PRIFYSGOL ABERYSTWYTH UNIVERSITY

Current and former volume and dynamics of mid-latitude glacier-like forms on Mars

Stephen Peter Brough

Thesis submitted in fulfilment of the requirements for the degree of PhD

Aberystwyth University

September 2017

Declaration and statements

Word count of thesis: 64423

Declaration

This work has not previously been accepted in substance for any degree and is not concurrently submitted in candidature for any degree.

Signed ..... Date .....

Statement 1

This thesis is the result of my own investigations, except where otherwise stated. Where correction services have been used, the extent and nature of the correction is clearly marked in a footnote. Other sources are acknowledged by footnotes giving explicit references. A bibliography is appended.

Signed ..... Date .....

Statement 2

I hereby give consent for my thesis, if accepted, to be available for photocopying and for inter-library loan, and for the title and summary to be made available to outside organisations.

Signed ..... Date .....

Acknowledgements

First and foremost I would like to thank Bryn and Alun Hubbard, both of whom provided seemingly inexhaustible support and advice over the course of this thesis. I am also indebted to Colin Souness for his input and guidance on various Mars related aspects. I also thank Peter Grindrod and Joel Davis for support in the processing and production of stereo DTMs, as well as to Matthew Balme and Tom Holt for constructive and challenging comments during the examination of this thesis.

The work undertaken in this thesis was funded by an Aberystwyth University Doctoral Career Development Scholarship. The British Society for Geomorphology and the Geological Remote Sensing Group are thanked for providing financial support for conference attendance. Acknowledgment is due to University College London for allowing access to the UK NASA RPIF during a research visit in 2014.

I am grateful to many staff members in the Department of Geography and Earth Sciences at Aberystwyth University and in the School of Geography, Geology and the Environment at Keele University for providing support, care and entertainment when needed. The list is long but Sam Doyle, Marie Busfield, Rhys Dafydd Jones, Peter Bunting, Harry Toland, Alix Cage, Richard Waller and Peter Knight deserve a special mention. To Jonathan Ryan, Morgan Gibson, Stephen Jennings and various other stablemates who I had the pleasure of sharing an office with, you will forever have my thanks for providing much needed relief and tea, of course.

To my family, I hope I can one day repay you for the support you have provided me during what has been, at times, a very demanding undertaking – *vis unita fortior*. I must save my last thanks for my dearest Rachel, without whom none of this would have been possible. Thank you for showing unwavering support and patience.

Stephen Brough
Aberystwyth

Abstract

The mid-latitudes of Mars host numerous ice-related landforms that bear many similarities to terrestrial ice masses. One particular landform has a strong resemblance to valley or debris-covered glaciers found on Earth and have subsequently become known as 'glacier-like forms' (GLFs). GLFs have detailed surface morphologies consistent with recent deposition and viscous deformation of ice, but there is still uncertainty regarding their formation, current and former volume, and dynamic evolution. Specifically, this thesis presents new observations and results that assess the current and former volume and dynamics of Mars' mid-latitude GLFs.

The findings presented in this thesis suggest that at the broadest level Mars' mid-latitudes appear to preserve a complex and spatially heterogeneous record of glaciation and that GLFs appear to be the manifestation of a more localised period of alpine glaciation. GLFs represent an active component of the near-surface water budget of Mars, locking away an estimated global equivalent water layer of between 3 ± 1 and 10 ± 3 mm. Evidence of recession and mass loss was identified in approximately one-third (n = 436) of the GLF population, suggesting that these landforms once contributed a larger volume of water to the near-surface water budget of Mars. Assessment of environmental and topographical controls over current ice volume and ice-mass loss revealed that their distribution and size is unlikely to be purely controlled by insolation forcing. Instead it is suggested that regional to local meteorological and topographical conditions also play an important role in GLF ice accumulation and/or preservation, with variation in physical environments providing microclimates favourable for accumulation and/or preservation of ice. The emerging picture shows that Mars' GLFs appear to have been dynamically active, and that they have played an important role in altering the surface landscape of Mars through erosion, transport and deposition of material.

Table of Contents

List of Figures

Chapter 4. Former extent of glacier-like forms on Mars

Chapter 5. Palaeo-glaciers on Mars: modelling their formation and evolution

Appendix A. Glacier-like forms on Mars

List of Tables

Chapter 1. Introduction

Chapter 2. Landscapes of polyphase glaciation: eastern Hellas Planitia, Mars

Chapter 3. Area and volume of mid-latitude glacier-like forms on Mars

Chapter 4. Former extent of glacier-like forms on Mars

Chapter 5. Palaeo-glaciers on Mars: modelling their formation and evolution

Appendix A. Glacier-like forms on Mars

List of Acronyms

CCF	Concentric crater fill
CTX	Context Camera
DEM/DTM	Digital elevation model/Digital terrain model
GCM	General circulation model
GIS	Geographic Information System
GLF	Glacier-like form
HiRISE	High Resolution Imaging Science Experiment
ISIS	Integrated Software for Imagers and Spectrometers
JMARS	Java Mission-planning and Analysis for Remote Sensing
LDA	Lobate debris apron
LMGM	Last martian glacial maximum
LVF	Lineated valley fill
MLR	Moraine-like ridge
MOC	Mars Orbiter Camera
MOLA	Mars Orbiter Laser Altimeter
MRO	Mars Reconnaissance Orbiter
MSGL	Mega-scale glacial lineations
SHARAD	Shallow Radar
THEMIS	Thermal Emission Imaging System
VFF	Viscous flow feature

CHAPTER 1

Introduction

To strive, to seek, to find, and not to yield

Alfred Tennyson

1. Introduction

This thesis seeks to improve our understanding of near-surface, ice flows in the mid-latitudes of Mars. It focuses on a suite of landforms termed glacier-like forms (e.g. Hubbard et al., 2011) and is motivated by the need to improve our understanding of geologically recent (Late Amazonian) climatic change on Mars. Glacier-like forms were targeted over other mid-latitude ice masses as they are the landform most similar – at least in overall appearance – to terrestrial glaciers. They thereby provide an opportunity to use terrestrial glacier analogues as a way to understand better cryospheric processes operating now and in the geologically recent past on Mars.

Below, a synthesis of key literature relating to the broad concept of mid-latitude glaciation on Mars is provided. This is followed by a summary of current understanding and knowledge gaps with respect to glacier-like forms. The aim and objectives of the thesis are then presented, followed by a summary of the thesis structure.

1.1. Mid-latitude glaciation on Mars

Current atmospheric conditions on Mars are both cold and dry with an average temperature of ~215 K (-58^{o}C) and an average vapour pressure of ~7 mbar (Read and Lewis, 2004; Barlow, 2008). These conditions prevent liquid water from being stable on the surface of Mars and only allow water ice to persist on the planet's surface in the polar regions (Mellon and Jakosky, 1995; Forget et al., 2006), with exposed surface ice sublimating into the atmosphere outside these regions (e.g. Byrne et al., 2009). However, such conditions are at odds with the geological and geomorphological records (Figure 1.1) that show compelling evidence of widespread fluvial and glacial activity (e.g. Baker, 2001; Kargel, 2004; Carr and Head, 2010; Souness and Hubbard, 2012).

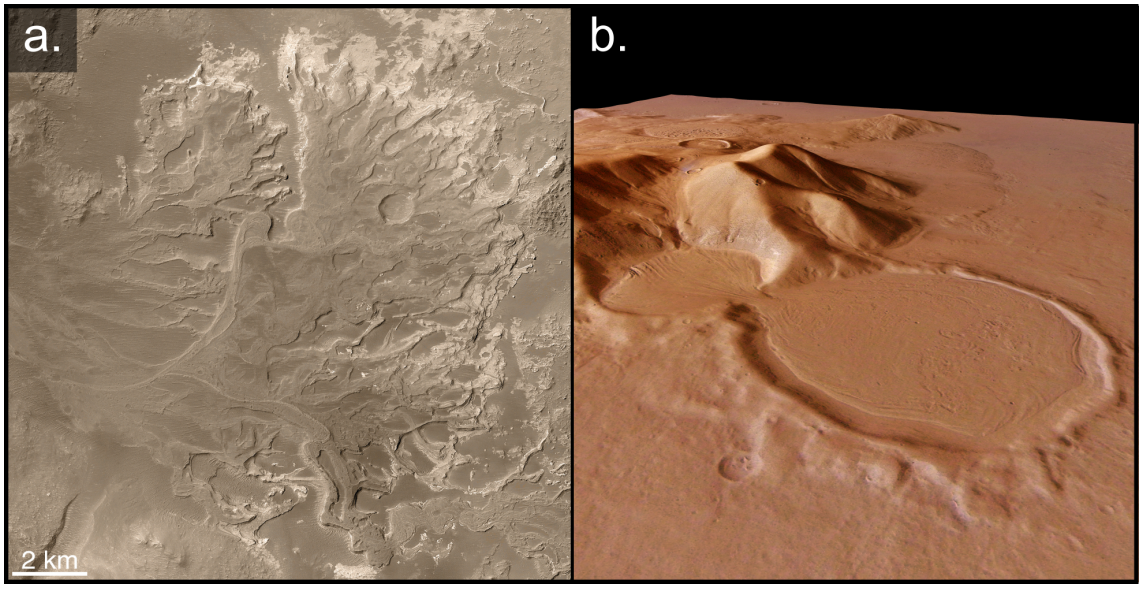

Figure 1.1: *Images indicating water-generated landscapes. (a) Fossil delta in Eberswalde Crater. Numerous inverted channels can be seen meandering and crisscrossing one another (Mars Orbiter Camera [MOC] mosaic MOC2-1225; centred on 33.61^{o} W, 23.84^{o} S). Image credit NASA/JPL/MSSS. (b) Hourglass Glacier in Promethei Terra. Icy material is thought to have flowed from the smaller, 9 km, wide crater into the larger, 16 km wide, crater below. The surface contains a number of lineations and lobate structures indicative of viscous flow (High Resolution Stereo Camera perspective view; centred on 102.83^{o} E, 38.92^{o} S). Image credit ESA/DLR/FU Berlin.*

Numerous landforms have been identified in the mid-latitudes (30 – 60^{o}) of Mars that have been attributed to viscous deformation and the flow of H_2O ice during the Amazonian epoch (~3 Ga BP to present) and predominately within the last 1 Ga BP (e.g. Sharp, 1973; Squyres, 1978, 1979; Squyres and Carr, 1986; Head et al., 2005; Holt et al., 2008). In many instances, these 'viscous flow features' (VFFs) share numerous characteristics with glaciers on Earth (e.g. Head et al., 2005, 2006, 2010; Marchant and Head, 2007; Holt et al., 2008). For a glacial scenario to be true, there must have been a marked shift in climate from that of today to one that favours ice emplacement and accumulation in the mid-latitudes. Based on converging theoretical (e.g. Head et al., 2003) and numerical studies – which have successfully reconstructed precipitation and accumulation of water ice in the locations where these ice-rich landforms have been identified (e.g. Forget et al., 2006; Madeleine et al., 2009) – it has been suggested that

changes in the orbital parameters of Mars (Figure 1.2) brought about climatic changes that have resulted in one or more 'ice ages' (Laskar et al., 2002, 2004; Head et al., 2003; Kargel, 2004).

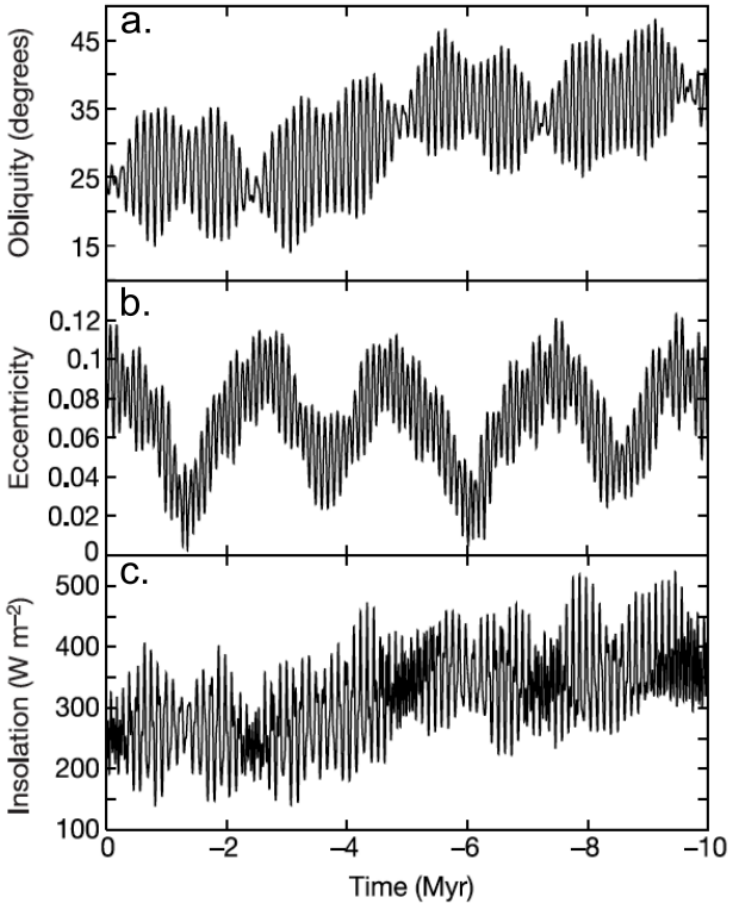

Figure 1.2: *Variations in orbital parameters of Mars for the last 10 Ma BP from numerical simulations. (a) Obliquity. (b) Eccentricity. (c) Insolation. Adapted from Laskar et al. (2002).*

These changes in orbital parameters are analogous to Milankovitch Cycles on Earth, which have been shown to induce and/or sustain glaciation (Imbrie and Imbrie, 1986). However, in contrast to the Earth scenario, glacial periods on Mars are thought to initiate during periods of higher (>30^{o}) obliquity (e.g. Head et al., 2003; Forget et al., 2006). During these periods of high obliquity, increased insolation at the poles causes

sublimation and ice redistribution to the mid-latitudes (Haberle et al., 2003; Head et al., 2003; Mischan et al., 2003).

Satisfactory reconstructions of orbital variations for Mars can only be generated for about the last 20 Ma, but show that during this time the obliquity has fluctuated between ~15 and 45^{o} (Laskar et al., 2004). As seen in Figure 1.2, the obliquity of Mars changed dramatically around 5 Ma ago, shifting from a mean obliquity period of ~35^{o} to a mean obliquity period of ~25^{o} for the last 5 Ma. This change in mean obliquity is hypothesised to have ended the most recent 'ice age' (Souness and Hubbard, 2012). Since that time, apart from during intermittent fluctuations where obliquity exceeded 30^{o}, mid-latitude ice would have been left to sublimate in the drier atmosphere, similar to the present day. Thus, the ice-rich landforms observed across large proportions of Mars' mid-latitudes are likely the relict remnants of once much larger ice masses, and their survival to today is only possible due to a debris cover protecting the ice from sublimation (Bryson et al., 2008; Holt et al., 2008; Plaut et al., 2009; Fastook et al., 2014). Notwithstanding the above, numerous questions still exist as to exactly how and when these VFFs formed, and to their geometrical change and dynamics since initial formation.

1.2. Glacier-like forms

Since their reporting within the literature in ~2003 (e.g. Hartmann et al., 2003; Marchant and Head, 2003; Milliken et al., 2003) various names have been applied in the description of small- to medium-scale (<10s km), lobate or tongue-like icy landforms (Figure 1.3). These include: rock glaciers (Marchant and Head, 2003); VFFs (Milliken et al., 2003); glacier-like flows (Arfstrom and Hartmann, 2005); superposed lineated valley fill (Levy et al., 2007); small-scale superposed lineated valley fill (Levy et al., 2007); and glacier-like forms (Hubbard et al., 2011). This thesis follows Hubbard et al. (2011) and uses the term 'glacier-like form' (GLF) throughout.

Figure 1.3: *A satellite image of a particularly well-developed tongue-shaped icy landform located in Crater Greg. A number of early studies focused on the 'glacier-like' nature of the landform, including the sequence of raised latero-terminal ridges surrounding the apparent margin of the landform, the deflated and degraded nature of the main body, and the chevron surface pattern of the upper basin (subset of MOC image M18-00897; centred on 113.16^{o} E, 38.15^{o}S). From Hartmann et al. (2003).*

1.2.1. GLF classification and geographical characteristics

GLFs represent perhaps the most distinctive subtype of VFF (see Souness and Hubbard, 2012 for detailed classification scheme), being similar in appearance and morphology to terrestrial valley glaciers. Broadly speaking, GLFs form in small cirque-like alcoves or valleys and appear to flow downslope, generally coalescing from a wide upper basin and terminating in a narrow elongate tongue that is often confined by moraine-like ridges (Figures 1.3 and 1.4).

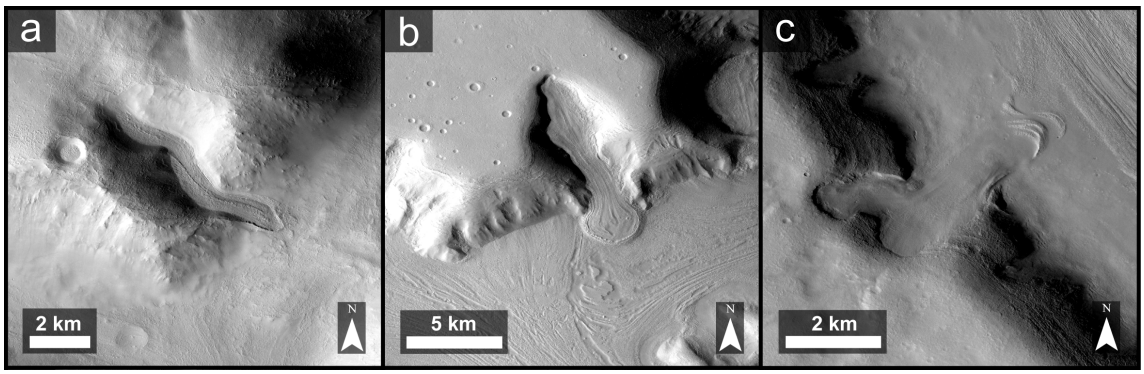

Figure 1.4: *Examples of GLFs, highlighting the diversity in their morphology and appearance. (a) Simple valley-like GLF terminating in non-ice terrain (subset of CTX image B04_011261_2146_XN_34N289W; centred on ~70.59^o E, 33.12^o N). (b) Piedmont type GLF terminating in an outer ice terrain. Note how the GLF lobe is superposed on the wider ice-rich terrain (subset of CTX image P22_009653_2224_XN_42N309W; centred on ~50.50^o E, 42.24^o N). (c) A dual alcove GLF. Note how the GLF merges with the wider ice-rich terrain (subset of CTX image P03_002112_2208_XN_40N337W; centred on ~22.27^o E, 40.07^o N).*

Building on earlier work of Milliken et al. (2003), Souness et al. (2012) produced formal criteria for the identification and classification of GLFs (Table 1.1) and, from visual inspection of >8000 Context Camera (CTX) images, identified 1309 GLFs between 25 and 65^o latitude in both hemispheres (Figure 1.5). Based on analysis of geographical and topographical data from point measurements and/or geometric buffers, the authors identified several inter- and intra-hemispheric similarities in the overall distribution and morphology of GLFs. Of the total GLF population, 727 (56%) were

Table 1.1: *Criteria for GLF identification following Souness et al. (2012).*

	Description
[i]	Be surrounded by topography showing general evidence of flow over or around obstacles
[ii]	Be distinct from the surrounding landscape exhibiting a texture or colour difference from adjacent terrains
[iii]	Display surface foliation indicative of down-slope flow; e.g. compressional/extensional ridges, surface lineations, arcuate surface morphologies or surface crevassing
[iv]	Have a length to width ratio >1 (i.e. be longer than it is wide)
[v]	Have either a discernible 'head' or a discernible 'terminus' indicating a compositional boundary or process threshold
[vi]	Appear to contain a volume of ice (or some other viscous substance), having a flat 'valley fill' surface, thus differentiating it from a previously glaciated 'GLF skeleton'

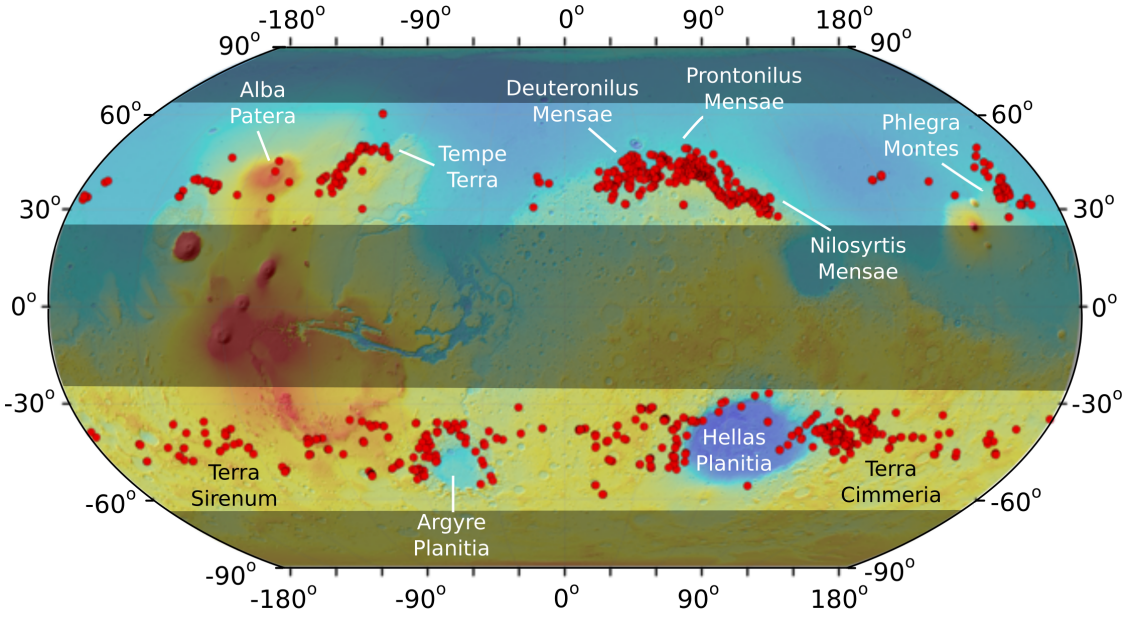

Figure 1.5: *Mid-latitude distribution of GLFs as identified by Souness et al. (2012). Note the preponderance of GLFs along the fretted terrain of Deuteronilus Mensae, Protonilus Mensae and Nili Fossae in the northern hemisphere, and surrounding the Hellas and Argyre impact basins in the southern hemisphere. Modified from Souness et al. (2012).*

identified in the northern hemisphere and 582 (44%) in the southern hemisphere, and were shown to have a preference for the mid-latitudes (centred on a mean latitude of ~ ±40^{o}). GLFs were also shown to have a remarkably similar mean length (4.91 km in the north and 4.35 km in the south) and width (1.26 km in the north and 1.34 km in the south), a strong preference for a poleward orientation (with a mean bearing of 26.6^{o} [NNE] in the north and 173.1^{o} [SSE] in the south) – indicating a strong sensitivity to insolation – and to be preferentially present in regions of moderate, but not high, relief.

Although GLFs are identified in isolation, where they terminate on bedrock (e.g. Figure 1.4a), they frequently feed into pre-existing VFFs where they either superpose (Figure 1.4b) or integrate (Figure 1.4c) and form part of what Head et al. (2010) referred to as Mars' integrated glacial landsystem. Following this model, GLFs represent the smallest component of this glacial landsystem and may merge downslope to form broad, rampart-like lobate debris aprons (LDAs [Squyres, 1978; Squyres. 1979]). In turn, LDAs may converge or coalesce, typically from opposing valley walls, to form lineated valley fills (LVFs), which commonly exhibit complex and contorted surfaces that show no obvious flow direction. However, it should again be noted, both LDAs and LVFs are commonly observed in isolation and need not require the inclusion of influent mass.

1.2.2. GLF mechanical and thermal properties

The precise composition of GLFs is a continuing point of discussion and remains largely unknown, mainly due to the occurrence of a ubiquitous layer of fine-grained regolith covering their surface. More broadly, the amount and quantity of water ice involved in VFF composition (including GLFs) is still debated, leading to a variety of feature-scale interpretations being proposed, including (i) ice assisted talus flows (~20 – 30% ice [Squyres 1978, 1979]); (ii) rock-glaciers (~30 – 80% ice [Colaprete and Jakosky, 1998; Mangold, 2003]); and (iii) debris-covered glaciers (>80% ice [Head et al., 2005; Li et al., 2005]). Given the limited number of direct observations of VFF interiors, coupled with the fact that the distinction between such forms and 'standard' glaciers is not clearly defined even on Earth (e.g. Berthling, 2011), it is unlikely that we are in a position to definitively attribute martian equivalents. That said, a number of recent observations appear to corroborate a more high-ice model of VFF formation. For

example, Head et al. (2005) argued that numerous surface textures, including sinuous ridges, irregular depressions and flowlines on a VFF in eastern Hellas Planitia (Figure 1.1b) were indicative of 'extremely ice-rich' glacier-like viscous flow. Further, Dundas and Bryne (2010) reported the capture of very recent meteorite strikes – in the mid-latitudes of Mars (between ~43 and 56^{o} N) – that indicated the presence of relatively clean (i.e., debris poor) massive ice at shallow depths below the surface. These results supported geophysical findings from the Shallow Radar (SHARAD), on board the Mars Reconnaissance Orbiter (MRO), that has detected massive H_2O ice deposits with minimal lithic content, buried beneath a thin (<10m) debris layer on VFFs in both the southern and northern hemispheres, respectively (e.g. Figure 1.6 [Holt et al., 2008; Plaut et al., 2009]). Such findings have led to the general acceptance that H_2O ice accounts for the dominant portion of VFF (including GLF) mass. However, our understanding of the internal structure, and the precise ratio of ice-rock mixture, of most VFFs – or indeed rock and debris-covered glaciers on Earth – remain elusive and have by no means been fully explored.

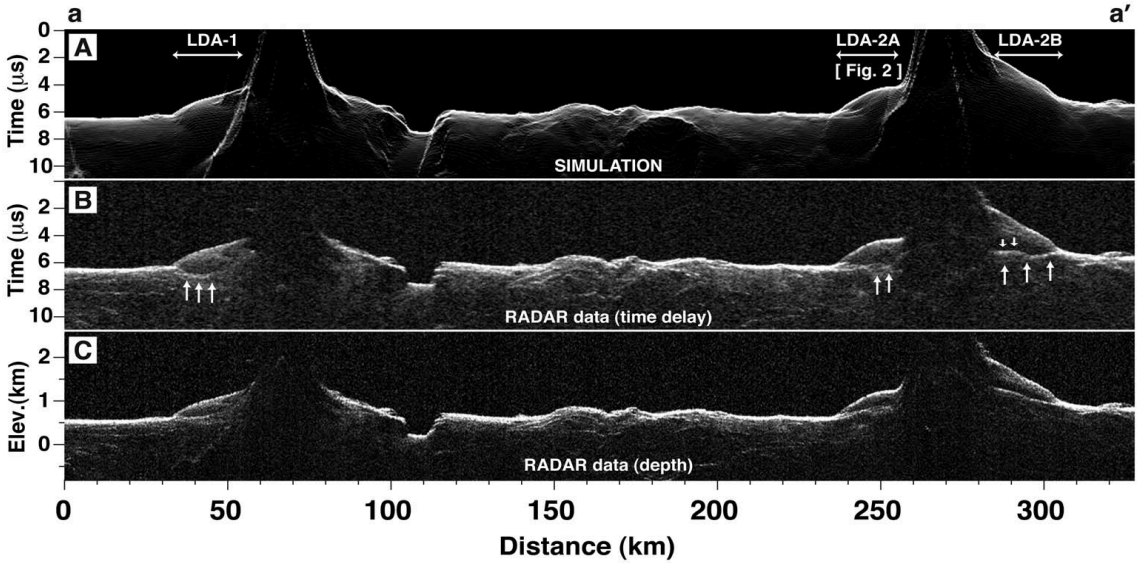

Figure 1.6: *SHARAD profiles of Holt et al. (2008) identifying 'buried glaciers' centred at ~104^{o} E, 43^{o} S in the eastern Hellas Planitia region. (a) Simulated radargram of expected off-nadir clutter echoes as one-way travel time. (b) SHARAD data represented in one-way travel time. White arrows indicate returns not present in the clutter simulation (a), and are interpreted to represent the subsurface. (c) SHARAD data converted to depth assuming a water-ice composition. From Holt et al. (2008).*

A second point of discussion that also remains largely unknown is the rheology of GLFs. This is particularly hampered by the fact that in no instance has GLF (or VFF) motion being observed, and our understanding of such motion has hitherto relied on modelling, or being inferred from their overall shape and surface flow structures, such as 'chevron' crevasses (e.g. Figure 1.3 [Marchant and Head, 2003]). For example, Milliken et al. (2003) implemented the multi-component constitutive relation of Goldsby and Kohlstedt (2001) to model the stress-strain rate within VFF, in order to assess the likelihood of motion. The authors based their analysis on typical ranges of VFF temperature, slope and (assumed) grain size, and calculated shear stresses of ~$10^{-1.5}$ – $10^{-2.5}$ MPa and consequent strain rates on the order of 10^{-11} – 10^{-16} a^{-1} for an estimated 10 m thick VFF deposit. Using these rates, Milliken et al. (2003) estimated that a period of between 3 Ka and 300 Ma would be required to produce a shear strain of 100 %, which was in broad agreement with the estimated age (10^5 – 10^7 a) of the material. It should be noted, that although representing a major advance at the time, the model was not applied to any particular GLF geometry and thus was not distributed spatially.

Coupled with the above, reliable estimates of GLF motion require knowledge of conditions, either at present and/or in the past, at the bed of the ice mass. Currently, there is a general consensus that most present-day GLFs (and VFFs) are cold-based (Head and Marchant, 2003; Shean et al., 2005) – i.e. they are frozen to their bed and involve little to no liquid water – with flow occurring through ductile or brittle ice deformation. This conclusion is driven by the absence of evidence for wet-based – i.e. ice at the glacier bed is at pressure melting point – glaciation (e.g. proglacial or lateral meltwater channels, and/or eskers that are visibly connected to the parent ice mass). Nonetheless, this is not to say that GLFs have been entirely cold-based throughout their history. For example, evidence for at least partial periods of wet-based glaciation has been proposed based on GLF morphology and associated landform assemblage (e.g. Arfstrom and Hartmann, 20005; Hubbard et al., 2011). Hubbard et al. (2011) conducted a geomorphological assessment of a GLF in Crater Greg, eastern Hellas Planitia (Figures 1.3 and 1.7), and concluded that the upper basin currently hosts a degraded GLF, with the lower basin zone now exhibiting relict bedforms. Two of these bedforms, their 'mound and tail' terrain and 'linear' terrain, were compared to terrestrial drumlins and mega-scale glacial lineations (MSGL), respectively. Given that both of these

landforms are associated with the influence of liquid water, this would appear to preclude an entirely cold-based scenario and suggest that the GLF may have, at least intermittently, experienced wet-based glaciation. Furthermore, outside of the current GLF basin, Hubbard et al. (2011) identified one further terrain that may have formed in the presence of liquid water. The authors likened their 'rectilinear ridge' terrain to moraine-mound complexes on Earth, which can form either from the direct presence of water (e.g. Lukas, 2005), or through the existence of polythermal – i.e. glaciers that have complex thermal structure where part of their bed is frozen and part of their bed is at the pressure melting point – glaciation (e.g. Hambrey et al., 2005). However, it is pertinent to point out that all three of theses terrains were also considered with alternate explanations that did not involve wet-based glaciation (Hubbard et al. 2011).

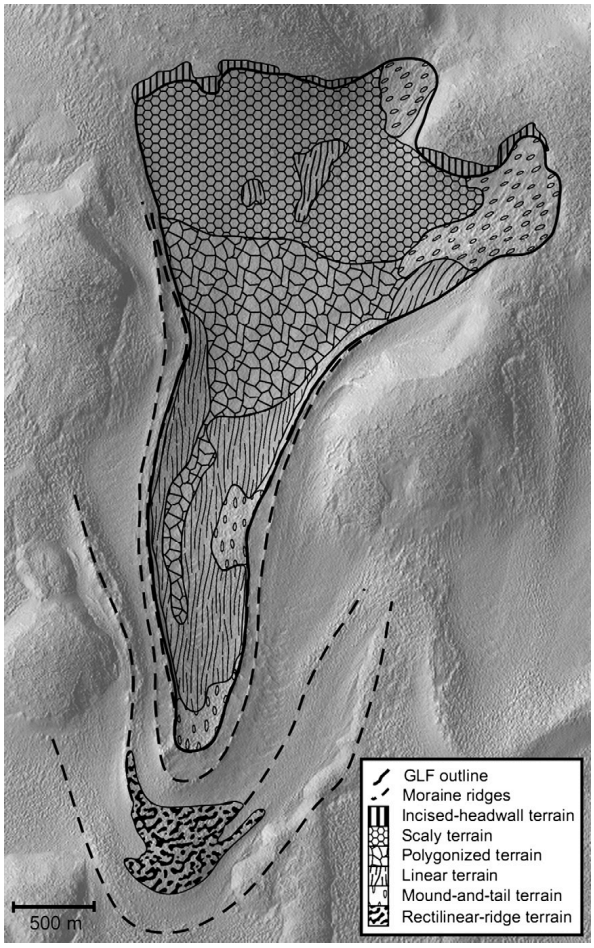

Figure 1.7: *Geomorphic map of Hubbard et al. (2011) identifying predominant surface terrains and features (subset of High Resolution Imaging Science Experiment [HiRISE] image PSP_002320_1415; centred on 113.16^{o} E, 38.15^{o}S). From Hubbard et al. (2011).*

At the broader VFF scale, several landforms have been interpreted as indicative of, or at least consistent with, the action of liquid water and therefore potentially wet-based glaciation. These include, for example, small supraglacial and proglacial valleys coincident with mid-latitude VFFs and interpreted as similar to glacier meltwater channels (Fassett et al., 2010), as well as sinuous and anastomosing ridge networks, bedforms and large-scale groves being interpreted as subglacial eskers, MSGL and glacial erosional grooving, respectively (Kargel et al., 1995; Banks and Pelletier, 2008; Banks et al., 2009). The association of the latter three landforms in Argyre Planitia has even led to suggestions that large, likely wet-based, ice masses once occupied portions of the martian surface (e.g. Kargel and Strom, 1992; Bernhardt et al., 2013). At the very least, some GLFs and VFFs do appear to preclude an entirely cold-based scenario, but our collective understanding of the thermal regime of these ice masses, and how this may vary both spatially and temporally remains largely unknown.

1.2.3. GLF formation and evolution

There is on-going debate as to exactly how and when GLFs formed, and as to how they have evolved since their initial formation. However, it is generally agreed that GLFs are extant forms relating to a past, but relatively recent, martian ice age (see Section 1.1 above). This hypothesis is supported by both flow modelling (see Section 1.2.2 above [Milliken et al., 2003; Turtle et al., 2003]) and investigations of surface crater density (e.g. Arfstrom and Hartmann, 2005), which place GLFs as geologically recent, and probably between ~10^5 and 10^7 years old. It should be noted that both of these dating techniques are not definitive and are potentially subject to errors because of uncertainties propagating from assumptions used in these types of analyses. For modelling, these uncertainties include the (i) internal geometry and (ii) rheology of GLFs (see Section 1.2.2 above), and for crater density analyses are related to (i) occlusion of craters via sublimation and/or viscous relaxation of the icy substrate (e.g. Pathare et al., 2005; Sinha and Murty, 2013), and (ii) the small areas often involved and thus numbers and size of craters used (e.g. Dauber et al., 2013).

Moreover, there is a growing body of evidence that GLFs (and other VFFs) are the remnants of once far larger ice masses (e.g. Dickson et al., 2008; Hubbard et al., 2011;

Sinha and Murty, 2013), which were most extensive during a hypothesised last martian glacial maximum, or LMGM (See Section 1.1 [e.g. Souness and Hubbard, 2013]). Such evidence has been presented in the form of detailed geomorphological reconstructions, that have identified former ice limits from variations in surface texture and from the presence of bounding or distal moraine-like ridges, or MLRs (Figures 1.3 and 1.4 [e.g. Arfstrom and Hartmann, 2005]). One particularly marked example of a GLF that has undergone apparent recession and mass loss has been the focus of much study (Figures 1.3 and 1.7 [e.g. Hartmann et al., 2003; Marchant and Head, 2003; Kargel, 2004; Arfstrom and Hartmann, 2005; Hubbard et al., 2011]). For example, in an analysis of this particular GLF, Hubbard et al. (2011) described a sequence of nested arcuate ridges surrounding the flanks and immediate forefield of this GLF (Figure 1.7). The authors argued that these ridges were equivalent to latero-terminal moraines on Earth, and discussed the possibility that the landform assemblage revealed a system that had been subject to general recession, punctuated by episodes (at least three) of minor advance of standstill (Hubbard et al., 2011), and that this behaviour could have been driven by recent climatic fluctuations (e.g. Arfstrom and Hartmann, 2005; Hubbard et al., 2011).

Beyond GLFs, an expanded former ice extent has also been identified on the regional scale of Mars' integrated glacial landsystem (see Section 1.2.1 above [e.g. Head et al., 2006; Dickson et al., 2008]), where former glacial highstands up to ~900 m above the present day surface have been inferred (Dickson et al., 2008). Indeed, the identification of features and landforms of glacial origin across large areas of Mars' present day surface has also led to inferences of former regional- to continental-scale ice sheet glaciation (Kargel and Strom, 1992; Kargel et al., 1995; Head and Marchant, 2003; Bernhardt et al., 2013). Furthermore, several studies have noted the superposed relationship (Figures 1.4 and 1.8) of some GLFs to the underlying ice-rich terrain (LDA or LVF) onto which they appear to have flowed – particularly along the fretted terrain (Sharp, 1973) of Deuteronilus Mensae, Prontonilus Mensae and Nili Fossae (Figures 1.5 and 1.8) – leading to suggestions of recurrent glacial phases with at least one 'local' glacial phase advancing over an earlier 'regional' glaciation (e.g. Levy et al., 2007; Dickson et al., 2008; Baker et al., 2010; Sinha and Murty, 2013).

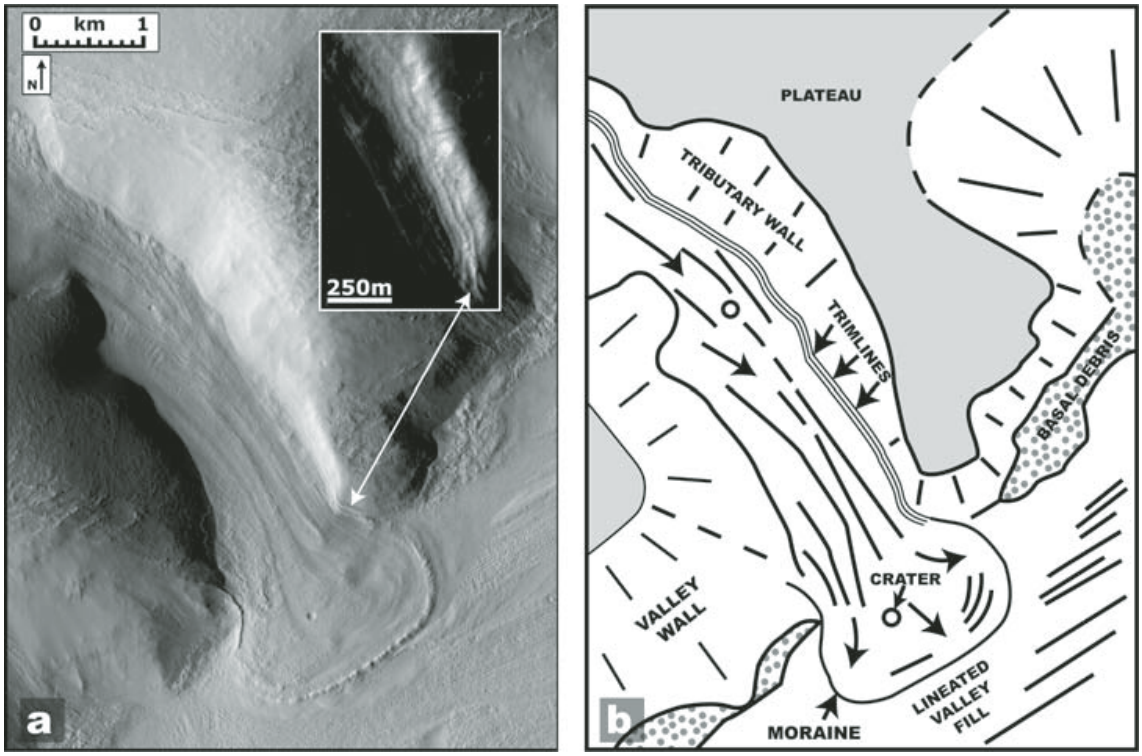

Figure 1.8: *Illustration of the stratigraphic relationship of GLFs to wider ice deposits. (a) Here a GLF can be seen emanating out of a valley and terminating in a distinctive lobate form. A raised latero-terminal ridge encompasses the terminus. The GLF is topographically superposed on the wider ice deposit – in this instance lineated valley fill. (b) Sketch map of (a). From Dickson et al. (2008).*

Despite these recent advances in understanding, we currently have limited knowledge of the mechanisms and climatic environments under which GLFs first accumulated sufficient ice-rich mass to flow downslope, the nature and timing of Mars' LMGM, the current and former volume of water contained within GLFs, and whether GLF (and VFF) recession has been spatially and/or temporally variable.

1.2.4. Summary of current GLF understanding and knowledge gaps

Given the observations presented in Sections 1.2.1 – 1.2.3 above, the current state of knowledge regarding GLFs is as follows:

- Souness et al. (2012) suggested that GLF(s): (i) are widespread across the mid-latitudes of Mars; (ii) share a common evolutionary history; (iii) appear to be influenced by, at least at some point in their history, climate/insolation; and (iv) flow is now influenced by local relief and gravity, but may have been in the recent past affected by an Earth-like mass-balance.

- Given the young age reported for GLFs and based on their stratigraphic relationships with other mid-latitude ice masses, it is possible that (some) GLFs represent a smaller more 'localised' glacial phase that is overriding an older 'regional' glaciation (Figure 1.8). Mars' mid-latitudes may thus contain evidence of multiple phases of glaciation.

- The identification of raised latero-terminal ridges surrounding the terminus of numerous GLFs suggests that, much like their Earth-based analogues (e.g. Zemp et al., 2009), GLFs have experienced an expanded former extent and have been subject to a period of mass loss since a former maximum. A further implication of this is that GLFs may therefore be, or have been, important landscaping agents through both deposition and erosion.

- Based on the above three points, GLFs that remain on the surface of Mars today are likely to be relict deposits that have survived from a potentially recent period of glaciation and may thus represent an important archive of information on recent climatic change on Mars.

Despite this relatively recent knowledge base, our understanding of the origin and evolution of GLFs is still in its infancy and a number of fundamental aspects of their behaviour remain virtually unknown. The most pressing of these knowledge gaps can be summarised as follows:

- What conditions can lead to GLF formation? Given the present climate of Mars is not favourable to ice accumulation in the mid-latitudes, significant climatic changes must have occurred in the geologically recent past in order for GLFs to have developed. By investigating the factors controlling the distribution of GLFs and assessing the potential climatic conditions required for their formation, we could begin to reconstruct these recent climatic perturbations and their spatial variation.

- What volume of water is stored in GLFs? Given the widespread presence of GLFs across the mid-latitudes of Mars (Figure 1.5) they potentially constitute an important reservoir of water. However, the contribution of GLFs to the nonpolar surface/near surface water inventory of Mars (e.g. Carr and Head, 2015) remains unknown. Furthermore, identifying the locations where, and the quantities in which, water exists on Mars may be highly relevant to future human and robotic exploration – water being a key component in the search for past life, and providing a potential resource for future explorers of Mars.

- How much mass has been removed from GLFs? Although instances of ice mass loss from GLFs have been reported (Figure 1.3), little attention has been paid to quantifying such loss. Better understanding the controls responsible for ice mass loss may provide valuable insights into recent/current climatic change and how GLFs, and their associated ice masses, might change under future climates.

- What are the mechanical properties and mechanisms of motion in GLFs? GLFs, and wider VFFs, show surface evidence for viscous flow; however, little is known about their (ice) rheology, mechanisms of GLF motion (e.g. velocity; stress-strain relationships), and their thermal regime.

- What role have GLFs played in landscaping the surface of Mars? Considering glaciers are a significant landscaping agent on Earth (e.g. Clark et al., 2004), ice masses on Mars could have played an important geomorphic role in altering the landscape of Mars.

1.3. Aim and objectives

The overarching aim of this thesis is to assess the current and former volume and dynamics of mid-latitude GLFs on Mars, in order to advance our understanding of the planet's recent glacial history. To achieve this aim, the following objectives have been identified:

(1) To map GLFs, associated ice masses and surrounding landforms to assess the style of glaciation.

(2) To investigate the physical glaciology of GLFs on Mars, including their former extent, motion, debris transport and hydrology.

(3) To conduct population-scale outline mapping of GLFs in order to estimate the ice volume from their areal extent.

(4) To identify, at the population-scale, GLFs that show evidence of recession and target an appropriate example for palaeo-glaciological reconstruction in order to assess area and volumetric change.

(5) Based on Objectives (3) and (4), examine the environmental and topographical controls influencing the distribution and stability of GLFs.

(6) To use computer-based numerical ice flow modelling to investigate the range of environmental and climatic conditions under which GLFs may have formed, and to assess their response to climatic forcing.

1.4. Thesis structure

1.4.1. Overview

This thesis has six chapters. An introduction to the broad subject of mid-latitude glaciation on Mars was provided in Chapter 1 that synthesised the current understanding and gaps in knowledge regarding GLFs, and provided context for the thesis. In Chapter 2, a geomorphic and structural assessment of a glacierised landscape in eastern Hellas Planitia in Mars' southern hemisphere is presented. In Chapter 3, the first comprehensive ice volume estimate of martian GLFs is presented and explanations for variation in their size and distribution offered. In Chapter 4, a population-scale inventory of GLF recession, including a palaeo-glaciological reconstruction of the former three-dimension extent of a GLF in Crater Greg, eastern Hellas Planitia, is presented. In Chapter 5, initial results from numerical ice flow modelling are presented. This modelling extended the investigations into the glacial history of the GLF reconstructed in Chapter 4 and assessed the environment and climatic conditions that could have led to the formation of the former maximum GLF extent, as recorded in the geomorphological record. In Chapter 6, a summary of Chapters 2 – 5 is given and an examination of how these outputs have contributed to addressing the aim of the thesis is presented, and is finished by providing avenues for future research.

Chapters 2 – 5 constitute published or near-published outputs that form standalone, but complementary, manuscripts, each of which represents original and new research. Therefore, each chapter consists of some, or all, of the following sections: Abstract; Introduction/Literature Review; Site Description; Data and Methods; Results; Discussion; Conclusions; References; and Supporting Material. Chapters 2 and 4 have been published in the *Journal of Maps* and *Icarus*, respectively, Chapter 3 is currently under review for the journal *Earth and Planetary Science Letters* and Chapter 5 is a manuscript in preparation for submission. Full details of these manuscripts and the contribution made by the author of this thesis are provided in Section 1.4.2. During the duration of this thesis, the author also co-authored complimentary work carried out by affiliated parties. These contributions are included in the publication of Hubbard et al. (2014) in the journal *The Cryosphere*. This publication is attached in Appendix A.

1.4.2. Summary of manuscript details and author contributions

Chapter 2

Brough, S., Hubbard, B., Souness, C., Grindrod, P. M., & Davis, J. (2016). Landscapes of polyphase glaciation: eastern Hellas Planitia, Mars. *Journal of Maps*, *12*(3), 530-542. doi: 10.1080/17445647.2015.1047907.

SB and BH conceived the study. SB, PG and JD produced the digital elevation models used in mapping. SB conducted all mapping, data analysis, figure production and led the manuscript writing. BH, CS, PG and JD provided conceptual and technical advice, and edited the manuscript. Mapping of the GLF is based on work presented in Hubbard et al. (2014 [Appendix A]) and Souness (2013).

Chapter 3

Brough, S., Hubbard, B., & Hubbard, A. (in review). Area and volume of mid-latitude glacier-like forms on Mars. *Earth and Planetary Science Letters*.

SB and BH conceived this study. SB conducted all mapping, data analysis, figure production and led the manuscript writing. BH and AH provided conceptual and technical advice and edited the manuscript.

Chapter 4

Brough, S., Hubbard, B., & Hubbard, A. (2016). Former extent of glacier-like forms on Mars. *Icarus*, *274*, 37-49. doi: 10.1016/j.icarus.2016.03.006.

SB and BH conceived this study. SB conducted all mapping, data analysis, figure production and led the manuscript writing. BH and AH provided conceptual and technical advice and edited the manuscript.

Chapter 5

Brough, S., Hubbard, A., & Hubbard, B. (in prep). Palaeo-glaciers on Mars: modelling their formation and evolution.

SB, BH and AH conceived this study. AH wrote and provided the model. SB modified the model, conducted all data analysis, figure production and led the manuscript writing. BH and AH provided conceptual and technical advice and edited the manuscript.

References

Arfstrom, J., & Hartmann, W. K. (2005). Martian flow features, moraine-like ridges, and gullies: Terrestrial analogs and interrelationships. *Icarus, 174*(2), 321-335. doi: 10.1016/j.icarus.2004.05.026.

Baker, V. R. (2001). Water and the martian landscape. *Nature, 412*(6843), 228-236. doi: 10.1038/35084172.

Baker, D. M. H., Head, J. W., & Marchant, D. R. (2010). Flow patterns of lobate debris aprons and lineated valley fill north of Ismeniae Fossae, Mars: Evidence for extensive mid-latitude glaciation in the Late Amazonian. *Icarus, 207*(1), 186-209. doi: 10.1016/j.icarus.2009.11.017.

Banks, M. E., & Pelletier, J. D. (2008). Forward modeling of ice topography on Mars to infer basal shear stress conditions. *Journal of Geophysical Research: Planets*, *113*(E1). doi: 10.1029/2007JE002895.

Banks, M. E., Lang, N. P., Kargel, J. S., McEwen, A. S., Baker, V. R., Grant, J. A., Pelletier, J. D., & Strom, R. G. (2009). An analysis of sinuous ridges in the southern Argyre Planitia, Mars using HiRISE and CTX images and MOLA data. *Journal of Geophysical Research: Planets*, *114*(E9). doi:10.1029/2008JE003244.

Barlow, N. G. (2008). *Mars: An Introduction to its Interior, Surface, and Atmosphere*. Cambridge: Cambridge University Press.

Berthling, I. (2011). Beyond confusion: Rock glaciers as cryo-conditioned landforms. *Geomorphology*, *131*, 98-106. doi: 10.1016/j.geomorph.2011.05.002.

Bernhardt, H., Hiesinger, H., Reiss, D., Ivanov, M., & Erkeling, G. (2013). Putative eskers and new insights into glacio-fluvial depositional settings in southern

Argyre Planitia, Mars. *Planetary and Space Science*, *85*, 261-278. doi: 10.1016/j.pss.2013.06.022.

Bryson, K., Chevrier, V., Sears, D., & Ulrich, R. (2008). Stability of ice on Mars and the water vapor diurnal cycle: Experimental study of the sublimation of ice through a fine-grained basaltic regolith. *Icarus, 196*(2), 446-458. doi: 10.1016/j.icarus.2008.02.011.

Byrne, S., Dundas, C. M., Kennedy, M. R., Mellon, M. T., McEwen, A. S., Cull, S. C., Dauber, I. J., Shean, D. E., Seelos, K. D., Murchie, S. L., Cantor, B. A., Arvidson, R. E., Edgett, K. S., Reufer, A., Thomas, N., Harrison, T. N., Posiolova, L. V., & Seelos, F. P. (2009). Distribution of mid-latitude ground ice on Mars from new impact craters. *Science, 325*(5948), 1674-1676. doi: 10.1126/science.1175307.

Carr, M. H., & Head, J. W. (2010). Geologic history of Mars. *Earth and Planetary Science Letters, 294*(3-4), 185-203. doi: 10.1016/j.epsl.2009.06.042.

Carr, M. H., & Head, J. W. (2015). Martian surface/near-surface water inventory: Sources, sinks, and changes with time. *Geophysical Research Letters*, 2014GL062464. doi: 10.1002/2014gl062464.

Clark, C. D., Evans, D. J. A., Khatwea, A., Bradwell, T., Jordan, C. J., Marsh, S. H., Mitchell, W. A., & Bateman, M. D. (2004). Map and GIS database of landforms and features related to the last British Ice Sheet. *Boreas, 33*(4), 359-375. doi: 10.1080/03009480410001983.

Colaprete, A., & Jakosky, B. M. (1998). Ice flow and rock glaciers on Mars. *Journal of Geophysical Research: Planets*, *103*(E3), 5897-5909. doi: 10.1029/97JE03371.

Daubar, I. J., McEwen, A. S., Byrne, S., Kennedy, M. R., & Ivanov, B. (2013). The current martian cratering rate. *Icarus, 225*(1), 506-516. doi: 10.1016/j.icarus.2013.04.009.

Dickson, J. L., Head, J. W., & Marchant, D. R. (2008). Late Amazonian glaciation at the dichotomy boundary on Mars: Evidence for glacial thickness maxima and multiple glacial phases. *Geology, 36*(5), 411-414. doi: 10.1130/g24382a.1.

Dundas, C. M., & Byrne, S. (2010). Modeling sublimation of ice exposed by new impacts in the martian mid-latitudes. *Icarus*, *206*(2), 716-728. doi: 10.1016/j.icarus.2009.09.007.

Fassett, C. I., Dickson, J., Head, J. W., Levy, J. S., & Marchant, D. R. (2010).

Supraglacial and proglacial valleys on Amazonian Mars. *Icarus*, *208*, 86-100. doi: 10.1016/j.icarus.2010.02.021.

Fastook, J. L., Head, J. W., & Marchant, D. R. (2014). Formation of lobate debris aprons on Mars: Assessment of regional ice sheet collapse and debris-cover armoring. *Icarus, 228*, 54-63. doi: 10.1016/j.icarus.2013.09.025.

Forget, F., Haberle, R. M., Montmessin, F., Levrard, B., & Head, J. W. (2006). Formation of glaciers on Mars by atmospheric precipitation at high obliquity. *Science, 311*(5759), 368-371. doi: 10.1126/science.1120335.

Goldsby, D. L., & Kohlstedt, D. L. (2001). Superplastic deformation of ice: Experimental observations. *Journal of Geophysical Research: Solid Earth*, *106*(B6), 11017-11030. doi: 10.1029/2000JB900336.

Haberle, R. M., Murphy, J. R., & Schaeffer, J. (2003). Orbital change experiments with a Mars general circulation model. *Icarus, 161*(1), 66-89. doi: 10.1016/S0019-1035(02)00017-9.

Hambrey, M. J., Murray, T., Glasser, N. F., Hubbard, A., Hubbard, B., Stuart, G., Hansen, S., & Kohler, J. (2005). Structure and changing dynamics of a polythermal valley glacier on a centennial timescale: Midre Lovenbreen, Svalbard. *Journal of Geophysical Research-Earth Surface*, *110*(F1). doi: 10.1029/2004JF000128.

Hartmann, W. K., Thorsteinsson, T., & Sigurdsson, F. (2003). Martian hillside gullies and Icelandic analogs. *Icarus, 162*(2), 259-277. doi: 10.1016/S0019-1035(02)00065-9.

Head, J. W., & Marchant, D. R. (2003). Cold-based mountain glaciers on Mars: Western Arsia Mons. *Geology, 31*(7), 641-644. doi: 10.1130/0091-7613(2003)031<0641:cmgomw>2.0.co;2.

Head, J. W., Marchant, D. R., Agnew, M. C., Fassett, C. I., & Kreslavsky, M. A. (2006). Extensive valley glacier deposits in the northern mid-latitudes of Mars: Evidence for Late Amazonian obliquity-driven climate change. *Earth and Planetary Science Letters, 241*(3-4), 663-671. doi: 10.1016/j.epsl.2005.11.016.

Head, J. W., Marchant, D. R., Dickson, J. L., Kress, A. M., & Baker, D. M. (2010). Northern mid-latitude glaciation in the Late Amazonian period of Mars: Criteria for the recognition of debris-covered glacier and valley glacier landsystem deposits. *Earth and Planetary Science Letters, 294*(3-4), 306-320. doi: 10.1016/j.epsl.2009.06.041.

Head, J. W., Mustard, J. F., Kreslavsky, M. A., Milliken, R. E., & Marchant, D. R. (2003). Recent ice ages on Mars. *Nature, 426*(6968), 797-802. doi: 10.1038/Nature02114.

Head, J. W., Neukum, G., Jaumann, R., Hiesinger, H., Hauber, E., Carr, M., Massson, P., Foing, B., Hoffmann, H., Kreslavsky, M., Werner, S., Milkovich, S., van Gasselt, S., & HRSC Co-Investigator Team. (2005). Tropical to mid-latitude snow and ice accumulation, flow and glaciation on Mars. *Nature, 434*(7031), 346-351. doi: 10.1038/Nature03359.

Holt, J. W., Safaeinili, A., Plaut, J. J., Head, J. W., Phillips, R. J., Seu, R., Kempft, S. D., Choudhary, P., Young, D. A., Putzig, N. E., Biccari, D., & Gim, Y. (2008). Radar Sounding Evidence for Buried Glaciers in the Southern Mid-Latitudes of Mars. *Science, 322*(5905), 1235-1238. doi: 10.1126/science.1164246.

Hubbard, B., Milliken, R. E., Kargel, J. S., Limaye, A., & Souness, C. (2011). Geomorphological characterisation and interpretation of a mid-latitude glacier-like form: Hellas Planitia, Mars. *Icarus, 211*(1), 330-346. doi: 10.1016/j.icarus.2010.10.021.

Imbre, J., & Imbre, K. P. (1986). *Ice Ages: Solving the Mystery*. London: Harvard University Press.

Kargel, J. S. (2004). *Mars: A Warmer, Wetter Planet*. London: Springer-Praxis.

Kargel, J. S., & Strom, R. G. (1992). Ancient glaciation on Mars. *Geology*, *20*(1), 3-7. doi: 10.1130/0091-7613(1992)020<0003:AGOM>2.3.CO;2.

Kargel, J. S., Baker, V. R., Beget, J. E., Lockwood, J. F., Pewe, T. L., Shaw, J. S., & Strom, R. G. (1995). Evidence of Ancient Continental-Glaciation in the Martian Northern Plains. *Journal of Geophysical Research-Planets, 100*(E3), 5351-5368. doi: 10.1029/94je02447.

Laskar, J., Levrard, B., & Mustard, J. F. (2002). Orbital forcing of the martian polar layered deposits. *Nature, 419*(6905), 375-377. doi: 10.1038/Nature01066.

Laskar, J., Correia, A. C. M., Gastineau, M., Joutel, F., Levrard, B., & Robutel, P. (2004). Long term evolution and chaotic diffusion of the insolation quantities of Mars. *Icarus, 170*(2), 343-364. doi: 10.1016/j.icarus.2004.04.005.

Levy, J. S., Head, J. W., & Marchant, D. R. (2007). Lineated valley fill and lobate debris apron stratigraphy in Nilosyrtis Mensae, Mars: Evidence for phases of glacial modification of the dichotomy boundary. *Journal of Geophysical*

Research, 112(E8). doi: 10.1029/2006je002852.

Li, H., Robinson, M. S., & Jurdy, D. M. (2005). Origin of martian northern hemisphere mid-latitude lobate debris aprons. *Icarus*, *176*(2), 382-394. doi: 10.106/j.icarus.2005.02.011.

Lukas, S. (2005). A test of the englacial thrusting hypothesis of 'hummocky' moraine formation: case studies from the northwest Highlands, Scotland. *Boreas*, *34*(3), 287-307. doi: 10.1111/j.1502-3885.2005.tb01102.x.

Madeleine, J. B., Forget, F., Head, J. W., Levrard, B., Montmessin, F., & Millour, E. (2009). Amazonian northern mid-latitude glaciation on Mars: A proposed climate scenario. *Icarus, 203*(2), 390-405. doi: 10.1016/j.icarus.2009.04.037.

Mangold, N. (2003). Geomorphic analysis of lobate debris aprons on Mars at Mars Orbiter Camera scale: Evidence for ice sublimation initiated by fractures. *Journal of Geophysical Research, 108*(E4), 8021. doi: 10.1029/2002je001885.

Marchant, D., & Head, J. W. (2003). Tongue-shaped lobes on Mars: Morphology, Nomenclature, and Relation to Rock Glacier Deposits. Abstract #3091, *Sixth International Conference on Mars, July 20-25, Pasadena, California.*

Marchant, D., & Head, J. W. (2007). Antarctic dry valleys: Microclimate zonation, variable geomorphic processes, and implications for assessing climate change on Mars. *Icaurs, 192*(1), 187-222. doi: 10.1016/j.icarus.2007.06.018.

Mellon, M. T., & Jakosky, B. M. (1995). The distribution and behavior of Martian ground ice during past and present epochs. *Journal of Geophysical Research: Planets, 100*(E6), 11781-11799. doi: 10.1029/95je01027.

Milliken, R. E., Mustard, J. F., & Goldsby, D. L. (2003). Viscous flow features on the surface of Mars: Observations from high-resolution Mars Orbiter Camera (MOC) images. *Journal of Geophysical Research-Planets, 108*(E6). doi: 10.1029/2002je002005.

Mischna, M. A., Richardson, M. I., Wilson, R. J., & McCleese, D. J. (2003). On the orbital forcing of Martian water and CO2 cycles: A general circulation model study with simplified volatile schemes. *Journal of Geophysical Research-Planets, 108*(E6). doi: 10.1029/2003je002051.

Pathare, A. V., Paige, D. A., & Turtle, E. (2005). Viscous relaxation of craters within the martian south polar layered deposits. *Icarus*, *174*, 396-418. doi: 10.1016/j.icarus.2004.10.031.

Plaut, J. J., Safaeinili, A., Holt, J. W., Phillips, R. J., Head, J. W., Seu, R., Putzig, N. E.,

& Frigeri, A. (2009). Radar evidence for ice in lobate debris aprons in the mid-northern latitudes of Mars. *Geophysical Research Letters, 36*(2), L02203. doi: 10.1029/2008gl036379.

Read, P. L., & Lewis, S. R. (2004). *The Martian Climate Revisited: Atmosphere and Environment of a Desert Planet*. London: Springer-Praxis.

Sharp, R. P. (1973). Mars - Fretted and Chaotic Terrains. *Journal of Geophysical Research, 78*(20), 4073-4083. doi: 10.1029/Jb078i020p04073.

Shean, D. E., Head, J. W., & Marchant, D. R. (2005). Origin and evolution of a cold-based tropical mountain glacier on Mars: The Pavonis Mons fan-shaped deposit. *Journal of Geophysical Research: Planets, 110*(E5), E05001. doi: 10.1029/2004je002360.

Sinha, R. K., & Murty, S. V. S. (2013). Evidence of extensive glaciation in Deuteronilus Mensae, Mars: Inferences towards multiple glacial events in the past epochs. *Planetary and Space Science, 86*, 10-32. doi: 10.1016/j.pss.2013.09.002.

Souness, C. (2013). *Distribution and character of mid-latitude glacier-like forms on Mars* (Doctoral dissertation, Aberystwyth University). Retrieved from: http://cadair.aber.ac.uk/dspace/handle/2160/13201.

Souness, C., & Hubbard, B. (2012). Mid-latitude glaciation on Mars. *Progress in Physical Geography, 36*(2), 238-261. doi: 10.1177/0309133312436570.

Souness, C., & Hubbard, B. (2013). An alternative interpretation of late Amazonian ice flow: Protonilus Mensae, Mars. *Icarus, 225*(1), 495-505. doi: 10.1016/j.icarus.2013.03.030.

Souness, C., Hubbard, B., Milliken, R. E., & Quincey, D. (2012). An inventory and population-scale analysis of martian glacier-like forms. *Icarus, 217*(1), 243-255. doi: 10.1016/j.icarus.2011.10.020.

Squyres, S. W. (1978). Martian Fretted Terrain: Flow of Erosional Debris. *Icarus, 34*(3), 600-613. doi: 10.1016/0019-1035(78)90048-9.

Squyres, S. W. (1979). Distribution of Lobate Debris Aprons and Similar Flows on Mars. *Journal of Geophysical Research, 84*, 8087-8096. doi: 10.1029/Jb084ib14p08087.

Squyres, S. W., & Carr, M. H. (1986). Geomorphic Evidence for the Distribution of Ground Ice on Mars. *Science, 231*(4735), 249-252. doi: 10.1126/science.231.4735.249.

Turtle, E. P., Pathare, A. V., Crown, D. A., Chaung, F. C., Hartmann, W. K., Greenham, J. C., & Bueno, N. F. (2003). Modeling the deformation of lobate debris aprons on Mars by creep of ice-rich permafrost. Abstract #8091, *Third International Conference on Mars Polar Science and Exploration, October 13-17, Alberta*.

Zemp, M., Hoelzle, M., & Haeberli, W. (2009). Six decades of glacier mass-balance observations: a review of the worldwide monitoring network. *Annals of Glaciology, 50*(50), 101-111. doi: 10.3189/172756409787769591.

CHAPTER 2

Landscapes of polyphase glaciation: eastern Hellas Planitia, Mars

Imagination will often carry us to worlds that never were.
But without it we go nowhere
Carl Sagan

Preface to manuscript 'Landscapes of polyphase glaciation: eastern Hellas Planitia, Mars'

Introduction and rationale

Although an extensive body of literature documenting and describing Mars' mid-latitude ice masses and their associated landforms exists (e.g. Pierce and Crown, 2003; Milliken et al., 2003; Levy et al., 2010; Head et al., 2010), our collective understanding of how these ice masses form and subsequently evolve is far from complete. For example, although it is now generally accepted that many of Mars' mid-latitude ice masses were once substantially larger than their present day configuration (e.g. Dickson et al., 2008), there is a paucity of investigations that have attempted to reconstruct their former extents and volumes. Furthermore, there is a growing body of literature suggesting that Mars' mid-latitudes may have experienced more than one glacial phase (e.g. Head et al., 2003; Dickson et al., 2008), but again, our understanding of the timing and spatial extent of such phases of glaciation remains poorly constrained – with much of this initial focus being directed on the northern hemisphere (see Section 1.2).

This chapter (published in the *Journal of Maps* [Brough et al., 2016]) describes a geomorphic and structural investigation of a glacial landscape in eastern Hellas Planitia, in a bid to better understand the region's glacial history. It serves to provide a map based example to key concepts that are further developed in later chapters of the thesis – for example, the current (Chapter 3) and former (Chapter 4) extent of mid-latitude ice masses – and to provide further insight into the knowledge gaps discussed above.

Eastern Hellas Planitia was targeted as the study area for a number of reasons: (i) it is located in Mars' southern hemisphere; (ii) climatic simulations have revealed the region to be a likely source for snow accumulation during periods of high (>45^{o}) obliquity (Forget et al., 2006); (iii) it is known to contain a high population of viscous flow features (VFFs), including lobate debris aprons (LDAs [e.g. Pierce and Crown, 2003]) and glacier-like forms (GLFs [e.g. Souness et al., 2012]); and (iv) there is strong morphological and geophysical evidence for these VFFs to be glacial in origin (e.g. Appendix A; Head et al., 2005; Holt et al., 2008). The specific study site (centred on

~103°E, 40.6°S) was chosen after an initial investigation of the massif revealed what appeared to be a discontinuity between the LDA and the higher altitude material (including a well-developed GLF), thus, affording an opportunity to test the hypothesis that multiple phases of glaciation may have occurred in eastern Hellas Planitia (e.g. contributing to Objective [1] of the thesis). The detailed geomorphic and structural mapping would also provide a platform to investigate the fundamental glaciological behaviour (e.g. extent; motion) of the VFFs in question (e.g. contributing to Objective [2] of the thesis). The remainder of this preface discusses the methods that were adopted during the study.

Geomorphic and structural mapping

There is an extensive body of terrestrial glaciological literature concerned with reconstructing glacial environments based on their landforms and structural assemblage (see Hubbard and Glasser, 2005). By compiling evidence left on the landscape with observations from modern glaciers, the extent and dynamics of both former (glaciated) and modern (glacierised) glacial environments can be reconstructed (e.g. Kleman et al., 1997; Evans and Twigg, 2002; Greeenwood and Clark, 2009). Furthermore, these analyses may provide an insight into how such ice masses have evolved over time and as to processes occurring within the ice mass. For example, by analysing the structure of a glacier it is possible to make inferences about the glacier's flow regime (e.g. Hambrey and Lawson, 2000; Goodsell et al., 2005). Given the useful insights that have been obtained from these studies on Earth, numerous authors have applied the same principles in a bid to describe glacial landscapes and landforms on Mars (e.g. Pierce and Crown, 2003; Milliken et al., 2003; Baker et al., 2010; Head et al., 2010; Levy et al., 2010; Souness and Hubbard, 2013). This study incorporated knowledge generated from both terrestrial and martian cryospheric communities in its analysis.

Geomorphic and structural features were mapped from manual inspection of satellite imagery within Geographic Information System (GIS) software. Mapping was conducted from a 6 metre per pixel orthorectified Context Camera (CTX) image, as this provided the highest-resolution continuous coverage of the study area. This CTX

coverage was supplemented with High Resolution Imaging Science Experiment (HiRISE) images, with spatial resolution of up to ~0.25 m, where available. Each geomorphic unit and structure was subsequently described within the text and explanations of their significance discussed. Whilst this method for glaciological investigation on Mars has been extensively used (e.g. Pierce and Crown, 2003; Milliken et al., 2003; Baker et al., 2010; Head et al., 2010; Levy et al., 2010; Souness and Hubbard, 2013), it should be noted that, as with all remote sensing projects, for a feature to be identified/mapped it must be greater than the observable resolution of the imaging sensor. Therefore, these types of analysis overlook features measuring less than this observable resolution. Naturally, as the coverage of higher spatial resolution imagery (e.g. HiRISE) increases, a more detailed assessment of surface landforms and structures may be sought. Notwithstanding this spatial dependence, major structures are often greater than the spatial resolution of the coarser CTX imagery (6 m), and therefore clearly identifiable for mapping.

Landscapes of polyphase glaciation: eastern Hellas Planitia, Mars

Stephen BROUGH[a], Bryn HUBBARD[a], Colin SOUNESS[a], Peter M. GRINDROD[b,c] and Joel DAVIS[b,d]

[a]*Department of Geography and Earth Sciences, Aberystwyth University, Aberystwyth, UK*

[b]*Centre for Planetary Sciences, University College London/Birkbeck, London, UK*

[c]*Department of Earth and Planetary Sciences, Birkbeck, University of London, London, UK*

[d]*Department of Earth Sciences, University College London, London, UK*

Link to published article

This is a manuscript of an article published by Taylor & Francis Group in *Journal of Maps* on 04/06/2015, available online: http://dx.doi.org/10.1080/17445647.2015.1047907.

Citation for published paper

Brough, S., Hubbard, B., Souness, C., Grindrod, P. M., & Davis, J. (2016). Landscapes of polyphase glaciation: eastern Hellas Planitia, Mars. *Journal of Maps*, *12*(3), 530-542. doi: 10.1080/17445647.2015.1047907.

Keywords: Mars; ice; glaciation; lobate debris apron; glacier-like form; mid-latitude; climate change

Abstract: The mid-latitudes of Mars host numerous ice-related landforms that bear many similarities to terrestrial ice masses. This collection of landforms, termed viscous flow features (VFFs), is composed primarily of H_2O ice and shows evidence of viscous deformation. Recent work has hypothesised that VFFs are the diminishing remains of once larger ice masses, formed during one or more previous ice ages, and the landscape therefore records evidence of polyphase glaciation. However, debate persists concerning the former extent and volume of ice, and style of former glaciations. The accompanying map (1:100,000 scale) presents a geomorphic and structural assessment of a glacial landscape in eastern Hellas Planitia, Mars. Here we present a description of the features identified, comprising four geomorphic units (plains, lobate debris apron, degraded glacial material, and glacier-like form) and 16 structures (craters, moraine-like ridges, flow unit boundaries, arcuate transvers structures, longitudinal surface structures, ring-mold craters, terraces, medial-moraine like ridges, raised textured areas, flow-parallel and flow-transverse lineations, crevasses and crevasse traces, and ridge clusters).

2.1. Introduction

The mid-latitudes of Mars host numerous ice-related landforms with many similarities to terrestrial ice masses (e.g. Arfstrom and Hartmann, 2005; Head et al., 2005; Baker et al., 2010; Hubbard et al., 2011; Souness et al., 2012; Sinha and Murty, 2013). These landforms are composed primarily of H_2O ice, have surface morphologies consistent with viscous deformation and have consequently become known as viscous flow features, or VFFs (Milliken et al., 2003; Holt et al., 2008; Plaut et al., 2009). Recent advances in orbital and climatic modelling have supported earlier arguments that VFFs are related to geologically recent ice ages. These ice ages are proposed to occur as a consequence of increased solar radiation forcing water stored in the polar caps of Mars to be transported towards lower latitudes, under periods of high ($>30^{o}$) obliquity (Touma and Wisdom, 1993; Head et al., 2003; Laskar et al., 2004; Forget et al., 2006).

Despite an increase in research into such non-polar ice deposits on Mars during recent decades, several fundamental planetary and glaciological issues remain, of which our collective understanding is still only in its infancy (see Souness and Hubbard, 2012;

Hubbard et al., 2014). Of particular prominence is the origin and subsequent evolution of mid-latitude VFFs (e.g. Pierce and Crown, 2003; Fastook et al., 2011; Parsons et al., 2011; Souness et al., 2012; Souness and Hubbard, 2013).

Such VFFs comprise four distinct subtypes (see review of Souness and Hubbard, 2012): (i) glacier-like forms, or GLFs (Hartmann, 2003; Hubbard et al., 2011); (ii) lobate debris aprons, or LDAs (Squyres, 1978; Pierce and Crown, 2003); (iii) lineated valley fill, or LVF (Squyres, 1978); and (iv) concentric crater fill, or CCF (Levy et al., 2010). However, VFFs commonly coalesce and interact to form what Head et al. (2010) described as Mars' integrated glacial landsystem (Figure 2.1). Following this model, GLFs represent the lowest order component of this glacial landsystem, generally forming in small valleys or cirque-like alcoves. Often multiple GLFs forming adjacent escarpments converge to form broad, rampart-like LDAs. In turn, LDAs may converge or coalesce to form an often complex and contorted LVF.

At present there is a growing body of evidence suggesting that mid-latitude ice deposits are the remnants of a once far larger ice mass (e.g. Dickson et al., 2008, 2010; Sinha and Murty, 2013; Hubbard et al., 2014) and the widespread identification of glacial features and landforms has led to suggestions that continental scale glaciation may have occurred on Mars (e.g. Kargel et al., 1995; Fastook et al., 2014). Reconstructing glacial environments based on their landforms and structural assemblage is a powerful concept applied in terrestrial glaciology (see Hubbard and Glasser, 2005). Through utilising evidence left on the landscape with observations from modern glaciers, we can reconstruct the extent and dynamics of both former (glaciated) and modern (glacierised) glacial environments (e.g. Kleman et al., 1997; Evans and Twigg, 2002; Greeenwood and Clark, 2009).

The map described herein documents the geomorphic units and structural features associated with a glacial landscape in eastern Hellas Planitia, Mars. Here, we present an overview of the data and methods used, and provide a description of the units recorded on the main map (which can be found in Supplementary Material Ch. 2).

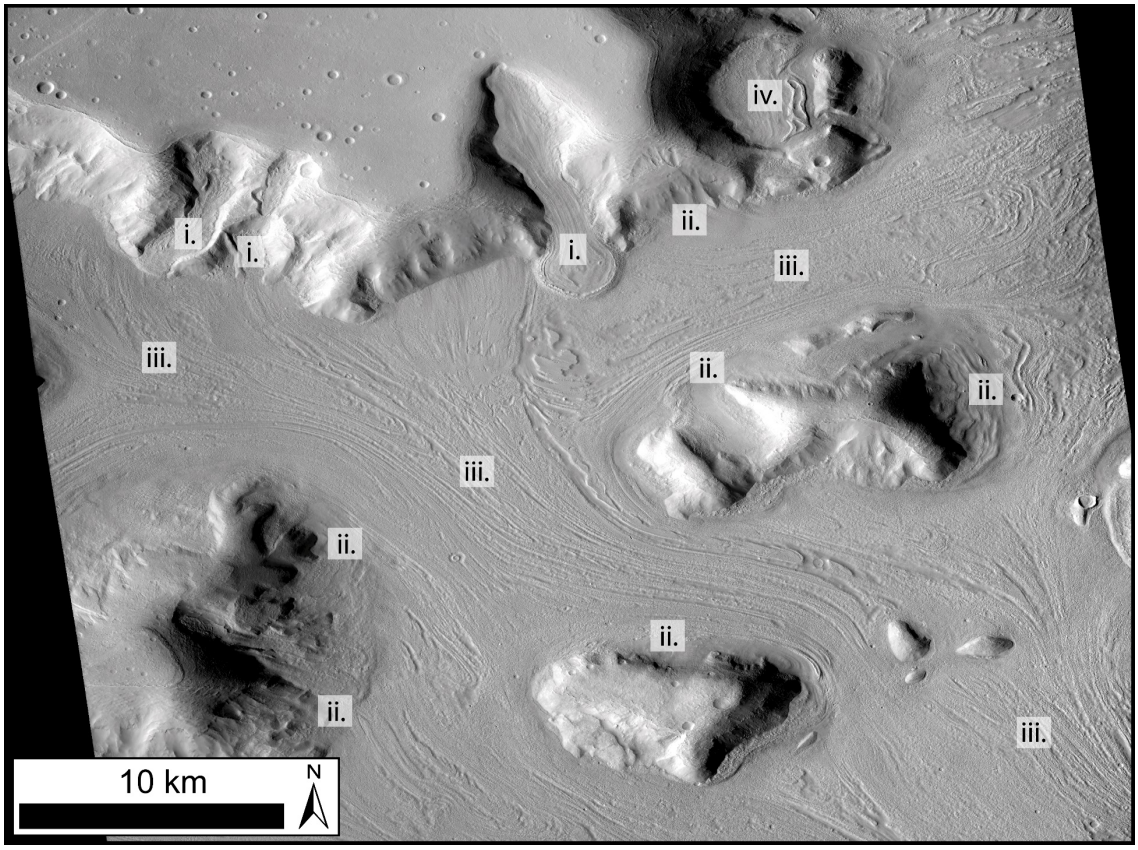

Figure 2.1: *Example of an integrated glacial landsystem as described by Head et al., 2010. Each component of the landsystem is labelled as follows: (i) GLFs; (ii) LDAs; (iii) LVFs; and (iv) CCF. The valley floor shows a complex, heavily distorted surface, typical of the integrated glacial landsystem. This scene is a subset of CTX image G02_018857_2226_XI_42N309W (centred 42.62^{o} N, 50.51^{o} E).*

2.2. Study site and brief review of previous work

2.2.1. Study site

Located to the east of Hellas Planitia, one of the largest impact structures on Mars, Reull Vallis is a morphologically complex outflow channel system comprising Noachian (~4.65 – 3.7 Ga BP), Hesperian (~3.7 – 3.0 Ga BP), and Amazonian (~3.0 Ga BP – present) materials (Tanaka and Leonard, 1995; Mest and Crown, 2001). Reull Vallis has an abundant population of VFFs (e.g. Souness et al., 2012), in particular LDAs, of which over 90 have been identified here (Mest and Crown, 2001; Pierce and Crown, 2003). Herein, we map a particularly well-developed LDA and associated

landforms which surround an isolated highland massif (Figure 2.2). The massif sits just to the north of the Reull Vallis outflow channel and is centred on ~103° E, 40.6° S. The study site covers an area of 2647 km^2 to the west of the massif and topography ranges between ~2700 and -650 m (relative to Mars datum). The LDA extends radially up to ~26 km from the base of the massif and has a maximum and minimum elevation of ~40 and -610 m, respectively, giving an overall elevation difference of ~650 m. Although not investigated, the eastern portion of the massif also contains several ice-related landforms (Figure 2.2c). The appearance of these landforms share several similarities with features described herein, and elsewhere on Mars (e.g. Whalley and Azizi, 2003), and likely reflect a wider cold climate landsystem in Reull Vallis.

2.2.2. Previous work

Eastern Hellas Planitia is a key region in martian climatic and glaciological studies. Climatic simulations have revealed the region to have experienced snow accumulation when Mars' obliquity exceeded 45° (Forget et al., 2006). Radar data from Mars Reconnaissance Orbiters' (MRO) Shallow Radar (SHARAD) have augmented these findings by detecting massive H_2O ice deposits, buried beneath thin (<10 m) debris layers surrounding LDAs near Reull Vallis (Holt et al., 2008). Furthermore, an analysis of craters and stratigraphic relationships of LDAs in the Reull Vallis region indicates that LDAs are Lower Amazonian in age, and are the youngest units in the region (Mest and Crown, 2001; Mest and Crown, 2014).

Investigations using high-resolution imagery have identified several lines of evidence for glacier-like flow in VFFs within eastern Hellas Planitia. Using Mars Express' High Resolution Stereo Camera images, Head et al. (2005) described numerous surface textures, including sinuous ridges, irregular depressions and flowlines on the surface of an LDA and within crater deposits. These were hypothesised as being indicative of ice-rich, glacier-like viscous flow. Hubbard et al. (2014) recently identified surface fracturing on a GLF in eastern Hellas Planitia. These authors argued that the location and geometry of the surface features are comparable to crevasses common on Earth's glaciers, and as such, are a direct indication of ice flow and brittle deformation.

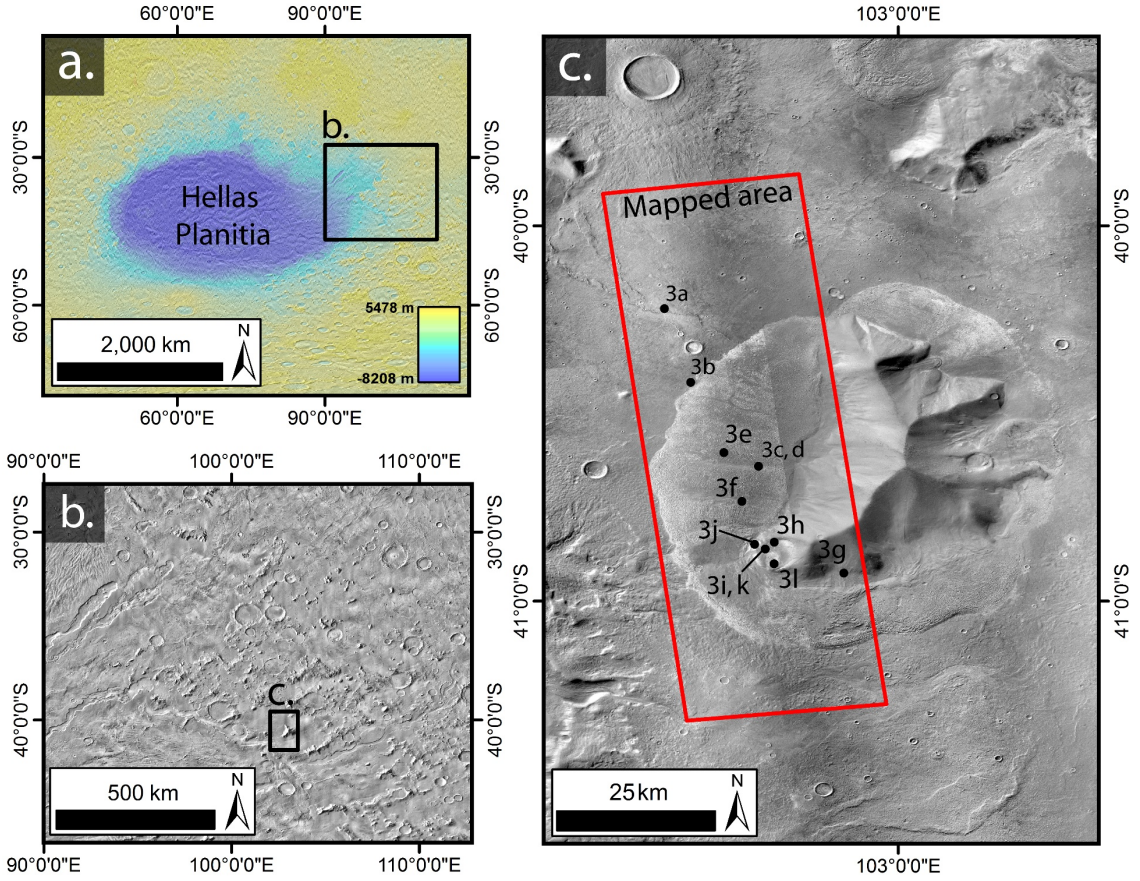

Figure 2.2: *Location and expansion of massif studied herein. (a) Global context indicting massifs location to the east of Hellas impact basin, illustrated as a MOLA elevation transparency overlain on a THEMIS-IR day mosaic. (b) Regional context of the Reull Vallis region as seen in THEMIS-IR day mosaic. The region is characterised by large outflow channel systems and abundant montane outcrops. Reull Vallis runs directly below the massif and portions of the Dao, Niger, and Harmakhis Vallis are also identifiable along the western part of the image (orientated NE-SW). (c) CTX mosaic of massif investigated. The LDA can be clearly seen encircling the massif. The area mapped in this study is identified by the red box and represents the DTM extent (section 2.3.1). Black dots indicate central location of features identified in Figure 2.3. Mosaic comprised from subset of CTX images D13_03226_1393_XI_40S256W; G16_024552_1394_XI_40S257W; D10_031066_1393_XI_40S257W; and P16_007397_1382_XN_41S257W.*

2.3. Data, methods and software

2.3.1. Image sources

We use both Context Camera (CTX [Malin et al., 2007]) and High Resolution Imaging Science Experiment (HiRISE [McEwen et al., 2007]) imagery, acquired from the MRO satellite (Table 2.1). CTX images have a spatial resolution of ~6 m per pixel and cover an area up to 30 x 160 km (Zurek and Smrekar, 2007). CTX imagery was supplemented by HiRISE imagery where available. HiRISE images have an unparalleled spatial resolution of up to ~0.25 m per pixel and cover an area up to 6 x 12 km (Zurek and Smrekar, 2007). For global and regional context, we also use the Mars Orbiter Laser Altimeter (MOLA [Smith et al., 1999]) gridded digital terrain model (DTM), with a typical resolution of 460 m per pixel, and the global mosaic of Thermal Emission Imaging System (THEMIS [Edwards et al., 2011]) daytime infra-red images, with a typical resolution of 100 m per pixel. All data used in this study are available through the NASA Planetary Data System.

Table 2.1: *List of imagery used in mapping.*

Instrument	Scene ID	Date (dd/mm/yyyy)	Resolution (m)	Scene Centre	
				Lat. (°)	Lon. (°)
CTX	D15_032978_1391_XN_40S257W	09/08/2013	6	-40.92	102.58
CTX	D16_033400_1391_XN_40S257W	11/09/2013	6	-40.94	102.59
HiRISE	PSP_004272_1390_RED	25/06/2007	0.25	-40.50	102.45
HiRISE	ESP_011669_1390_RED	21/01/2009	0.50	-40.88	102.50
HiRISE	ESP_019462_1390_RED	20/09/2010	0.25	-40.76	102.37
HiRISE	ESP_033400_1390_RED	11/11/2013	0.25	-40.84	102.62
HiRISE	ESP_033901_1390_RED	20/10/2013	0.25	-40.86	102.74
HiRISE	ESP_035391_1390_RED	13/02/2014	0.50	-40.49	102.56

We created a 20 m per pixel DTM using standard techniques with Integrated Software for Imagers and Spectrometers (ISIS) and SOCET SET software packages (Kirk et al., 2008) and the CTX stereo image pair D15_032978_1391_XN_40S257W and D16_033400_1391_XN_40S257W. Using previous methods (Kirk et al., 2003; 2008; Okubo, 2010), we estimate the vertical precision of our CTX stereo DTM to be 3.5 m. We then used this DTM to produce a 6 m per pixel orthorectified image, which was the main data product used in this study.

2.3.2. Surface mapping

All mapping and analysis was carried out in ESRI's ArcMap 10.1 Geographic Information System (GIS) software. Mapping was conducted through manual inspection of the imagery. Geomorphic unit and structural classifications were guided by both terrestrial and martian cryospheric literature (e.g. Goodsell et al., 2005; Hubbard and Glasser, 2005; Baker et al., 2010; Souness and Hubbard, 2013). Standard image enhancement procedures (e.g. histogram equalisation and standard deviation) were applied on an image-by-image basis to enhance the appearance and maximise the contrast between features during digitisation.

Features mapped include an LDA, a GLF, degraded glacial material, crevasses, moraine-like ridges, lineations, terraces, craters, and flow units. Digitisation was carried out at two main scales: (i) 1:50,000 was used for large scale features, including LDA and plains and (ii) 1:25,000 was used for less well-resolved features such as crevasses, lineations, and moraine-like ridges. Features which varied in size, such as craters and terraces, were mapped at scales appropriate to their characteristics.

2.4. Description of geomorphic units and structural features

This section describes the geomorphic units and their associated structural features progressing from the distal to proximal end of the glacial system as follows: (i) plains; (ii) LDA; (iii) degraded glacial material; and (iv) GLF. To avoid repetition, although

presented in all relevant geomorphic units, a structure will only be described in the first unit where it occurs in the text.

2.4.1. Plains

Plains form the distal part of the glacial landscape, representing an area of ice-free or ice-poor terrain that is texturally distinct from the surrounding ice-related surfaces. The distal plains are characterised by a heavily cratered, but otherwise relatively smooth surface. There is no evidence of surface flow within this unit. Identifying such areas of terrain that appear unaffected by ice flow is important when looking at glacial reconstruction, as it provides a clear outer boundary for active glaciation. Structures observed within the plains unit are: (i) craters and (ii) sinuous ridges.

2.4.1.1. Craters

Craters are identified as surface depressions caused by the impact of a hypervelocity object – usually a meteoroid (Figure 2.3a). They are typically bowl-shaped, and quasi-circular in planform, but their appearance can change over time. Deformation within the substrate of the material can cause the craters to distort and therefore provide an indication of local strain (e.g. Sinha and Murty, 2013). The appearance or sharpness of craters may also change over time, as surface processes degrade their surface terrains and edges (e.g. Baker et al., 2010). Craters form an essential part of planetary investigation, as they provide a means by which surfaces may be dated (e.g. Hartmann and Neukum, 2001).

2.4.1.2. Sinuous ridges

Sinuous ridges are identified as ridges that display both positive raised relief from their surroundings and a sinuous morphology (Figure 2.3a). Ridges may be branched and connected to each other, or occur in isolation. They often interact with craters where

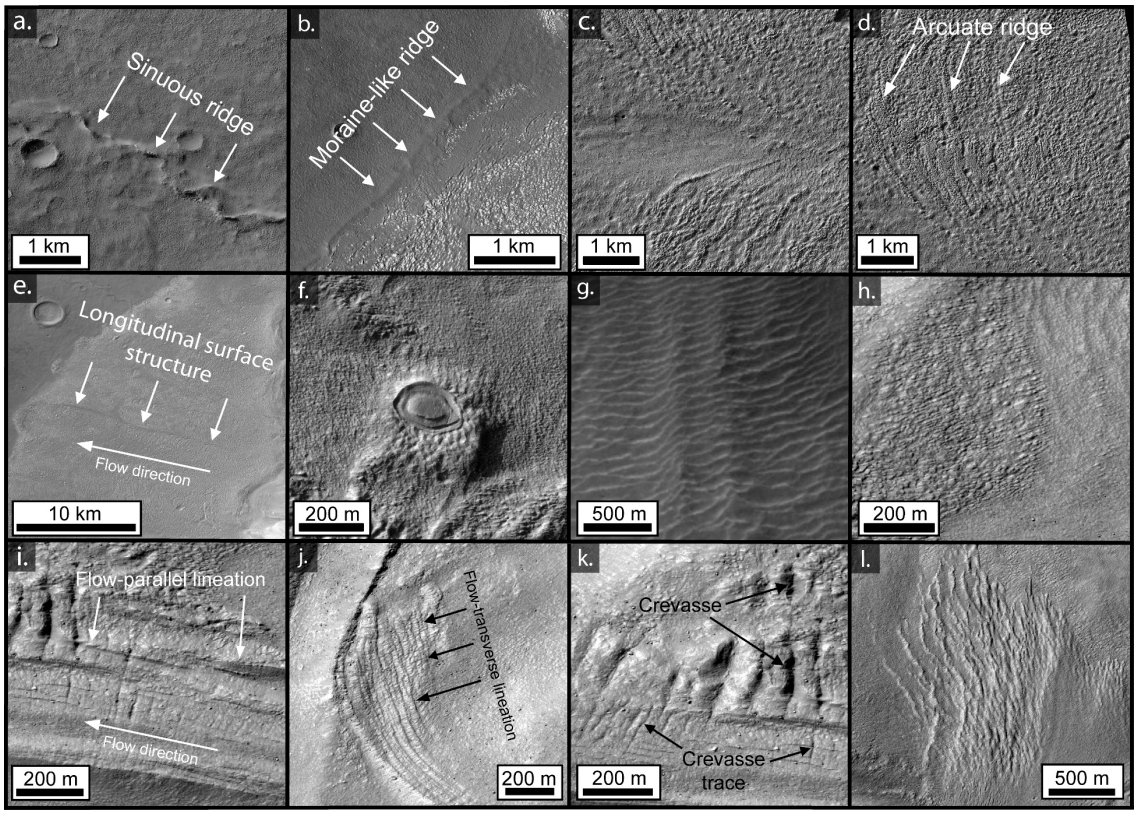

Figure 2.3: *Feature identification in CTX and HiRISE imagery, as discussed in the main text. Images orientated north up. (a) Craters and sinuous ridge. (b) Moraine-like ridge surrounding LDA. (c) Flow unit boundary - arcuate structures can be seen deforming along the flow unit boundary in the centre of the image. (d) Arcuate transverse ridges. (e) Longitudinal surface structure. (f) Well-formed ring-mold crater. (g) Terraces and medial moraine-like ridges – terraces appear to cut across the two medial moraine-like ridges, which run longitudinally from the top centre to bottom centre of the image. (h) Raised textured area – visible on the western and central portion of the image is a lumpy, raised surface texture that clearly contrasts the smoother terrain to the east. (i) Flow-parallel lineations. (j) Flow-transverse lineations. (k) Crevasses (open fracture) and crevasse traces (closed fracture). (l) ridge clusters. Images used: a, c, d, f -ESP_035391_1390_RED; b - PSP_004272_1390_RED; e, g - D15_032978_1391_XN_40S257W orthorectified image (see Section 3.1); and h, i, j, k, l -ESP_033400_1390_RED.*

they appear to emanate away from, or are dissected by them. These ridges are predominantly located in the northern part of the map. However, one particular prominent sinuous ridge appears to be buried under the upper northern part of the LDA, before emanating into the foreground in a northwest direction. It is possible that these ridges are subglacial in origin (i.e. similar to eskers on Earth); however, their morphology is more consistent with 'wrinkle' and degraded ridges in the Reull Valles region, the origin of which are interpreted to be fluvial or volcanic (Mest and Crown, 2001; Mest and Crown, 2014).

2.4.2. Lobate debris apron

The surface morphology and convexity described above have previously been used to infer that LDAs show viscous flow and that the mechanism by which flow is achieved is a result of ice deformation (e.g. Squyres, 1978; Colaprete and Jakosky, 1998; Pierce and Crown, 2003; Head et al., 2005; Holt et al., 2008; Grindrod and Fawcett, 2011). Structures observed within the LDA unit are: (i) moraine-like ridges; (ii) flow unit boundaries; (iii) arcuate transverse structures; (iv) longitudinal surface structures; (v) ring-mold craters; and (vi) craters (Section 2.4.1.1).

2.4.2.1. Moraine-like ridges

Moraine-like ridges are long (10's km), often narrow (10^{-2} – 10^{-1} km), ridges that are raised above their surroundings (Figure 2.3b). Moraine-like ridges run parallel to the terminus of VFFs, commonly in an arcuate manner and are similar to terminal or ice-marginal moraines associated with terrestrial glaciers (Arfstrom and Hartmann, 2005). Such moraines (including on Mars) mark the former terminal position of an ice mass and are, therefore, indicators of ice recession, and can also indicate a former boundary between a previously glaciated and currently glacierised terrain. On Earth, moraines form an essential component of glacial reconstruction in both glacierised (e.g. Evans and Twigg, 2002) and glaciated environments (e.g. Greenwood and Clark, 2009).

2.4.2.2. Flow unit boundaries

A flow unit boundary is identified as a boundary between two flow units that have distinctive velocity fields with an associated discontinuity in orientation of deformation-related features (Figure 2.3c). Structures may also appear smeared along the junction (Goodsell et al., 2005).

2.4.2.3. Arcuate transverse structures

Arcuate transverse structures are identified as linear structures with positive or negative relief that are arranged roughly transverse to the apparent flow direction. These linear structures can be followed down the LDA, where they become highly arcuate or deformed (Figure 2.3d). Arcuate transverse structures can provide an indication of local flow rates and the distribution of stresses within the flowing material.

2.4.2.4. Longitudinal surface structures

Longitudinal structures are identified as extended linear features (up to ~20 km long) that are arranged roughly parallel to the apparent flow direction (Figure 2.3e). These structures are similar in appearance and persistence to longitudinal foliation identified on terrestrial glaciers. However, there is an ongoing debate as to the terminology, origin, and significance of these features (see Glasser and Gudmundsson, 2012). This debate notwithstanding, both flow-transverse (Section 2.4.2.3) and flow-parallel structures can be used to elucidate local flow direction, deformation and strain history (e.g. Baker et al., 2010; Souness and Hubbard, 2013).

2.4.2.5. Ring-mold craters

In contrast to (standard) craters (Section 2.4.1.1), ring-mold craters are identified as an almost rimless depression with an annular moat enclosing an inner circular plateau of varying morphology (Figure 2.3f [e.g. Kress and Head, 2008]). The morphology of

ring-mold craters is consistent with previous laboratory experiments of impact craters forming in relatively pure ice (e.g. Kato et al., 1995) and shows a distinctly different morphology from craters formed in ice-poor surfaces. This distinct difference in morphology between ring-mold and bowl-shaped craters has led to the interpretation that ring-mold craters are formed in an ice-rich substrate (Kress and Head, 2008). Furthermore, ring-mold craters appear to be exclusively located within VFFs and therefore have the potential to be a diagnostic indicator for the presence of subsurface ice (Kress and Head, 2008).

2.4.3. Degraded glacial material

Occupying the base and encroaching up the slopes of the massif is an area of homogeneous terrain characterised by a texturally smoothed surface, abundant terrace structures, and a concave down-slope profile. In contrast to the plains and LDA, there is little evidence of surface cratering on this homogeneous terrain. Several small alcoves appear to be cut into the massif, but two larger alcoves (one located towards the centre of the massif and one on the southern face) are associated with structures, including raised textured areas and moraine-like ridges, similar to the adjacent GLF (Section 2.4.4). This overall appearance suggests a deflated or degraded terrain, possibly formed during the region's current state of periglaciation. Based on structural evidence within the alcoves, it may also be possible that GLFs once occupied these localities, and therefore localised glaciation may have previously occurred in this unit. Structures observed within this degraded glacial material unit are: (i) terraces; (ii) raised textured areas; (iii) medial moraine-like ridges; (iv) moraine-like ridges (Section 2.4.2.1); and (v) craters (Section 2.4.1.1).

2.4.3.1. Terraces

Terraces are identified as an interlinked network of step-like ridges that form sub-perpendicular to slope (Figure 2.3g). Their length, size and coherence appear highly variable, which correspondingly produces a variety of patterns. Terraces cut across

other structures (such as moraine- and medial moraine-like ridges), suggesting that these features represent a later age of formation relative to the structure across which they cut.

2.4.3.2. Medial moraine-like ridges

Medial moraine-like ridges, in contrast to moraine-like ridges (section 2.4.2.1), persist longitudinally within an ice mass (Figure 2.3g), rather than forming an arcuate structure demarking a limit of glaciation. Medial moraines are important structures on glaciers on Earth as they can be used to identify flow pathways and the deformation of debris within a glacier (e.g. Hambrey et al., 1999). They are also often flow unit boundaries (section 2.4.2.2).

2.4.3.3. Raised textured areas

Raised textured areas are identified as areas showing a distinct lumpy surface texture that is raised above the surrounding mass (Figure 2.3h). The occurrence of a markedly different surface texture from adjacent areas suggests that there is a local change in mechanical process or material composition.

2.4.4. Glacier-like form (GLF)

A well-pronounced GLF with clearly distinguishable outlines occupies a small, cirque-like alcove on the southwestern flank of the massif. The GLF has a discernible head and terminus, the latter of which appears to have breached a cirque lip to the northwest of the feature. Running parallel to the terminus of the breached snout is an extensive moraine-like ridge (Section 2.4.2.1), enclosing the GLF. Within the body of the GLF are several distinct structures indicative of flow and transportation of mass down-slope, including fractures and surface lineations (Hubbard et al., 2014). Two large textured areas are identifiable on the lower surface of the GLF, the southernmost of which is associated with a cluster of ridges. Like the degraded glacial material (Section 2.4.3),

the GLF surface has a distinct lack of craters. The GLF appears to reflect a currently glacierised environment, indicative of local ice accumulation and subsequent flow. Structures observed in the GLF unit are: (i) flow-parallel and flow-transverse lineations; (ii) crevasses and crevasse traces; (iii) ridge clusters; (iv) moraine-like ridges (Section 2.4.2.1); (v) raised textured areas (Section 2.4.3.3); (vi) craters (Section 2.4.1.1); and (vii) ring-mold craters (Section 2.4.2.5).

2.4.4.1. Flow-parallel and flow-transverse lineations

Flow-parallel and flow-transverse lineations show many similarities to the longitudinal and arcuate structures found in the LDA unit (Figure 3i – j [Section 2.4.2]). However, both flow-parallel and flow-transverse lineations only show positive relief and their length is an order of magnitude smaller (up to ~1 km long). Like longitudinal and arcuate surface structures, flow-parallel and flow-traverse lineations can be used to elucidate local flow direction, deformation, and strain history (e.g. Baker et al., 2010; Souness and Hubbard, 2013).

2.4.4.2. Crevasses and crevasse traces

Crevasses are identified as open fractures on the GLF surface which may cut across other structures (Figure 2.3k). Crevassing occurs where the tensile strain rate of ice exceeds a temperature-dependant threshold (Vaughan, 1993). Crevasses are correspondingly orientated perpendicular to the direction of maximum extensional strain (Hambrey and Lawson, 2000). Crevasse traces are identified by distinct, often dark, lines in areas of crevassing that do not have a visible opening or fracture. Crevasse traces are former crevasses, which have subsequently closed, likely due to the crevasse passing through a compressive flow regime (Figure 2.3k [Hambrey and Lawson, 2000]).

2.4.4.3. Ridge clusters

Ridge clusters are a series of sub-parallel, nested, elongate ridges (Figure 2.3l). Ridges are clustered towards the southwest of the GLF where they merge with the raised textured area and are difficult to identify individually. However, individual structures are easily identifiable to the north of the feature, where ridges become well defined.

2.5. Conclusions

This paper presents a detailed geomorphic and structural map of glacial landforms in eastern Hellas Planitia, Mars. Initial evidence suggests that the region has undergone at least two, possibly three, phases of glaciation, with a wider, more extensive glacial period being recorded in the LDA, and a secondary, more localised glaciation recorded in the GLF. The work presented here is part of a wider ongoing project addressing the extent and dynamics of mid-latitude VFFs on Mars (e.g. Hubbard et al., 2014). It also provides further evidence, and extends the spatial scale, for the hypothesis that Mars has experienced multiple phases of glaciation.

Software

Image pre-processing was carried out in the freely available ISIS provided by the United States Geological Survey. Stereo DTM production was carried out in the commercial software package SOCET SET ® provided by BAE Systems. Image processing and mapping was carried out using ESRI ArcMap 10.1 GIS. Figures and final map were produced in ESRI ArcMap 10.1. Figures were subsequently exported to Adobe Illustrator CS for annotation.

Acknowledgements

The authors would like to thank Hannes Bernhardt, John Abrahams and Stephan Harrison for reviewing an earlier version of this manuscript and accompanying map, and both Mike Smith and Monica Pondrelli for editing. The stereo DTM processing was carried out at the UK NASA RPIF at University College London. SB is funded by an Aberystwyth University Doctoral Career Development Scholarship. PMG is funded by the UK Space Agency (Aurora Fellowship grant ST/L00254X/1).

References

Arfstrom, J., & Hartmann, W. K. (2005). Martian flow features, moraine-like ridges, and gullies: Terrestrial analogs and interrelationships. *Icarus, 174*(2), 321-335. doi: 10.1016/j.icarus.2004.05.026.

Baker, D. M. H., Head, J. W., & Marchant, D. R. (2010). Flow patterns of lobate debris aprons and lineated valley fill north of Ismeniae Fossae, Mars: Evidence for extensive mid-latitude glaciation in the Late Amazonian. *Icarus, 207*(1), 186-209. doi: 10.1016/j.icarus.2009.11.017.

Colaprete, A., & Jakosky, B. M. (1998). Ice flow and rock glaciers on Mars. *Journal of Geophysical Research-Planets, 103*(E3), 5897-5909. doi: 10.1029/97je03371.

Dickson, J. L., Head, J. W., & Marchant, D. R. (2008). Late Amazonian glaciation at the dichotomy boundary on Mars: Evidence for glacial thickness maxima and multiple glacial phases. *Geology, 36*(5), 411-414. doi: 10.1130/g24382a.1.

Dickson, J. L., Head, J. W., & Marchant, D. R. (2010). Kilometer-thick ice accumulation and glaciation in the northern mid-latitudes of Mars: Evidence for crater-filling events in the Late Amazonian at the Phlegra Montes. *Earth and Planetary Science Letters, 294*(3-4), 332-342. doi: 10.1016/j.epsl.2009.08.031.

Edwards, C. S., Nowicki, K. J., Christensen, P. R., Hill, J., Gorelick, N., & Murray, K. (2011). Mosaicking of global planetary image datasets: 1. Techniques and data processing for Thermal Emission Imaging System (THEMIS) multi-spectral data. *Journal of Geophysical Research: Planets, 116*(E10), E10008. doi: 10.1029/2010je003755.

Evans, D. J. A., & Twigg, D. R. (2002). The active temperate glacial landsystem: a model based on Breioamerkurjokull and Fjallsjokull, Iceland. *Quaternary Science Reviews, 21*(20-22), 2143-2177. doi: 10.1016/S0277-3791(02)00019-7.

Fastook, J. L., Head, J. W., & Marchant, D. R. (2014). Formation of lobate debris aprons on Mars: Assessment of regional ice sheet collapse and debris-cover armouring. *Icarus, 228*, 54-63. doi: 10.1016/j.icarus.2013.09.025.

Fastook, J. L., Head, J. W., Forget, F., Madeleine, J.-B., & Marchant, D. R. (2011). Evidence for Amazonian northern mid-latitude regional glacial landsystems on Mars: Glacial flow models using GCM-driven climate results and comparisons to geological observations. *Icarus, 216*(1), 23-39. doi: 10.1016/j.icarus.2011.07.018.

Forget, F., Haberle, R. M., Montmessin, F., Levrard, B., & Head, J. W. (2006). Formation of glaciers on Mars by atmospheric precipitation at high obliquity. *Science, 311*(5759), 368-371. doi: 10.1126/science.1120335.

Glasser, N. F., & Gudmundsson, G. H. (2012). Longitudinal surface structures (flowstripes) on Antarctic glaciers. *The Cryosphere, 6*(2), 383-391. doi: 10.5194/tc-6-383-2012.

Goodsell, B., Hambrey, M. J., Glasser, N. F., Nienow, P., & Mair, D. (2005). The structural glaciology of a temperate valley glacier: Haut Glacier d'Arolla, Valais, Switzerland. *Arctic Antarctic and Alpine Research, 37*(2), 218-232. doi:10.2307/4139080.

Greenwood, S. L., & Clark, C. D. (2009). Reconstructing the last Irish Ice Sheet 1: changing flow geometries and ice flow dynamics deciphered from the glacial landform record. *Quaternary Science Reviews, 28*(27-28), 3085-3100. doi: 10.1016/j.quascirev.2009.09.008.

Grindrod, P. M., & Fawcett, S. A. (2011) Possible climate-related signals in high resolution topography of lobate debris aprons in Tempe Terra, Mars. Geophysical Research Letters, 38, L19201, doi: 10.1029/2011GL049295.

Hambrey, M. J., Bennett, M. R., Dowdeswell, J. A., Glasser, N. F., & Huddart, D. (1999). Debris entrainment and transfer in polythermal valley glaciers. *Journal of Glaciology, 45*(149), 69-86. doi: 10.1017/S0022143000003051.

Hambrey, M. J., & Lawson, W. (2000). Structural styles and deformation fields in glaciers: a review. *Geological Society, London, Special Publications, 176*(1), 59-83. doi: 10.1144/gsl.sp.2000.176.01.06.

Hartmann, W. (2003). Martian hillside gullies and Icelandic analogs. *Icarus, 162*(2), 259-277. doi: 10.1016/s0019-1035(02)00065-9.

Hartmann, W. K., & Neukum, G. (2001). Cratering chronology and the evolution of Mars. *Space Science Reviews, 96*(1-4), 165-194. doi: 10.1023/A:1011945222010.

Head, J. W., Marchant, D. R., Dickson, J. L., Kress, A. M., & Baker, D. M. (2010). Northern mid-latitude glaciation in the Late Amazonian period of Mars: Criteria for the recognition of debris-covered glacier and valley glacier landsystem deposits. *Earth and Planetary Science Letters, 294*(3-4), 306-320. doi: 10.1016/j.epsl.2009.06.041.

Head, J. W., Mustard, J. F., Kreslavsky, M. A., Milliken, R. E., & Marchant, D. R. (2003). Recent ice ages on Mars. *Nature, 426*(6968), 797-802. doi: 10.1038/Nature02114.

Head, J. W., Neukum, G., Jaumann, R., Hiesinger, H., Hauber, E., Carr, M., Masson, P., Foing, B., Hoffmann, H., Kreslavsky, M., Werner, S., Milkovich, S., van Gasselt, S., & HRSC Co-Investigator Team (2005). Tropical to mid-latitude snow and ice accumulation, flow and glaciation on Mars. *Nature, 434*(7031), 346-351. doi: 10.1038/Nature03359.

Holt, J. W., Safaeinili, A., Plaut, J. J., Head, J. W., Phillips, R. J., Seu, R., Kempft, S. D., Choudhary, P., Young, D. A., Putzig, N. E., Biccari, D., & Gim, Y. (2008). Radar Sounding Evidence for Buried Glaciers in the Southern Mid-Latitudes of Mars. *Science, 322*(5905), 1235-1238. doi: 10.1126/science.1164246.

Hubbard, B., & Glasser, N. F. (2005). *Field Techniques in Glaciology and Glacial Geomorphology*. Chichester: Wiley.

Hubbard, B., Souness, C., & Brough, S. (2014). Glacier-like forms on Mars. *The Cryosphere, 8*(6), 2047-2061. doi: 10.5194/tc-8-2047-2014.

Hubbard, B., Milliken, R. E., Kargel, J. S., Limaye, A., & Souness, C. (2011). Geomorphological characterisation and interpretation of a mid-latitude glacier-like form: Hellas Planitia, Mars. *Icarus, 211*(1), 330-346. doi: 10.1016/j.icarus.2010.10.021.

Kargel, J. S., Baker, V. R., Beget, J. E., Lockwood, J. F., Pewe, T. L., Shaw, J. S., & Strom, R. G. (1995). Evidence of Ancient Continental-Glaciation in the Martian

Northern Plains. *Journal of Geophysical Research: Planets, 100*(E3), 5351-5368. doi: 10.1029/94je02447.

Kato, M., Iijima, Y., Arakawa, M., Okimura, Y., Fujimura, A., Maeno, N., & Mizutani, H. (1995). Ice-on-Ice Impact Experiments. *Icarus, 113*(2), 423-441. doi: 10.1006/icar.1995.1032.

Kirk, R. L., Howington-Kraus, E., Redding, B., Galuszka, D., Hare, T. M., Archinal, B. A., Soderblom, L. A., & Barrett, J. M. (2003). High-resolution topomapping of candidate MER landing sites with Mars Orbiter Camera narrow-angle images. *Journal of Geophysical Research: Planets, 108*(E12). doi: 10.1029/2003je002131.

Kirk, R. L., Howington-Kraus, E., Rosiek, M. R., Anderson, J. A., Archinal, B. A., Becker, K. J., Cook, D. A., Gaulszka, D. M., Geissler, P. E., Hare, T. M., Holmberg, I. M., Keszthelyi, L. P., Redding, B. L., Delamere, W. A., Gallagher, D., Chapel, J. D., Eliason, E. M., King, R., & McEwen, A. S. (2008). Ultrahigh resolution topographic mapping of Mars with MRO HiRISE stereo images: Meter-scale slopes of candidate Phoenix landing sites. *Journal of Geophysical Research, 113*. doi: 10.1029/2007je003000.

Kleman, J., Hattestrand, C., Borgstrom, I., & Stroeven, A. (1997). Fennoscandian palaeoglaciology reconstructed using a glacial geological inversion model. *Journal of Glaciology, 43*(144), 283-299. doi: 10.3189/S0022143000003233.

Kress, A. M., & Head, J. W. (2008). Ring-mold craters in lineated valley fill and lobate debris aprons on Mars: Evidence for subsurface glacial ice. *Geophysical Research Letters, 35*(23). doi: 10.1029/2008gl035501.

Laskar, J., Correia, A. C. M., Gastineau, M., Joutel, F., Levrard, B., & Robutel, P. (2004). Long term evolution and chaotic diffusion of the insolation quantities of Mars. *Icarus, 170*(2), 343-364. doi: 10.1016/j.icarus.2004.04.005.

Levy, J., Head, J. W., & Marchant, D. R. (2010). Concentric crater fill in the northern mid-latitudes of Mars: Formation processes and relationships to similar landforms of glacial origin. *Icarus, 209*(2), 390-404. doi: 10.1016/j.icarus.2010.03.036.

Malin, M. C., Bell, J. F., Cantor, B. A., Caplinger, M. A., Calvin, W. M., Clancy, R. T., Edgett, K. S., Edwards, L., Haberle, R. M., James, P. B., Lee, S. W., Ravine, M. A., Thomas, P. C., & Wolff, M. J. (2007). Context Camera Investigation on

board the Mars Reconnaissance Orbiter. *Journal of Geophysical Research, 112*(E5). doi: 10.1029/2006je002808.

McEwen, A. S., Eliason, E. M., Bergstrom, J. W., Bridges, N. T., Hansen, C. J., Delamere, W. A., Grant, J. A., Gulick, V. C., Herkenhoff, K. E., Keszthelyi, L., Kirk, R. L., Mellon, M. T., Squres, S. W., Thomas, N., & Weitz, C. M. (2007). Mars Reconnaissance Orbiter's High Resolution Imaging Science Experiment (HiRISE). *Journal of Geophysical Research, 112*(E5). doi: 10.1029/2005je002605.

Mest, S. C., & Crown, D. A. (2001). Geology of the Reull Vallis Region, Mars. *Icarus, 153*, 89-110. doi: 10.1006/icar.2001.6655.

Mest, S. C., & Crown, D. A. (2014). Geologic map of MTM –30247, –35247, and –40247 quadrangles, Reull Vallis region of Mars. U.S. Geological Survey Scientific Investigations Map *3245,* scale 1:1,000,000, pamphlet 20 p. doi: 10.3133/sim3245.

Milliken, R. E., Mustard, J. F., & Goldsby, D. L. (2003). Viscous flow features on the surface of Mars: Observations from high-resolution Mars Orbiter Camera (MOC) images. *Journal of Geophysical Research, 108*(E6). doi: 10.1029/2002je002005.

Okubo, C. H. (2010), Structural geology of Amazonian-aged layered sedimentary deposits in southwest Candor Chasma, Mars, *Icarus*, 207, 210-225, doi: 10.1016/j.icarus.2009.11.012.

Parsons, R. A., Nimmo, F., & Miyamoto, H. (2011). Constraints on martian lobate debris apron evolution and rheology from numerical modeling of ice flow. *Icarus, 214*(1), 246-257. doi: 10.1016/j.icarus.2011.04.014.

Pierce, T. L., & Crown, D. A. (2003). Morphologic and topographic analyses of debris aprons in the eastern Hellas region, Mars. *Icarus, 163*(1), 46-65. doi: 10.1016/s0019-1035(03)00046-0.

Plaut, J. J., Safaeinili, A., Holt, J. W., Phillips, R. J., Head, J. W., Seu, R., Putzig, N. E., & Frigeri, A. (2009). Radar evidence for ice in lobate debris aprons in the mid-northern latitudes of Mars. *Geophysical Research Letters, 36*(2), doi: 10.1029/2008gl036379.

Sinha, R. K., & Murty, S. V. S. (2013). Evidence of extensive glaciation in Deuteronilus Mensae, Mars: Inferences towards multiple glacial events in the past epochs. *Planetary and Space Science, 86*, 10-32. doi: 10.1016/j.pss.2013.09.002.

Smith, D. E., Zuber, M. T., Solomon, S. C., Phillips, R. J., Head, J. W., Garvin, J. B., Banerdt, W. B., Muhleman, D. O., Pettengill, G. H., Neumann, G. A., Lemoine, F. G., Abshire, J. B., Aharonson, O., Brown, C. B., Hauck, S. A., Ivanov, A. B., McGovern, P. J., Zwalley, H. J., & Duxbury, T, C. (1999). The Global Topography of Mars and Implications for Surface Evolution. *Science, 284*(5419), 1495-1503. doi: 10.1126/science.284.5419.1495.

Souness, C., & Hubbard, B. (2012). Mid-latitude glaciation on Mars. *Progress in Physical Geography, 36*(2), 238-261. doi: 10.1177/0309133312436570.

Souness, C., & Hubbard, B. (2013). An alternative interpretation of late Amazonian ice flow: Protonilus Mensae, Mars. *Icarus, 225*(1), 495-505. doi: 10.1016/j.icarus.2013.03.030.

Souness, C., Hubbard, B., Milliken, R. E., & Quincey, D. (2012). An inventory and population-scale analysis of martian glacier-like forms. *Icarus, 217*(1), 243-255. doi: 10.1016/j.icarus.2011.10.020.

Squyres, S. W. (1978). Martian Fretted Terrain - Flow of Erosional Debris. *Icarus, 34*(3), 600-613. doi: 10.1016/0019-1035(78)90048-9.

Tanaka, K. L., & Leonard, G. J. (1995). Geology and Landscape Evolution of the Hellas Region of Mars. *Journal of Geophysical Research: Planets, 100*(E3), 5407-5432. doi: 10.1029/94je02804.

Touma, J., & Wisdom, J. (1993). The Chaotic Obliquity of Mars. *Science, 259*(5099), 1294-1296. doi: 10.1126/science.259.5099.1294.

Vaughan, D. G. (1993). Relating the Occurrence of Crevasses to Surface Strain Rates. *Journal of Glaciology, 39*(132), 255-266. doi: 10.3189/S0022143000015926.

Whalley, W. B., & Azizi, F. (2003). Rock glaciers and protalus landforms: Analogous forms and ice sources on Earth and Mars. *Journal of Geophysical Research: Planets, 108*(E4). doi: 10.1029/2002je001864.

Zurek, R. W., & Smrekar, S. E. (2007). An overview of the Mars Reconnaissance Orbiter (MRO) science mission. *Journal of Geophysical Research, 112*(E5). doi: 10.1029/2006je0027.

Supplementary Material Ch. 2

Landscapes of polyphase glaciation: eastern Hellas Planitia, Mars

Stephen BROUGH[a], Bryn HUBBARD[a], Colin SOUNESS[a], Peter M. GRINDROD[b,c] and Joel DAVIS[b,d]

[a]*Department of Geography and Earth Sciences, Aberystwyth University, Aberystwyth, UK*

[b]*Centre for Planetary Sciences, University College London/Birkbeck, London, UK*

[c]*Department of Earth and Planetary Sciences, Birkbeck, University of London, London, UK*

[d]*Department of Earth Sciences, University College London, London, UK*

Link to published article

This is supplementary material to an article published by Taylor & Francis Group in *Journal of Maps* on 04/06/2015, available online: http://dx.doi.org/10.1080/17445647.2015.1047907.

Citation for published paper

Brough, S., Hubbard, B., Souness, C., Grindrod, P. M. & Davis, J. (2016). Landscapes of polyphase glaciation: eastern Hellas Planitia, Mars. *Journal of Maps*. *12*(3), 530-542. doi: 10.1080/17445647.2015.1047907.

This supplementary material consists of a geomorphic and structural map. The supplementary material is organised as follows:

Landscapes_of_polyphases_glaciation.pdf: An A1 geomorphic and structural map (1:100,000 scale) of the glacial landscape described in the text and can be accessed at: https://www.dropbox.com/s/ujv54zzom0kre3o/Landscapes_of_polyphases_glaciation.pdf?dl=0.

Summary to manuscript 'Landscapes of polyphase glaciation: eastern Hellas Planitia, Mars'

Chapter 2 has presented a geomorphic and structural investigation of a glacial landscape in eastern Hellas Planitia. The key outcomes to carry forward are as such:

1. Two units showed significant evidence of glacial flow: (i) at the broad scale the lobate debris apron (LDA) preserved a convex-up profile and numerous arcuate and longitudinal structures indicative of the downslope flow of ice; and (ii) at the more localised scale the glacier-like form (GLF) also preserved several structures indicative of flow and transport of ice downslope. A third terrain, degraded glacial material, also showed evidence for the downslope flow of mass, but structures lacked clear indication of a present day ice core and are more akin to slope processes of periglacial environments.

2. There is a clear discontinuity between material in the GLF and degraded glacial material, and the LDA. Certainly, the GLF preserves evidence for localised ice accumulation and subsequent flow of mass within a well-defined cirque basin that is raised above the LDA surface. Two further alcoves (one located towards the centre of the massif and one on the southern face) within the degraded glacial material are associated with structures similar to the adjacent GLF and perhaps were former centres of localised ice accumulation, that have subsequently deflated. Nonetheless, there is a clear ridge at the confluence of the degraded glacial material and the LDA, again suggesting a material or process threshold between the two units.

3. There is an apparent (qualitative) difference in the density and size of craters between geomorphic units. The LDA, GLF and degraded glacial material contain a lower density and size distribution relative to the outer plain, consistent with a younger age for the deposition or exposure of the former terrains. Further, both the GLF and degraded glacial material generally lack resolvable craters on their surface, and although insufficient in numbers to

formally analyse, would suggest that these features are of a geologically very young age, and younger than the encompassing LDA.

4. Given points (2) and (3) above, it is interpreted that the LDA represents a larger and more extensive phase of glaciation, and that the GLF (and likely the degraded glacial material) represent a smaller, more localised, phase of glaciation. Such an interpretation is consistent with the hypothesis that Mars' mid-latitudes preserve evidence of multiple phases of glaciation, but extends the spatial scale at which these observations have been reported.

5. The identification of numerous moraine-like ridges (MLRs) surrounding both the LDA and GLF are clear indications of ice mass loss since emplacement. This mass loss has occurred through both surface lowering and terminus recession. The identification of numerous MLR and medial moraine-like ridges further implies that these viscous flow features (VFFS) are, or at least have been at some point in their history, capable of entraining, transporting and depositing debris.

6. Analysis of several surface structures, for example the identification of fractures and arcuate transverse ridges, revealed insights into the dynamics of these ice masses and indicate that, much like terrestrial glaciers, Mars' VFFs (GLF and LDA in this instance) have experienced variable flow regimes.

CHAPTER 3

Area and volume of mid-latitude glacier-like forms on Mars

If the Sun & Moon should doubt
They'd immediately go out
William Blake

Preface to manuscript 'Area and volume of mid-latitude glacier-like forms on Mars'

Introduction and rationale

As introduced in Chapter 1 (see Section 1.2), a substantial reservoir of buried ice has been identified within viscous flow features in the mid-latitudes of Mars (e.g. Holt et al., 2008; Levy et al. 2014). However, there is uncertainty regarding the formation, current and former volume, and dynamic evolution of these ice masses. Reducing such uncertainties is important if we are to better understand how water moves through the martian hydrological cycle through time (e.g. Carr and Head, 2015). With respect to glacier-like forms (GLFs), although their distribution has been well documented and constrained in previous studies (e.g. Chapter 2; Milliken et al., 2003; Souness et al., 2012) – and unlike the wider lobate debris aprons, lineated valley fill and concentric crater fill deposits (e.g. Levy et al., 2014; Karlsson et al., 2015) – no study has attempted to estimate the potential ice volume contained within these landforms.

This chapter (submitted to *Earth and Planetary Science Letters*) looks to build upon the local- to regional-scale mapping of GLFs that was introduced in Chapter 2 (see also Appendix A), and presents a systematic population-scale mapping investigation in to the areal and volumetric extent of martian GLFs. The analysis draws on techniques similar to those used by terrestrial glaciologists interested in glacier monitoring (e.g. Paul et al., 2009) and/or reconstructing ice volume in inaccessible areas (e.g. Bahr et al., 2015). These results will fill a knowledge gap within our understanding of the contribution of GLFs to the to the nonpolar surface/near surface water inventory of Mars (e.g. contributing to Objective [3] of the thesis), and provide an opportunity to evaluate environmental and topographical controls over the resulting volume distribution (e.g. contributing to Objective [5] of the thesis). The remainder of this preface discusses the methods that were adopted during the study.

GLF inventory compilation

In 2012, Souness et al. published by far the most complete inventory of GLFs. This study built upon the earlier work of Milliken et al. (2003) to formally define, and analyse the distribution of GLFs between the latitudes of 25 and 65^{o} in both hemispheres. Although representing a major advancement at the time, this analysis was conducted on the basis of point measurements and/or geometric buffers (rectangles/circles from Mars Orbiter Laser Altimeter [MOLA] derived background topography) rather than from directly mapped GLF boundaries. The later are of great importance for accurately assessing current ice extents and for providing baselines to assess past and future change in response to climate (e.g. Paul et al., 2009). The initial phase of this study therefore focused on deriving such boundaries, in the form of digital vector outlines, and the second phase looked to derive a volumetric estimate.

Mapping GLFs

Using the location and imagery information contained within the inventory of Souness et al. (2012), all Context Camera (CTX) images where a GLF had been identified were processed with a standard routine to map projected 6 m per pixel resolution images, via USGS' Integrated Software for Imagers and Spectrometers (https://isis.astrogeology.usgs.gov/fixit/projects/isis/wiki/Working_with_Mars_Reconnaissance_Orbiter_CTX_Data). Given the nature of this imagery (panchromatic and single band), and the fact that GLFs are covered in a ubiquitous layer of debris, it was not possible to utilise automated techniques commonly applied to terrestrial glaciers (see Racoviteanu et al., 2009) for delineation of GLF outlines. Therefore, GLFs were manually delineated using the identification criteria of Souness et al. (2012), within Geographic Information System (GIS) software.

Inventory data

With the GLF outlines in digital format, it was possible to couple these data with the MOLA digital elevation model – the best globally available dataset – in order to include valuable environmental and topographical data with the inventory. Within the GIS, it is possible to derive grid-based (zonal) statistics for each glacier from the digital

intersection of both datasets. Inventory parameters calculated in this way were: ID, area, centroid x-y coordinates; elevations of maximum, minimum, mean, median and standard deviation; mean slope; and the mean aspect (also classified into eight cardinal and inter-cardinal directions). This method and parameter selection followed the recommendation of the terrestrial glaciological community (see Paul et al., 2009), and was chosen as it produces reproducible data that can be used in change assessment.

Volumetric analysis

Perhaps the biggest challenge was to derive the volumetric estimate of ice contained within the GLF population, given that our knowledge of the composition and ice thickness distribution of GLFs on Mars is severely limited (see Section 1.2.2) and difficult to obtain using currently available satellite-based geophysical methods (Appendix A). Although a number of sophisticated methods for estimating ice mass thickness of terrestrial glaciers exist (see Farinotti et al., 2017 and references therein), many of these approaches include data that is simply not available for their martian counterparts (e.g. surface velocity; mass balance; large-scale, high-resolution DEMs). One method that has been applied by terrestrial glaciologist interested in estimating ice volume from inaccessible/large areas is volume-area scaling (see Bahr et al., 2015 and references therein). Such ‘scaling’ approaches rest on the principle that (glacier) volume can be estimated from the (glacier) surface area alone. Although volume-area scaling has a number of assumptions and limitations that can influence the accuracy of the volume estimation (see detailed discussion in Section 3.2.5), given the availability of GLF area generated previously, it leaves volume-area scaling as the most viable option for volume estimation for the entire GLF population.

Area and volume of mid-latitude glacier-like forms on Mars

Stephen BROUGH[a], Bryn HUBBARD[a] and Alun HUBBARD[a,b]

[a]*Department of Geography and Earth Sciences, Aberystwyth University, Aberystwyth, UK*

[b]*Centre for Arctic Gas Hydrate, Environment and Climate, Department of Geology, University of Tromsø, Tromsø, Norway*

This is a manuscript of an article under review for publication in *Earth and Planetary Science Letters*, submitted on 15/08/2017.

Keywords: Mars; glaciation; glacier; water; climate change; GIS

Abstract: Although a substantial ice reservoir has been identified within the mid-latitudes of Mars, there is uncertainty regarding the formation, current and former volume, and dynamic evolution of these ice masses. Here, we present the first comprehensive ice volume estimate of martian glacier-like forms (GLFs) from systematic population scale mapping and volumetric analysis. The outlines of 1243 GLFs were manually delineated from 6 m per pixel Context Camera (CTX) images and the volume of each determined using a volume-area scaling approach. Our results show that GLFs cover a surface area of 11344 ± 393 km^2 and have a total volume of 1744 ± 441 km^3. Using two end-member scenarios for ice concentration by volume of 30 % (pore ice) and 90 % (debris-covered glacier ice), we calculate the volume of ice contained within GLFs to be between 523 ± 132 km^3 (480 ± 121 Gt) and 1570 ± 397 km^3 (1439 ± 364 Gt), equivalent to a mean global water layer 3 ± 1 – 10 ± 3 mm thick. We investigate the local topographic setting of each GLF by reference to the Mars Orbiter Laser Altimeter (MOLA) digital elevation model. Our analysis reveals that globally GLFs are on average larger in latitudes >36^o and on slopes between 2 and 8^o. In the northern hemisphere GLFs between 500 and 2500 m in elevation and in the southern hemisphere GLFs with a northern aspect are also larger on average. The observed spatial patterns of GLF landform and volume distribution suggests that regional to local meteorological and topographical conditions play an important role in GLF ice accumulation and/or preservation. Assuming a net accumulation rate of 10 mm a^{-1} typical of climatic excursions with high obliquity, we estimate a period of at least 13 ka is required to yield the average calculated GLF ice thickness of ~130 m. Such a period is well within the timeframe of a high obliquity cycle (20 – 40 ka), suggesting that the current GLF volume could have formed during a single climate excursion.

3.1. Introduction

Extensive evidence has been presented for the existence and character of buried water ice within Mars' mid-latitudes (30 – 60^o [e.g. Squyres, 1978, 1979; Squyres and Carr 1986; Mustard et al., 2001; Head et al., 2003; Milliken et al., 2003; Arfstrom and Hartmann, 2005; Levy et al., 2007; Dickson et al., 2008; Holt et al., 2008; Head et al., 2010, Dickson et al., 2012; Souness et al., 2012; Hartmann et al., 2014; Levy et al., 2014]). Pervasive landforms consistent with viscous deformation and the resulting flow

of ice are of particular interest. Collectively, these landforms have been termed viscous flow features, or VFFs (Milliken et al., 2003; Souness et al., 2012). Among some of the earliest VFFs identified were lobate debris aprons (LDA [Squyres, 1978, 1979]), lineated valley fill (LVF [Squyres 1978, 1979]), and concentric crater fill (CFF [Squyres and Carr, 1986]). The original interpretations of these landforms were that they were either ice assisted (<30% ice) or were formed by debris/talus flows from ground ice emplaced by vapour diffusion (e.g. Squyres 1978, 1979). However, more recent investigations – corroborated with geophysical evidence showing many, if not all, of these landforms are composed of a substantial core (~90%) of water ice (Holt et al., 2008; Plaut et al., 2009) – have noted several similarities between VFFs and debris-covered glaciers on Earth (e.g. Head et al., 2010; Mackay and Marchant, 2017).

Given that water ice is not presently stable across much of the latitudinal range where these ice-rich landforms are observed (Mellon and Jakosky, 1995; Mellon et al., 2004), VFFs are suggested to have formed as a result of climatic excursions redistributing ice from polar to mid-latitude regions during periods of high (>30^{o}) obliquity (Head et al., 2003; Forget et al., 2006; Madeleine et al., 2009; Fassett et al., 2014). VFF survival to the present day is due, at least in part, to the ice being protected from sublimation by surface debris (Holt et al., 2008; Fastook et al., 2014). Constraining the timing of high obliquity periods required for VFF formation is hindered by the fact that numerical models can only satisfactorily predict orbital variations for approximately the last 20 Ma (e.g. Laskar et al., 2004). However, crater-related age estimates for LDA, LVF and CFF constrain the age of formation to between 60 Ma and 1 Ga BP (see Berman et al., 2015). Furthermore, ice volume estimates from analysis of mapped outlines of >11,000 mid-latitude VFFs (LDA, LVF, CCF), suggest a total of between 1.25 x 10^5 and 3.74 x 10^5 km^3 of ice is potentially held within in these landforms; the equivalent of a global water layer between 0.8 and 2.4 m thick (Levy et al., 2014; Karlsson et al., 2015). Thus, VFFs constitute: (i) an important component of the surface/near-surface water inventory of Mars (Carr and Head, 2015); and (ii) have become an important proxy for improving our understanding of long term climate change throughout the Amazonian Epoch of Mars (e.g. Fassett et al., 2014; Fastook et al., 2014; Parsons and Holt, 2016).

In recent years, growing attention has focused on a set of smaller scale VFFs that, in planform, appear similar to (debris-covered) valley glaciers on Earth (e.g. Milliken et

al., 2003; Arfstrom and Hartmann, 2005; Hubbard et al., 2011; Souness et al., 2012; Hubbard et al., 2014). Such landforms have become known as glacier-like forms, or GLFs (Hubbard et al., 2011; noting that these landforms have also been subject to a range of nomenclature within the literature, including: VFFs [Milliken et al., 2003]; glacier-like flows [Arfstrom and Hartmann, 2005]; superposed lineated valley fill [Levy et al., 2007] and small-scale superposed lineated valley fill [Levy et al., 2007]). GLFs appear to flow downslope, generally coalescing from cirque-like alcoves or valleys to a narrow elongate tongue that is commonly demarcated by raised latero-terminal ridges. The identification of such ridges suggests that GLFs are relict remains of more extensive ice masses that have receded since a climatic optimum (Hubbard et al., 2011; Hartmann et al., 2014; Brough et al., 2016a), perhaps as a result of the last major change from a high (~35^{o}) to low (~25^{o}) mean obliquity period ~4 Ma – 6 Ma BP (Laskar et al., 2004). Although identified in isolation, GLFs often feed into pre-existing VFFs to form what Head et al. (2010) described as Mars' integrated glacial landsystem.

In total ~1300 GLFs have been identified between 30 and 60^{o} latitude in both hemispheres and inter-hemispheric similarities in their morphology (e.g. length and width) and environmental settings suggests a common evolutionary history (Souness et al., 2012; Brough et al., 2016a). Age estimates for several GLFs in Crater Greg, although somewhat speculative due to the small areas involved and thus numbers of craters used (e.g. Dauber et al., 2013), indicate that they are likely <10 Ma old, with an upper boundary of <50 Ma (Arfstrom and Hartmann, 2005; Hartmann et al., 2014). Furthermore, numerous studies have noted a distinct stratigraphic relationship between GLFs and other ice-rich landforms (LDA, LVF and CCF), with the former being superposed on the later (e.g. Levy et al., 2007). The apparent younger age of GLFs and their stratigraphic relationships with other ice-rich landforms has provided supporting evidence for the hypothesis that GLFs represent a more recent, perhaps localised and small-scale, glacial phase and the more extensive LDA, LVF and CCF deposits record an earlier, regional, glacial phase (Levy et al., 2007; Dickson et al., 2008; Brough et al., 2016b). Therefore, GLFs may represent: (i) important archives of geologically recent climatic change (e.g. Hartmann et al., 2014; Brough et al., 2016a); (ii) an active/recently active hydrological store; and (iii) effective landscaping agents through erosion, transportation and deposition of material. Despite these important questions, and unlike the wider LDA, LVF and CCF deposits (e.g. Levy et al., 2014; Karlsson et al., 2015),

no population-scale outline mapping or estimation of the water ice volume of GLFs exist and our understanding of the basic physical and mechanical properties of GLFs is still being added to (e.g. Souness et al., 2012; Hubbard et al., 2014; Brough et al., 2016a). The study by Souness et al. (2012) represents the most comprehensive analysis of GLFs to date, providing the geographic coordinates and morphometric data for each individual GLF identified at the time. However, this analysis was conducted on the basis of point measurements and/or geometric buffers (rectangles/circles from Mars Orbiter Laser Altimeter [MOLA] derived background topography) rather than from directly mapped GLF boundaries.

The aim of this paper is to advance our understanding of the glacial history of Mars' GLFs by providing the first population-scale outline mapping and estimation of the water ice volume of GLFs, as well as evaluating controls over the resulting volume distribution. Specifically, we provide: (i) manually digitised outlines for all GLFs; (ii) an estimate of the volume of water ice held within GLFs, using a volume-area scaling approach commonly applied to ice masses on Earth (cf. Bahr et al., 2015 and references therein) and more recently to Mars (Karlsson et al., 2015); (iii) an assessment of potential controlling environmental variables on GLF volume; and (iv) an updated GLF inventory to that of Souness et al. (2012).

3.2. Data and methods

3.2.1. Datasets

Analysis of GLFs in this study was based on all 1293 landforms identified in the database of Souness et al. (2012)[1]. This database contained two pieces of information used in the present study: (i) the Context Camera (CTX) image ID, and (ii) the location (latitude and longitude) of all GLFs. Where a GLF had been identified, map projected (level 2) CTX images at 6 m pixel resolution were produced using the USGS' Integrated Software for Imagers and Spectrometers. The processed CTX images, GLF

[1] Souness et al. (2012) originally identified 1309 GLFs. However, Brough et al. (2016a) recently refined this number to 1293 due to the identification of duplicate entries.

[2] Many of the environmental parameters described above formed part of the study by Souness et al. (2012). Our intention was not to replicate but to update the inventory of Souness et al. (2012) based on directly mapped, rather than approximated, outlines of individual GLFs. Herein, we only report on new

centroid coordinates and a gridded MOLA digital elevation model (DEM) were then analysed in ESRI's ArcMap 10.1 Geographic Information System (GIS) software. MOLA elevation data at ~463 m horizontal resolution was used to define a number of topographic related parameters including slope and aspect (in radians and broken down into linear, sine and cosine, form).

3.2.2. GLF outline mapping and area calculation

GLF outlines (vector polygons) were manually digitised by a single user (SB) at a scale of 1:25 000 following the criteria set out in Souness et al. (2012) and summarised in Table 3.1. Three scenarios were identified and classified in demarcating the GLF boundaries (Figure 3.1). Type 1 GLFs (n = 249) were the easiest to demarcate, terminating on a non-ice surface and with their complete boundary being constrained by the surrounding topography (e.g. Figure 3.1a, d). Type 2 GLFs (n = 216) are similar to Type 1 but differ in that they terminate within a wider icy terrain, often superposed on the wider LDA/LVF (e.g. Figure 3.1b, e). Type 3 GLFs (n = 778) similarly terminate in wider icy terrain but do not have an unequivocal continuous boundary (e.g. Figure 3.1c, f). In this scenario, the boundary is identified based on observable changes in surface texture as indicated by criterion [ii] of Table 3.1.

Table 3.1: *Criteria for GLF identification following Souness et al. (2012).*

	Description
[i]	Be surrounded by topography showing general evidence of flow over or around obstacles
[ii]	Be distinct from the surrounding landscape exhibiting a texture or colour difference from adjacent terrains
[iii]	Display surface foliation indicative of down-slope flow; e.g. compressional/extensional ridges, surface lineations, arcuate surface morphologies or surface crevassing
[iv]	Have a length to width ratio >1 (i.e. be longer than it is wide)
[v]	Have either a discernible 'head' or a discernible 'terminus' indicating a compositional boundary or process threshold
[vi]	Appear to contain a volume of ice (or some other viscous substance), having a flat 'valley fill' surface, thus differentiating it from a previously glaciated 'GLF skeleton'

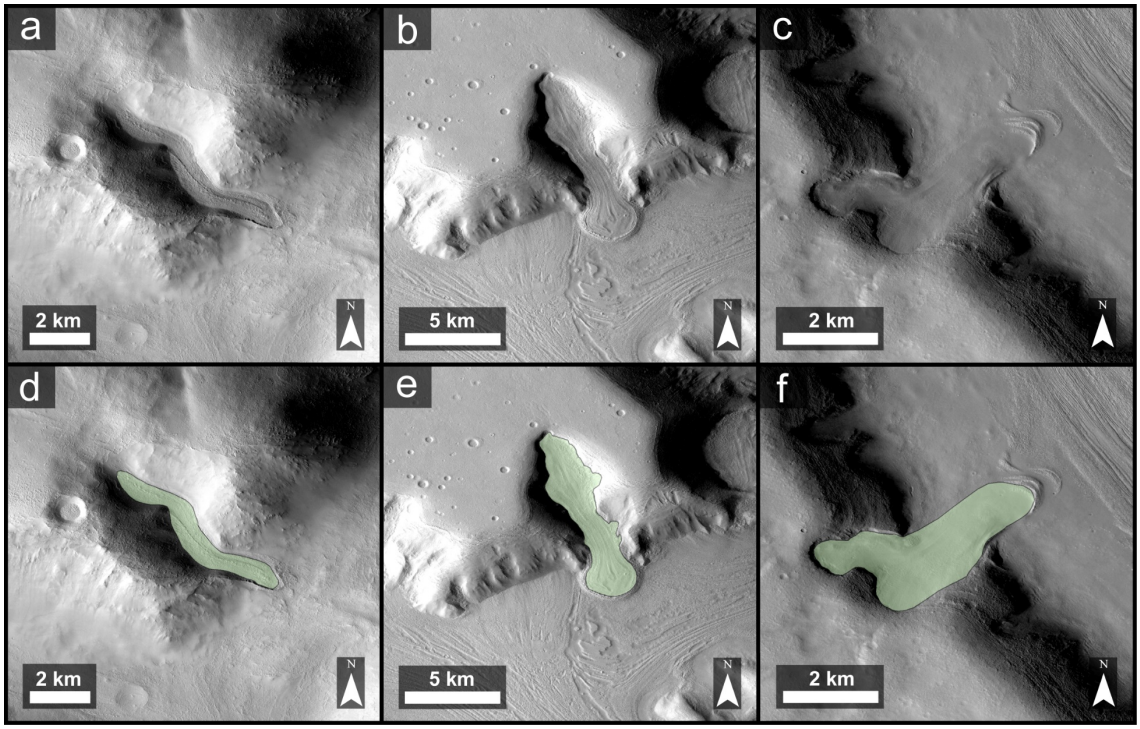

Figure 3.1: *Examples of GLFs (a – c) and their manually digitized outlines (d – f). (a) A Type 1 GLF. The boundary is readily demarcated with the GLF constrained within a valley and the terminus identified by moraine-like ridges (Subset of CTX image B04_011261_2146_XN_34N289W; centred on ~70.59^{o} E, 33.12^{o} N). (b) A Type 2 GLF. The boundary is again clear, but in this case the GLF is superposed on LVF (Subset of CTX image P22_009653_2224_XN_42N309W; centred on ~50.50^{o} E, 42.24^{o} N). (c) A Type 3 GLF. The boundary is somewhat unclear as the GLF emerges out of the alcove and merges with the outer LVF deposit (Subset of CTX image P03_002112_2208_XN_40N337W; centred on ~22.27^{o} E, 40.07^{o} N).*

Compound GLFs (i.e. where two or more GLFs share a border) were treated as follows. GLFs flowing in different directions from a common source area were each classified separately and mapped from the drainage divide (Figure SF1 in Supplementary Material Ch. 3). In contrast, ice flow units originating from separate source areas and converging into a single distinct terminus (e.g. Figure SF1) were classified as a single GLF. In all scenarios, when the GLF margin was flanked by a moraine-like ridge (MLR) the boundary was placed on the inside of the MLR. If multiple MLRs were visible, then the innermost ridge was used. Once the outline of the GLF had been mapped, any internal bedrock/nunatak perturbations were removed from the GIS polygon.

Each GLF was assigned to the unique ID corresponding to Souness et al. (2012), with GLFs that here are treated as one, rather than multiple entries, assigned the first corresponding ID. Subsequently, the area for each GLF was calculated in ArcMap using an Albers Equal Area Conic map projection.

3.2.3. GLF volume calculation

Knowledge of the composition and ice thickness distribution of GLFs on Mars is severely limited and difficult to obtain using currently available satellite-based geophysical methods (Hubbard et al., 2014). Numerous methods for estimating ice volume exist for ice masses on Earth (see Farinotti et al., 2017). However, the more sophisticated of these require input data not presently available for Mars (e.g., surface velocity; mass balance; large-scale, high-resolution DEMs). Here we applied a simple and commonly used volume-area scaling method (cf. Bahr et al., 2015 and references therein) based solely on (glacier) area.

Volume-area scaling rests on the principle that (glacier) volume (V) can be estimated from the (glacier) surface area (A) with the relationship: $V = kA^{\gamma}$ or $\log(V) = \log(k) + \gamma \log(A)$, where k and γ are scaling parameters derived from data, or through theoretical considerations (Bahr et al., 2015). Although a number of regional and global volume-area scaling relationships have been proposed for glaciers on Earth (see Bahr et al., 2015), given the general absence of ancillary data, volume-area scaling relationships for martian ice masses are scant and, to our knowledge, the only scaling relationship for mid-latitude VFFs is provided by Karlsson et al. (2015). Based on radar-validated measurements of ice thickness from LDAs on Mars, Karlsson et al. (2015) determined a volume-area relationship: $\log(V) = 1.12 \log(A) - 0.978$. Although obtained from LDA, in the absence of contemporaneous radar-validated measurements for GLFs, we adopted this relationship and applied it to our outline mapping (see Section 3.2.2) to calculate the volume for each individual GLF.

3.2.4. GLF inventory attributes

3.2.4.1. Environmental parameters

As well as the ID, Type, area and volume values already attributed to each GLF (see Sections 3.2.2 and 3.2.3), several environmental parameters were calculated from the MOLA topographic datasets (see Section 3.2.1) including: the centroid x-y coordinates; elevations of maximum, minimum, mean, median and standard deviation; mean slope; and the mean aspect (also classified into eight cardinal and inter-cardinal directions) [2]. The mean aspect for each GLF was derived following Paul (2007) and the resulting orientations were classified into 45° bins corresponding to the eight cardinal and inter-cardinal directions. The mapped GLF outlines and corresponding environmental parameters are provided as supplementary material.

3.2.4.2. Analysis of environmental parameters

Several environmental parameters were extracted and analysed to evaluate controls over GLF volume. Mean GLF volume (km^3) was calculated as a function of longitude (^{o}), latitude (^{o}), aspect (cardinal and inter-cardinal directions), slope (^{o}) and elevation (m relative to Mars datum), and two sample t-tests were run, using an alpha (*P*) level of 0.05, to assess for significant differences between populations (Table ST1 in Supplementary Material Ch. 3). Global and hemispheric GLF counts and total GLF volume were also plotted and can be found in Supplementary Material Ch. 3 (Figures SF2 – SF5 and Tables ST2 – ST6).

[2] Many of the environmental parameters described above formed part of the study by Souness et al. (2012). Our intention was not to replicate but to update the inventory of Souness et al. (2012) based on directly mapped, rather than approximated, outlines of individual GLFs. Herein, we only report on new findings obtained from this study or through results obtained from previously unreported analysis.

3.2.5. Uncertainty in GLF mapping and volume calculation

3.2.5.1. Outline mapping

Manual classification is prone to errors that reflect a users' ability to identify the features of interest (Smith, 2011). Glacier boundaries, and particularly those of debris-covered glaciers, are inherently difficult to define from remotely-sensed imagery alone (e.g. Paul et al., 2013). However, these difficulties can be mitigated to some degree by a single interpreter following a consistent and tightly constrained mapping technique in terms of e.g., criteria and scale (Smith, 2011), both of which were followed in the present study (see Section 3.2.2).

In order to quantify uncertainty associated with this study's outline mapping, we followed standard procedure (e.g. Paul et al., 2013) and conducted an error analysis by performing multiple and independent digitisations of a selection of GLFs. Each of the three GLF Types (see Section 3.2.2) presented in Figure 3.1 was digitised independently at a scale of 1:25 000 five times, and the resulting GLF areas were compared. This yielded, a mean standard deviation of 2.0, 2.2 and 4.0 % of the area for Types 1, 2 and 3 GLFs respectively. The uncertainty in the total mapped GLF area reported in this study was consequently calculated by applying these Type-dependant (1 std. dev.) variations to each individual GLF as appropriate.

3.2.5.2. Volume estimation

Karlsson et al. (2015) constrained their volume-area relationship by interpolating Shallow Radar (SHARAD) measurements into bed elevation maps for seven LDAs, where sufficient SHARAD coverage was available, in order to calculate their thickness and thus estimate their volume. By comparing misfit in their interpolated bed elevation maps with individual SHARAD tracks, Karlsson et al. (2015) assigned an uncertainty of 25 % to their calibration data set. In the absence of SHARAD data for GLFs we adopt this value and add it to the area uncertainty of 2.0, 2.2 and 4.0 % to Type 1, 2 and 3 GLFs, respectively (see Section 3.2.5.1).

Furthermore, volume-area scaling has a number of assumptions and limitations that can influence the accuracy of the volume estimation (see review by Bahr et al., 2015 for detailed discussion). For example, at the individual glacier scale, the use of a scaling parameter *k* that has not been established for that glacier (i.e. the use of a mean, global value) can lead to large volume errors, as the fractional error in estimated volume is equal to the fractional error in *k* (Bahr et al., 2015). Applying a mean value of *k* to a single randomly selected glacier can cause volume errors of ~34%, based on a one standard deviation error in *k* (Bahr et al., 2015). However, for large populations of glaciers (n >100), volume-area scaling can give accurate estimates of their total volume even with significant errors in *k* (Bahr et al., 2015). Another issue that needs consideration is that when applied only to a part or subsection of a glacier, volume-area scaling significantly underestimates the correct volume, producing underestimations as large as 100% for those glaciers (Bahr et al., 2015). Given that some part of the boundary of Type 3 GLFs is connected to another ice body (Figure 3.1c), our volume estimation is likely conservative and the actual volume of ice stored in GLFs larger than that reported herein. Given the challenges of obtaining data able to resolve this issue (e.g. radar) and the likely range of differing conditions across the GLF population, it is difficult to quantify the value of this underestimation with any confidence and its constraint remains to be addressed by future studies.

3.3. Results

3.3.1. GLF outline mapping

From a total population of 1293 GLFs identified by Souness et al. (2012), we positively identified 1273 (~98 %) of them, with the remaining 20 being either unidentifiable or repeated GLFs in the earlier inventory. Mapping these 1273 GLFs resulted in 1243 unique entries, with 30 compound GLFs being re-classified as single GLFs. Of the total number of 1243 mapped GLFs, 698 (~56 %) are located in the northern hemisphere and 545 (~44 %) in the southern hemisphere (Figure 3.2).

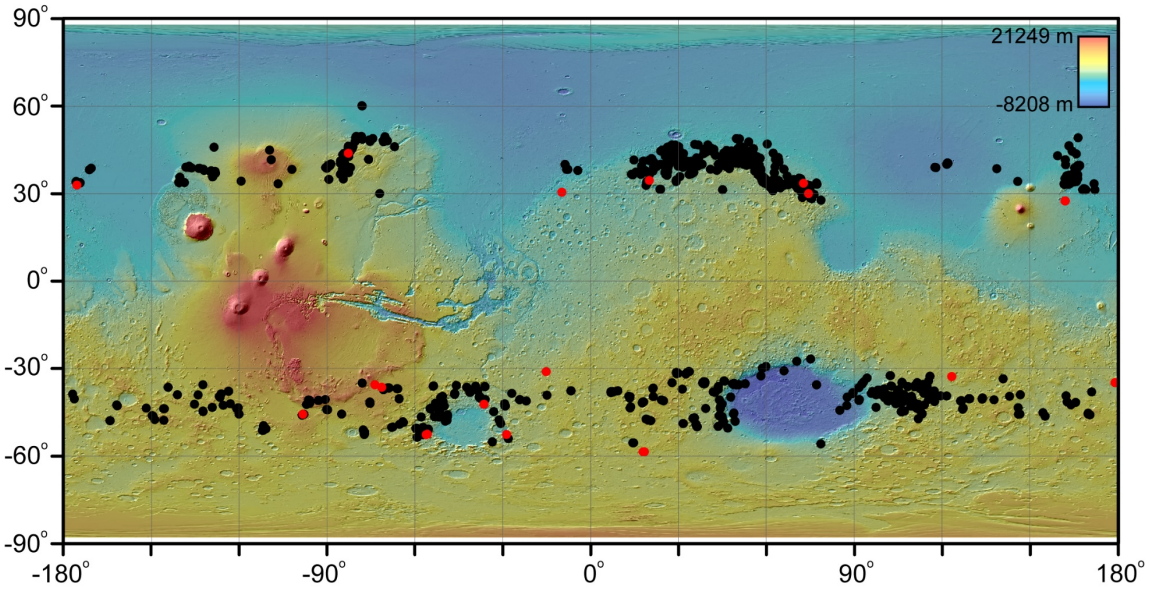

Figure 3.2: *Map of Mars showing the mid-latitude distribution of each mapped GLF (black dots). 1243 GLFs were mapped globally: 698 were located in the northern hemisphere and 545 were located in the southern hemisphere. Red dots identify the locations of the 20 GLFs not mapped in this study. Background map is MOLA elevation transparency overlain on a MOLA hillshade projection.*

3.3.2. GLF area

In total, the 1243 GLFs identified have a surface area of 11344 ± 393 km^2 (Table 3.2), equivalent to 0.01% of the total surface area of Mars. Of this surface area, 6680 ± 240 km^2 (~59 %) is in the northern hemisphere and 4664 ± 154 km^2 (~41 %) is in the southern hemisphere (Table 3.2). Global mean GLF area is 9.13 km^2 (std. dev. = 18.69), comprising 9.57 km^2 (std. dev. = 21.78) and 8.56 km^2 (std. dev. = 13.76) in the northern and southern hemispheres, respectively (Table 3.2).

3.3.3. GLF volume

The following analyses were carried out in terms of GLF volume only but, given the scaling method applied, similar relationships apply to GLF area.

Table 3.2: *Basic descriptive statistics for GLF area and volume.*

ROI	Area				Volume			
	Total (km^2)	Total (%)	Mean (km^2)	Std. dev.	Total (km^3)	Total (%)	Mean (km^3)	Std. dev.
Global	11343.93	100.0	9.13	18.69	1743.60	100.0	1.40	3.54
North	6679.75	58.9	9.57	21.78	1045.10	59.9	1.50	4.22
South	4664.17	41.1	8.56	13.76	698.49	40.1	1.28	2.41

3.3.3.1. Population-scale volume distribution

Spatial distribution by volume

We calculate the total martian GLF volume to be 1744 ± 441 km^3 (Table 3.2). Of this volume, 1045 ± 265 km^3 (~60 %) is in the northern hemisphere and 698 ± 175 km^3 (~40 %) is in the southern hemisphere (Table 3.2). Global mean GLF volume is 1.40 km^3 (std. dev. = 3.54), comprising 1.50 km^3 (std. dev. = 4.22) and 1.28 km^3 (std. dev. = 2.41) in the northern and southern hemispheres, respectively (Table 3.2).

Several regions show high volumetric contributions, including the 'fretted terrain' of the northern hemisphere and regions surrounding the Hellas impact basin in the southern hemisphere (Figures 3.3 and SF4). This distribution broadly reflects the overall GLF population (Figure SF2): mean GLF volume in these regions is similar to the hemispheric GLF mean (Figure 3.3). However, there are two regions where mean GLF volume has a statistically significant difference from the respective hemispheric mean; these are Tempe Terra (between -95 and -65^o longitude) in the northern hemisphere (P = 0.023) and surrounding the Argyre impact basin (between -65 and -20^o longitude) in the southern hemisphere (P = 0.016), where mean GLF volume increases to 2.85 and 2.31 km^3, respectively (Figure 3.3 and Table ST1).

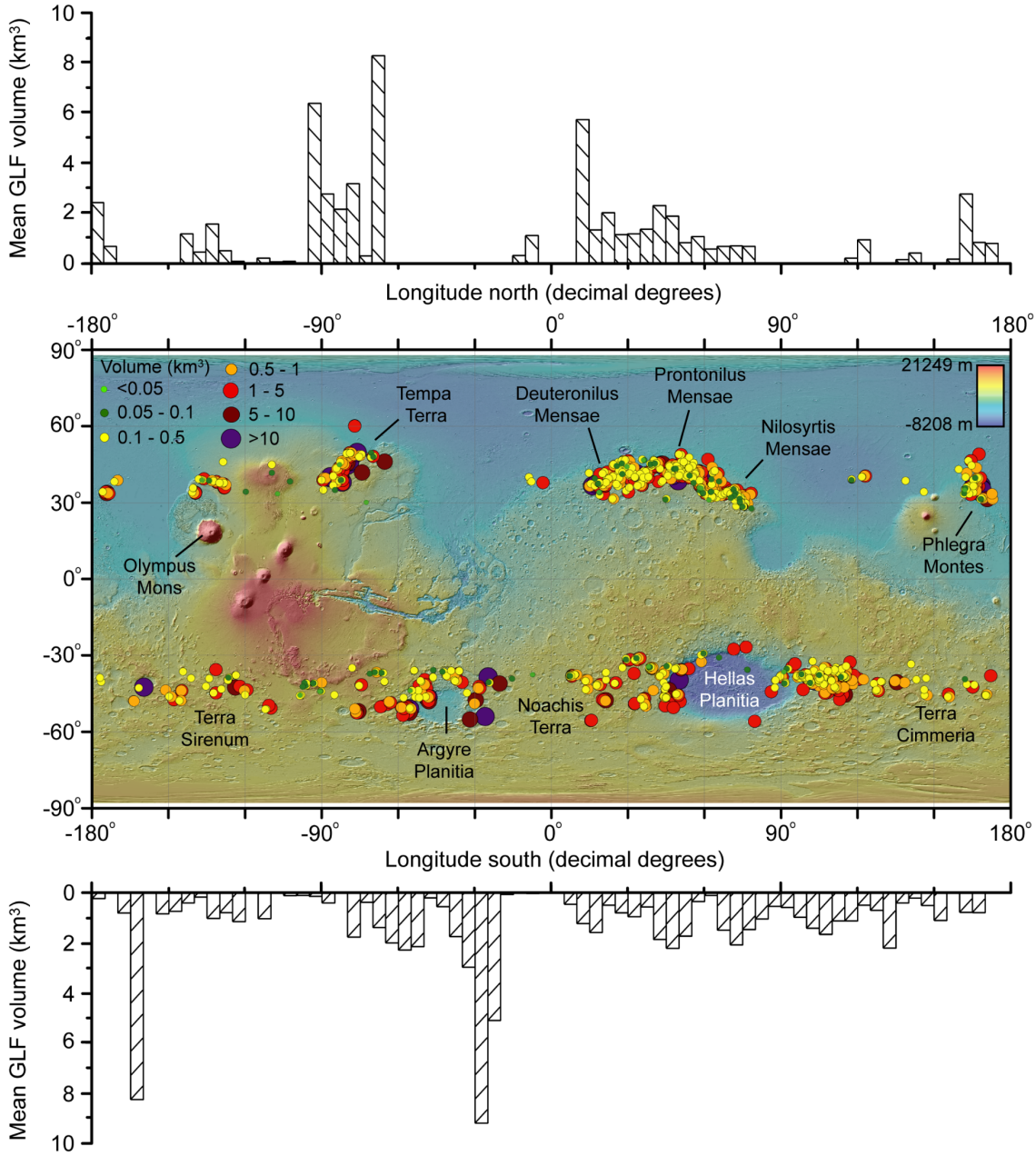

Figure 3.3: *Map of Mars showing the mid-latitude distribution of individual GLF volume. The colour and size of the circles represents the volume (km^3) of each GLF (green through to purple; larger circles = more volume). GLF volume is 1743.60 km^3 globally: 1045.10 km^3 is in the northern hemisphere and 698.49 km^3 is in the southern hemisphere. Bar plots, showing mean GLF volume in 5° longitude bins, for each hemisphere are presented above and below the distribution map. Background map as in Figure 3.2.*

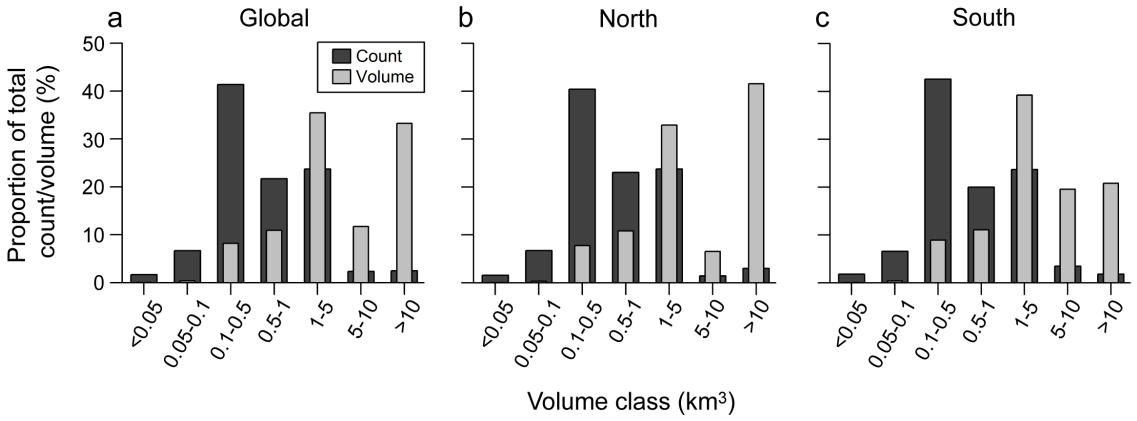

Figure 3.4: *GLF count and volume per size class for: (a) global, (b) northern hemisphere, and (c) southern hemisphere GLF populations.*

Size-class distribution by volume

The distribution of GLFs by count and total volume for selected size classes is summarised in Table ST7 of the supplementary material and the normalised (%) distribution presented in Figure 3.4. Globally, the distribution appears to be dominated by middle size-class GLFs, with ~87 % of the total count and ~55 % of the total volume contained within GLFs of volume 0.1 – 5 km^3. The two smallest size classes for volume (e.g. GLFs <0.1 km^3) host ~8 % of the total count but contain <1 % of the total volume. In contrast, only ~5 % of GLFs are in the two largest size classes for volume (e.g. GLFs >5 km^3), but they contribute ~45 % of the total volume (Figure 3.4a and Table ST7). On the whole, GLF size-class distribution is similar for both hemispheres (Figure 3.4b – c and Table ST7).

3.3.3.2. Environmental controls over GLF volume distribution

Latitude

Mean GLF volume increases with latitude such that GLFs located <36° north or south have mean volumes of 0.98 and 0.62 km^3 respectively, compared to mean volumes of 1.69 and 1.42 km^3 for those located >36° (Figure 3.5a and Table ST3). This difference in mean volume between GLFs located <36° and GLFs located >36° is statistically significant for both the northern (P = 0.006) and southern hemispheres (P = <0.001), thus revealing those lower-latitude GLFs have smaller average volumes than those

GLFs at higher-latitudes. This association is particularly strong in the southern hemisphere, where mean GLF volume increases to 3.27 km^3 at latitudes >48^o (Figure 3.5a and Table ST3).

Aspect

In both hemispheres GLFs flowing towards the north (NW, N, NE) are larger than those flowing towards the south (SE, S, SW) (Figure 3.5b – d and Table ST4). In the northern hemisphere GLFs with a northern aspect have a mean volume of 1.55 km^3 in contrast to a mean volume of 1.19 km^3 for GLFs with a southern aspect. This difference is stronger in the southern hemisphere where GLFs have mean volumes of 1.91 and 1.10 km^3 for northern and southern aspects, respectively. However, a statistically significant difference in mean volume between northern and southern flowing GLFs is noted only for the southern hemisphere (P = 0.024).

Slope

Mean GLF volume peaks on slopes between 2 and 4^o in the northern and southern hemispheres, respectively (Figure 3.5e – g and Table ST5). In both hemispheres, there is a statistically significant difference in mean volume between GLFs located on 2 – 8^o slopes and GLFs located on slopes outside the range of 2 – 8^o (P = <0.001), with the former having larger mean volumes of 2.94 and 2.46 km^3 and the later having smaller mean volumes of 0.71 and 0.95 km^3 for the northern and southern hemispheres, respectively. This association is enhanced in the northern hemisphere where a mean GLF volume of 7.13 km^3 is noted for GLFs on slopes between 2 and 4^o (Figure 3.5e – g and Table ST5). Plotting mean slope against GLF size (Figure 3.6) reveals that smaller GLFs show increased variability in slope where they are located compared to larger GLFs which show less variability and cover a narrower range of lower slope values.

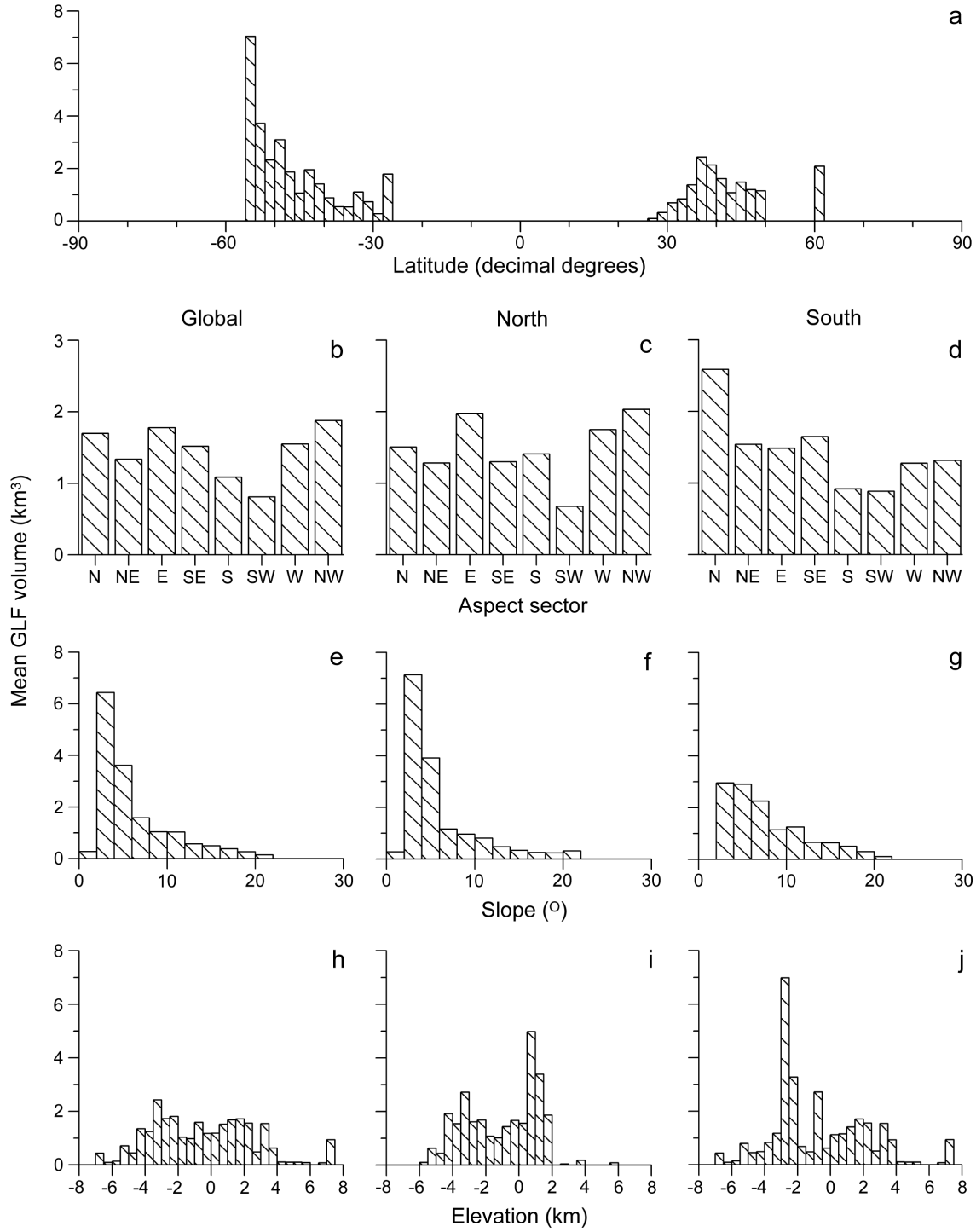

Figure 3.5: *Bar plots showing mean GLF volume (km^3) for: (a) global and hemispheric latitude in 2^o bins; (b) global, (c) northern and (d) southern hemispheric aspect in the eight cardinal and inter-cardinal directions; (e) global, (f) northern and (g) southern hemispheric slope in 2^o bins; (h) global, (i) northern hemisphere and (j) southern hemisphere elevation in 500 m bins.*

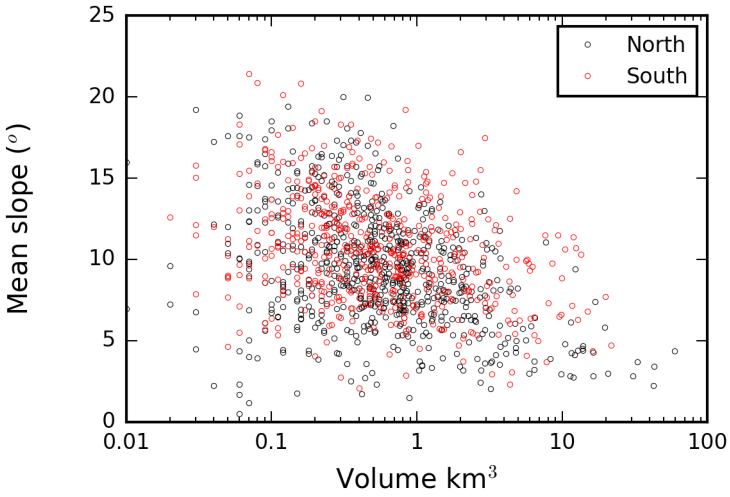

Figure 3.6: *Scatter plot showing GLF volume against mean GLF slope for each individual GLF. The distribution reveals inter-hemispheric similarity between the northern (black open circles) and southern hemispheres (red open circles).*

Elevation

Two zones host GLFs of increased mean volume, these are between -3500 and -2000 m, with a mean GLF volume of 1.86 km^3, and between 500 and 2500 m, with a mean GLF volume of 1.67 km^3 (Figure 3.5h – j and Table ST6). Although these peaks are visible in both the northern and southern hemisphere it does mask an inter-hemispheric contrast: in the northern hemisphere the mean GLF volume is greatest between 500 and 2500 m (3.73 km^3) and in the southern hemisphere mean GLF volume is greatest between -3500 and -2000 m (2.99 km^3). However, this difference in mean GLF volume is only statistically significant for those northern hemispheric GLFs between 500 and 2500 m ($P = 0.049$).

3.4. Interpretation and discussion

3.4.1. GLF volume distribution and contribution to mid-latitude ice

Globally, GLF volume is distributed similarly to the parent GLF population (Figures 3.3 and SF2), with several regions of high volume concentration along the martian dichotomy boundary, Tempa Terra and Phlegra Montes in the northern hemisphere and

to the east of the Hellas impact basin in the southern hemisphere. This spatial distribution is similar to the wider volume distribution of VFFs (LDA and LVF) in the mid-latitudes of Mars (e.g. Levy et al., 2014), indicating similarity in controls on GLF and VFF formation and/or preservation. Coupled with the observed spatial variation in GLF volume (Figures 3.3 and 3.4), these observations add further support to the hypothesis that regional to local meteorological and topographical conditions play an important role in VFF formation due to ice accumulation and preservation (Dickson et al., 2012; Levy et al., 2014; Brough et al., 2016a), and it is not exclusively a result of latitude-dependent insolation forcing. Under this scenario, specific atmospheric circulation patterns, driven by changes in orbital parameters, strongly influence the locations where glacial conditions persist, and could be an explanation for the spatial heterogeneity noted in the distribution of GLFs and the wider VFFs (e.g. Levy et al., 2014). Indeed, several studies using general circulation models (GCMs) for Mars have predicted, during periods of increased obliquity and atmospheric dust, ice accumulation in regions that match the observed VFF distribution (e.g. Forget et al., 2006; Madeleine et al., 2009).

Our estimated volume of 1744 ± 441 km^3 from mid-latitude GLFs does not take into account variations in the ice content of GLFs. Following Levy et al. (2014), we chose two end member scenarios to calculate ice content (see Section 3.1): scenario (i) favours a low ice content value of 30% by volume, as suggested by the ice assisted debris/rock glacier origin (e.g. Squyres, 1978, 1979); and scenario (ii) favours a high ice content value of 90% by volume, as suggested by the debris-covered glacier origin (e.g. Holt et al., 2008; Head et al., 2010). These two end member scenarios yield ice contributions of 523 ± 132 km^3 (480 ± 121 Gt) and 1570 ± 397 km^3 (1439 ± 364 Gt) for mid-latitude GLFs, or the equivalent of a global water layer between 3 ± 1 and 10 ± 3 mm thick. Although it is unlikely that all GLFs, and by extension VFFs, are compositionally homogeneous (e.g. Parson et al., 2011), converging evidence from morphological (Head et al., 2010), geophysical (Holt et al., 2008; Plaut et al., 2009) and numerical (Forget et al., 2006; Madeleine et al., 2009; Fastook et al., 2014) studies, point towards VFF formation through the accumulation of atmospherically derived ice. We therefore favour the (higher) debris-covered glacier ice volume estimate of 1570 ± 397 km^3 (1439 ± 364 Gt).

The VFF inventory of Levy et al. (2014), although being the most comprehensive to date, did not include GLFs in their ice volume estimation. Thus, the contribution of mid-latitude VFFs to the present day surface/near-surface water budget should be revised upwards to account for this. We note the concurrence of some 130 GLFs mapped in this inventory and those identified as part of the wider VFF analysis by Levy et al. (2014). These 130 GLFs have an estimated ice volume of 606 ± 154 km^3. Therefore, the remaining 1203 GLFs add an additional ice volume of between 341 ± 86 and 1024 ± 258 km^3 to the VFF estimate of Levy et al. (2014), based on our two end member scenarios.

Comparing the volume of GLFs (on the order of 10^3) to other ice deposits located in Mars' mid-latitudes (Table 3.3) reveals that they contribute about an order of magnitude less (on the order of 10^4) than the latitude-dependent mantle (Mustard et al., 2001; Kreslavsky and Head, 2002; Conway and Balme, 2014), LVF and CCF, and are of about two orders of magnitude less (on the order of 10^5) than LDA (Levy et al., 2014; Karlsson et al., 2015). In total, GLFs contribute an additional ice volume of ~0.4% to Mars' currently known mid-latitude deposits. On a global scale, GLFs contain <0.1% of the volume of ice stored in the polar ice caps (Table 3.3), thus GLFs contribute only a minor component to the present day surface/near-surface water budget (e.g. Carr and Head 2015). However, taking into account the degraded nature of many GLFs (Brough et al., 2016a), it is possible that they once contributed a much larger volume to Mars' water budget. Furthermore, given that many GLFs are clearly demarcated by metres high MLR (e.g. Hubbard et al., 2011) and/or coalesce into the wider glacial valley landsystem (e.g. Head et al., 2010), they likely constitute an important component to the erosion and supply of debris in mid-latitude environments (Levy et al., 2016) and, given their Late Amazonian age, may represent some of the most recent geomorphological activity on Mars (Hubbard et al., 2014; Brough et al., 2016a).

Table 3.3: *Ice volume estimates and global equivalent water layer thickness for several mid-latitude landforms. The two polar caps are included for comparison.*

Landform	Ice volume (km^3)	Global equivalent water layer (m)	References
Glacier-like forms	$0.52 – 1.57 \times 10^3$	0.003 – 0.010	This study
North Polar Cap	$0.82 – 1.14 \times 10^6$	5.2 – 7.2	Smith et al., 2001; Putzig et al., 2009
South Polar Cap	$1.20 – 1.70 \times 10^6$	7.6 – 10.8	Zubar et al., 1998; Plaut et al., 2007
Lobate debris aprons	$0.79 – 2.36 \times 10^5$	0.50 – 1.50	Levy et al., 2014; Karlsson et al., 2015
Concentric crater fill	$2.63 – 7.88 \times 10^4$	0.17 – 0.50	Levy et al., 2014
Lineated valley fill	$1.95 – 5.86 \times 10^4$	0.12 – 0.37	Levy et al., 2014
Latitude-dependent mantle	$1.00 – 8.00 \times 10^4$	0.06 – 0.51	Mustard et al., 2001; Kreslavsk and Head, 2002; Conway and Balme, 2014

3.4.2. Controls on GLF volume

3.4.2.1. Latitude

Latitude has a systematic control over GLF volume with an increase in mean GLF volume with increasing latitude, particularly enhanced in the southern hemisphere (Figure 3.5a and Table ST3). This relationship is highlighted by the difference in mean GLF volume when comparing GLFs at lower latitudes ($<36^o$) to those GLFs at higher latitudes ($>36^o$). There are two potential explanations as to why lower latitude GLFs are on average smaller than higher latitude GLFs. First, on Earth, the distribution of glacier ice (area and volume) can, other things being equal, be controlled by the proximity to a precipitation source with glaciers in regions farther from a source diminishing in size (Koerner, 1977). Thus, given that the polar regions are the principal source areas of mass exchange with the mid-latitudes during climatic fluctuations (e.g. Head et al.,

2003), it is possible that lower latitude regions receive less mass during initial emplacement due to their distance from the contributing moisture source. Second, the latitudinal boundary of 36°, above which mean GLF volume increases, is close to the current stability threshold for shallow ground ice, which places ice stability at latitudes pole-ward of 40 – 45° (Mellon and Jakosky, 1995; Mellon et al., 2004). Therefore, the mean volume difference between GLFs below and above 36° north and south can be explained by the fact that ice below the latitudinal threshold for ice stability is susceptible to preferential removal via sublimation/ablation – indeed GLFs at latitudes <40° have previously been shown as preferential sites of recession compared to GLFs at latitudes >40° (Brough et al., 2016a). Accordingly, it is possible that at least two differing signals are contributing to the observed latitudinal pattern in mean GLF volume, with one related to initial reduced ice emplacement in, and the other to preferential ice removal from, GLFs at latitudes <36°. Although the exact influence and contribution of these two factors to GLF size remains unknown, it does offer viable explanations for the observed difference in mean GLF volume between latitudes above and below 36°.

3.4.2.2. Aspect

Although, as expected, pole-ward facing GLFs predominate in the southern hemisphere (Figure SF3 [Souness et al., 2012]), these GLFs are smaller and contain less mass on average than those facing north (Figure 3.5d). In terrestrial scenarios pole-ward facing alcoves are often preferential locations for ice accumulation and/or preservation due to reduced insolation (Unwin, 1973). However, our observations of equator-facing GLFs being on average larger than pole-ward facing GLFs suggests that a purely insolation driven argument cannot be invoked for GLFs in the southern hemisphere, or the effect is overwhelmed by a counteracting process. This pattern suggests that insolation alone does not control GLF volume in the southern hemisphere and again points to the possibility that local meteorological and topographical conditions can play an important role in ice accumulation and preservation (Dickson et al., 2012; Levy et al., 2014; Brough et al., 2016a).

3.4.2.3. Slope

GLFs located on slopes between 2 and 8^{o} have the largest average volume (Figure 3.5e – g and Table ST5). The influence of slope on glacier thickness on Earth is well-established and shows that larger glaciers tend to have lower mean slopes and smaller glaciers tend to have steeper slopes, principally due to the influence of slope on driving stress and hence velocity (Cuffey and Paterson, 2010). Thus, suggesting that slope process may have a similar influence on martian GLFs as their Earth based counterparts.

In terms of the relationship between mean slope and GLF size (Figure 3.6), the increase in the variability of slope values for smaller GLFs reveals that smaller GLFs are less sensitive to their topographic settings than larger GLFs, implying that smaller GLFs can form in a wider range of terrain. This again suggests that, for smaller GLFs, local meteorological and topographical conditions can combine to provide microclimates favourable for the accumulation and/or preservation of ice. A similar effect has been reported in relation to the topographic setting of glaciers in the European Alps on Earth (e.g. Paul et al., 2011). As a consequence, the increased topographic variability observed for small GLFs may affect their response to current/future climatic perturbations, such that small GLFs that are of comparable size may show variable responses to the same climatic perturbation.

3.4.2.4. Elevation

Mean GLF volume is noticeably larger between the elevations of 500 and 2500 m in the northern hemisphere, suggesting this zone holds some control over GLF volume (Figure 3.5h – j and Table ST6). Plotting the distribution of these northern hemisphere GLFs indicates that they cluster around Tempa Terra (Figure 3.7). This suggests that GLF volume may be related to a combination of both elevation and local to regional meteorological conditions providing favourable conditions for ice accumulation and/or preservation. Indeed, large-scale martian atmospheric modelling indicates that high net ice accumulation is predicted in Tempa Terra under high obliquity conditions (e.g. Madeleine et al., 2009).

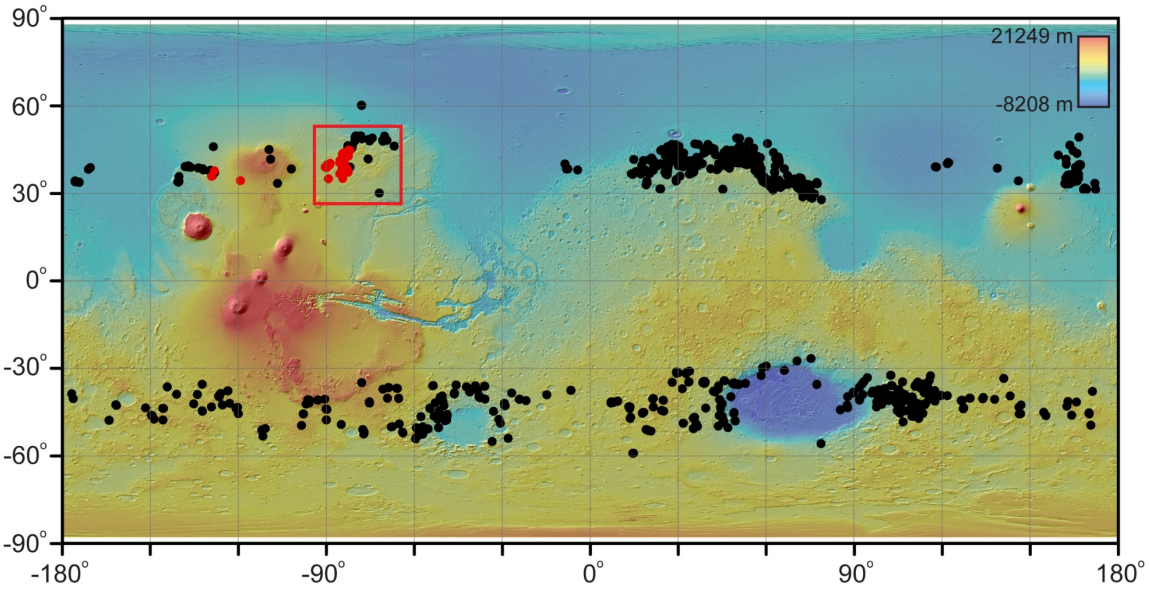

Figure 3.7: *Map of Mars showing distribution of elevation zones of high mean GLF volume. Red circles (n = 34) denote the distribution of northern hemisphere GLFs between 500 and 2500 m. Note the predominance of GLFs in the Tempa Terra region (red box).*

3.4.3. Implications for Late Amazonian glaciation on Mars

Age estimates place GLFs as young surface landforms <50 Ma and likely <10 Ma old (Arfstrom and Hartmann, 2005; Hartmann et al., 2014), but our understanding of when or for how long glacial conditions are required for GLF formation is uncertain. A mean ice thickness of ~130 m was calculated from the area and volume of each GLF in our analysis. Under a 10 mm a^{-1} accumulation rate possible during climatic excursions of high obliquity (e.g. Madeleine et al., 2009), ice of this thickness could have accumulated within ~13 ka assuming no influent mass from beyond GLF boundaries. Considering each high obliquity excursion, which were common earlier than 300 ka ago, last on the order of 20 – 40 ka (Laskar et al., 2002; Head et al., 2003) it is possible that Mars' current GLF volume could have been emplaced during a single event – as suggested for the associated latitude-dependant mantle (Conway and Balme, 2014). However, as ~33 % of the GLF population shows evidence of ablation and mass loss (Brough et al., 2016a) it is likely that a more complex formation history exists, perhaps requiring multiple high obliquity accumulation cycles, a scenario proposed to explain

the formation of some larger VFFs (e.g. Parsons and Holt, 2016). Considering there has been over 15 high obliquity periods during the last 2 Ma (Laskar et al., 2002; Head et al., 2003), such a scenario is plausible and indeed, likely (e.g. Milliken et al., 2003). Therefore, the timespan for formation of ~13 ka should be viewed as an absolute minimum limit. As with the wider VFF deposits (e.g. Fastook et al., 2014; Parsons and Holt, 2016), constraining the environmental conditions and timespan required to form GLFs can be tested with numerical ice flow models if appropriate boundary conditions are known and is a direction for future research.

3.5. Conclusions

A new population-scale GLF inventory was compiled through a combination of MOLA topographic data and directly mapped outlines of 1243 GLFs from CTX imagery. We used these products to: (i) provide the first ice volume estimate of GLFs to the mid-latitude surface/near surface water budget on Mars; (ii) improve our understanding of the controls on GLF formation and evolution; and (iii) assess their formation in relation to the most recent high obliquity climatic excursions on Mars. From these investigations, we conclude the following:

- GLF area was calculated to be 11344 ± 393 km^2, equivalent to ~0.01 % of the total surface area of Mars. Of this surface area, 6680 ± 240 km^2 (~59 %) is in the northern hemisphere and 4664 ± 154 km^2 (~41 %) is in the southern hemisphere.

- GLF volume was calculated to be 1744 ± 441 km^3. Using two end member scenarios the actual population-scale ice volume contribution is found to be 523 ± 132 km^3 (480 ± 121 Gt) for a pore ice content (30 % ice by volume) scenario and 1570 ± 397 km^3 (1439 ± 364 Gt) for a debris-covered glacier (90 % ice by volume) scenario. This mapped out to a global equivalent water layer of between 3 ± 1 and 10 ± 3 mm thick. Based on converging morphological, geophysical and numerical evidence pointing towards GLF/VFF formation through the accumulation of atmospherically derived ice, we favour the (higher) debris-covered glacier estimate.

- GLF deposits represent an ice volume contribution on the order of 10^3 km^3, between one and two orders of magnitude less than those reported for LDM, LDA, LVF and CCF (Mustard et al., 2001; Kreslavsky and Head, 2002; Conway and Balme, 2014; Levy et al., 2014; Karlsson et al., 2015). GLFs contribute an equivalent of 0.4 % of currently known mid-latitude ice deposits.

- Coupling mean thickness estimates with GCM derived ice accumulation rates (e.g. Madeleine et al., 2009) suggests that GLFs require at least 13 ka to obtain the equivalent mass currently stored in these features. This places a minimum boundary on the duration of ice emplacement that is less than one high obliquity cycle. Although we do not rule out the possibility that formation requires multiple depositional cycles and suggest that better understanding the required formation conditions for GLFs be a priority research area.

- Spatial patterns of GLF landform and volume distribution suggest that regional to local meteorological and topographical conditions play an important role in GLF ice accumulation and preservation. Specifically, GLF location and volume, although influenced by, is not simply a relation of latitudinal dependence or insolation driven factors and that variation in physical environments is also important in providing microclimates favourable for the accumulation and/or preservation of ice.

- Assessment of the environmental conditions that influence GLF accumulation and/or preservation revealed that GLF size is, to a certain extent, controlled by their physical setting. Specifically, GLFs globally are on average larger in latitudes >36^o and on slopes between 2 and 8^o. In the northern hemisphere GLFs between 500 and 2500 m in elevation and in the southern hemisphere GLFs with a northern aspect are also larger on average.

Acknowledgements

SB is funded by an Aberystwyth University Doctoral Career Development Scholarship. AH gratefully acknowledges support from the Research Council of Norway through its Centres of Excellence funding scheme, project number 223259. We are grateful to Souness et al. (2012) and Levy et al. (2014) for making their inventory data, analysed within this study, freely available.

References

Arfstrom, J., & Hartmann, W. K. (2005). Martian flow features, moraine-like ridges, and gullies: Terrestrial analogs and interrelationships. *Icarus, 174*(2), 321-335. doi: 10.1016/j.icarus.2004.05.026.

Bahr, D. B., Pfeffer, W. T., & Kaser, G. (2015). A review of volume-area scaling of glaciers. *Reviews of Geophysics, 53*(1), 95-140. doi: 10.1002/2014RG000470.

Berman, D. C., Crown, D. A., & Joseph, E. C. S. (2015). Formation and mantling ages of lobate debris aprons on Mars: Insights from categorized crater counts. *Planetary and Space Science, 111*, 83-99. doi: 10.1016/j.pss.2015.03.013.

Brough, S., Hubbard, B., & Hubbard, A. (2016a). Former extent of glacier-like forms on Mars. *Icarus, 274*, 37-49. doi: 10.1016/j.icarus.2016.03.006.

Brough, S., Hubbard, B., Souness, C., Grindrod, P. M., & Davis, J. (2016b). Landscapes of polyphase glaciation: eastern Hellas Planitia, Mars. *Journal of Maps, 12*(3), 530-542. doi: 10.1080/17445647.2015.1047907.

Carr, M. H., & Head, J. W. (2015). Martian surface/near-surface water inventory: Sources, sinks, and changes with time. *Geophysical Research Letters*, 2014GL062464. doi: 10.1002/2014gl062464.

Conway, S. J., & Balme, M. R. (2014). Decameter thick remnant glacial ice deposits on Mars. *Geophysical Research Letters, 41*(15), 2014GL060314. doi: 10.1002/2014gl060314.

Cuffey, K. M., & Paterson, W. S. B. (2010). *The Physics of Glaciers* (4th ed.). Oxford: Butterworth-Heinemann.

Daubar, I. J., McEwen, A. S., Byrne, S., Kennedy, M. R., & Ivanov, B. (2013). The current martian cratering rate. *Icarus, 225*(1), 506-516. doi:

10.1016/j.icarus.2013.04.009.

Dickson, J. L., Head, J. W., & Marchant, D. R. (2008). Late Amazonian glaciation at the dichotomy boundary on Mars: Evidence for glacial thickness maxima and multiple glacial phases. *Geology, 36*(5), 411-414. doi: 10.1130/g24382a.1.

Dickson, J. L., Head, J. W., & Fassett, C. I. (2012). Patterns of accumulation and flow of ice in the mid-latitudes of Mars during the Amazonian. *Icarus, 219*(2), 723-732. doi: 10.1016/j.icarus.2012.03.010.

Farinotti, D., Brinkerhoff, D. J., Clarke, G. K. C., Fürst, J. J., Frey, H., Gantayat, P., Gillet-Chaulet, F., Girard, C., Huss, M., Leclercq, P. W., Linsbauer, A., Machguth, H., Martin, C., Maussion, F., Morlighem, M., Mosbeux, C., Pandit, A., Portmann, A., Rabatel, A., Ramsankaran, R. A. A. J., Reerink, T. J., Sanchez, O., Stentoft, P. A., Kumari, S. S., van Pelt, W. J. J., Anderson, B., Benham, T., Binder, D., Dowdeswell, J. A., Fischer, A., Helfricht, K., Kutuzov, S., Lavrentiev, I., McNabb, R., Gudmundsson, G. H., Li, H., & Andreassen, L. M. (2017). How accurate are estimates of glacier ice thickness? Results from ITMIX, the Ice Thickness Models Intercomparison eXperiment. *The Cryosphere, 11*(2), 949-970. doi: 10.5194/tc-11-949-2017.

Fassett, C. I., Levy, J. S., Dickson, J. L., & Head, J. W. (2014). An extended period of episodic northern mid-latitude glaciation on Mars during the Middle to Late Amazonian: Implications for long-term obliquity history. *Geology, 42*(9), 763-766. doi: 10.1130/g35798.1.

Fastook, J. L., Head, J. W., & Marchant, D. R. (2014). Formation of lobate debris aprons on Mars: Assessment of regional ice sheet collapse and debris-cover armoring. *Icarus, 228*, 54-63. doi: 10.1016/j.icarus.2013.09.025.

Forget, F., Haberle, R. M., Montmessin, F., Levrard, B., & Head, J. W. (2006). Formation of glaciers on Mars by atmospheric precipitation at high obliquity. *Science, 311*(5759), 368-371. doi: 10.1126/science.1120335.

Hartmann, W. K., Ansan, V., Berman, D. C., Mangold, N., & Forget, F. (2014). Comprehensive analysis of glaciated martian crater Greg. *Icarus, 228*, 96-120. doi: 10.1016/j.icarus.2013.09.016.

Head, J. W., Mustard, J. F., Kreslavsky, M. A., Milliken, R. E., & Marchant, D. R. (2003). Recent ice ages on Mars. *Nature, 426*(6968), 797-802. doi: 10.1038/Nature02114.

Head, J. W., Marchant, D. R., Dickson, J. L., Kress, A. M., & Baker, D. M. (2010).

Northern mid-latitude glaciation in the Late Amazonian period of Mars: Criteria for the recognition of debris-covered glacier and valley glacier landsystem deposits. *Earth and Planetary Science Letters, 294*(3-4), 306-320. doi: 10.1016/j.epsl.2009.06.041.

Holt, J. W., Safaeinili, A., Plaut, J. J., Head, J. W., Phillips, R. J., Seu, R., Kempf, S. D., Choudhary, P., Young, D. A., Putzig, N. E., Biccari, D., & Gim, Y. (2008). Radar Sounding Evidence for Buried Glaciers in the Southern Mid-Latitudes of Mars. *Science, 322*(5905), 1235-1238. doi: 10.1126/science.1164246.

Hubbard, B., Souness, C., & Brough, S. (2014). Glacier-like forms on Mars. *The Cryosphere, 8*(6), 2047-2061. doi: 10.5194/tc-8-2047-2014.

Hubbard, B., Milliken, R. E., Kargel, J. S., Limaye, A., & Souness, C. (2011). Geomorphological characterisation and interpretation of a mid-latitude glacier-like form: Hellas Planitia, Mars. *Icarus, 211*(1), 330-346. doi: 10.1016/j.icarus.2010.10.021.

Karlsson, N. B., Schmidt, L. S., & Hvidberg, C. S. (2015). Volume of Martian midlatitude glaciers from radar observations and ice flow modeling. *Geophysical Research Letters, 42*(8), 2015GL063219. doi: 10.1002/2015gl063219.

Koerner, R. M. (1977). Ice thickness measurements and their implications with respect to past and present ice volumes in the Canadian High Arctic ice caps. *Canadian Journal of Earth Sciences, 14*(12), 2697-2705. doi: 10.1139/e77-237.

Kreslavsky, M. A., & Head, J. W. (2002). Mars: Nature and evolution of young latitude-dependent water-ice-rich mantle. *Geophysical Research Letters, 29*(15). doi: 10.1029/2002gl015392.

Laskar, J., Levrard, B., & Mustard, J. F. (2002). Orbital forcing of the martian polar layered deposits. *Nature, 419*(6905), 375-377. doi: 10.1038/Nature01066.

Laskar, J., Correia, A. C. M., Gastineau, M., Joutel, F., Levrard, B., & Robutel, P. (2004). Long term evolution and chaotic diffusion of the insolation quantities of Mars. *Icarus, 170*(2), 343-364. doi: 10.1016/j.icarus.2004.04.005.

Levy, J. S., Head, J. W., & Marchant, D. R. (2007). Lineated valley fill and lobate debris apron stratigraphy in Nilosyrtis Mensae, Mars: Evidence for phases of glacial modification of the dichotomy boundary. *Journal of Geophysical Research, 112*(E8). doi: 10.1029/2006je002852.

Levy, J. S., Fassett, C. I., & Head, J. W. (2016). Enhanced erosion rates on Mars during Amazonian glaciation. *Icarus, 264*, 213-219. doi: 10.1016/j.icarus.2015.09.037.

Levy, J. S., Fassett, C. I., Head, J. W., Schwartz, C., & Watters, J. L. (2014). Sequestered glacial ice contribution to the global Martian water budget: Geometric constraints on the volume of remnant, midlatitude debris-covered glaciers. *Journal of Geophysical Research: Planets, 119*(10), 2014JE004685. doi: 10.1002/2014je004685.

Mackay, S. L., & Marchant, D. R. (2017). Obliquity-paced climate change recorded in Antarctic debris-covered glaciers. *Nature Communications, 8*, 14194. doi: 10.1038/ncomms14194.

Madeleine, J. B., Forget, F., Head, J. W., Levrard, B., Montmessin, F., & Millour, E. (2009). Amazonian northern mid-latitude glaciation on Mars: A proposed climate scenario. *Icarus, 203*(2), 390-405. doi: 10.1016/j.icarus.2009.04.037.

Mellon, M. T., & Jakosky, B. M. (1995). The distribution and behavior of Martian ground ice during past and present epochs. *Journal of Geophysical Research: Planets, 100*(E6), 11781-11799. doi: 10.1029/95je01027.

Mellon, M. T., Feldman, W. C., & Prettyman, T. H. (2004). The presence and stability of ground ice in the southern hemisphere of Mars. *Icarus, 169*(2), 324-340. doi: 10.1016/j.icarus.2003.10.022.

Milliken, R. E., Mustard, J. F., & Goldsby, D. L. (2003). Viscous flow features on the surface of Mars: Observations from high-resolution Mars Orbiter Camera (MOC) images. *Journal of Geophysical Research: Planets, 108*(E6). doi: 10.1029/2002je002005.

Mustard, J. F., Cooper, C. D., & Rifkin, M. K. (2001). Evidence for recent climate change on Mars from the identification of youthful near-surface ground ice. *Nature, 412*(6845), 411-414. doi: 10.1038/35086515.

Parsons, R., & Holt, J. (2016). Constraints on the formation and properties of a Martian lobate debris apron: Insights from high-resolution topography, SHARAD radar data, and a numerical ice flow model. *Journal of Geophysical Research: Planets*, 2015JE004927. doi: 10.1002/2015je004927.

Parsons, R., Nimmo, F., & Miyamoto, H. (2011). Constraints on martian lobate debris apron evolution and rheology from numerical modeling of ice flow. *Icarus*, *214*(1), 246-257. doi: 10.1016/j.icarus.2011.04.014.

Paul, F. (2007). *The new Swiss glacier inventory 2000 - application of remote sensing and GIS*. Universitat Zurich: Schriftenreihe Physische Geographie.

Paul, F., Frey, H., & Le Bris, R. (2011). A new glacier inventory for the European Alps

from Landsat TM scenes of 2003: challenges and results. *Annals of Glaciology, 52*(59), 144-152. doi: 10.3189/172756411799096295.

Paul, F., Barry, R. G., Cogley, J. G., Frey, H., Haeberli, W., Ohmura, A., Ommanney, C. S. L., Raup, B., Rivera, A., & Zemp, M. (2009). Recommendations for the compilation of glacier inventory data from digital sources. *Annals of Glaciology*, *50*(53), 119-126. doi: 10.3189/172756410790595778.

Paul, F., Barrand, N. E., Baumann, S., Berthier, E., Bolch, T., Casey, K., Frey, H., Joshi, S. P., Konovalov, V., Le Bris, R., Molg, N., Nosenko, G., Nuth, C., Pope, A., Racoviteanu, A., Rastner, P., Raup, B., Scharrer, K., Steffen, S., & Winsvold, S. (2013). On the accuracy of glacier outlines derived from remote-sensing data. *Annals of Glaciology, 54*(63), 171-182. doi: 10.3189/2013AOG63A296.

Plaut, J. J., Safaeinili, A., Holt, J. W., Phillips, R. J., Head, J. W., Seu, R., Putzig, N. E., & Frigeri, A. (2009). Radar evidence for ice in lobate debris aprons in the mid-northern latitudes of Mars. *Geophysical Research Letters, 36*(2). doi: 10.1029/2008gl036379.

Plaut, J. J., Picardi, G., Safaeinili, A., Ivanov, A. B., Milkovich, S. M., Cicchetti, A., Kofman, W., Mouginot, J., Farrell, W. M., Phillips, R. J., Clifford, S. M., Frigeri, A., Orosei, R., Federico, C., Williams, I. P., Gurnett, D. A., Nielsen, E., Hagfors, T., Heggy, E., Stofan, E. R., Plettemeier, D., Watters, T. R., Leuschen, C. J., & Edenhofer, P. (2007). Subsurface radar sounding of the south polar layered deposits of Mars. *Science, 316*(5821), 92-95. doi: 10.1126/science.1139672.

Putzig, N. E., Phillips, R. J., Campbell, B. A., Holt, J. W., Plaut, J. J., Carter, L. M., Egan, A. F., Bernardini, F., Safaeinili, A., & Seu, R. (2009). Subsurface structure of Planum Boreum from Mars Reconnaissance Orbiter Shallow Radar soundings. *Icarus, 204*(2), 443-457. doi: 10.1016/j.icarus.2009.07.034.

Racoviteanu, A. E., Paul, F., Raup, B., Khalsa, S. J. S., & Armstrong, R. (2009). Challenges and recommendations in mapping of glacier parameters from space: results of the 2008 Global Land Ice Measurements from Space (GLIMS) workshop, Boulder, Colorado, USA. *Annals of Glaciology*, *50*(53), 53-69. doi: 10.3189/172756410790595804.

Smith, D. E., Zuber, M. T., Frey, H. V., Garvin, J. B., Head, J. W., Muhleman, D. O., Pettergill, G. H., Phillips, R. J., Solomon, S. C., Zwally, H. J., Banerdt, W. B., Duxbury, T. C., Golombek, M. P., Lemoine, F. G., Neumann, G. A., Rowlands,

D. D., Aharonson, O., Ford, P. G., Ivanov, A. B., Johnson, C. L., McGovern, P. J., Abshire, J. B., Afzal, R. S., & Sun, X. (2001). Mars Orbiter Laser Altimeter: Experiment summary after the first year of global mapping of Mars. *Journal of Geophysical Research: Planets, 106*(E10), 23689-23722. doi: 10.1029/2000je001364.

Smith, M. J. (2011). Digital Mapping: Visualisation, Interpretation and Quantification of Landforms. In Smith, M. J., Paron, P., & Griffiths, J. (Eds.), *Geomorphological Mapping: Methods and Applications*. Oxford: Elsevier, 225 – 251.

Souness, C., Hubbard, B., Milliken, R. E., & Quincey, D. (2012). An inventory and population-scale analysis of martian glacier-like forms. *Icarus, 217*(1), 243-255. doi: 10.1016/j.icarus.2011.10.020.

Squyres, S. W. (1978). Martian Fretted Terrain - Flow of Erosional Debris. *Icarus, 34*(3), 600-613. doi: 10.1016/0019-1035(78)90048-9.

Squyres, S. W. (1979). Distribution of Lobate Debris Aprons and Similar Flows on Mars. *Journal of Geophysical Research, 84*, 8087-8096. doi: 10.1029/Jb084ib14p08087.

Squyres, S. W., & Carr, M. H. (1986). Geomorphic Evidence for the Distribution of Ground Ice on Mars. *Science, 231*(4735), 249-252. doi: 10.1126/science.231.4735.249.

Unwin, D. J. (1973). The Distribution and Orientation of Corries in Northern Snowdonia, Wales. *Transactions of the Institute of British Geographers*(58), 85-97. doi: 10.2307/621583.

Zuber, M. T., Smith, D. E., Solomon, S. C., Abshire, J. B., Afzal, R. S., Aharonson, O., Fishbaugh, K., Ford, P. G., Frey, H. V., Garvin, J. B., Head, J. W., Ivanov, A. B., Johnson, C. L., Muhleman, D. O., Neumann, G. A., Pettengill, G. H., Phillips, R. J., Sun, X., Zwally, H. J., Banerdt, W. B. & Duxbury, T. C. (1998). Observations of the North Polar Region of Mars from the Mars Orbiter Laser Altimeter. *Science, 282*(5396), 2053-2060. doi: 10.1126/science.282.5396.2053.

Supplementary Material Ch. 3

Area and volume of mid-latitude glacier-like forms on Mars

Stephen BROUGH[a], Bryn HUBBARD[a] and Alun HUBBARD[a,b]

[a]*Department of Geography and Earth Sciences, Aberystwyth University, Aberystwyth, UK*

[b]*Centre for Arctic Gas Hydrate, Environment and Climate, Department of Geology, University of Tromsø, Tromsø, Norway*

This is supplementary material to an article under review for publication in *Earth and Planetary Science Letters*, submitted on 15/08/2017.

This supplementary material consists of five figures, seven tables and a geographic information system (GIS) ready version of the glacier-like form (GLF) inventory. The supplementary material is organised as follows:

Supplementary figures and tables: Figure SF1 presents two examples of compound GLFs and their manually digitised outlines. Figures SF2 – SF5 present the raw GLF count and total volume of those GLFs in various size classes for longitude (^{o}), latitude (^{o}), aspect sector (cardinal and inter-cardinal direction), slope (^{o}) and elevation (m). The numerical values for these size classes are presented in Tables ST2 – ST6; this data provides the basis for Figures 3.3 and 3.5 of the corresponding manuscript. Table ST1 summarises two sample t-test results for selected longitude (^{o}), latitude (^{o}), aspect sector (cardinal and inter-cardinal direction), slope (^{o}) and elevation (m) zones discussed in the corresponding manuscript. Table ST7 summarises the distribution of GLFs by count and total volume of those GLFs in selected size classes; this data provides the basis for Figure 3.4 of the corresponding manuscript.

GLF_inventroy.zip: The GIS shapefile and associated metadata for the GLF inventory can be accessed at:
https://www.dropbox.com/s/p9hoe3idotzp8ts/GLF_inventory.zip?dl=0.

The header information for the GIS attribute table is summarised below:

Parameter	Description	Unit
GLF_ID	Unique ID for each GLF entry	-
GLF_ID_Sou	Corresponding ID from the inventory of Souness et al. (2012) *Icarus*, **217**, 243-255	-
x_dd	Longitude coordinate in decimal degrees	^{o}
y_dd	Latitude coordinate in decimal degrees	^{o}
area_km2	GLF area	km^2
vol_km3	GLF volume	km^3
elev_min	Minimum GLF elevation	m
elev_max	Maximum GLF elevation	m
elev_mean	Mean GLF elevation	m
elev_media	Median GLF elevation	m
elev_std	Standard deviation of GLF elevation	m
slope_mean	Mean GLF slope (degrees)	^{o}
aspect_360	GLF aspect (0-360)	^{o}
aspect_sec	GLF aspect divided into eight cardinal and inter-cardinal directions (N, NE, E, SE, S, SW, W, NW)	-
deposit_ty	Relationship of GLF to surrounding terrain classified into Type 1; Type 2 or Type 3 (see Section 2.2 of the corresponding manuscript for full description)	-
Levy_2014	Does GLF overlap with VFFs of Levy et al. (2014) *JGR: Planets*, **119**, 2188-2196? 1 = no; 2 = yes	-

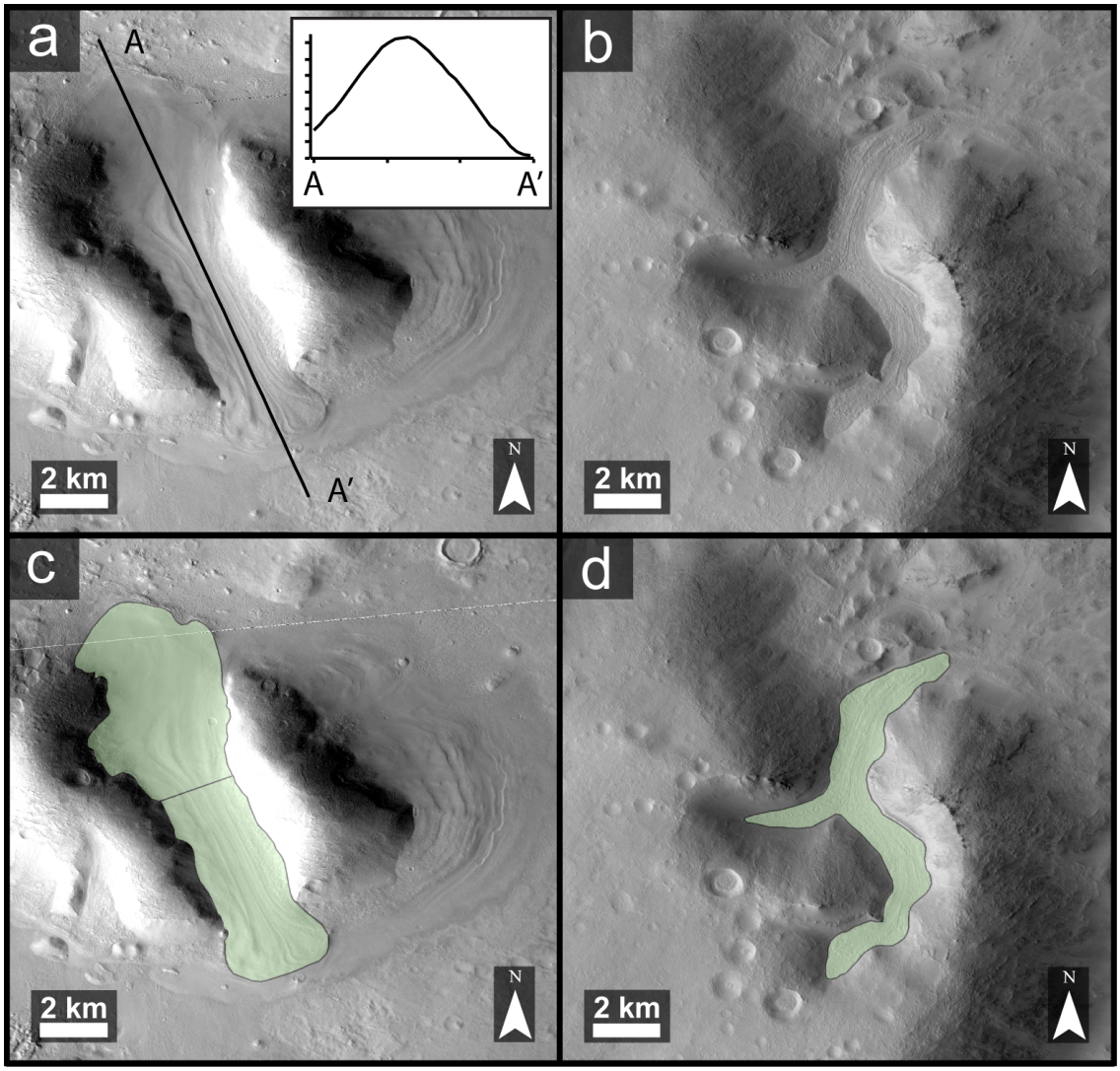

SF1: *Examples of compound GLFs (a and b) and their manually digitised outlines (c and d). (a) Divergent GLFs. As depicted in transect A – A' (x-axis 0 to 15 km; y-axis -2700 to -2000 m) two GLFs flow away from a central divide and both terminate with a distinct lobate form. Such entries are mapped as two separate GLFs, with the divide located at the topographic peak (Subset of CTX image P16_007451_2211_XI_41N303W; centred on ~56.35° E, 42.14° N). (b) Converging GLFs. Two GLFs in separate valleys coalesce and terminate in one trunk. Such entries are mapped as one single GLF in this study (Subset of CTX image P17_007490_2095_XN_29N286W; centred on ~73.60° E, 30.43° N).*

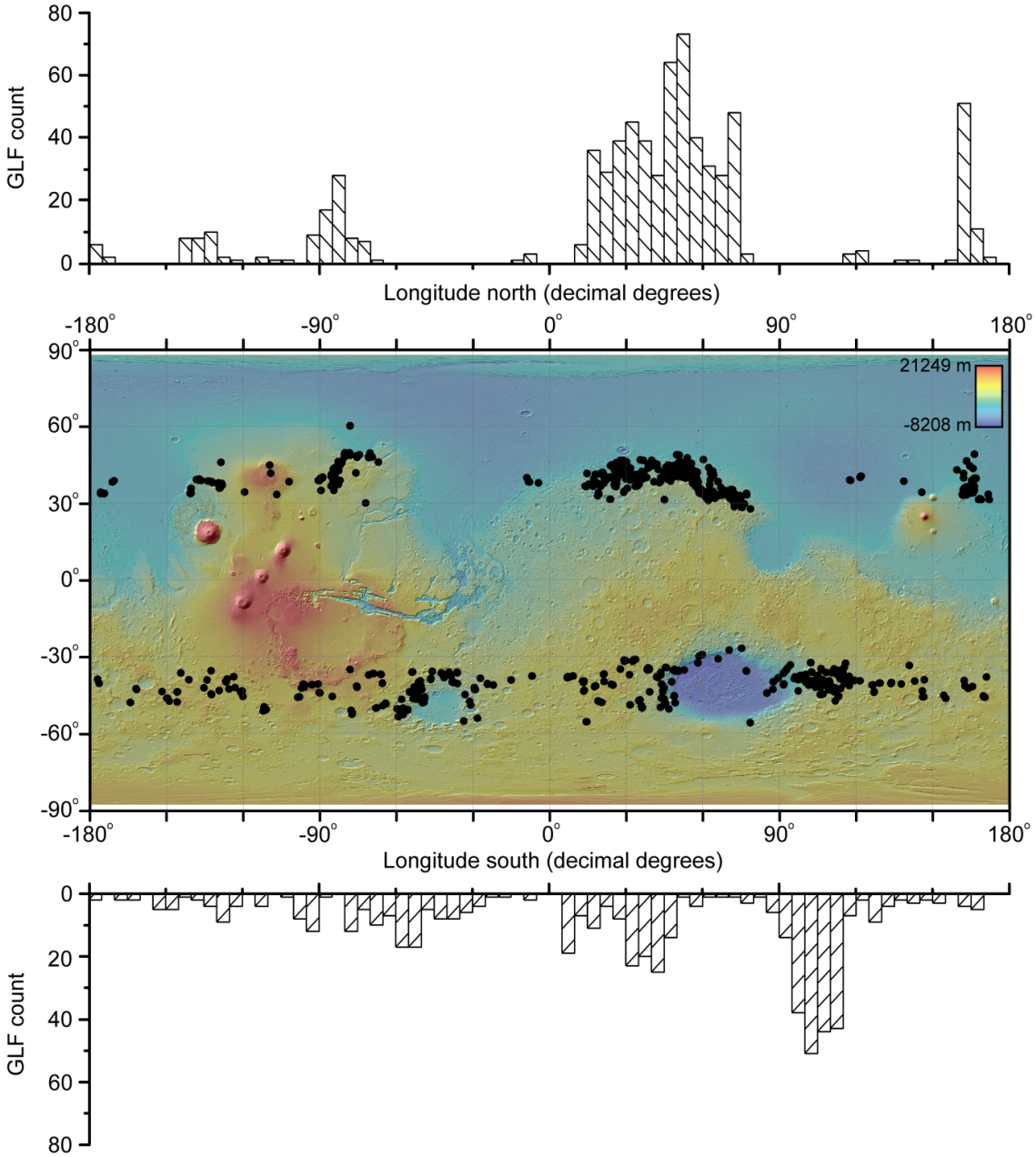

SF2: *Map of Mars showing the mid-latitude distribution of mapped GLFs (data from Souness et al., 2012). 1243 GLFs were mapped globally: 698 were located in the northern hemisphere and 545 were located in the southern hemisphere. Histograms, showing GLF count in 5° longitude bins, for each hemisphere are presented above and below the distribution map. Background map is MOLA elevation transparency overlain on a MOLA hillshade projection.*

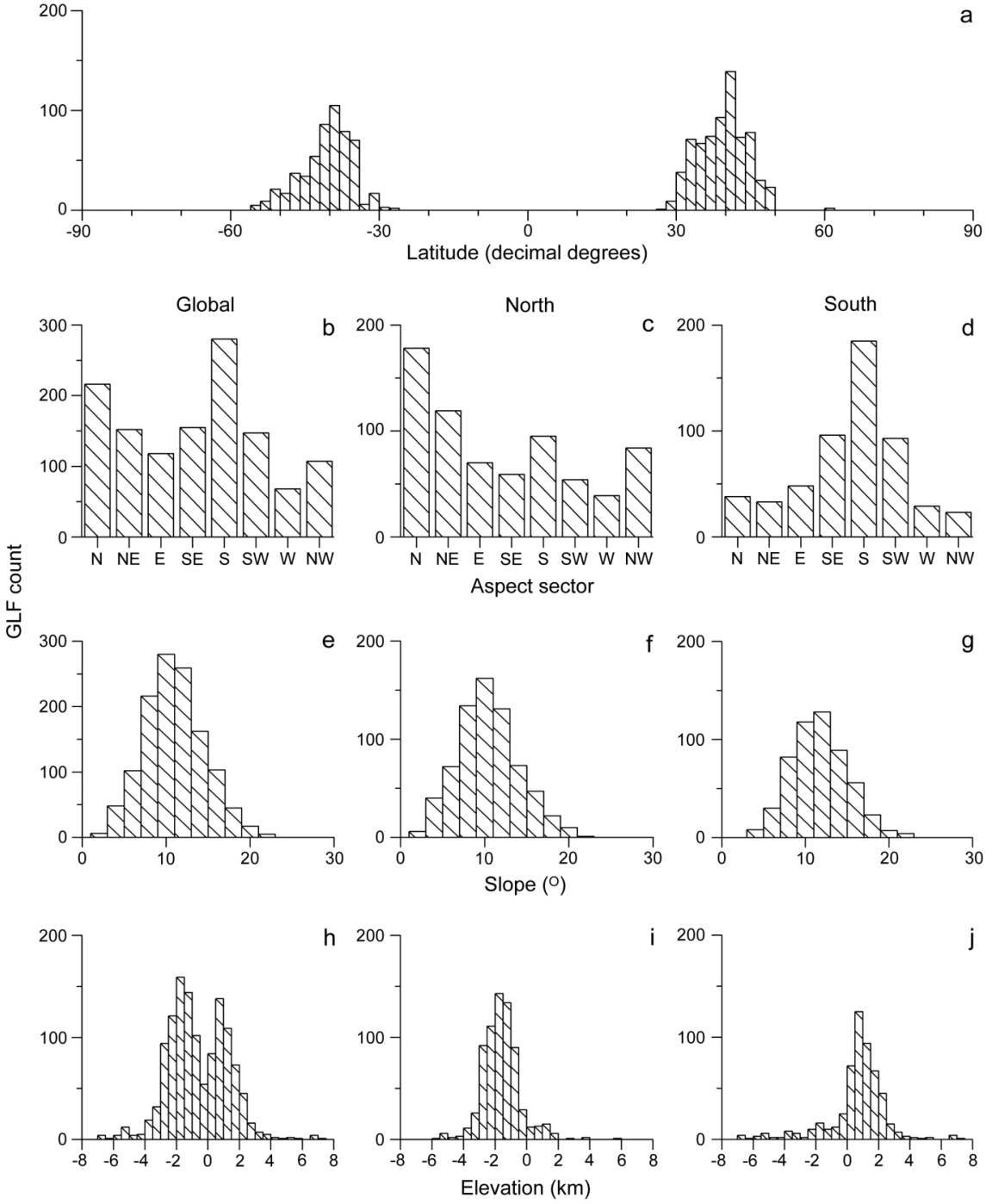

SF3: *Histograms showing GLF count for: (a) global and hemispheric latitude in 2° bins; (b) global, (c) northern and (d) southern hemispheric aspect in the eight cardinal and inter-cardinal directions; (e) global, (f) northern and (g) southern hemispheric slope in 2° bins; (h) global, (i) northern and (j) southern hemispheric elevation in 500 m bins.*

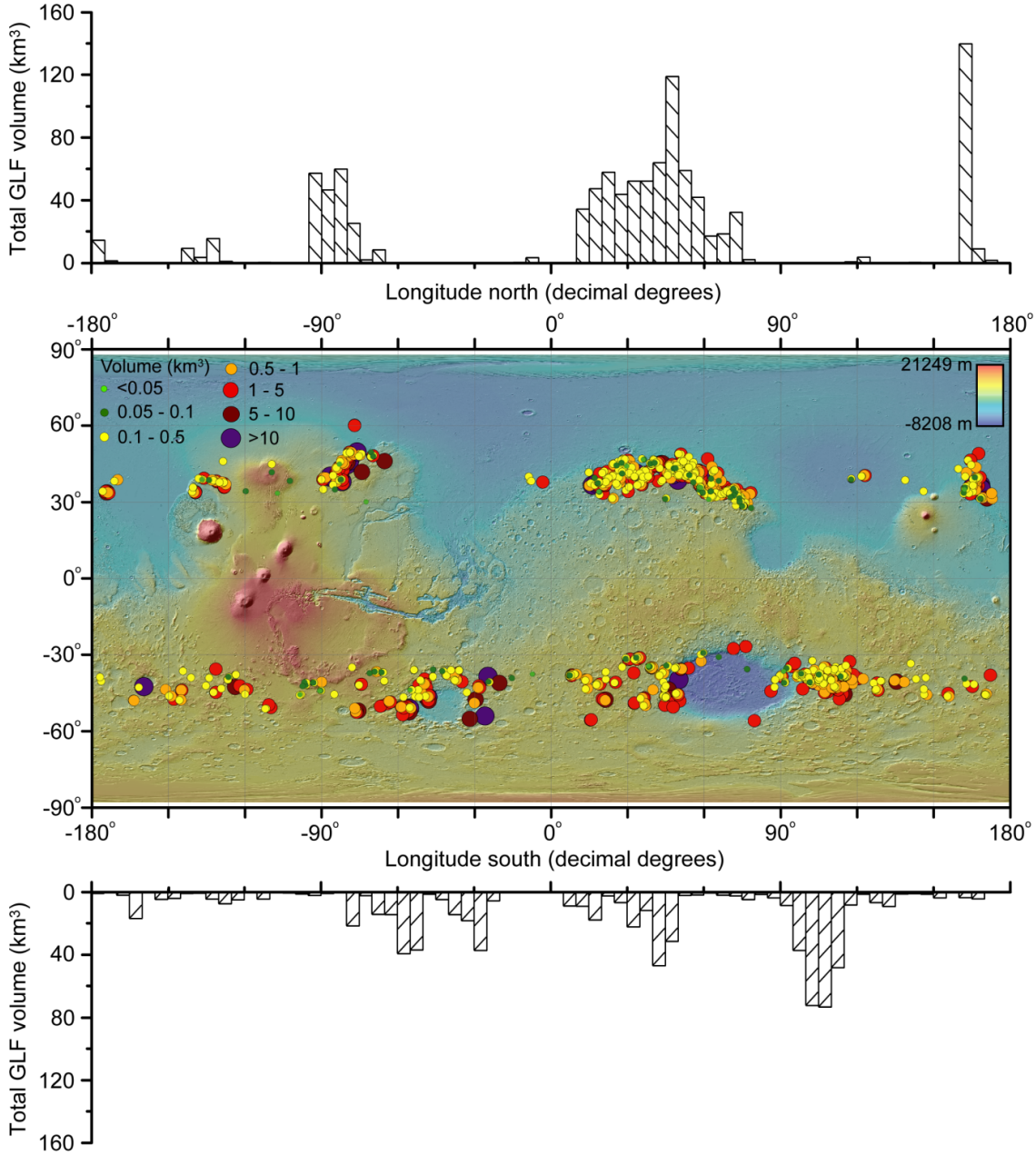

SF4: *Map of Mars showing the mid-latitude distribution of GLF volume. The colour and size of the circles represents the volume (km^3) of each GLF (green through to purple; larger circles = more volume). GLF volume is 1743.60 km^3 globally: 1045.10 km^3 is in the northern hemisphere and 698.49 km^3 is in the southern hemisphere. Bar plots, showing total GLF volume in 5° longitude bins, for each hemisphere are presented above and below the distribution map. Background map as in Figure SF2.*

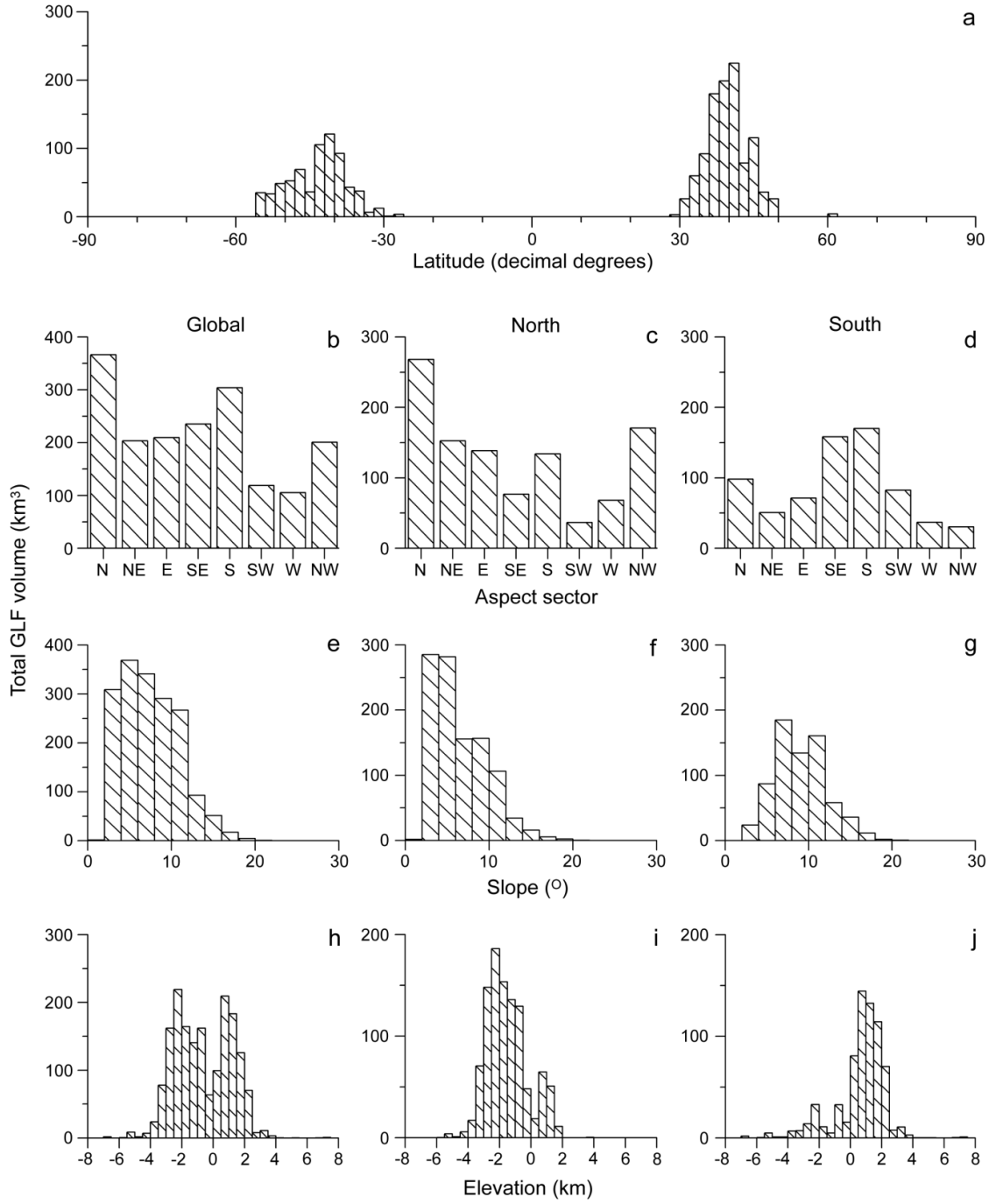

SF5: *Bar plots showing total GLF volume (km^3) for: (a) global and hemispheric latitude in 2^o bins; (b) global, (c) northern and (d) southern hemispheric aspect in the eight cardinal and inter-cardinal directions; (e) global, (f) northern and (g) southern hemispheric slope in 2^o bins; (h) global, (i) northern and (j) southern hemispheric elevation in 500 m bins.*

ST1: *The statistical similarity of GLF properties discussed in the corresponding manuscript, calculated using a two sample t-test. Those properties with 'P' values highlighted in bold are statistically different at an alpha level of 0.05.*

Parameter	Independent Variables	Hem.	Count (#)	Mean (km^3)	Std. dev. (km^3)	d.f.	*t*	*P*
Longitude	-95° to -65°	N	70	2.85	5.25	78.5	2.31	**0.023**
	≠ -95° to -65°	N	628	1.35	4.07			
	-65° to -20°	S	73	2.31	4.01	77.7	2.47	**0.016**
	≠ -65° to -20°	S	472	1.12	2.01			
Latitude	<36°	N	186	0.98	1.98	684.9	2.78	**0.006**
	>36°	N	512	1.69	4.77			
	<36°	S	98	0.62	0.75	511.8	5.54	**<0.001**
	>36°	S	447	1.43	2.62			
Aspect	N (NW, N, NE)	N	381	1.55	4.51	501.2	1.06	0.291
	S (SE, S, SW)	N	208	1.19	3.69			
	N (NW, N, NE)	S	94	1.91	3.28	113.9	2.28	**0.024**
	S (SE, S, SW)	S	374	1.10	2.15			
Slope	2 to 8°	N	246	2.94	6.76	250.7	5.13	**<0.001**
	≠ 2 to 8°	N	452	0.71	0.99			
	2 to 8°	S	120	2.46	3.86	131.6	4.19	**<0.001**
	≠ 2 to 8°	S	425	0.95	1.66			
Elevation	500 to 2500	N	34	3.73	6.65	34.3	2.03	**0.049**
	≠ 500 to 2500	N	664	1.38	4.04			
	-3500 to -2000	S	18	2.99	5.48	17.2	1.36	0.190
	≠ -3500 to -2000	S	527	1.22	2.22			

ST2: *GLF count and total volume of those GLFs per longitude in 5^o bins. The percentages of the total count and volume, along with the mean GLF volume per size class are also shown.*

ROI	Longitude (^{o})	Count (#)	Count (%)	Volume (km^3)	Volume (%)	Mean GLF volume (km^3)	ROI	Longitude (^{o})	Count (#)	Count (%)	Volume (km^3)	Volume (%)	Mean GLF volume (km^3)
North	-180 to -175	6	0.9	14.42	1.4	2.40	South	-180 to -175	2	0.4	0.46	0.1	0.23
	-175 to -170	2	0.3	1.31	0.1	0.65		-175 to -170	0	0.0	0.00	0.0	0.00
	-170 to -165	0	0.0	0.00	0.0	0.00		-170 to -165	2	0.4	1.61	0.2	0.81
	-165 to -160	0	0.0	0.00	0.0	0.00		-165 to -160	2	0.4	16.54	2.4	8.27
	-160 to -155	0	0.0	0.00	0.0	0.00		-160 to -155	0	0.0	0.00	0.0	0.00
	-155 to -150	0	0.0	0.00	0.0	0.00		-155 to -150	5	0.9	4.16	0.6	0.83
	-150 to -145	0	0.0	0.00	0.0	0.00		-150 to -145	5	0.9	3.67	0.5	0.73
	-145 to -140	8	1.1	9.23	0.9	1.15		-145 to -140	1	0.2	0.40	0.1	0.40
	-140 to -135	8	1.1	3.48	0.3	0.43		-140 to -135	2	0.4	0.34	0.0	0.17
	-135 to -130	10	1.4	15.47	1.5	1.55		-135 to -130	4	0.7	4.07	0.6	1.02
	-130 to -125	2	0.3	0.96	0.1	0.48		-130 to -125	9	1.7	7.03	1.0	0.78
	-125 to -120	1	0.1	0.06	0.0	0.06		-125 to -120	4	0.7	4.58	0.7	1.14
	-120 to -115	0	0.0	0.00	0.0	0.00		-120 to -115	0	0.0	0.00	0.0	0.00
	-115 to -110	2	0.3	0.37	0.0	0.19		-115 to -110	4	0.7	4.10	0.6	1.03
	-110 to -105	1	0.1	0.04	0.0	0.04		-110 to -105	0	0.0	0.00	0.0	0.00
	-105 to -100	1	0.1	0.06	0.0	0.06		-105 to -100	1	0.2	0.11	0.0	0.11
	-100 to -95	0	0.0	0.00	0.0	0.00		-100 to -95	8	1.5	0.79	0.1	0.10
	-95 to -90	9	1.3	57.29	5.5	6.37		-95 to -90	12	2.2	1.66	0.2	0.14
	-90 to -85	17	2.4	46.64	4.5	2.74		-90 to -85	1	0.2	0.40	0.1	0.40
	-85 to -80	28	4.0	59.90	5.7	2.14		-85 to -80	0	0.0	0.00	0.0	0.00
	-80 to -75	8	1.1	25.23	2.4	3.15		-80 to -75	12	2.2	21.17	3.0	1.76
	-75 to -70	7	1.0	1.91	0.2	0.27		-75 to -70	5	0.9	1.87	0.3	0.37
	-70 to -65	1	0.1	8.26	0.8	8.26		-70 to -65	10	1.8	13.84	2.0	1.38
	-65 to -60	0	0.0	0.00	0.0	0.00		-65 to -60	7	1.3	14.00	2.0	2.00
	-60 to -55	0	0.0	0.00	0.0	0.00		-60 to -55	17	3.1	38.83	5.6	2.28

ST2 continued

ROI	Longitude (°)	Count (#)	Count (%)	Volume (km^3)	Volume (%)	Mean GLF volume (km^3)	ROI	Longitude (°)	Count (#)	Count (%)	Volume (km^3)	Volume (%)	Mean GLF volume (km^3)
North	-35 to -30	0	0.0	0.00	0.0	0.00	South	-35 to -30	6	1.1	17.85	2.6	2.98
	-30 to -25	0	0.0	0.00	0.0	0.00		-30 to -25	4	0.7	36.81	5.3	9.20
	-25 to -20	0	0.0	0.00	0.0	0.00		-25 to -20	1	0.2	5.10	0.7	5.10
	-20 to -15	0	0.0	0.00	0.0	0.00		-20 to -15	1	0.2	0.06	0.0	0.06
	-15 to -10	1	0.1	0.30	0.0	0.30		-15 to -10	0	0.0	0.00	0.0	0.00
	-10 to -5	3	0.4	3.26	0.3	1.09		-10 to -5	2	0.4	0.03	0.0	0.02
	-5 to 0	0	0.0	0.00	0.0	0.00		-5 to 0	0	0.0	0.00	0.0	0.00
	0 to 5	0	0.0	0.00	0.0	0.00		0 to 5	0	0.0	0.00	0.0	0.00
	5 to 10	0	0.0	0.00	0.0	0.00		5 to 10	19	3.5	8.53	1.2	0.45
	10 to 15	6	0.9	34.31	3.3	5.72		10 to 15	7	1.3	8.57	1.2	1.22
	15 to 20	36	5.2	47.35	4.5	1.32		15 to 20	11	2.0	17.36	2.5	1.58
	20 to 25	29	4.2	57.91	5.5	2.00		20 to 25	4	0.7	1.98	0.3	0.49
	25 to 30	39	5.6	43.80	4.2	1.12		25 to 30	8	1.5	6.32	0.9	0.79
	30 to 35	45	6.4	52.25	5.0	1.16		30 to 35	23	4.2	21.83	3.1	0.95
	35 to 40	39	5.6	52.29	5.0	1.34		35 to 40	20	3.7	11.24	1.6	0.56
	40 to 45	28	4.0	63.99	6.1	2.29		40 to 45	25	4.6	46.54	6.7	1.86
	45 to 50	64	9.2	119.04	11.4	1.86		45 to 50	14	2.6	30.99	4.4	2.21
	50 to 55	73	10.5	58.91	5.6	0.81		50 to 55	1	0.2	1.73	0.2	1.73
	55 to 60	40	5.7	41.81	4.0	1.05		55 to 60	4	0.7	1.37	0.2	0.34
	60 to 65	31	4.4	17.15	1.6	0.55		60 to 65	1	0.2	0.09	0.0	0.09
	65 to 70	28	4.0	18.43	1.8	0.66		65 to 70	1	0.2	1.49	0.2	1.49
	70 to 75	48	6.9	32.37	3.1	0.67		70 to 75	1	0.2	2.08	0.3	2.08
	75 to 80	3	0.4	1.98	0.2	0.66		75 to 80	3	0.6	4.38	0.6	1.46
	80 to 85	0	0.0	0.00	0.0	0.00		80 to 85	1	0.2	1.04	0.1	1.04
	85 to 90	0	0.0	0.00	0.0	0.00		85 to 90	6	1.1	3.22	0.5	0.54
	90 to 95	0	0.0	0.00	0.0	0.00		90 to 95	14	2.6	8.09	1.2	0.58
	95 to 100	0	0.0	0.00	0.0	0.00		95 to 100	38	7.0	36.83	5.3	0.97

ST2 continued

ROI	Longitude (°)	Count (#)	Count (%)	Volume (km^3)	Volume (%)	Mean GLF volume (km^3)	ROI	Longitude (°)	Count (#)	Count (%)	Volume (km^3)	Volume (%)	Mean GLF volume (km^3)
North	100 to 105	0	0.0	0.00	0.0	0.00	South	100 to 105	51	9.4	71.97	10.3	1.41
	105 to 110	0	0.0	0.00	0.0	0.00		105 to 110	44	8.1	73.01	10.5	1.66
	110 to 115	0	0.0	0.00	0.0	0.00		110 to 115	43	7.9	47.86	6.9	1.11
	115 to 120	3	0.4	0.55	0.1	0.18		115 to 120	7	1.3	7.80	1.1	1.11
	120 to 125	4	0.6	3.67	0.4	0.92		120 to 125	2	0.4	0.99	0.1	0.49
	125 to 130	0	0.0	0.00	0.0	0.00		125 to 130	9	1.7	6.26	0.9	0.70
	130 to 135	0	0.0	0.00	0.0	0.00		130 to 135	4	0.7	8.81	1.3	2.20
	135 to 140	1	0.1	0.12	0.0	0.12		135 to 140	2	0.4	0.81	0.1	0.41
	140 to 145	1	0.1	0.39	0.0	0.39		140 to 145	3	0.6	0.62	0.1	0.21
	145 to 150	0	0.0	0.00	0.0	0.00		145 to 150	2	0.4	1.01	0.1	0.50
	150 to 155	0	0.0	0.00	0.0	0.00		150 to 155	3	0.6	3.30	0.5	1.10
	155 to 160	1	0.1	0.14	0.0	0.14		155 to 160	0	0.0	0.00	0.0	0.00
	160 to 165	51	7.3	139.92	13.4	2.74		160 to 165	4	0.7	3.10	0.4	0.78
	165 to 170	11	1.6	8.96	0.9	0.81		165 to 170	5	0.9	3.93	0.6	0.79
	170 to 175	2	0.3	1.56	0.1	0.78		170 to 175	0	0.0	0.00	0.0	0.00
	175 to 180	0	0.0	0.00	0.0	0.00		175 to 180	0	0.0	0.00	0.0	0.00
	Total	698	100.0	1045.10	100.0	-		Total	545	100.0	698.49	100.0	-

ST3: *GLF count and total volume of those GLFs per latitude in 2^o bins. The percentages of the total count and volume, along with the mean GLF volume per size class are also shown.*

ROI	Latitude (^{o})	Count (#)	Count (%)	Volume (km^3)	Volume (%)	Mean GLF volume (km^3)
North	26 to 28	1	0.1	0.09	0.1	0.09
	28 to 30	9	1.3	2.92	0.3	0.32
	30 to 32	38	5.4	26.24	2.5	0.69
	32 to 34	71	10.2	59.92	5.7	0.84
	34 to 36	67	9.6	92.24	8.8	1.38
	36 to 38	74	10.6	179.88	17.2	2.43
	38 to 40	93	13.3	198.64	19.0	2.14
	40 to 42	139	19.9	224.76	21.5	1.62
	42 to 44	73	10.5	78.59	7.5	1.08
	44 to 46	78	11.2	115.35	11.0	1.48
	46 to 48	30	4.3	35.92	3.4	1.20
	48 to 50	23	3.3	26.39	2.5	1.15
	50 to 52	0	0.0	0.00	0.0	0.00
	52 to 54	0	0.0	0.00	0.0	0.00
	54 to 56	0	0.0	0.00	0.0	0.00
	56 to 58	0	0.0	0.00	0.0	0.00
	58 to 60	0	0.0	0.00	0.0	0.00
	60 to 62	2	0.3	4.17	0.4	2.08
	Total	698	100.0	1045.10	100.0	-
South	-26 to -28	2	0.4	3.57	0.5	1.79
	-28 to -30	3	0.6	0.82	0.1	0.27
	-30 to -32	17	3.1	12.47	1.8	0.73
	-32 to -34	6	1.1	6.62	0.9	1.10
	-34 to -36	70	12.8	37.50	5.4	0.54
	-36 to -38	79	14.5	43.02	6.2	0.54
	-38 to -40	105	19.3	92.79	13.3	0.88
	-40 to -42	86	15.8	121.17	17.3	1.41
	-42 to -44	54	9.9	105.35	15.1	1.95
	-44 to -46	34	6.2	36.22	5.2	1.07
	-46 to -48	37	6.8	68.95	9.9	1.86
	-48 to -50	17	3.1	52.60	7.5	3.09
	-50 to -52	21	3.9	48.79	7.0	2.32
	-52 to -54	9	1.7	33.48	4.8	3.72
	-54 to -56	5	0.9	35.16	5.0	7.03
	-56 to -58	0	0.0	0.00	0.0	0.00
	-58 to -60	0	0.0	0.00	0.0	0.00
	-60 to -62	0	0.0	0.00	0.0	0.00
	Total	545	100.0	698.49	100.0	-

ST4: *GLF count and total volume of those GLFs per aspect class (cardinal and inter-cardinal directions). The percentages of the total count and volume, along with the mean GLF volume per size class are also shown.*

ROI	Aspect class	Count		Volume		Mean GLF volume
		(#)	(%)	(km^3)	(%)	(km^3)
All	N	216	17.4	366.43	21.0	1.70
	NE	152	12.2	203.31	11.7	1.34
	E	118	9.5	209.72	12.0	1.78
	SE	155	12.5	235.07	13.5	1.52
	S	280	22.5	304.00	17.5	1.09
	SW	147	11.8	118.89	6.8	0.81
	W	68	5.5	105.27	6.0	1.55
	NW	107	8.6	200.91	11.5	1.88
	Total	1243	100.0	1743.60	100.0	-
North	N	178	25.5	268.13	25.7	1.51
	NE	119	17.1	152.52	14.6	1.28
	E	70	10.0	138.47	13.3	1.98
	SE	59	8.5	76.66	7.3	1.30
	S	95	13.6	133.90	12.8	1.41
	SW	54	7.7	36.53	3.5	0.68
	W	39	5.6	68.25	6.5	1.75
	NW	84	12.0	170.64	16.3	2.03
	Total	698	100.0	1045.10	100.0	-
South	N	38	7.0	98.30	14.1	2.59
	NE	33	6.1	50.79	7.3	1.54
	E	48	8.8	71.25	10.2	1.48
	SE	96	17.6	158.41	22.7	1.65
	S	185	33.9	170.10	24.3	0.92
	SW	93	17.1	82.36	11.8	0.89
	W	29	5.3	37.01	5.3	1.28
	NW	23	4.2	30.27	4.3	1.32
	Total	545	100.0	698.49	100.0	-

ST5: *GLF count and total volume of those GLFs per slope in 2^o bins. The percentages of the total count and volume, along with the mean GLF volume per size class are also shown.*

ROI	Slope (^{o})	Count (#)	Count (%)	Volume (km^3)	Volume (%)	Mean GLF volume (km^3)
All	0 – 2	6	0.5	1.64	0.1	0.27
	2 – 4	48	3.9	308.80	17.7	6.43
	4 – 6	102	8.2	368.56	21.1	3.61
	6 – 8	216	17.4	340.70	19.5	1.58
	8 – 10	280	22.5	290.75	16.7	1.04
	10 – 12	259	20.8	266.72	15.3	1.03
	12 – 14	162	13.0	92.65	5.3	0.57
	14 – 16	103	8.3	51.45	2.9	0.50
	16 – 18	45	3.6	17.10	1.0	0.38
	18 – 20	17	1.4	4.48	0.3	0.26
	20 – 22	5	0.4	0.74	0.1	0.15
	Total	1243	100.0	1743.60	100.0	-
North	0 – 2	6	0.9	1.64	0.2	0.27
	2 – 4	40	5.7	285.19	27.3	7.13
	4 – 6	72	10.3	281.55	26.9	3.91
	6 – 8	134	19.2	155.76	14.9	1.16
	8 – 10	162	23.2	156.49	15.0	0.97
	10 – 12	131	18.8	106.09	10.2	0.81
	12 – 14	73	10.5	34.45	3.3	0.47
	14 – 16	47	6.7	15.68	1.5	0.33
	16 – 18	22	3.2	5.57	0.5	0.25
	18 – 20	10	1.4	2.37	0.2	0.24
	20 – 22	1	0.1	0.31	0.1	0.31
	Total	698	100.0	1045.10	100.0	-
South	0 – 2	0	0.0	0.00	0.0	0.00
	2 – 4	8	1.5	23.62	3.4	2.95
	4 – 6	30	5.5	87.01	12.5	2.90
	6 – 8	82	15.0	184.93	26.5	2.26
	8 – 10	118	21.7	134.26	19.2	1.14
	10 – 12	128	23.5	160.63	23.0	1.25
	12 – 14	89	16.3	58.21	8.3	0.65
	14 – 16	56	10.3	35.77	5.1	0.64
	16 – 18	23	4.2	11.53	1.7	0.50
	18 – 20	7	1.3	2.11	0.3	0.30
	20 – 22	4	0.7	0.43	0.1	0.11
	Total	545	100.0	698.49	100.0	-

ST6: *GLF count and total volume of those GLFs per elevation in 500 m bins. The percentages of the total count and volume, along with the mean GLF volume per size class are also shown.*

ROI	Elevation (m)	Count (#)	Count (%)	Volume (km^3)	Volume (%)	Mean GLF volume (km^3)
All	-7000 to -6500	4	0.3	1.74	0.1	0.44
	-6500 to -6000	1	0.1	0.09	0.0	0.09
	-6000 to -5500	4	0.3	0.54	0.0	0.13
	-5500 to -5000	12	1.0	8.54	0.5	0.71
	-5000 to -4500	4	0.3	1.77	0.1	0.44
	-4500 to -4000	5	0.4	6.74	0.4	1.35
	-4000 to -3500	19	1.5	23.63	1.4	1.24
	-3500 to -3000	32	2.6	77.75	4.5	2.43
	-3000 to -2500	94	7.6	162.12	9.3	1.72
	-2500 to -2000	121	9.7	218.92	12.6	1.81
	-2000 to -1500	159	12.8	164.31	9.4	1.03
	-1500 to -1000	144	11.6	140.63	8.1	0.98
	-1000 to -500	102	8.2	161.96	9.3	1.59
	-500 to 0	54	4.3	63.68	3.7	1.18
	0 to 500	84	6.8	99.47	5.7	1.18
	500 to 1000	138	11.1	209.20	12.0	1.52
	1000 to 1500	109	8.8	183.34	10.5	1.68
	1500 to 2000	73	5.9	125.55	7.2	1.72
	2000 to 2500	45	3.6	70.19	4.0	1.56
	2500 to 3000	16	1.3	7.66	0.4	0.48
	3000 to 3500	7	0.6	10.78	0.6	1.54
	3500 to 4000	5	0.4	3.13	0.2	0.63
	4000 to 4500	2	0.2	0.21	0.0	0.10
	4500 to 5000	1	0.1	0.10	0.0	0.10
	5000 to 5500	2	0.2	0.20	0.0	0.10
	5500 to 6000	1	0.1	0.09	0.0	0.09
	6000 to 6500	0	0.0	0.00	0.0	0.00
	6500 to 7000	4	0.3	0.32	0.0	0.08
	7000 to 7500	1	0.1	0.94	0.1	0.94
	Total	1243	100.0	1743.60	100.0	-
North	-7000 to -6500	0	0.0	0.00	0.0	0.00
	-6500 to -6000	0	0.0	0.00	0.0	0.00
	-6000 to -5500	1	0.1	0.10	0.0	0.10
	-5500 to -5000	6	0.9	3.78	0.4	0.63
	-5000 to -4500	2	0.3	0.86	0.1	0.43
	-4500 to -4000	3	0.4	5.76	0.6	1.92
	-4000 to -3500	11	1.6	16.99	1.6	1.54
	-3500 to -3000	26	3.7	70.69	6.8	2.72
	-3000 to -2500	92	13.2	148.16	14.2	1.61
	-2500 to -2000	111	15.9	186.14	17.8	1.68
	-2000 to -1500	143	20.5	153.42	14.7	1.07
	-1500 to -1000	134	19.2	135.83	13.0	1.01
	-1000 to -500	90	12.9	129.35	12.4	1.44
	-500 to 0	29	4.2	48.15	4.6	1.66
	0 to 500	12	1.7	18.69	1.8	1.56

ST6 continued

ROI	Elevation (m)	Count (#)	Count (%)	Volume (km^3)	Volume (%)	Mean GLF volume (km^3)
	500 to 1000	13	1.9	64.74	6.2	4.98
	1000 to 1500	15	2.1	50.80	4.9	3.39
	1500 to 2000	6	0.9	11.16	1.1	1.86
	2000 to 2500	0	0.0	0.00	0.0	0.00
	2500 to 3000	1	0.1	0.04	0.0	0.04
	3000 to 3500	0	0.0	0.00	0.0	0.00
	3500 to 4000	2	0.3	0.34	0.0	0.17
	4000 to 4500	0	0.0	0.00	0.0	0.00
	4500 to 5000	0	0.0	0.00	0.0	0.00
	5000 to 5500	0	0.0	0.00	0.0	0.00
	5500 to 6000	1	0.1	0.09	0.0	0.09
	6000 to 6500	0	0.0	0.00	0.0	0.00
	6500 to 7000	0	0.0	0.00	0.0	0.00
	7000 to 7500	0	0.0	0.00	0.0	0.00
	Total	698	100.0	1045.10	100.0	-
South	-7000 to -6500	4	0.7	1.74	0.2	0.44
	-6500 to -6000	1	0.2	0.09	0.0	0.09
	-6000 to -5500	3	0.6	0.44	0.1	0.15
	-5500 to -5000	6	1.1	4.76	0.7	0.79
	-5000 to -4500	2	0.4	0.91	0.1	0.45
	-4500 to -4000	2	0.4	0.98	0.1	0.49
	-4000 to -3500	8	1.5	6.64	1.0	0.83
	-3500 to -3000	6	1.1	7.06	1.0	1.18
	-3000 to -2500	2	0.4	13.97	2.0	6.98
	-2500 to -2000	10	1.8	32.78	4.7	3.28
	-2000 to -1500	16	2.9	10.88	1.6	0.68
	-1500 to -1000	10	1.8	4.79	0.7	0.48
	-1000 to -500	12	2.2	32.62	4.7	2.72
	-500 to 0	25	4.6	15.53	2.2	0.62
	0 to 500	72	13.2	80.78	11.6	1.12
	500 to 1000	125	22.9	144.46	20.7	1.16
	1000 to 1500	94	17.2	132.53	19.0	1.41
	1500 to 2000	67	12.3	114.38	16.4	1.71
	2000 to 2500	45	8.3	70.19	10.0	1.56
	2500 to 3000	15	2.8	7.62	1.1	0.51
	3000 to 3500	7	1.3	10.78	1.5	1.54
	3500 to 4000	3	0.6	2.79	0.4	0.93
	4000 to 4500	2	0.4	0.21	0.0	0.10
	4500 to 5000	1	0.2	0.10	0.0	0.10
	5000 to 5500	2	0.4	0.20	0.0	0.10
	5500 to 6000	0	0.0	0.00	0.0	0.00
	6000 to 6500	0	0.0	0.00	0.0	0.00
	6500 to 7000	4	0.7	0.32	0.0	0.08
	7000 to 7500	1	0.2	0.94	0.1	0.94
	Total	545	100.0	698.49	100.0	-

ST7: *GLF count and total volume of those GLFs by size class. The percentages of the total count and volume per size class are also shown.*

ROI	Volume class (km^3)	Count (#)	Count (%)	Volume (km^3)	Volume (%)
Global	<0.05	21	1.7	0.70	0.1
	0.05-0.1	83	6.7	6.28	0.4
	0.1-0.5	514	41.4	143.31	8.2
	0.5-1	270	21.7	190.86	10.9
	1-5	295	23.7	617.90	35.4
	5-10	29	2.3	204.98	11.8
	>10	31	2.5	579.57	33.2
	Total	1243	100.0	1743.60	100.0
North	<0.05	11	1.6	0.34	0.1
	0.05-0.1	47	6.7	3.57	0.3
	0.1-0.5	282	40.4	81.08	7.8
	0.5-1	161	23.1	113.43	10.8
	1-5	166	23.8	344.12	32.9
	5-10	10	1.4	68.23	6.5
	>10	21	3.0	434.33	41.6
	Total	698	100.0	1045.10	100.0
South	<0.05	10	1.8	0.36	0.1
	0.05-0.1	36	6.6	2.71	0.4
	0.1-0.5	232	42.6	62.22	8.9
	0.5-1	109	20.0	77.44	11.1
	1-5	129	23.7	273.78	39.2
	5-10	19	3.5	136.74	19.5
	>10	10	1.8	145.24	20.8
	Total	545	100.0	698.49	100.0

Summary to manuscript 'Area and volume of mid-latitude glacier-like forms on Mars'

Chapter 3 has presented a population-scale mapping investigation in to the areal and volumetric extent of martian GLFs. The key outcomes to carry forward are as such:

1. GLF area was calculated to be 11344 ± 393 km^2 and GLF volume was calculated to be 1744 ± 441 km^3. Two end member scenarios were used to characterise the actual population-scale ice volume contribution, and were found to be 523 ± 132 km^3 (480 ± 121 Gt) for a pore ice content (30 % ice by volume) scenario and 1570 ± 397 km^3 (1439 ± 364 Gt) for a debris-covered glacier (90 % ice by volume) scenario. This is equivalent to a contribution of a global water layer between 3 ± 1 and 10 ± 3 mm thick to the present day surface/near-surface water budget of Mars.

2. Assessment of the environmental conditions that influence(d) GLF accumulation and/or preservation revealed that GLF size is, to a certain extent, controlled by their physical setting. In particular, at the global scale, GLFs are larger at higher latitudes and on shallower slopes; in the northern hemisphere, GLFs with elevations between 500 and 2500 m; and in the southern hemisphere, GLFs with a northern aspect are also larger on average.

3. Given the spatial pattern of GLF landform and volume distribution, GLF ice accumulation and/or preservation appears to be sensitive to a combination of regional to local meteorological and topographical conditions and, although influenced by (see point 2 above), is not simply a relation of latitudinal dependence or insolation driven factors.

4. GLF size appeared particularly sensitive to slope, therefore suggesting that like glaciers on Earth, slope processes play(ed) an important role in driving GLF motion.

5. Smaller GLFs are less sensitive to their topographic setting, and as such small GLFs of comparable size are likely to show a heterogeneous response to the same climatic perturbation.

CHAPTER 4

Former extent of glacier-like forms on Mars

How great would be the desire in every admirer of nature to behold,
if such we possible,
the scenery of another planet
Charles Darwin

Preface to manuscript 'Former extent of glacier-like forms on Mars'

Introduction and rationale

Although the concept of ice mass loss and reconstruction of Mars' mid-latitude ice masses was introduced in Chapter 2 and its associated preface, many studies – including Chapter 2 – have focused on local- to regional-scale mapping investigations of the former extents of these ice masses (e.g. Dickson et al., 2010). Furthermore, relatively few studies have tried to quantify the actual volumetric loss from these ice masses (e.g. Shean et al., 2005; Dickson et al., 2008). This is particularly true for glacier-like forms (GLFs) where studies have mainly focused on the detailed description of a single, or a small collection of landforms (e.g. Appendix A; Hubbard et al., 2011; Hartmann et al, 2014), and all of these studies stop short of calculating volumetric change. Addressing these knowledge gaps is important as better understanding the distribution of, and controls responsible for, ice mass loss may provide valuable insights into recent/current climatic change and how GLFs, and their associated ice masses, might change under future climates.

In Chapters 2 and 3 regional- and population-scale analysis have been undertaken in a bid to improve our understanding of the current and former extent and volume of GLFs. This chapter (published in *Icarus* [Brough et al., 2016]) looks to further contribute to this wider goal and aims to advance our understanding of the evolutional history of Mars' GLFs. Specifically, it presents a population-scale investigation assessing and quantifying the distribution of, and controls on, GLF recession (e.g. contributing to Objectives [2] and [4] of the thesis). This population-scale recessional survey is supplemented by the three-dimensional reconstruction of the maximum extent and morphology of a specific GLF in Crater Greg, eastern Hellas Planitia in order to calculate its volume and area change (e.g. contributing to Objectives [2] and [4] of the thesis). These results will contribute to better understanding of the evolution of Mars' GLFs through time and provide an opportunity to investigating the environmental and topographical controls responsible for ice mass loss (e.g. contributing to Objective [5]

of the thesis). The remainder of this preface discusses the methods that were adopted during the study.

GLF recessional inventory and glacial reconstruction

Recessional inventory

Identification of recessional GLFs was based on analysis of all GLFs in the database of Souness et al. (2012). This database was chosen as it was the most comprehensive to date and importantly, contained the Context Camera (CTX [6 m per pixel]) image ID, for all identified GLFs. All GLFs in the database were manually examined by eye using Arizona State University's Mars Image Explorer (http://viewer.mars.asu.edu/) and JMARS software (https://jmars.asu.edu/), as this allowed for the fast ingestion and viewing at full resolution of the CTX imagery, and negated the need to download/process large volumes of data. To allow for the investigation of the environmental settings of recessional GLFs and to assess likely controlling variables on their spatial distribution, all GLFs showing evidence of an expanded former extent were ingested in to Geographic Information System (GIS) software and plotted based on the coordinate data of Souness et al. (2012). This spatial information was coupled with the published environmental parameters of the aforementioned study, which included latitude, longitude, elevation, relief and orientation.

The method Souness et al. (2012) used for their relief calculation was more involved than taking a point measurement for other parameters such as latitude. These authors calculated the relief from the standard deviation of elevation taken from a 5 km radius buffer from the GLFs' head. While this measure does capture relief, for example a smooth terrain with little elevation variation within this buffer will provide a small standard deviation, it is per se, a closer measure of landscape roughness. A closer approximation of relief could have been sought from taking the maximum and minimum elevation from the 5 km buffer, or more directly from mapped outlines, as discussed in Chapter 3 and its associated preface.

GLF reconstruction

The GLF targeted for reconstruction is located in Crater Greg, eastern Hellas Planitia, thus, as in Chapter 2, it is located in a likely region for snow accumulation during periods of high (>45^{o}) obliquity (Forget et al., 2006). More specifically, the GLF was selected due to the previous identification of sequential moraine-like ridges in the forefield (e.g. Hubbard et al., 2011) and, due to the availability of High Resolution Imaging Science Experiment (HiRISE) satellite imagery and corresponding digital elevation model. In order to reconstruct the palaeo-ice surface of the GLF the maximum former extent needs to be demarcated. The mapping of the maximum former extent uses the knowledge gained in Chapter 2 and applies this mapping approach to the aforementioned GLF to demarcate its boundary using geomorphological evidence (e.g. moraine-like ridges and trimlines).

The second stage is to recreate the palaeo-ice surface of the GLF using the constraining geomorphological information generated in the previous stage (e.g. former upper and lower GLF limits). Theoretical solutions of the palaeo-surface can be obtained using a simple, steady-state, model that uses an adaptation of Nye's (1951, 1952) perfect-plasticity approximation for ice flow. This approach rests on the assumption that ice deforms at an infinite rate when the driving stress exceeds a critical yield strength. Such models are commonly used to reconstruct palaeo-ice surface for glaciers on Earth (e.g. Wolff et al., 2013) due to the fact that the model only requires two input parameters; the bed topography along a flowline and a yield strength for ice (Van der Veen, 1999). This approach has previously been used for Mars (Shean et al., 2005) and is utilised in this study given that the required input data can be derived from the available data products. The major difference between using such an approach for glaciers on Earth and Mars is the value used for the ice yield strength. On Earth this value is typically between 50 and 150 kPa (Cuffey and Paterson, 2010), but empirical studies have placed this value between ~10 and ~40 kPa for Mars (Karlsson et al., 2015). Using these Mars derived yield strength values in the model, rather than their higher Earth counterparts, will ultimately result in a reduction in the reconstructed ice thickness.

Former extent of glacier-like forms on Mars

Stephen BROUGH[a], Bryn HUBBARD[a] and Alun HUBBARD[a, b]

[a]*Department of Geography and Earth Sciences, Aberystwyth University, Aberystwyth, UK*

[b]*Centre for Arctic Gas Hydrate, Environment and Climate, Department of Geology, University of Tromsø, Tromsø, Norway*

Link to published article

This is a manuscript of an article published by Elsevier Inc. in Icarus on 11/03/2016, available online: http://dx.doi.org/10.1016/j.icarus.2016.03.006.

Citation for published paper

Brough, S., Hubbard, B. & Hubbard, A. (2016). Former extent of glacier-like forms on Mars. *Icarus*, *274*, 37-49. doi: 10.1016/j.icarus.2016.03.006.

Keywords: Mars; Ices; Mars, climate; Mars, surface; Geological processes

Abstract: Mars' mid-latitude glacier-like forms (GLFs) have undergone substantial mass loss and recession since a hypothesised last martian glacial maximum (LMGM) stand. To date, there is a lack of knowledge of the nature and timing of the LMGM, the subsequent mass loss and whether this mass loss has been spatially variable. Here, we present the results of a population-scale inventory of recessional GLFs, derived from analysis of 1293 GLFs[1] identified within Context Camera (CTX) imagery, to assess the distribution and controls on GLF recession. A total of 436 GLFs were identified showing strong evidence of recession: 197 in the northern hemisphere and 239 in the southern hemisphere. Relative to their parent populations, recessional GLFs are over-represented in the low latitude belts between 25 and 40º and in areas of high relief, suggesting that these zones exert some control over GLF sensitivity and response to forcing. This analysis is complemented by the reconstruction of the maximum extent and morphology of a specific GLF for which High Resolution Imaging Science Experiment (HiRISE) derived digital elevation data are available. Using Nye's (Nye, J. F. [1951] *Proc. Roy. Soc. Lond, Ser. A-Mat. Phys. Sci, 207, 554-572*) perfect plastic approximation of ice flow applied to multiple flow-lines under an optimum yield strength of 22 kPa, we calculate that the reconstructed GLF has lost an area of 6.86 km^2 with a corresponding volume loss of 0.31 km^3 since the LMGM. Assuming the loss reconstructed at this GLF occurred at all mid-latitude GLFs yields a total planetary ice loss from Mars' GLFs of 135 km^3, similar to the current ice volume in the European Alps on Earth.

4.1. Introduction

Although water ice is not presently stable across much of Mars' mid-latitudes (Mellon and Jakosky, 1995; Mellon et al., 2004), evidence of pervasive ice-rich landforms between 30 and 60º latitude has been presented (Sharp, 1973; Squyres, 1978, 1979; Lucchitta, 1984; Mangold, 2003; Milliken et al., 2003; Levy et al., 2007; Baker et al., 2010; Dickson et al., 2010; Head et al., 2010, Souness et al., 2012; Hubbard et al., 2014; Brough et al., 2016; Sinha and Murty, 2015). Based on evidence from the Shallow Radar (SHARAD) instrument on board the Mars Reconnaissance Orbiter, the

[1] In their inventory Souness et al. (2012) identified 1309 GLFs. We refine the number of GLFs to 1293, due to the identification of duplicate entries.

composition of these ice-rich deposits is consistent with water ice (Holt et al., 2008; Plaut et al., 2009), and their surface morphologies are indicative of viscous flow of that ice (e.g. Squyres, 1979; Mangold, 2003; Head et al., 2005). Collectively, these ice-rich deposits have become known as viscous flow features, or VFFs (Milliken et al., 2003), and are hypothesised to have been formed during a previous 'ice age' as a result of changes in orbital and atmospheric parameters providing preferential conditions for mid-latitude ice accumulation during periods of high (>30^{o}) obliquity (Head et al., 2003; Forget et al., 2006; Madeleine et al., 2009; Fassett et al., 2014). The last major change from a high (~35^{o}) to low (~25^{o}) mean obliquity period occurred ~4 – 6 Ma BP (Laskar et al., 2004), perhaps causing the end of the hypothesised last martian glacial maximum, or LMGM (Souness and Hubbard, 2013). The persistence of VFFs to the present day is therefore probably due, at least partly, to their ubiquitous debris cover protecting the underlying ice from sublimating into the atmosphere (Bryson et al., 2008; Holt et al., 2008; Plaut et al., 2009; Fastook et al., 2014).

Glacier-like forms (GLFs) are a distinctive subtype of VFFs, similar in planform appearance to terrestrial valley glaciers or debris-covered glaciers (e.g. Arfstrom and Hartmann, 2005; Hubbard et al., 2011; Souness et al., 2012). GLFs form in cirque-like alcoves or valleys and appear to flow downslope, generally coalescing from a wide upper basin to a narrow elongate tongue that is often confined by raised latero-terminal ridges. GLFs may or may not feed into pre-existing VFFs and form what Head et al. (2006, 2010) described as Mars' integrated glacial landsystem. Following this model, GLFs represent the smallest component of this glacial landsystem and may converge downslope to form broad, rampart-like lobate debris aprons (LDAs). Where LDAs converge or coalesce, complex and contorted surfaces termed lineated valley fill (LVF) are commonly observed (Squyres, 1978, 1979; Lucchitta, 1984).

GLFs and other VFFs (LDA or LVF) have been interpreted as relict remains of once far larger ice masses (Dickson et al., 2008; Sinha and Murty, 2013; Hubbard et al., 2014; Brough et al., 2016), that were most extensive during a hypothesised LMGM (Souness and Hubbard, 2013). For example, in a two-dimensional planform analysis of a GLF in Phlegra Montes, Hubbard et al. (2014) noted a set of pronounced ridges resembling terrestrial moraines, encompassing a texturally distinct 'arcuate' terrain, devoid of many

impact craters, in the forefield of a GLF. The contrast between this distinct landform and the wider surface led the authors to suggest that the proglacial arcuate terrain represented a phase of expanded glaciation, and that the GLF had subsequently receded by up to ~3.3 km. Such an expanded former extent has also been identified on GLFs elsewhere on Mars (Hubbard et al., 2011; Hartmann et al., 2014), as well as on the regional scale of Mars' integrated glacial landsystem (e.g. Head et al., 2006; Dickson et al., 2008; Fastook et al., 2014), where surface lowering of up to ~900 m has been inferred (Dickson et al., 2008). Indeed, the identification of relict landforms of glacial origin across large areas of Mars has led to inferences of former regional- to continental-scale ice sheet glaciation (Kargel et al., 1995; Hobley et al., 2014; Souček et al., 2015). Furthermore, several studies have noted the superposed relationship of some GLFs to the underlying ice-rich terrain (LDA or LVF) onto which they appear to have flowed, leading to suggestions of recurrent glacial phases with at least one 'local' glacial phase advancing over an earlier 'regional' glaciation (Levy et al., 2007; Dickson et al., 2008; Baker et al., 2010; Sinha and Murty, 2013; Brough et al., 2016). Despite these inferred changes, we currently have limited knowledge of the nature and timing of Mars' LMGM, the volume of ice lost since that time, and whether such GLF recession has been spatially variable (e.g. Hubbard et al., 2014).

On Earth, the vast majority of valley glaciers have experienced an expanded former extent, or glacial maximum, and have receded since that time (Zemp et al., 2009; Radić and Hock, 2014; Fischer et al., 2015). The visible imprint of such recession, or in some cases complete deglaciation, is recorded to varying degrees in the geomorphic and sedimentary record. Detailed investigation of these remnant landform and sediment assemblages can therefore be used to reconstruct former glacier limits and thermal conditions (e.g. Kleman et al., 1997; Hambrey and Glasser, 2012). Furthermore, due to their short response times, valley glaciers have become important indicators of climatic change (Hambrey et al., 2005; Raper and Braithwaite, 2009; Carrivick et al., 2015). Thus, if the processes and responses of martian GLFs are broadly equivalent to their terrestrial counterparts, they may represent: (i) effective geomorphic agents, through both erosion and deposition; and (ii) important archives of recent climatic change on Mars.

The aim of this paper is to advance our understanding of the glacial history of Mars'

GLFs by assessing and quantifying the distribution of, and controls on, GLF recession. Specifically, we: (i) provide a population-scale inventory detailing the locations of GLFs that show evidence of recession; (ii) analyse the environmental settings of recessional GLFs to assess likely controlling variables on their spatial distribution; and (iii) provide a high-resolution three-dimensional reconstruction of a typical recessional GLF to calculate its volume and area change.

4.2. Data and methods

4.2.1. Population-scale recessional GLF inventory

4.2.1.1. Mapping distribution and morphology

Identification of recessional GLFs was based on analysis of all GLFs in the database of Souness et al. (2012). This database contains the Context Camera (CTX [6 m per pixel]) image ID, coordinate information and basic morphometric and environmental data for all identified GLFs. All GLFs in the database were manually examined by eye using Arizona State University's Mars Image Explorer (http://viewer.mars.asu.edu/) and JMARS software (https://jmars.asu.edu/). GLFs showing evidence of an expanded former extent (Figure 4.1) were recorded into a separate database (provided in Supplementary Material Ch. 4) and subsequently imported and plotted, based on the coordinate data of Souness et al. (2012), using ESRI's ArcMap 10.1 Geographic Information System (GIS) software.

4.2.1.2. Spatial distribution

To determine what, if any, controls are responsible for the observed spatial distribution of recessional GLFs, several environmental parameters were extracted and analysed. These include latitude (°), longitude (°), elevation (m relative to Mars datum), relief (m) and orientation (°). Following Souness et al. (2012) relief was calculated as the standard

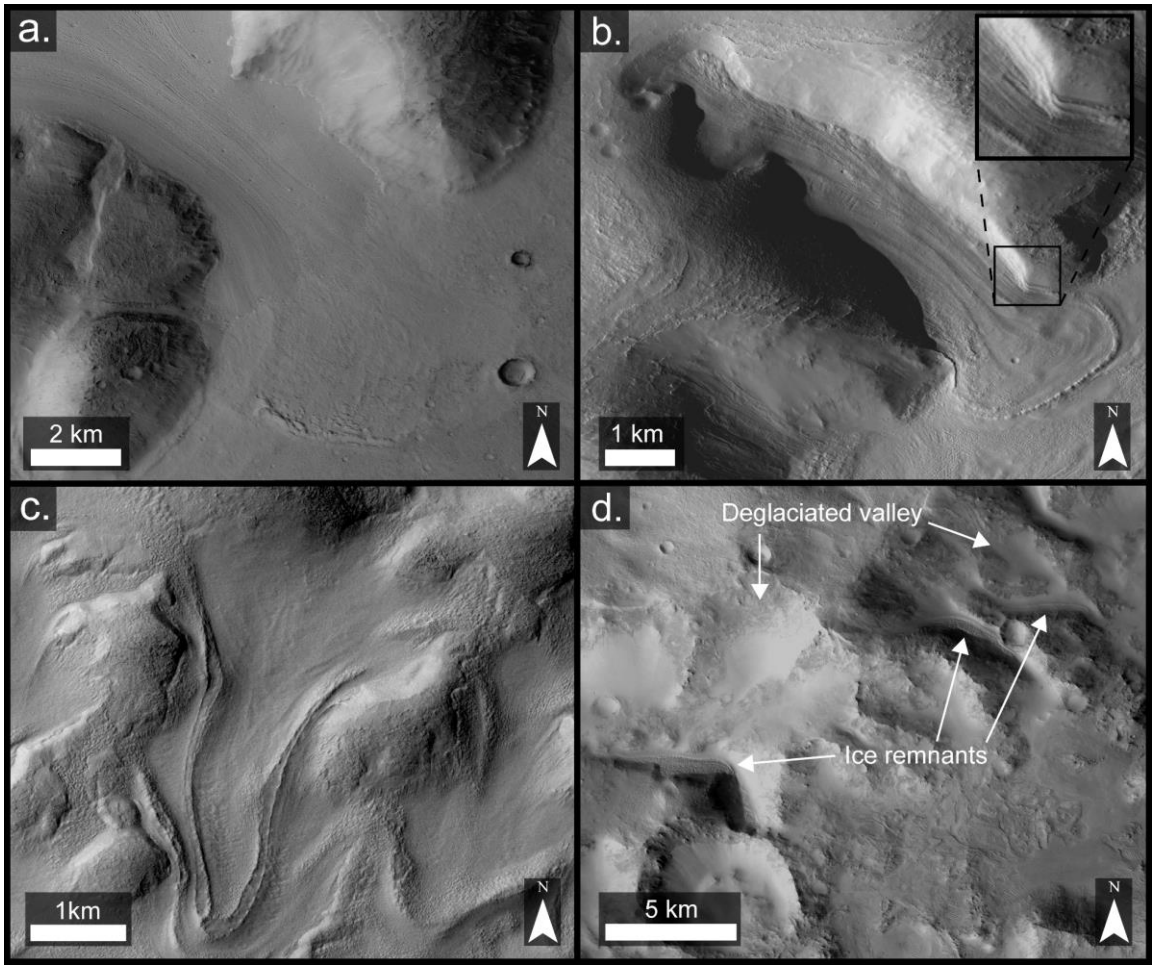

Figure 4.1: *Montage of CTX images exemplifying GLFs identified as showing evidence of recession. (a) A well-developed set of arcuate moraine ridges demarcating a deglaciated terrain in the foreground of a GLF in Phlegra Montes (subset of CTX image P16_007368_2152_XN_35N195; centred on ~164.54º E, 34.05º N). (b) Lateral moraine ridges on eastern sidewall of a GLF in Protonilus Mensae. Note multiple ridges are visible, suggesting progressive or phased recession has occurred (subset of CTX image P01_001570_2213_XI_41N305W; centred on ~54.71º E, 41.27º N). (c) Tongue-shaped GLF with pronounced sequence of latero-terminal moraine ridges (subset of CTX image G05_020121_1412_XN_38S247W; centred on ~113.16º E, 38.15º S). (d) Palimpsest landscape. Located in close proximity to current GLFs were landscapes indicative of former glaciation. However, as no GLFs are identified in these regions they were not included in the inventory (subset of CTX image P06_003231_2090_XI_29N286W; centred on ~73.15º E, 30.01º N).*

deviation of elevation values extracted from a 5 km radius buffer from the GLF's head. As well as plotting recessional GLF counts against these variables, both the recessional GLF population and the total GLF population were normalised against their total counts (436 and 1293, respectively), and the subsequent normalised ratio of recessional GLFs relative to total GLF population plotted to evaluate the relative abundance of recessional GLFs (with a ratio >1 indicating over-representation and <1 indicating under-representation).

The normalised ratio plots for global and hemispheric GLF coverage are presented herein. The global and hemispheric recessional GLF counts can be found in Supplementary Material Ch. 4 (Figures SF1–SF4).

4.2.2. Case study: Crater Greg GLF reconstruction

The presence of overlapping High Resolution Imaging Science Experiment (HiRISE) satellite imagery allows high-resolution digital elevation models (DEMs) to be created (e.g. Kirk et al., 2008). Here we utilise a 2 m per pixel DEM (stereo pair PSP_002320_1415_RED and PSP_003243_1415_RED [see Hubbard et al., 2011 for details]) and corresponding orthorectified HiRISE image, with a resolution of ~0.25 m per pixel, to reconstruct the former extent of a well-studied GLF (e.g. Hartmann et al., 2003; Marchant and Head, 2003; Milliken et al., 2003; Kargel, 2004; Hubbard et al., 2011 [Figure 4.2d]).

4.2.2.1. Study site

Our case study reconstruction is based on the analysis of a GLF located in Crater Greg, eastern Hellas Planitia (Figure 4.2). This crater is located in a climatically important zone with global climate models suggesting that it was positioned in one of two regions of high ice deposition outside of the polar ice-caps during periods of high obliquity (Forget et al., 2006; Hartmann et al., 2014).

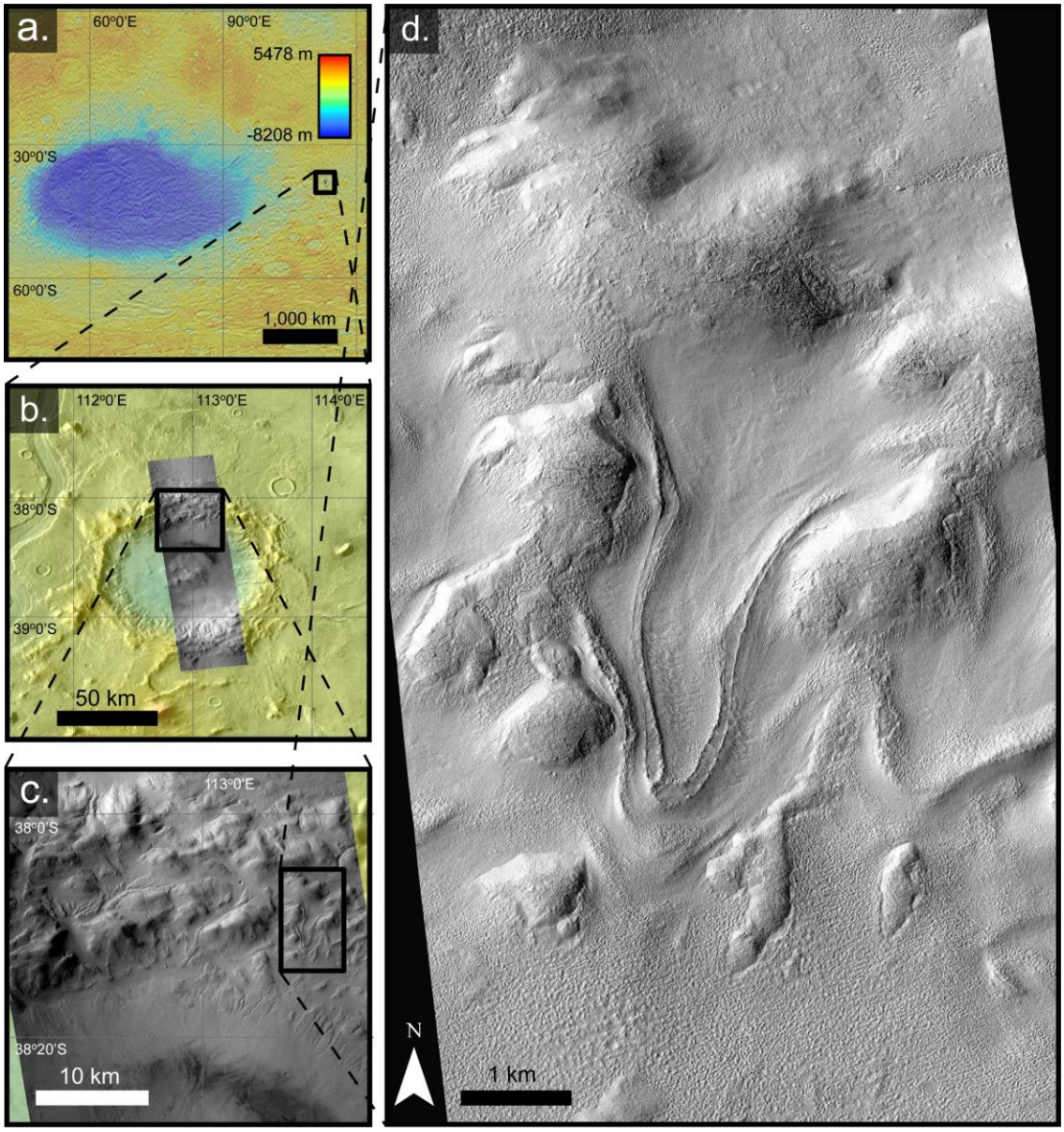

Figure 4.2: *Location and expansion of our case study GLF reconstruction. (a) Global context map indicating location of host crater, Greg, illustrated as a MOLA elevation transparency overlain on a THEMIS-IR day mosaic. (b, c) Expansion of Crater Greg, illustrating local context and abundance of GLFs on the crater's northern headwall (CTX image G05_020121_1412_XN_38S247W). (d) The subject GLF to reconstruction, illustrated as a subset of HiRISE image PSP_002320_1415_RED (centred on ~113.16^{o} E, 38.15^{o} S).*

Several lobate tongues classified as GLFs are located on the northern wall of Crater Greg (Arfstrom and Hartmann, 2005; Hubbard et al., 2011; Souness et al., 2012; Hartmann et al., 2014 [Figure 4.2c]). The GLF studied herein (Figure 4.2d), is ~4 km

long and ~1 – 2 km wide, extends down-slope at an angle of ~10^{o}, and according to Hartmann et al. (2014) is likely younger than ~50 Ma BP, with a best estimate of ~2–9 Ma BP. Several arcuate ridges visible in the immediate forefield of the GLF (Figure 4.2d) have been interpreted as latero-terminal moraines (Hubbard et al., 2011; Hartmann et al., 2014) – a type of moraine that demarcates not only the frontal position of an ice mass but also provides geometric constraints on former lateral and vertical extents, an important component of glacier reconstruction on Earth (e.g. Benn et al. 2005). Based on the GLF's overall geomorphological characteristics, Hubbard et al. (2011) concluded that the upper basin currently hosts a degraded GLF, while the lower basin zone represents deglaciated terrain. Although several authors have commented on the degraded nature of this GLF, with previous estimates of thinning based on heights of the innermost set of lateral moraines of between 30 and 50 m (Hubbard et al., 2011; Hartmann et al., 2014), no attempt has been made to reconstruct the GLF's former three-dimensional extent, or to quantify the volume of ice lost since that maximum extent.

4.2.2.2. Glacial reconstruction

In order to assess changes in volume and area of our selected GLF we use standard GIS routines in ESRI's ArcMap v10.1 (e.g. Wolff et al., 2013). Below, we detail the methods used to reconstruct the GLFs palaeo-ice surface and to calculate morphometric change since the time of that extent. We summarise sources of potential uncertainty that may arise during our reconstruction in Section 4.2.3.

The outlines of the current and former GLF surface were manually digitised on screen. The former GLF outline was mapped on the basis of clear moraine ridges (Section 4.2.2.1) and associated geomorphological evidence such as the locations of trimlines (Figure 4.3). To demarcate the current GLF surface we follow the interpretation of Hubbard et al. (2011) to isolate the surface with a relatively fresh, sharp appearance (including their 'scaly' and 'polygonized' terrains). These terrains contrast sharply with the surrounding material, which is dominated by heavily dissected unconsolidated material to the north (termed 'incised-headwall' terrain by Hubbard et al. [2011]; Figure

4.3b), and regions of round to elongate ridges to the south (their 'mound-and-tail' and 'linear' terrain; Figure 4.3c). These outer terrains were interpreted by Hubbard et al. (2011) as consistent with regions of former glaciation.

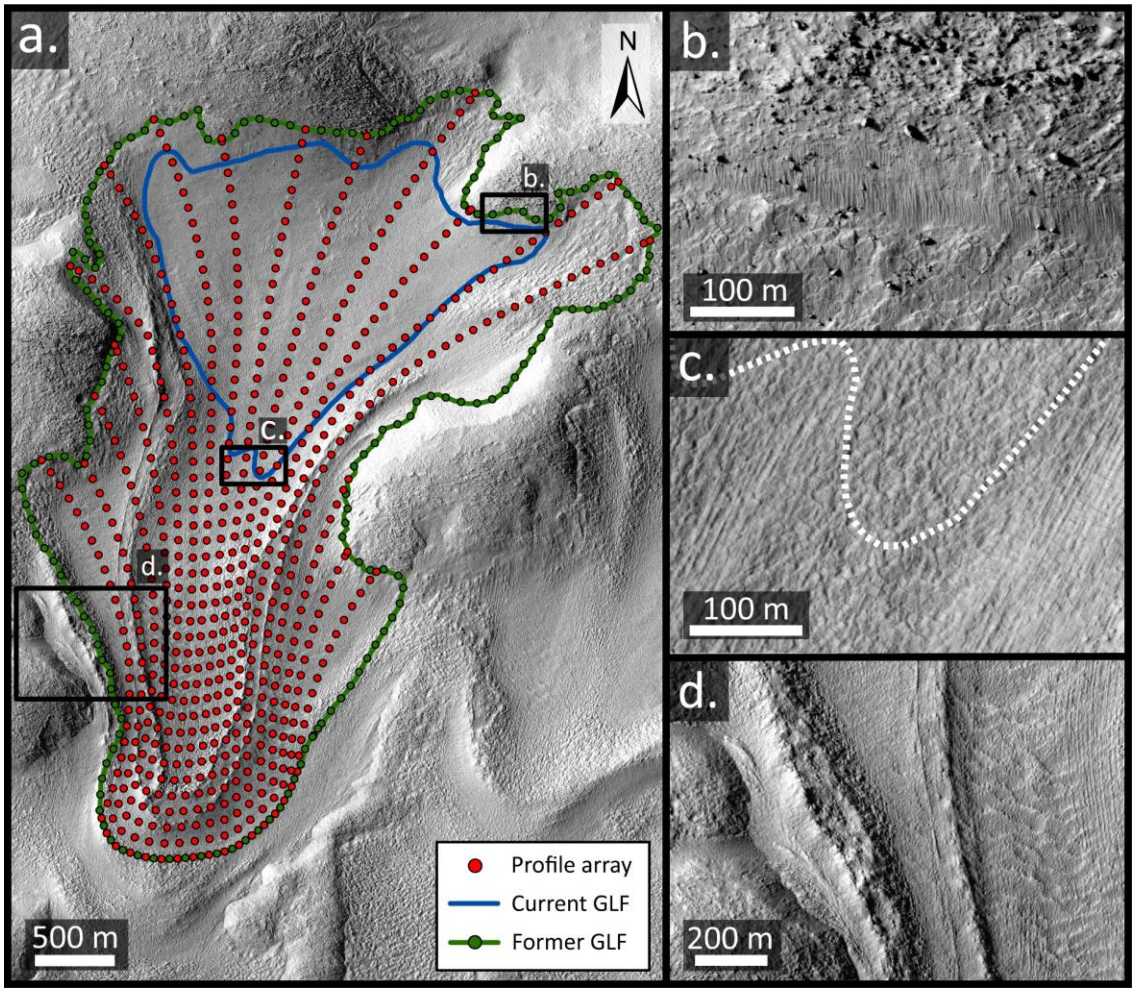

Figure 4.3: *Interpreted GLF limits and reconstruction array (subset of HiRISE image PSP_002320_1415_RED). (a) Overview of mapped current (blue line) and former (green line) GLF limits with glacier surface (red) and constraining marginal (green) reconstruction nodes overlain. (b–d) Geomorphological and surface evidence used in demarcating the current and former GLF limits: (b) incised headwall terrain, (c) compositional boundary between relatively fresh 'polygonized' terrain and contrasting 'linear' terrain (dashed white line marks the inferred current GLF terminus) and (d) clearly visible moraine ridges.*

In order to recreate the former GLF's bed, we removed the later set of moraine ridges located between the current and former GLF surfaces by clipping them from the DEM and re-interpolating the surface using ArcMap's 'Topo to Raster' (ANUDEM algorithm) tool.

To reconstruct the palaeo-ice surface, we calculated the ice thickness along an array of 17 flow-line profiles that extend from the terminus of the outer moraine ridge up to the GLF's headwall. Flow-lines were created based on geometric considerations of terrestrial glacier flow. Each flow-line was converted into a series of nodes at 100 m intervals (Figure 4.3a) and, following Van der Veen's (1999, pg 149 – EQ. 6.2.3) adaptation of Nye's (1951, 1952) perfect-plasticity approximation for ice flow, the GLF surface elevation was solved at each node from the margin iterating up-glacier to the headwall. The perfect-plasticity approximation assumes that ice deforms at an infinite rate when the driving stress exceeds a critical yield strength (Van der Veen, 1999). Yield strength values for terrestrial glaciers typically range from 50–150 kPa (Cuffey and Paterson, 2010). However, recent SHARAD-validated measurements of ice thickness on Mars using the same perfect-plastic approach utilised herein, reveal a critical yield strength value of 22 kPa (Karlsson et al., 2015); a value markedly lower than those derived for terrestrial glaciers due, potentially, to the impurity content of martian ice, which is estimated to be between 5 and 10 % (Holt et al., 2008; Grima et al., 2009; Karlsson et al., 2015). For our GLF reconstruction we adopted this yield strength value bracketed by two additional scenarios to reflect low (12 kPa) and high (38 kPa) yield strengths (Karlsson et al., 2015). Calculation of driving stress followed Van der Veen (1999) and accordingly uses a lower gravitational constant of 3.71 m s^{-2} for Mars compared to Earth. To constrain the zero-thickness boundary around the reconstructed GLF, we converted the mapped former margin to nodes at 50 m intervals and extracted the elevation from the HiRISE DEM (Figure 4.3a). Finally, by combining these values, the former GLF's palaeo-ice surface was interpolated using ArcMap's 'Topo to Raster' tool, which has previously provided robust results for glacier surface interpolation (e.g. Racoviteanu et al., 2007; Carrivick et al., 2015). Our reconstructed GLFs were generated at a resolution of 2 m per pixel to allow direct comparison with the original DEM. We estimated the GLF's former ice thickness by subtracting the GLF's current DEM (with the inner moraines removed) from each of the three

reconstructed surfaces. Volume and area change was calculated using Arc Map's 'cut and fill' tool.

4.2.3. Uncertainty in recession identification and reconstruction

Both the identification of recession and the GLF reconstruction used herein are subject to uncertainties, some of which are constrained and others are not. Below we summarise the sources of these uncertainties and outline their management.

4.2.3.1. Identification of recession

As with all remotely sensed manual classification studies, there is a potential degree of human error, mainly reflecting the user's ability to identify their features of interest (Smith, 2011). However, evidence of GLF recession was considered to be unambiguous, with geometric changes visible in clearly identifiable latero-terminal moraine ridges and/or in clear surface depressions. Further, the identification of recession depends on the production and subsequent survival of evidence until the time of image acquisition, while any feature must be greater than the observable resolution of the imaging sensor (Smith, 2011).

4.2.3.2. Identification and digitisation of GLF extent

In the absence of field validation, demarcating the current and former limit of a GLF is solely based on geomorphological and surface features identified in satellite imagery. The identification of glacier boundaries, particularly exemplified on debris-covered glaciers, is inherently difficult in remotely-sensed imagery and subject to variable observer interpretation (e.g. Nuimura et al., 2015). Although mitigated by the high resolution of the satellite imagery and DEM used, defining exact boundaries involves some error.

4.2.3.3. Removal of moraine ridges

Care was taken to remove only the proportion of the surface affected by the inner set of moraine ridges, rather than any natural surface perturbation. This is effectively mitigated because moraine ridges were easily identifiable in contours where they appear as sharp crested peaks.

4.2.3.4. Creation of DEMs

The choice of interpolation routine causes variation in the reconstructed surface depending on the method used (e.g. inverse distance weighting, spline, kriging, tin). We use the Topo to Raster interpolation method as it has been shown to produce improved results relative to other interpolation methods (Racoviteanu et al., 2007), and has previously provided reliable estimates of former ice surfaces (Racoviteanu et al., 2007; Carrivick et al., 2015). Although the choice of pixel size used in interpolation is user-defined, it has previously been shown to have a negligible influence on volume calculations (e.g. Villa et al., 2007).

4.2.3.5. Surface reconstruction and change analysis

In the absence of SHARAD-validating measurements, we do not remove the current GLF volume or potential proglacial sediment in-fill from our DEM. However, under the GLF's current degraded state, it is unlikely that either of these materials is greater than metres to tens of metres thick (Hubbard et al., 2011). We therefore assume the present valley floor, with the innermost moraine ridges removed (Sections 4.2.2.2 & 4.2.3.3), represented the former GLF bed for our reconstruction scenarios.

4.3. Results

4.3.1. Population-scale distribution of recessional GLFs

From a total population of 1293 GLFs located in Mars' mid-latitudes, 436 (33.7 %) show evidence of an expanded former extent (Figure 4.4). Of these 436 recessional GLFs, 197 (45.2 %) are located in the northern hemisphere, and 239 (54.8 %) in the southern hemisphere. Several clusters of recessional GLFs are visible, e.g., across the 'fretted terrain' of the northern dichotomy boundary and surrounding the Hellas impact basin (Figure 4.4). This distribution broadly reflects concentration variations in the parent population, resulting in recessional:total GLF ratios close to 1 (Figure 4.4).

4.3.2. Environmental controls over recessional GLF distribution

4.3.2.1. Latitude

The latitudinal distribution of recessional GLFs shows inter-hemispheric similarity, with a mean of 38.4º in the northern hemisphere and 39.0º in the southern hemisphere (Table 4.1). However, in both hemispheres, the lower-latitude regions between ~25 and 40º are over-represented by recessional GLFs, with a mean ratio of 1.33, relative to the regions between 40 and 65º, where a mean (under-represented) ratio of 0.64 is observed (Figure 4.5a). This effect strengthens at even lower latitudes within the surveyed region, such that the mean ratio rises to 1.83 between 28 and 32º in the northern hemisphere and to 1.72 between 26 and 30º in the southern hemisphere (Figure 4.5a).

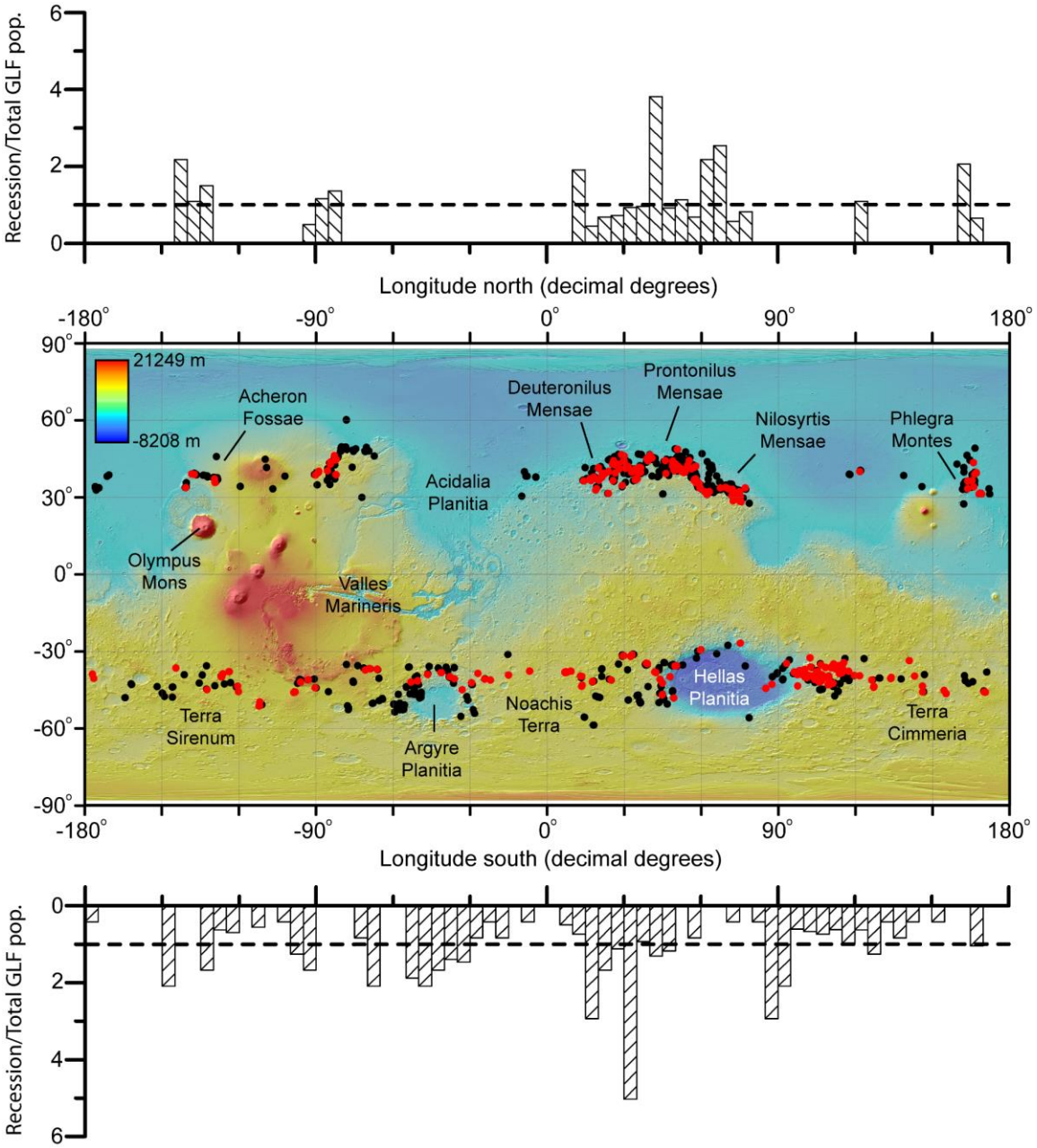

Figure 4.4: *Mars global map showing the mid-latitude distribution of recessional GLFs (red dots) relative to the total GLF population (black dots). 436 recessional GLFs were identified globally: 197 were located in the northern hemisphere and 239 were located in the southern hemisphere. Ratio bar plots in 5° longitude bins, showing normalised concentration of recessional GLFs relative to the normalised concentration of the total GLF population, for each hemisphere are presented above and below the distribution map. Background map is MOLA elevation transparency overlain on MOLA hillshade projection.*

Table 4.1: *Basic descriptive statistics for the environmental parameters of orientation, elevation, relief and latitude for (a) all GLFs (after Souness et al., 2012) and (b) recessional GLFs. See also Figures SF2 and SF4.*

(a) All GLFs	Parameter	Mean	Std. dev.	(b) Recessional GLFs	Parameter	Mean	Std. dev.
All (n = 1293)	Orientation (º)	145	117	All (n = 436)	Orientation (º)	167	87.0
	Elevation (m)	-363	1950		Elevation (m)	-33	1760
	Relief (m)	364	171		Relief (m)	394	176
	Latitude (º)	-	-		Latitude (º)	-	-
North (n = 723)	Orientation (º)	26	105	North (n = 197)	Orientation (º)	49	119
	Elevation (m)	-1370	1290		Elevation (m)	-1170	1180
	Relief (m)	323	161		Relief (m)	340	158
	Latitude (º)	39.3	4.90		Latitude (º)	38.4	4.80
South (n = 570)	Orientation (º)	173	73.0	South (n = 239)	Orientation (º)	175	55.0
	Elevation (m)	911	1900		Elevation (m)	900	1600
	Relief (m)	416	169		Relief (m)	439	178
	Latitude (º)	-40.8	5.30		Latitude (º)	-39.0	3.60

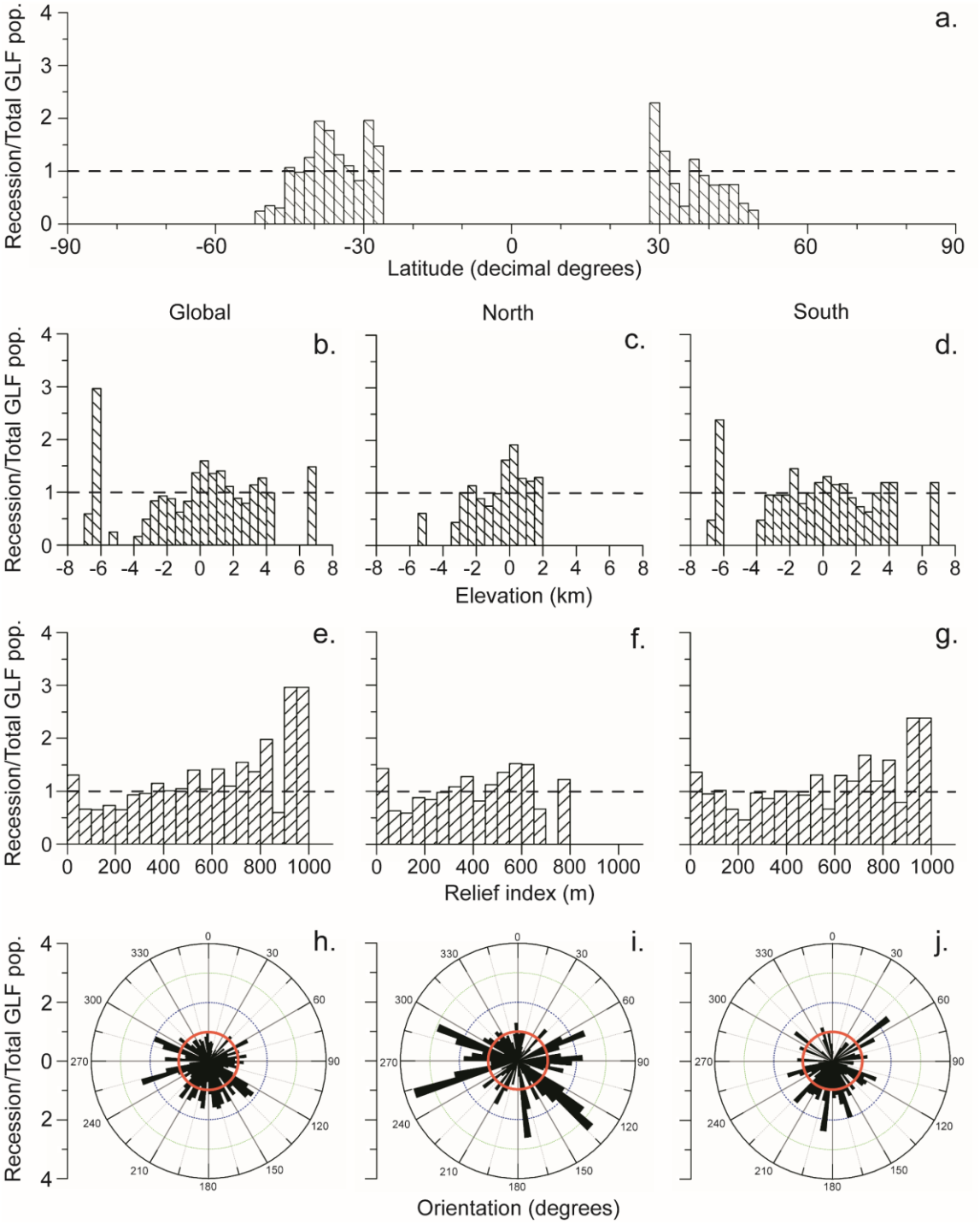

Figure 4.5: *Ratio plots showing normalised concentration of recessional GLFs relative to the normalised concentration of the total GLF population for: (a) global and hemispheric latitude in 2º bins; (b) global, (c) northern- and (d) southern-hemispheric elevation in 500 m bins; (e) global, (f) northern- and (g) southern-hemispheric relief index in 50 m bins; (h) global, (i) northern- and (j) southern-hemispheric orientation in 5º bins.*

4.3.2.2. Elevation

In contrast to latitudinal distribution of recessional GLFs, there are distinct inter-hemispheric differences in terms of elevation. Mean recessional GLF elevation of the northern and southern hemispheres was -1170 and (+)900 m (Table 4.1) respectively. In the northern hemisphere, recessional GLFs appear over-represented (ratio up to 2) at elevations close to 0 m, particularly between -500 and (+)2000 m (Figure 4.5c). In the southern hemisphere, apart from one isolated peak between -6500 and -6000 m (ratio ~2.5) and some minor fluctuations between -2000 and (+)7500 m, the elevation of recessional GLFs appears to generally reflect that of the parent GLF population (e.g. ratio of ~1).

4.3.2.3. Relief

The relief of recessional GLFs generally shows that they are over-represented towards the higher relief index values between 700 and 1000 m (Figure 4.5e–g). The mean relief index of recessional GLFs has a value of 340 m (standard deviation = 158 m) in the northern hemisphere and a slightly higher value of 439 m (standard deviation = 178 m) in the southern hemisphere (Table 4.1).

4.3.2.4. Orientation

Overall, recessional GLFs are over-represented in a broadly southward-facing orientation range between ~120 and 290º (Figure 4.5h). However, this general pattern masks an inter-hemispheric contrast: the mean bearing of recessional GLFs is 49º in the northern hemisphere, with little preference for orientation (Figure 4.5i), compared to the southern hemisphere where there is a mean bearing of 175º, and a pronounced southerly (i.e. pole-facing) orientation bias of between 150 and 225º (Figure 4.5j, Table 4.1).

4.3.3. Case study: Crater Greg GLF reconstruction

The reconstructed GLF's plan-form geometry was larger in all directions than its present day configuration. Overall, the reconstructed GLF appears to have coalesced from a wide upper basin down through a bedrock confined channel, which coupled with two lower alcoves provided mass to the narrow GLF terminus (Figures 4.3 and 4.6). The current GLF has a maximum length and width of 2.3 and 2.5 km respectively, and covers an area of 2.81 km^2. The reconstructed GLF extended ~2.5 km southward down the wall of Crater Greg to the lowest moraine ridge and northward up the steep headwall by ~400 – 500 m (Figure 4.3). The reconstructed GLF's lateral margins extended by ~700 m to the east and ~500 m to the west of the current GLFs margins (Figure 4.3). These geometric changes result in the reconstructed GLF having a maximum length and width of 5.2 and 3.5 km respectively, and covering an area of 9.67 km^2. The GLF has therefore experienced a reduction in area of 6.86 km^2, or ~70 %, since its maximum extent.

For each of the three reconstruction scenarios (Figure 4.6) we calculated the former GLF's maximum and average ice thickness (Figure 4.7), and ice volume loss relative to the present-day surface. For our low (12 kPa), mean (22 kPa) and high (38 kPa) yield strength scenarios we calculate: (i) maximum ice thickness as 38, 62, and 97 m; (ii) mean ice thickness as 19, 32, and 54 m; and (iii) ice volume loss as 0.18, 0.31, and 0.52 km^3 respectively. In general, an increase in yield strength equated to an increase in mean and maximum ice thickness, and ice volume loss, such that all values for the high yield strength reconstruction were ~2.5 times greater than the low yield strength reconstruction.

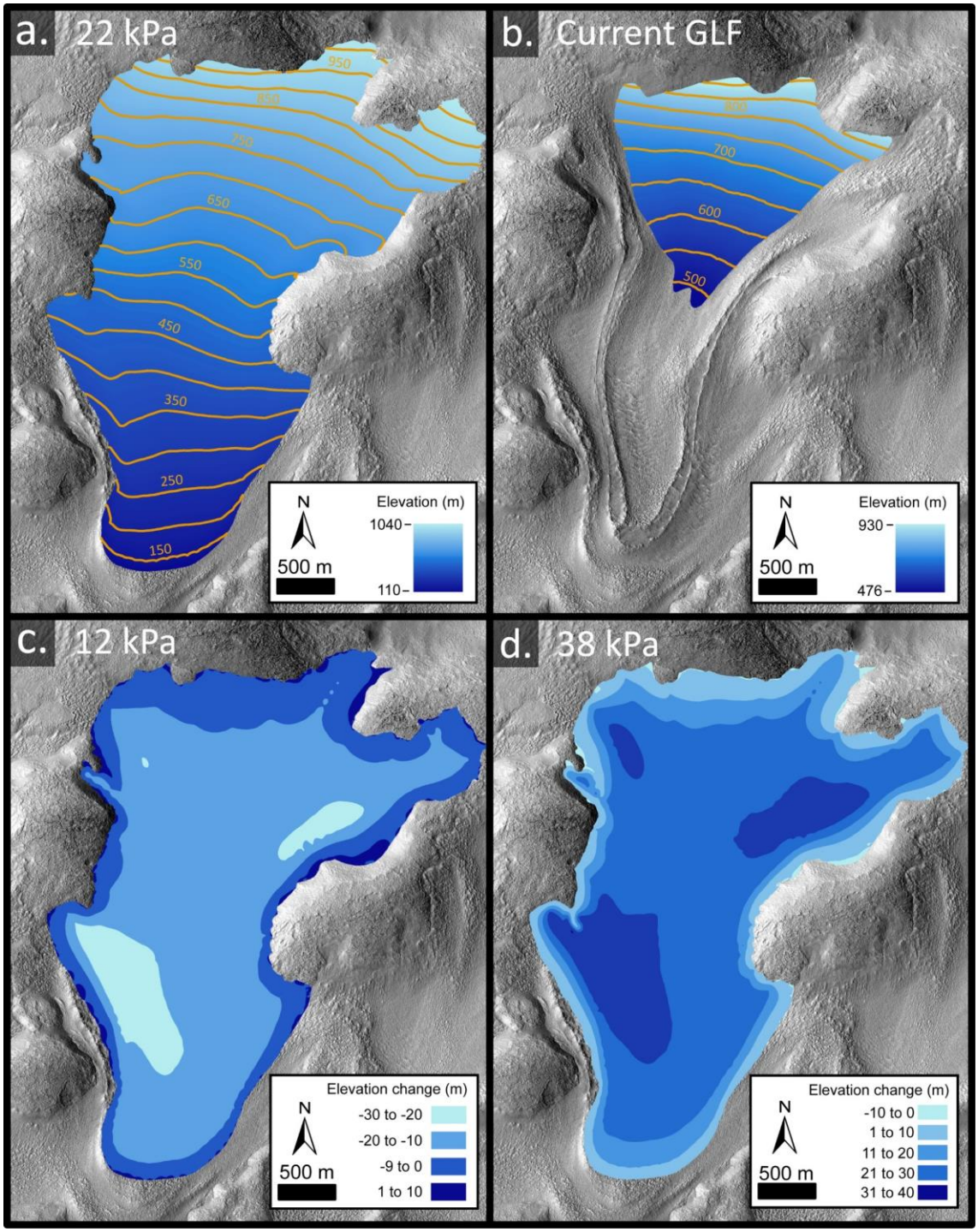

Figure 4.6: *Crater Greg GLF reconstructed palaeo-ice surface. (a) Reconstructed palaeo-ice surface based on yield strength of 22 kPa, with 50 m contours. (b) Current ice surface with 50 m contours for comparison. Difference in reconstructed palaeo-ice surface from (a) for yield strength of 12 kPa (c) and 38 kPa (d).*

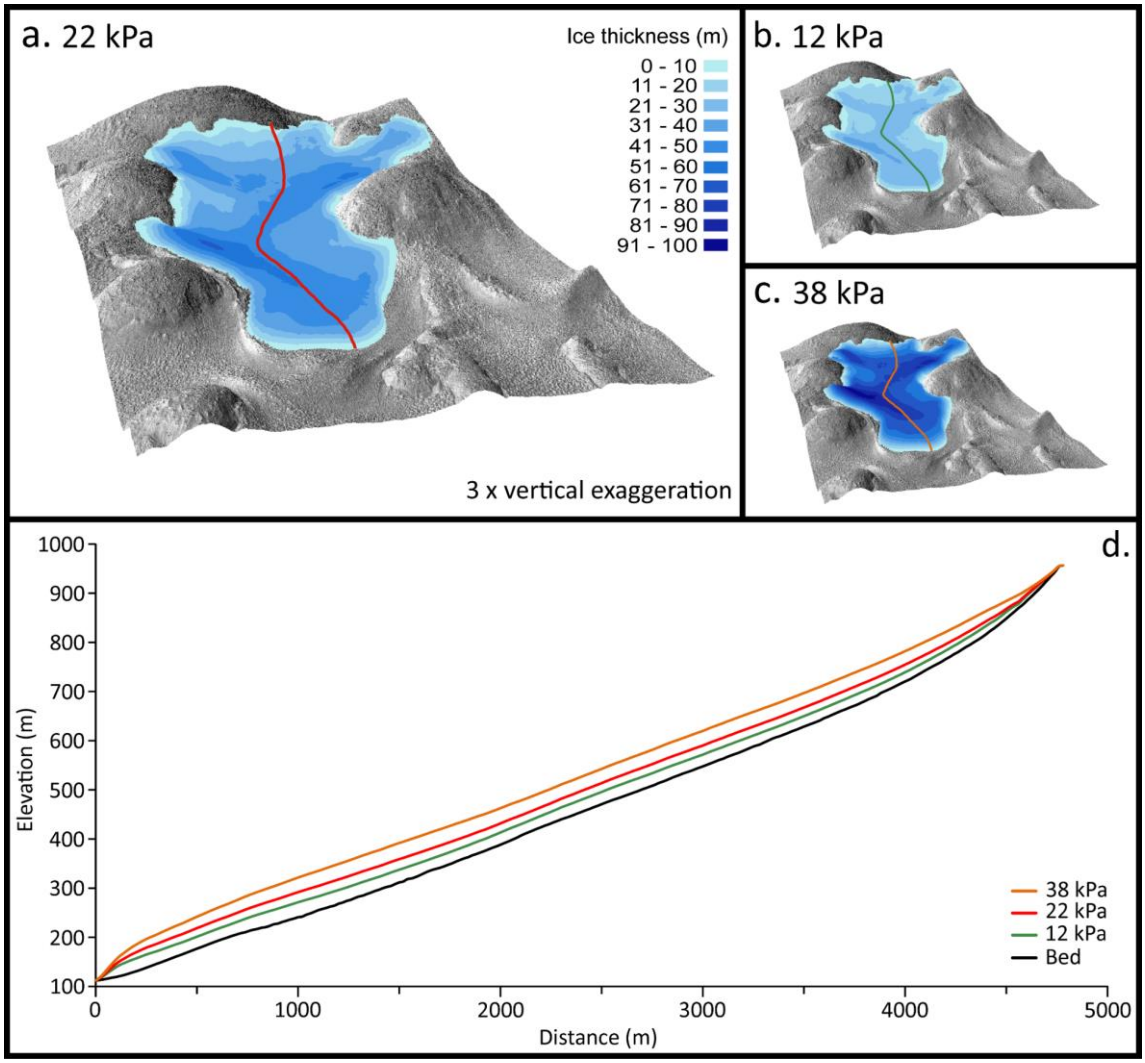

Figure 4.7: *Crater Greg GLF reconstructed three-dimensional geometry and ice thickness. Reconstructed palaeo-ice thickness for yield strength of (a) 22 kPa, (b) 12 kPa and (c) 38 kPa. (d) Palaeo-ice surface elevation of (a–c) along a central flow-line.*

4.4. Interpretation and discussion

4.4.1. Controls on GLF recession

One third of all GLFs showed evidence of recession. Such recession appears widespread in both the northern and southern hemispheres (Figure 4.4) and covers all latitude, elevation, relief and orientation ranges (Figure 4.5). This widespread evidence of recession is therefore indicative of global rather than regional or hemispheric changes in controlling, likely climatic, conditions. On Earth, the locality and survival of glaciers

are a result of the interplay of effective precipitation, temperature and topography (Cuffey and Paterson, 2010). These three factors are in turn governed by variation in latitude and altitude on the macro-scale and orientation, relief and distance from a precipitation source at a regional or more local scale.

Latitude and relief appear to exert a systematic control on where recessional GLFs occur on Mars. Both of these environmental parameters show statistical over-representation of recessional GLFs towards the boundary of their environmental ranges (Figure 4.5), although it should be noted that total numbers of GLFs are lower in these regions than towards the centre of the ranges (Figures SF2 and SF4).

In terms of latitude, recessional GLFs are over-represented relative to the total GLF population at lower latitudes (i.e. closer to the equator). This over-representation occurs within the latitudinal range between 25 and 40^{o} in both the northern and southern hemisphere and was particularly enhanced between 26 and 32^{o} in both (Figure 4.5a). This association was not apparent for the higher pole-ward latitudes between 40 and 65^{o}, where recessional GLFs are conversely equally- or under-represented (Figure 4.5a). The over-representation of recessional GLFs in the lower latitudinal domain may be a direct reflection of the current stability of shallow ground ice on the planet. At present, ground ice is suggested to be stable at depths of less than 5 m pole-ward of ~45^{o} (Mellon et al., 2004; Bryne et al., 2009; Schorghofer and Forget, 2012). This limit provides an effective threshold such that near surface ice at lower latitudes is at best meta-stable and susceptible to sublimation/ablation. Thus, although recession is identified across all latitudes, over-representation of recessional GLFs at lower latitudes (25 – 40^{o} in particular) suggests that ice is being preferentially removed from these localities, with corresponding implications for preferential GLF recession.

In terms of relief, recessional GLFs were over-represented in areas of higher relief index values in both the northern and southern hemispheres (Figure 4.5e – g), albeit covering a slightly lower index value in the northern hemisphere (550 – 800 m) than in the southern hemisphere (700 – 1000 m [Figure 4.5e–g]). This hemispheric difference mirrors that of the overall GLF population (Figures SF2 and SF4 [Souness et al., 2012]), and also potentially that identified at the wider VFF scale (e.g. Karlsson et al., 2015). On Earth, relief plays an important role in glacier formation and preservation. On higher

relief (steeper) slopes, glaciers are prone to particularly rapid mass change due to a high sensitivity to changes in mass balance and potentially increased solar insolation if they are tilted towards the Sun (see discussion below), or even complete mass loss as a result of avalanching (e.g. Raper and Braithwaite, 2009). While there is little evidence of ice avalanching on Mars, steeper GLFs are still likely to respond more rapidly to climatic change. Although recession is observed across all relief values, the over-representation of recessional GLFs at higher relief values may therefore reflect that they have already re-adjusted their mass distribution to recent climatic change(s), whereas lower relief GLFs are still re-adjusting to climatic perturbations. Furthermore, surface debris can accumulate to thicker depths on shallower slopes, a process that would further dampen the rate in mass response of lower-relief GLFs (e.g. Marchant et al., 2002).

The over-represented recessional GLF latitude and relief domains often host low total GLF numbers (Figures SF2 and SF4 [Souness et al., 2012]). We attribute this association to environmental conditions that are marginal for initial GLF formation, and/or their subsequent preservation.

In terms of elevation and orientation, there was no clear systematic pattern of recessional GLFs visible at either the global or hemispheric scale. For example, Souness et al. (2012) found that GLFs showed a strong pole-ward bias in orientation in both the northern and southern hemisphere. These authors related this bias to the fact that pole-facing alcoves received lower insolation than equatorial facing alcoves and therefore, much like terrestrial glaciers, were more likely to be conducive to accumulation and preservation of ice. Thus, if orientation was to exert a dominant control over GLF recession, one would expect to see GLFs facing away from their nearest pole (i.e. equatorial facing: south in the northern hemisphere and north in the southern hemisphere) to be over-represented – a pattern that was not identified (Figure 4.5h – j).

There are at least two potential explanations as to why no orientation bias was observed in the distribution of recessional GLFs. First, this inventory only considers current GLFs and does not consider potential sites of former GLFs that have been either partially removed (e.g. Figure 4.1d), and therefore no longer conform to the definition of a GLF as set out by Souness et al. (2012), or completely removed so that a glaciated

(ice free) landscape now prevails (e.g. Figure 4.1d). During lower obliquity periods, equator-facing slopes are likely to receive higher insolation than pole-facing slopes, and equator-facing GLFs are therefore more likely to be preferentially removed than pole-facing GLFs. Second, it may be possible that a regime similar to those used to explain scalloped terrain development (e.g. Lefort et al., 2009; Ulrich et al., 2010; Séjourné et al., 2011) and gully formation (Costard et al., 2002) may also affect GLFs. Here, it is argued that during periods of very high obliquity (≥45^{o}) pole-facing slopes become the more likely regions of higher insolation and day-averaged summer temperatures, and thus preferential sites for ice removal, relative to equator-facing slopes (Costard et al., 2002). If we take into account obliquity variation over the last 20 Ma, a period for which reliable obliquity solutions have been obtained (Laskar et al., 2004) and one which covers the possible age of GLFs (Hartmann et al., 2014), Mars has experienced at least six periods of obliquity of ≥45^{o} (Laskar et al., 2004). However, it should be noted that these high obliquity excursions are relatively short lived and that the last 20 Ma has been dominated by obliquity ≤45^{o} (Laskar et al., 2004). Therefore, it is possible that at least two contrasting signals are manifested in the orientation distribution of recessional GLFs, with one preferentially reducing/removing equator-facing GLFs and the other preferentially reducing/removing pole-facing GLFs. Although the exact contribution and importance of these processes to ice removal remains unknown, it does provide a potential explanation for the observed orientation distribution of recessional GLFs.

Taken together, these results can add further perspective to the development and evolution of glacial/periglacial landforms in Mars' mid-latitudes. Several landforms or terrains, including dissected mantle terrain (Mustard et al., 2001; Kreslavsky and Head, 2002; Milliken and Mustard, 2003), banded terrain (Diot et al., 2014), scalloped depressions (Lefort et al., 2009; Ulrich et al., 2010; Séjourné et al., 2011), polygons (Mangold, 2005), and VFFs (Milliken et al., 2003; Souness et al., 2012; Levy et al., 2014) appear between 30 and 60^{o} in both hemispheres, and have been, to various degrees, attributed to latitude-dependent insolation forcing. The identification of a latitudinal threshold at ~40^{o} in both hemispheres, below which GLFs are preferentially removed (Figure 4.5), would conform to this hypothesis, particularly as this latitude falls close to the current stability of shallow ground ice on the planet (Mellon et al., 2004; Bryne et al., 2009; Schorghofer and Forget, 2012). However, there is also some degree of heterogeneity in recession, whereby GLFs in a similar setting do not show a

similar response (Figures 4.4 and 4.5). It is therefore likely that regional or local meteorological conditions also play a role in GLF survival and/or initial emplacement, as may be the scenario for other mid-latitude glacial/periglacial landforms (Conway and Balme, 2014; Levy et al., 2014).

4.4.2. Crater Greg GLF reconstruction and population ice loss potential

Our reconstructed GLF in Crater Greg has changed substantially since its former maximum. The GLF has receded 3 km, or ~60 %, of its maximum length, and lost an area of 6.86 km^2, or ~70 %, of its maximum extent (Figures 4.6 and 4.7). Assuming that the mean yield strength of 22 kPa (Section 4.2.2.2) is the most appropriate value for our GLF reconstruction, we calculate that the GLF had a maximum and mean ice thickness of 62 and 32 m respectively (Figure 4.7), and has lost an ice volume of 0.31 km^3. The GLF in Crater Greg has therefore undergone substantial mass loss since the LMGM, with these changes manifested in both surface lowering and terminus recession.

The identification of over 400 GLFs showing evidence of recession, coupled with substantial mass and area loss for our reconstructed case study GLF, suggests that a large proportion of ice has been removed from GLFs since the LMGM. Although tentative, assuming that the volume loss of 0.18 – 0.52 km^3 from the reconstructed Crater Greg GLF (Section 4.3.3) is typical of all recessional GLFs (n = 436), yields a first-order estimate of global ice volume loss from GLFs since the LMGM of between 78 and 227 km^3, with a best estimate of 135 km^3 for an optimum yield strength of 22 kPa – an equivalent ice volume to that currently stored in the Alpine glaciers of central Europe (Huss and Farinotti, 2012), although the mass balance terms are likely very different in the two settings.

This generalised estimate does emphasise the requirement for regional- or population-scale reconstruction studies if we are to improve our current understanding of the evolution of mid-latitude ice deposits under a changing martian climate. For example, recessional GLFs in the northern hemisphere have an overall lower elevation and relief index than those in the southern hemisphere (Section 4.2 and Figure SF4). Thus, these

spatially varying conditions, coupled with potential endogenic environmental variability in, for example, ice-debris content, ice grain size or supra-glacial debris layer thickness, are likely to exert some control over the rates of individual GLF recession and volume loss (i.e. a non-uniform recession rate and ice volume change in GLFs [Parsons et al., 2011]) – a ubiquitous occurrence on terrestrial glaciers (e.g. Scherler et al., 2011). Such variability would be captured by high-resolution mapping and reconstruction of all recessional GLFs. Similar studies have proven useful on terrestrial glaciers (e.g. Glasser et al., 2011), and would be a beneficial avenue for future research on Mars.

Several lines of evidence have been presented for partial to complete degradation of non-polar ice deposits (e.g. Head and Marchant, 2003; Dickson et al., 2008; Hauber et al., 2008), and although not formally analysed herein, several instances of alcoves adjacent to GLFs containing ice remnants were observed (e.g. Figure 4.1d). It is possible that such deposits are the remains of former GLFs that have partially, or completely, receded since ice emplacement. Thus, in restricting this analysis to identified GLFs (Souness et al., 2012), total ice volume loss has likely been underestimated. Therefore, due to the potential sources of over- or under-estimation outlined above, the estimate of ice volume loss from GLFs reported here should be viewed only as an initial approximation, pending refinement based on a more granular-level analysis.

The estimated ice volume loss from GLFs (135 km^3) is minor relative to the volume of ice contained in the Northern Polar Layered Deposits (~821,000 km^3 [Putzig et al., 2009]), which potentially serves as a likely reservoir exchanging mass with the mid-latitudes (e.g. Head et al., 2003, Levrard et al., 2004). Thus, although not a significant mass exchange at the planetary level, the GLF ice loss we report is potentially important for mid-latitude environmental conditions and landform development.

4.5. Conclusions

Visual analysis of 1293 GLFs reveals that 436 show evidence of an expanded former extent. This recession is distributed across both the northern and southern hemispheres, thereby indicating widespread climatic change on Mars. Although recession is observed

across all environmental parameters, the statistical over-representation of recessional GLFs is particularly pronounced in (i) low latitude and (ii) high relief domains, suggesting that these parameters exert some control over GLF recession. With respect to latitude, GLFs between 25 and 40^{o} in both hemispheres appear to be preferentially experiencing mass loss. Here, the higher latitudinal boundary coincides with the limit of present day ground ice stability, and, as such, may represent a threshold between the effective preservation and sublimation/ablation of GLFs. The over-representation of recessional GLFs in regions of higher relief would suggest that, like their terrestrial counterparts, these ice masses have a shorter response time to climatic perturbations than lower relief GLFs, reflecting the influence of slope on mass redistribution both directly and indirectly via the stability of supraglacial debris. These two domains of over-representation of recessional GLFs are characterised by low total GLF numbers, suggesting that the areas already represent zones of marginal glaciation, which have subsequently become un-stable under martian climatic change.

Our GLF reconstruction provides, to our knowledge, the first estimate of both area and volume loss from a GLF (noting that similar studies have previously been applied to other, often large scale, ice masses [e.g. Shean et al., 2005]). Results indicate that the case study Crater Greg GLF has receded in area by ~70 % and has lost an ice volume between 0.18 and 0.52 km^3, with a best estimate of 0.31 km^3, since its former maximum extent. Scaling this up to all recessional GLFs (n = 436) suggests a global first-order estimate of ice volume loss from Mars' mid-latitude GLFs of between 78 and 227 km^3, with a best estimate of 135 km^3. Future research should focus on refining this estimate through consideration of volume change at all individual recessional GLFs, as well as on the much wider VFF scale (e.g. Levy et al., 2014).

Acknowledgements

We thank various parties including University of Arizona, NASA/JPL, Arizona State University and Malin Space Science Systmes for their efforts in capturing and making the various forms of data we investigated herein available to the public. We thank Ajay Limaye for preparing the HiRISE DEM utilised in our GLF reconstruction. Finally, we

thank the Editor Jeffrey Johnson and two anonymous reviewers for their helpful and insightful comments; they ultimately helped improve the quality of the manuscript. SB is funded by an Aberystwyth University Doctoral Career Development Scholarship. AH gratefully acknowledges support from the Research Council of Norway through its Centres of Excellence funding scheme, project number 223259.

References

Arfstrom, J., & Hartmann, W. K. (2005). Martian flow features, moraine-like ridges, and gullies: Terrestrial analogs and interrelationships. *Icarus, 174*(2), 321-335. doi: 10.1016/j.icarus.2004.05.026.

Baker, D. M. H., Head, J. W., & Marchant, D. R. (2010). Flow patterns of lobate debris aprons and lineated valley fill north of Ismeniae Fossae, Mars: Evidence for extensive mid-latitude glaciation in the Late Amazonian. *Icarus, 207*(1), 186-209. doi: 10.1016/j.icarus.2009.11.017.

Benn, D. I., Owen, L. A., Osmaston, H. A., Seltzer, G. O., Porter, S. C., & Mark, B. (2005). Reconstruction of equilibrium-line altitudes for tropical and sub-tropical glaciers. *Quaternary International, 138-139*, 8-21. doi: 10.1016/j.quaint.2005.02.003.

Brough, S., Hubbard, B., Souness, C. J., Grindrod, P. M., & Davis, J. (2016). Landscapes of polyphase glaciation: eastern Hellas Planitia, Mars. *Journal of Maps, 12*(3), 530-542. doi: 10.1080/17445647.2015.1047907.

Bryson, K., Chevrier, V., Sears, D., & Ulrich, R. (2008). Stability of ice on Mars and the water vapor diurnal cycle: Experimental study of the sublimation of ice through a fine-grained basaltic regolith. *Icarus, 196*(2), 446-458. doi: 10.1016/j.icarus.2008.02.011.

Byrne, S., Dundas, C. M., Kennedy, M. R., Mellon, M. T., McEwen, A. S., Cull, S. C., Dauber, I. J., Shean, D. E., Seelos, K. D., Murchie, S. L., Cantor, B. A., Arvidson, R. E., Edgett, K. S., Reufer, A., Thomas, N., Harrison, T. N., Posiolova, L. V., & Seelos, F. P. (2009). Distribution of mid-latitude ground ice on Mars from new impact craters. *Science, 325*(5948), 1674-1676. doi: 10.1126/science.1175307.

Carrivick, J. L., Berry, K., Geilhausen, M., James, W. H. M., Williams, C., Brown, L. E., Rippin, D. M., & Carver, S. J. (2015). Decadal-scale changes of the Ödenwinkelkees, Central Austria, suggest increasing control of topography and evolution towards steady state. *Geografiska Annaler: Series A, Physical Geography, 97*(3), 543-562. doi: 10.1111/geoa.12100.

Conway, S. J., & Balme, M. R. (2014). Decameter thick remnant glacial ice deposits on Mars. *Geophysical Research Letters, 41*(15), 2014GL060314. doi: 10.1002/2014gl060314.

Costard, F., Forget, F., Mangold, N., & Peulvast, J. P. (2002). Formation of recent Martian debris flows by melting of near-surface ground ice at high obliquity. *Science, 295*(5552), 110-113. doi: 10.1126/science.1066698.

Cuffey, K. M., & Paterson, W. S. B. (2010). *The Physics of Glaciers* (4th ed.). Oxford: Butterworth-Heinemann.

Dickson, J. L., Head, J. W., & Marchant, D. R. (2008). Late Amazonian glaciation at the dichotomy boundary on Mars: Evidence for glacial thickness maxima and multiple glacial phases. *Geology, 36*(5), 411-414. doi: 10.1130/g24382a.1.

Dickson, J. L., Head, J. W., & Marchant, D. R. (2010). Kilometer-thick ice accumulation and glaciation in the northern mid-latitudes of Mars: Evidence for crater-filling events in the Late Amazonian at the Phlegra Montes. *Earth and Planetary Science Letters, 294*(3-4), 332-342. doi: 10.1016/j.epsl.2009.08.031.

Diot, X., El-Maarry, M. R., Schlunegger, F., Norton, K. P., Thomas, N., & Grindrod, P. M. (2014). The geomorphology and morphometry of the banded terrain in Hellas basin, Mars. *Planetary and Space Science, 101*, 118-134. doi: 10.1016/j.pss.2014.06.013.

Fassett, C. I., Levy, J. S., Dickson, J. L., & Head, J. W. (2014). An extended period of episodic northern mid-latitude glaciation on Mars during the Middle to Late Amazonian: Implications for long-term obliquity history. *Geology, 42*(9), 763-766. doi: 10.1130/g35798.1.

Fastook, J. L., Head, J. W., & Marchant, D. R. (2014). Formation of lobate debris aprons on Mars: Assessment of regional ice sheet collapse and debris-cover armoring. *Icarus, 228*, 54-63. doi: 10.1016/j.icarus.2013.09.025.

Fischer, M., Huss, M., & Hoelzle, M. (2015). Surface elevation and mass changes of all Swiss glaciers 1980–2010. *The Cryosphere*, *9*(2), 525-540. doi: 10.5194/tc-9-525-2015.

Forget, F., Haberle, R. M., Montmessin, F., Levrard, B., & Heads, J. W. (2006). Formation of glaciers on Mars by atmospheric precipitation at high obliquity. *Science, 311*(5759), 368-371. doi: 10.1126/science.1120335.

Glasser, N. F., Harrison, S., Jansson, K. N., Anderson, K., & Cowley, A. (2011). Global sea-level contribution from the Patagonian Icefields since the Little Ice Age maximum. *Nature Geoscience, 4*(5), 303-307. doi: 10.1038/ngeo1122.

Grima, C., Kofman, W., Mouginot, J., Phillips, R. J., Hérique, A., Biccari, D., Seu, R., & Ccutigni, M. (2009). North polar deposits of Mars: Extreme purity of the water ice. *Geophysical Research Letters, 36*(3), L03203. doi: 10.1029/2008gl036326.

Hambrey, M. J., & Glasser, N. F. (2012). Discriminating glacier thermal and dynamic regimes in the sedimentary record. *Sedimentary Geology, 251–252*, 1-33. doi: 10.1016/j.sedgeo.2012.01.008.

Hambrey, M. J., Murray, T., Glasser, N. F., Hubbard, A., Hubbard, B., Stuart, G., Hansen, S., & Kohler, J. (2005). Structure and changing dynamics of a polythermal valley glacier on a centennial timescale: Midre Lovénbreen, Svalbard. *Journal of Geophysical Research: Earth Surface, 110*(F1), F01006. doi: 10.1029/2004jf000128.

Hartmann, W. K., Thorsteinsson, T., & Sigurdsson, F. (2003). Martian hillside gullies and Icelandic analogs. *Icarus, 162*(2), 259-277. doi: 10.1016/S0019-1035(02)00065-9.

Hartmann, W. K., Ansan, V., Berman, D. C., Mangold, N., & Forget, F. (2014). Comprehensive analysis of glaciated martian crater Greg. *Icarus, 228*, 96-120. doi: 10.1016/j.icarus.2013.09.016.

Hauber, E., van Gasselt, S., Chapman, M. G., & Neukum, G. (2008). Geomorphic evidence for former lobate debris aprons at low latitudes on Mars: Indicators of the Martian paleoclimate. *Journal of Geophysical Research, 113*(E2), E02007. doi: 10.1029/2007je002897.

Head, J. W., & Marchant, D. R. (2003). Cold-based mountain glaciers on Mars: Western Arsia Mons. *Geology, 31*(7), 641-644. doi: 10.1130/0091-7613(2003)031<0641:cmgomw>2.0.co;2.

Head, J. W., Marchant, D. R., Agnew, M. C., Fassett, C. I., & Kreslavsky, M. A. (2006). Extensive valley glacier deposits in the northern mid-latitudes of Mars: Evidence for Late Amazonian obliquity-driven climate change. Earth and Planetary Science Letters, 241(3-4), 663-671. doi: 10.1016/j.epsl.2005.11.016.

Head, J. W., Marchant, D. R., Dickson, J. L., Kress, A. M., & Baker, D. M. (2010). Northern mid-latitude glaciation in the Late Amazonian period of Mars: Criteria for the recognition of debris-covered glacier and valley glacier landsystem deposits. *Earth and Planetary Science Letters, 294*(3-4), 306-320. doi: 10.1016/j.epsl.2009.06.041.

Head, J. W., Mustard, J. F., Kreslavsky, M. A., Milliken, R. E., & Marchant, D. R. (2003). Recent ice ages on Mars. *Nature, 426*(6968), 797-802. doi: 10.1038/Nature02114.

Head, J. W., Neukum, G., Jaumann, R., Hiesinger, H., Hauber, E., Carr, M., Massson, P., Foing, B., Hoffmann, H., Kreslavsky, M., Werner, S., Milkovich, S., van Gasselt, S., & HRSC Co-Investigator Team. (2005). Tropical to mid-latitude snow and ice accumulation, flow and glaciation on Mars. *Nature, 434*(7031), 346-351. doi: 10.1038/Nature03359.

Hobley, D. E. J., Howard, A. D., & Moore, J. M. (2014). Fresh shallow valleys in the Martian midlatitudes as features formed by meltwater flow beneath ice. *Journal of Geophysical Research-Planets, 119*(1), 128-153. doi: 10.1002/2013je004396.

Holt, J. W., Safaeinili, A., Plaut, J. J., Head, J. W., Phillips, R. J., Seu, R., Kempft, S. D., Choudhary, P., Young, D. A., Putzig, N. E., Biccari, D., & Gim, Y. (2008). Radar Sounding Evidence for Buried Glaciers in the Southern Mid-Latitudes of Mars. *Science, 322*(5905), 1235-1238. doi: 10.1126/science.1164246.

Hubbard, B., Souness, C., & Brough, S. (2014). Glacier-like forms on Mars. *The Cryosphere, 8*(6), 2047-2061. doi: 10.5194/tc-8-2047-2014.

Hubbard, B., Milliken, R. E., Kargel, J. S., Limaye, A., & Souness, C. J. (2011). Geomorphological characterisation and interpretation of a mid-latitude glacier-like form: Hellas Planitia, Mars. *Icarus, 211*(1), 330-346. doi: 10.1016/j.icarus.2010.10.021.

Huss, M., & Farinotti, D. (2012). Distributed ice thickness and volume of all glaciers around the globe. *Journal of Geophysical Research: Earth Surface, 117*(F4), F04010. doi: 10.1029/2012jf002523.

Kargel, J. S. (2004). *Mars: A Warmer, Wetter Planet*. London: Springer-Praxis.

Kargel, J. S., Baker, V. R., Beget, J. E., Lockwood, J. F., Pewe, T. L., Shaw, J. S., & Strom, R. G. (1995). Evidence of Ancient Continental-Glaciation in the Martian Northern Plains. *Journal of Geophysical Research-Planets, 100*(E3), 5351-5368. doi: 10.1029/94je02447.

Karlsson, N. B., Schmidt, L. S., & Hvidberg, C. S. (2015). Volume of Martian midlatitude glaciers from radar observations and ice flow modeling. *Geophysical Research Letters, 42*(8), 2672-2633. doi: 10.1002/2015gl063219.

Kirk, R. L., Howington-Kraus, E., Rosiek, M. R., Anderson, J. A., Archinal, B. A., Becker, K. J., Cook, D. A., Galuszka, D. M., Geissler, P. E., Hare, T. M., Holmberg, I. M., Keszthelyi, L. P., Redding, B. L., Delamere, W. A., Gallagher, D., Chapel, J. D., Eliason, E. M., King, R., & McEwen, A. S. (2008). Ultrahigh resolution topographic mapping of Mars with MRO HiRISE stereo images: Meter-scale slopes of candidate Phoenix landing sites. *Journal of Geophysical Research, 113*, E00A24. doi: 10.1029/2007je003000.

Kleman, J., Hattestrand, C., Borgstrom, I., & Stroeven, A. (1997). Fennoscandian palaeoglaciology reconstructed using a glacial geological inversion model. *Journal of Glaciology, 43*(144), 283-299. Doi: 10.1017/S0022143000003233.

Kreslavsky, M. A., & Head, J. W. (2002). Mars: Nature and evolution of young latitude-dependent water-ice-rich mantle. *Geophysical Research Letters, 29*(15). doi: 10.1029/2002gl015392.

Laskar, J., Correia, A. C. M., Gastineau, M., Joutel, F., Levrard, B., & Robutel, P. (2004). Long term evolution and chaotic diffusion of the insolation quantities of Mars. *Icarus, 170*(2), 343-364. doi: 10.1016/j.icarus.2004.04.005.

Lefort, A., Russell, P. S., Thomas, N., McEwen, A. S., Dundas, C. M., & Kirk, R. L. (2009). Observations of periglacial landforms in Utopia Planitia with the High Resolution Imaging Science Experiment (HiRISE). *Journal of Geophysical Research: Planets, 114*(E4), E04005. doi: 10.1029/2008je003264.

Levrard, B., Forget, F., Montmessin, F., & Laskar, J. (2004). Recent ice-rich deposits formed at high latitudes on Mars by sublimation of unstable equatorial ice during low obliquity. *Nature, 431*(7012), 1072-1075. doi: 10.1038/nature03055.

Levy, J. S., Head, J. W., & Marchant, D. R. (2007). Lineated valley fill and lobate debris apron stratigraphy in Nilosyrtis Mensae, Mars: Evidence for phases of

glacial modification of the dichotomy boundary. *Journal of Geophysical Research, 112*(E8), E08004. doi: 10.1029/2006je002852.

Levy, J. S., Fassett, C. I., Head, J. W., Schwartz, C., & Watters, J. L. (2014). Sequestered glacial ice contribution to the global Martian water budget: Geometric constraints on the volume of remnant, midlatitude debris-covered glaciers. *Journal of Geophysical Research: Planets, 119*(10), 2014JE004685. doi: 10.1002/2014je004685.

Lucchitta, B. K. (1984). Ice and debris in the Fretted Terrain, Mars. *Journal of Geophysical Research: Solid Earth, 89*(S02), B409-B418. doi: 10.1029/JB089iS02p0B409.

Madeleine, J. B., Forget, F., Head, J. W., Levrard, B., Montmessin, F., & Millour, E. (2009). Amazonian northern mid-latitude glaciation on Mars: A proposed climate scenario. *Icarus, 203*(2), 390-405. doi: 10.1016/j.icarus.2009.04.037.

Mangold, N. (2003). Geomorphic analysis of lobate debris aprons on Mars at Mars Orbiter Camera scale: Evidence for ice sublimation initiated by fractures. *Journal of Geophysical Research, 108*(E4), 8021. doi: 10.1029/2002je001885.

Mangold, N. (2005). High latitude patterned grounds on Mars: Classification, distribution and climatic control. *Icarus, 174*(2), 336-359. doi: 10.1016/j.icarus.2004.07.030.

Marchant, D., & Head, J. W. (2003). Tongue-shaped lobes on Mars: Morphology, Nomenclature, and Relation to Rock Glacier Deposits. Abstract #3091, *Sixth International Conference on Mars, July 20-25, Pasadena, California.*

Marchant, D. R., Lewis, A. R., Phillips, W. M., Moore, E. J., Souchez, R. A., Denton, G. H., Sugden, D. E., Potter Jr, N., & Landis, G. P. (2002). Formation of patterned ground and sublimation till over Miocene glacier ice in Beacon Valley, southern Victoria Land, Antarctica. *Geological Society of America Bulletin 114*(6), 718-730. doi: 10.1130/0016-7606(2002)114<0718:fopgas>2.0.co;2.

Mellon, M. T., & Jakosky, B. M. (1995). The distribution and behavior of Martian ground ice during past and present epochs. *Journal of Geophysical Research: Planets, 100*(E6), 11781-11799. doi: 10.1029/95je01027.

Mellon, M. T., Feldman, W. C., & Prettyman, T. H. (2004). The presence and stability of ground ice in the southern hemisphere of Mars. *Icarus, 169*(2), 324-340. doi: 10.1016/j.icarus.2003.10.022.

Milliken, R. E., & Mustard, J. F. (2003). Erosional morphologies and characteristics of latitude-dependant surface mantles on Mars. Abstract #3240, *Sixth International Conference on Mars, July 20-25, Pasadena, California*.

Milliken, R. E., Mustard, J. F., & Goldsby, D. L. (2003). Viscous flow features on the surface of Mars: Observations from high-resolution Mars Orbiter Camera (MOC) images. *Journal of Geophysical Research-Planets, 108*(E6), 5057. doi: 10.1029/2002je002005.

Mustard, J. F., Cooper, C. D., & Rifkin, M. K. (2001). Evidence for recent climate change on Mars from the identification of youthful near-surface ground ice. *Nature, 412*(6845), 411-414. doi: 10.1038/35086515.

Nuimura, T., Sakai, A., Taniguchi, K., Nagai, H., Lamsal, D., Tsutaki, S., Kozawa, A., Hoshina, Y., Takenaka, S., Omiya, S., Tsunematsu, K., Tshering, P., & Fujita, K. (2015). The GAMDAM glacier inventory: a quality-controlled inventory of Asian glaciers. *The Cryosphere, 9*(3), 849-864. doi: 10.5194/tc-9-849-2015.

Nye, J. F. (1951). The Flow of Glaciers and Ice-Sheets as a Problem in Plasticity. *Proceedings of the Royal Society of London Series a-Mathematical and Physical Sciences, 207*(1091), 554-572. doi: 10.1098/rspa.1951.0140.

Nye, J. F. (1952). A Method of Calculating the Thicknesses of the Ice-Sheets. *Nature, 169*(4300), 529-530. doi: 10.1038/169529a0.

Parsons, R. A., Nimmo, F., & Miyamoto, H. (2011). Constraints on martian lobate debris apron evolution and rheology from numerical modeling of ice flow. *Icarus, 214*(1), 246-257. doi: 10.1016/j.icarus.2011.04.014.

Plaut, J. J., Safaeinili, A., Holt, J. W., Phillips, R. J., Head, J. W., Seu, R., Putzig, N. E., & Frigeri, A. (2009). Radar evidence for ice in lobate debris aprons in the mid-northern latitudes of Mars. *Geophysical Research Letters, 36*(2), L02203. doi: 10.1029/2008gl036379.

Putzig, N. E., Phillips, R. J., Campbell, B. A., Holt, J. W., Plaut, J. J., Carter, L. M., Egan, A. F., Bernardini, F., Safaeinili, A., & Seu, R. (2009). Subsurface structure of Planum Boreum from Mars Reconnaissance Orbiter Shallow Radar soundings. *Icarus, 204*(2), 443-457. doi: 10.1016/j.icarus.2009.07.034.

Racoviteanu, A. E., Manley, W. F., Arnaud, Y., & Williams, M. W. (2007). Evaluating digital elevation models for glaciologic applications: An example from Nevado Coropuna, Peruvian Andes. *Global and Planetary Change, 59*(1–4), 110-125. doi: 10.1016/j.gloplacha.2006.11.036.

Radić, V., & Hock, R. (2014). Glaciers in the Earth's Hydrological Cycle: Assessments of Glacier Mass and Runoff Changes on Global and Regional Scales. *Surveys in Geophysics, 35*(3), 813-837. doi: 10.1007/s10712-013-9262-y.

Raper, S. C. B., & Braithwaite, R. J. (2009). Glacier volume response time and its links to climate and topography based on a conceptual model of glacier hypsometry. *The Cryosphere, 3*(2), 183-194. doi: 10.5194/tc-3-183-2009.

Scherler, D., Bookhagen, B., & Strecker, M. R. (2011). Spatially variable response of Himalayan glaciers to climate change affected by debris cover. *Nature Geoscience, 4*(3), 156-159. doi: 10.1038/ngeo1068.

Schorghofer, N., & Forget, F. (2012). History and anatomy of subsurface ice on Mars. *Icarus, 220*(2), 1112-1120. doi: 10.1016/j.icarus.2012.07.003.

Séjourné, A., Costard, F., Gargani, J., Soare, R. J., Fedorov, A., & Marmo, C. (2011). Scalloped depressions and small-sized polygons in western Utopia Planitia, Mars: A new formation hypothesis. *Planetary and Space Science, 59*(5–6), 412-422. doi: 10.1016/j.pss.2011.01.007.

Sharp, R. P. (1973). Mars - Fretted and Chaotic Terrains. *Journal of Geophysical Research, 78*(20), 4073-4083. doi: 10.1029/Jb078i020p04073.

Shean, D. E., Head, J. W., & Marchant, D. R. (2005). Origin and evolution of a cold-based tropical mountain glacier on Mars: The Pavonis Mons fan-shaped deposit. *Journal of Geophysical Research: Planets, 110*(E5), E05001. doi: 10.1029/2004je002360.

Sinha, R. K., & Murty, S. V. S. (2013). Evidence of extensive glaciation in Deuteronilus Mensae, Mars: Inferences towards multiple glacial events in the past epochs. *Planetary and Space Science, 86*, 10-32. doi: 10.1016/j.pss.2013.09.002.

Sinha, R. K., & Murty, S. V. S. (2015). Amazonian modification of Moreux crater: Record of recent and episodic glaciation in the Protonilus Mensae region of Mars. *Icarus, 245*, 122-144. doi: 10.1016/j.icarus.2014.09.028.

Smith, M. J. (2011). Digital Mapping: Visualisation, Interpretation and Quantification of Landforms. In Smith, M. J., Paron, P., & Griffiths, J. (Eds.), *Geomorphological*

Mapping: Methods and Applications. Oxford: Elsevier, 225 – 251.

Souček, O., Bourgeois, O., Pochat, S., & Guidat, T. (2015). A 3 Ga old polythermal ice sheet in Isidis Planitia, Mars: Dynamics and thermal regime inferred from numerical modeling. *Earth and Planetary Science Letters, 426*, 176-190. doi: 10.1016/j.epsl.2015.06.038.

Souness, C. J., & Hubbard, B. (2013). An alternative interpretation of late Amazonian ice flow: Protonilus Mensae, Mars. *Icarus, 225*(1), 495-505. doi: 10.1016/j.icarus.2013.03.030.

Souness, C. J., Hubbard, B., Milliken, R. E., & Quincey, D. (2012). An inventory and population-scale analysis of martian glacier-like forms. *Icarus, 217*(1), 243-255. doi: 10.1016/j.icarus.2011.10.020.

Squyres, S. W. (1978). Martian Fretted Terrain: Flow of Erosional Debris. *Icarus, 34*(3), 600-613. doi: 10.1016/0019-1035(78)90048-9.

Squyres, S. W. (1979). The Distribution of Lobate Debris Aprons and Similar Flows on Mars. *Journal of Geophysical Research, 84*, 8087-8096. doi: 10.1029/Jb084ib14p08087.

Ulrich, M., Morgenstern, A., Günther, F., Reiss, D., Bauch, K. E., Hauber, E., Rössler, S., & Schirrmeister, L. (2010). Thermokarst in Siberian ice-rich permafrost: Comparison to asymmetric scalloped depressions on Mars. *Journal of Geophysical Research: Planets, 115*(E10), E10009. doi: 10.1029/2010je003640.

Van der Veen, C. J. (1999). Fundamentals of Glacier Dynamics. Rotterdam: A. A. Balkema.

Villa, F., De Amicia, M., & Maggi, V. (2007). GIS analysis of Rutor Glacier (Aosta Valley, Italy) volume and terminus variations. *Geografia Fisica e Dinamica Quaternaria, 30*(1), 87-95.

Wolff, I. W., Glasser, N. F., & Hubbard, A. (2013). The reconstruction and climatic implication of an independent palaeo ice cap within the Andean rain shadow east of the former Patagonian ice sheet, Santa Cruz Province, Argentina. *Geomorphology, 185*, 1-15. doi: 10.1016/j.geomorph.2012.10.018.

Zemp, M., Hoelzle, M., & Haeberli, W. (2009). Six decades of glacier mass-balance observations: a review of the worldwide monitoring network. *Annals of Glaciology, 50*(50), 101-111. doi: 10.3189/172756409787769591.

Supplementary Material Ch. 4

Former extent of glacier-like forms on Mars

Stephen BROUGH[a], Bryn HUBBARD[a] and Alun HUBBARD[a, b]

[a]*Department of Geography and Earth Sciences, Aberystwyth University, Aberystwyth, UK*

[b]*Centre for Arctic Gas Hydrate, Environment and Climate, Department of Geology, University of Tromsø, Tromsø, Norway*

Link to published article

This is supplementary material to an article published by Elsevier Inc. in Icarus on 11/03/2016, available online: http://dx.doi.org/10.1016/j.icarus.2016.03.006.

Citation for published paper

Brough, S., Hubbard, B. & Hubbard, A. (2016). Former extent of glacier-like forms on Mars. *Icarus*, *274*, 37-49. doi: 10.1016/j.icarus.2016.03.006.

This supplementary material consists of four figures and a glacier-like form (GLF) recessional inventory. The supplementary material is organised as follows:

Supplementary figures: Figures SF1 and SF2 present the raw GLF count in various size classes for longitude (º), latitude (º), elevation (m), relief index (m), and orientation (º). Figures SF3 and SF4 as in SF1 and SF2 but for recessional GLFs only.

Former_extent_GLF_inventory.xlxs: The recessional GLF inventory can be accessed at:
https://www.dropbox.com/s/o7szseuc9dwkxrn/Former_extent_GLF_inventory.xlsx?dl=0.

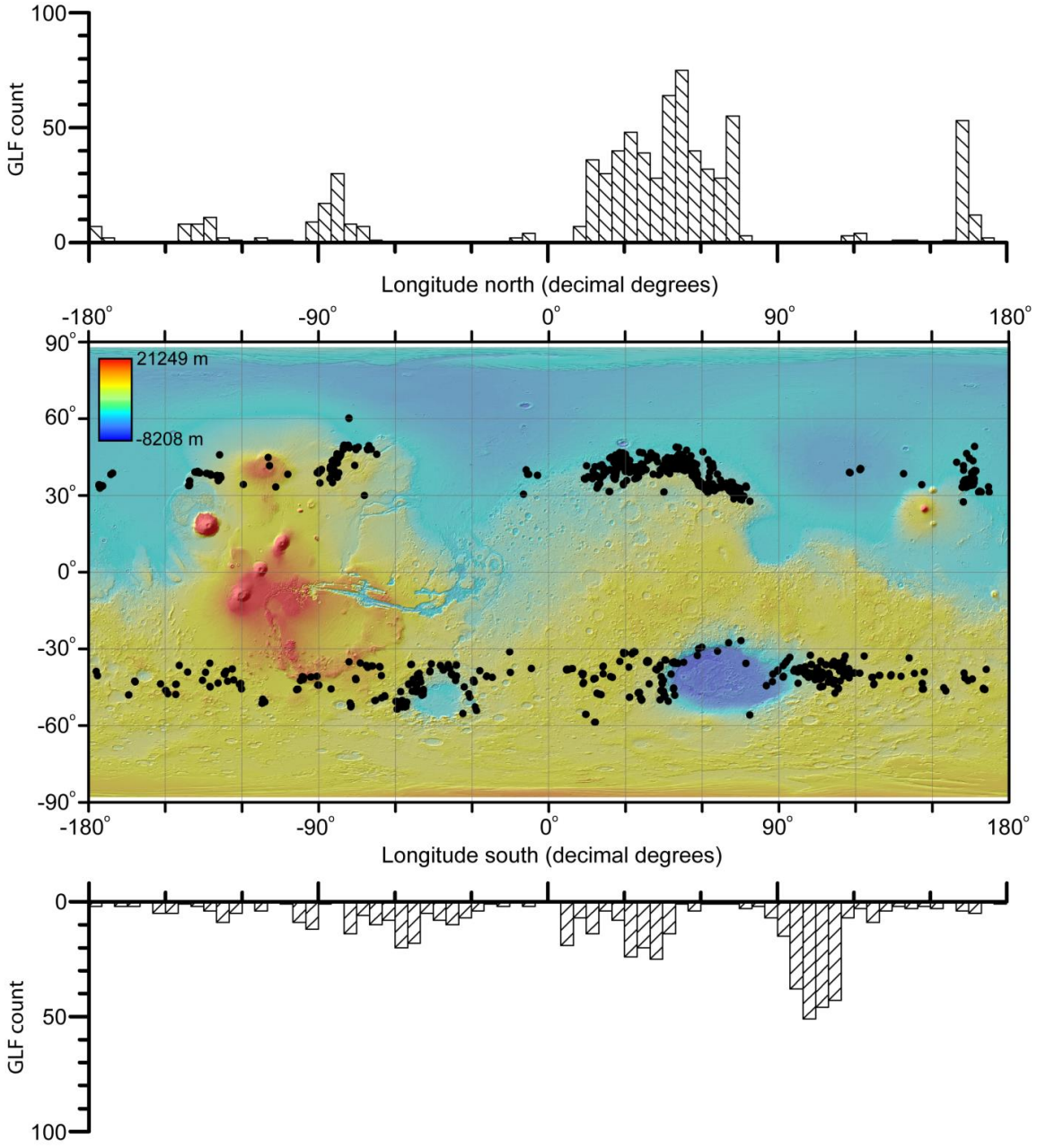

SF1: *Mars global map showing the mid-latitude distribution of GLFs (data from Souness et al., 2012). 1293 GLFs were identified globally: 723 were located in the northern hemisphere and 570 were located in the southern hemisphere. Histograms of GLF concentration in 5º longitude bins are presented above and below the distribution map. Background map is MOLA elevation transparency overlain on MOLA hillshade projection.*

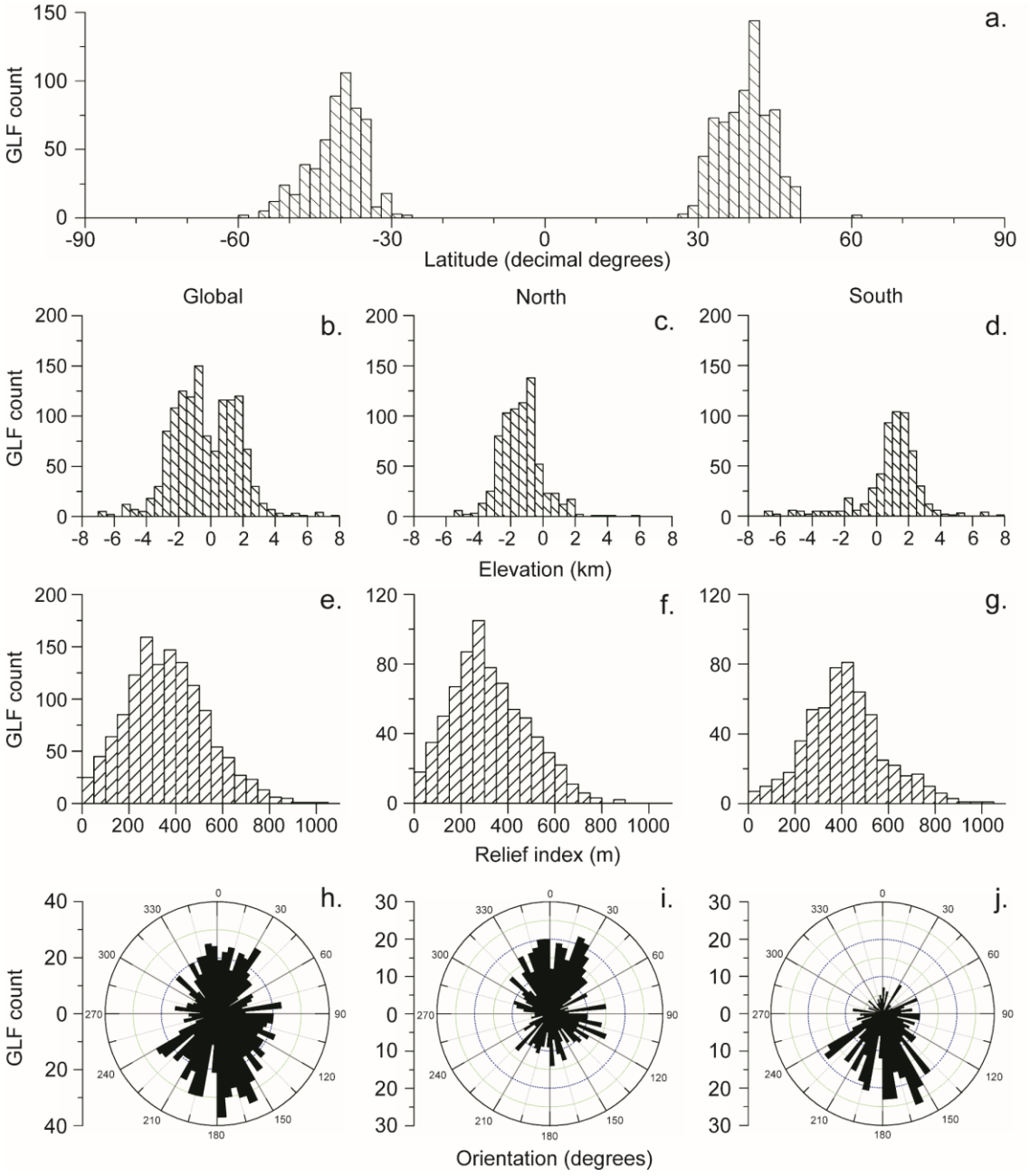

SF2: *Histograms of GLF population distribution relative to latitude, elevation, relief and orientation (data from Souness et al., 2012): (a) global and hemispheric latitude in 2º bins; (b) global, (c) northern- and (d) southern-hemispheric elevation in 500 m bins; (e) global, (f) northern- and (g) southern-hemispheric relief index in 50 m bins; (h) global, (i) northern- and (j) southern-hemispheric orientation in 5º bins.*

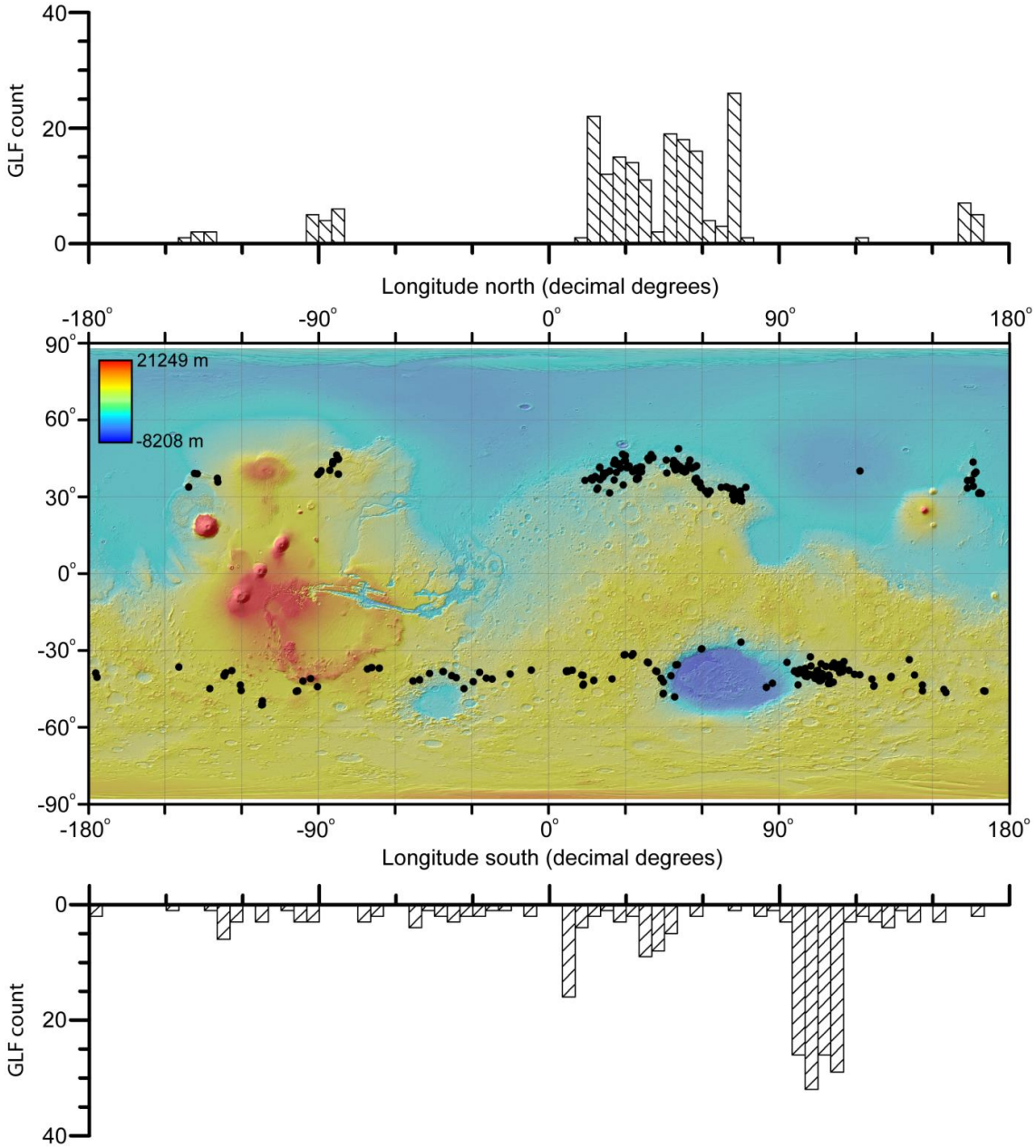

SF3: *Mars global map showing the mid-latitude distribution of recessional GLFs. 436 recessional GLFs were identified globally: 197 were located in the northern hemisphere and 239 were located in the southern hemisphere. Histograms of GLF concentration in 5^o longitude bins are presented above and below the distribution map. Background map is MOLA elevation transparency overlain on MOLA hillshade projection.*

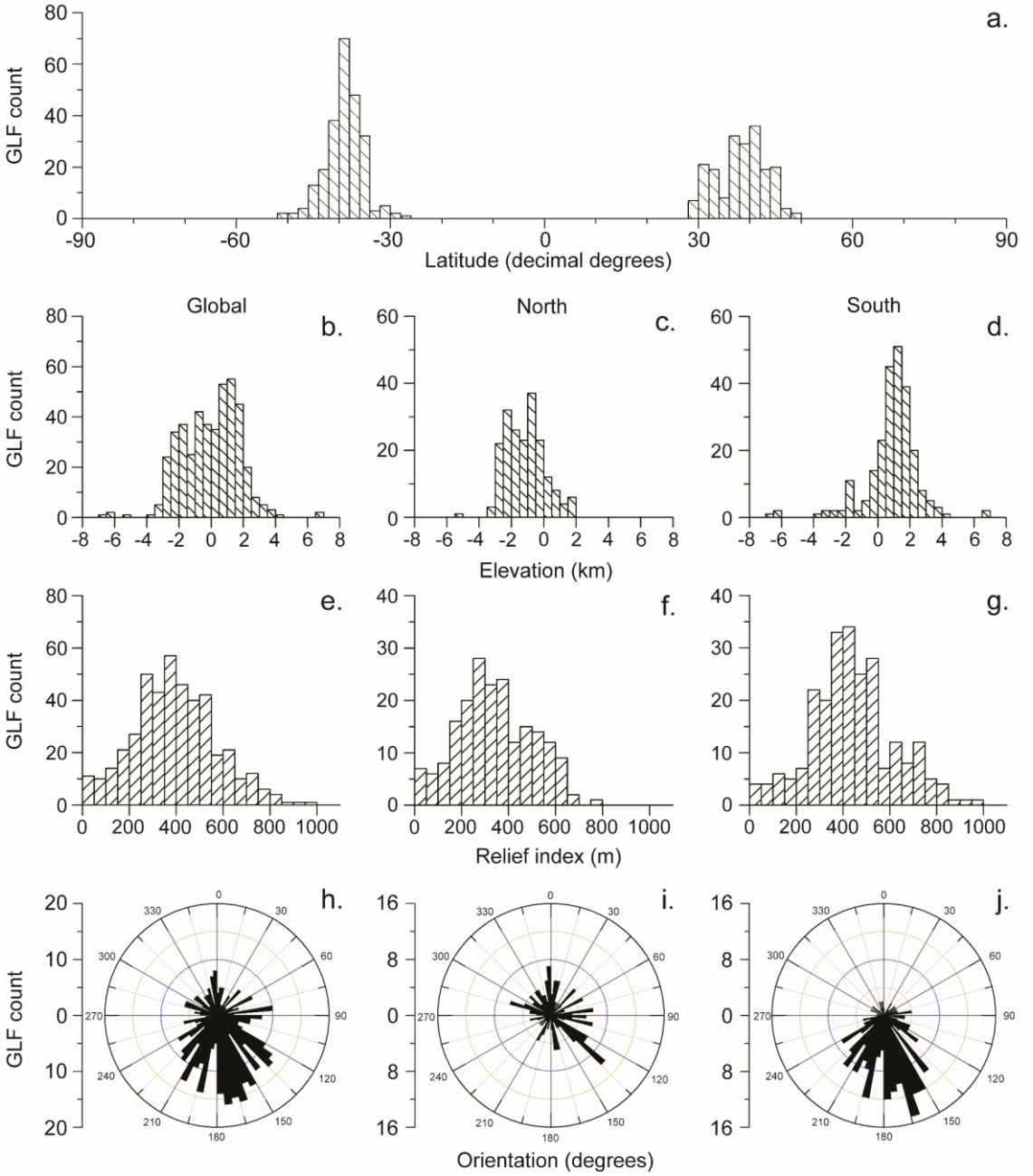

SF4: *Histograms of recessional GLF population distribution relative to latitude, elevation, relief and orientation: (a) global and hemispheric latitude in 2º bins; (b) global, (c) northern- and (d) southern-hemispheric elevation in 500 m bins; (e) global, (f) northern- and (g) southern-hemispheric relief index in 50 m bins; (h) global, (i) northern- and (j) southern-hemispheric orientation in 5º bins.*

Summary to manuscript 'Former extent of glacier-like forms on Mars'

Chapter 4 has presented a population-scale inventory of recessional GLFs. Coupled with this inventory was a glacial reconstruction of the maximum extent and morphology of a typical GLF. The key outcomes to carry forward are as such:

1. A total of 436 GLFs showed evidence of an expanded former extent. This recession appears widespread in both the northern and southern hemispheres and covers all latitude, elevation, relief and orientation ranges. Such widespread evidence of recession is therefore interpreted to be indicative of global rather than regional or hemispheric climatic change.

2. Assessment of the environmental settings of recessional GLFs revealed that latitude and relief exert(ed) some control over GLF sensitivity and response to climatic forcing. These results suggested that GLFs are particularly sensitive to the planetary limit of shallow ground ice stability and that GLFs in areas of higher relief (rougher topography) likely have a shorter response time to climatic perturbations than GLFs in areas of lower relief (smoother topography).

3. Although GLFs that showed evidence of recession appeared to be sensitive to their latitude and relief (see point 2 above), there was also some degree of heterogeneity in GLF recession, whereby GLFs in a similar setting did not show a similar response. It is therefore likely that a combination of regional to local meteorological conditions also play(ed) a role in GLF survival and/or initial emplacement.

4. The reconstruction of a GLF in Crater Greg, eastern Hellas Planitia, revealed a loss in area of ~70 % and volume of between 0.18 and 0.52 km^3 since its maximum extent. This analysis suggested that, at least some, GLFs have undergone substantial change and mass lass since their initial emplacement. Scaling this volume loss up to all recessional GLFs (n = 436) suggested a first-

order estimate of ice volume loss from Mars' GLFs of between 78 and 227 km^3, with a best estimate of 135 km^3.

5. As discussed in the summary to Chapter 2, the identification of MLRs in the forefield of the reconstructed GLF are a clear indication of ice mass loss through both surface lowering and terminus recession. The identification of these structures also provided further evidence that GLFs are, or at least have been at some point in their history, landscape altering agents capable of entraining, transporting and depositing debris.

CHAPTER 5

Palaeo-glaciers on Mars: modelling their formation and evolution

All models are wrong,
but some are useful
George Box

Preface to manuscript 'Palaeo-glaciers on Mars: modelling their formation and evolution'

Introduction and rationale

The results and conclusions of work presented in previous chapters have improved our understanding of the current and former extent, volume and dynamics of Mars' glacier-like forms. However, in spite of these new advancements, relatively little is still known about the processes and climates responsible for GLF formation, and how they respond to climatic forcing (see Section 1.2.3). Better constraining the environmental and climatic conditions that can lead to GLF formation is of particular significance given that GLFs may represent some of the most recent ice flows on Mars (Arfstrom and Hartmann, 2005; Hartmann et al., 2014), therefore, by investigating the potential conditions responsible for their formation, we could begin to reconstruct the magnitude of these recent climatic perturbations and their spatial variation.

This chapter presents ice flow modelling experiments that investigate the climates under which one particular GLF may have formed in Crater Greg, eastern Hellas Planitia. It builds upon the glacial geomorphological reconstruction presented in Chapter 4 to specifically investigate: (i) the long-term ELA and temperature required to best reproduce the maximum frontal position and vertical extent recorded in the geomorphological record; and (ii) the effect and response of the GLF to transient climatic forcing (e.g. contributing to Objectives [2] and [6] of the thesis). These results provide the opportunity to link geological observations of GLF fluctuations to the environmental and climatic conditions that were potentially responsible for producing them. The remainder of this preface discusses the methods that were adopted during the study.

Numerical modelling

A number of ice flow models with a varying range of complexity exist. Here we use a time-evolving, plane-strain model of ice flow that is based on a finite-difference, first-order solution of the ice-flow equations (Blatter, 1995; Blatter et al., 1998; Hubbard, 2006). The model includes the effects of longitudinal or deviatoric stress and although such schemes are more elaborate than the often used driving stress approximation (e.g. Fastook et al., 2011), the inclusion of longitudinal stresses have been shown to be an important component of valley glacier modelling on Earth (e.g. van der Veen et al., 1999; Hubbard, 2000), and more recently on Mars (e.g. Parsons and Holt, 2016). The use of such a model is justified given the valley-like topographic setting of the GLF studied herein is likely to induce changes in gradients at the glacier bed and surface, or through variability in basal and lateral friction.

The model itself is driven by a mass balance parameterisation forced by altering the equilibrium line altitude (ELA) through time. For this approach the mass balance function is based on the altitudinal-derived mass balance parameterisation of Fastook et al. (2008), which provided a linear mass balance gradient of 0.005 mm water equivalent per m of elevation for our modelling domain (their Figure 5b). In reality the parameterisation of Fastook et al. (2008) can be seen as more of a climate tuning function, as both accumulation and ablation are ultimately dependant on the base temperature via the lapse rate (Fastook et al., 2008). Offsetting the base temperature can simulate a change in climate by changing the mass balance distribution (their Figure 5c). This change in climate is achieved by altering (raising/lowering) the ELA in our modelling domain rather than changing the mass balance function, and given the small altitudinal range (~1300 m) of our domain, is a sufficient approximation to the method of Fastook et al. (2008). Furthermore, this approach closely aligns with comparative studies for Earth based glaciers (e.g. Hubbard, 1997a). Ultimately, a more robust approach would be to use regional/site specific temperature and ice accumulation rates generated from a general circulation model (e.g. Forget et al., 2006), this is currently precluded by the resolution differences in modelling domains.

Other boundary conditions that are required were the glacier (or GLF) bed along a central flowline, down-glacier width distribution, ice rheology and subglacial conditions. Apart from the bed and the width distribution, these inputs are only poorly constrained for Mars and thus can introduce uncertainty into the modelling process (see detailed discussion provided in section 5.3.2). This issue underlies the modelling approach adopted here and cannot be avoided given the limited empirical data available to constrain the problem. However, that does not make the approach invalid and by careful parameter selection (using well investigated Earth analogues), coupled with forthright presentation of model assumptions, the experiments conducted remain valid and arguably provide important insights in themselves and that can be further refined in future studies, particularly as new data and evidence becomes available. Developments in martian palaeo-climatic reconstruction, remote sensing/DEM analysis and satellite-born geophysical instrumentation including in ice penetrating radar (e.g. Karlsson et al., 2015; Parsons and Holt, 2016), are presently on-going and will combine to incrementally improve constraints on such glacier flow modelling as has conducted here, thereby leading to improved understanding of these little known and understood, yet extremely remote, glacial systems and their associated landforms.

Palaeo-glaciers on Mars: modelling their formation and evolution

Stephen BROUGH[a], Alun HUBBARD[a,b] and Bryn HUBBARD[a]

[a]*Department of Geography and Earth Sciences, Aberystwyth University, Aberystwyth, UK*

[b]*Centre for Arctic Gas Hydrate, Environment and Climate, Department of Geology, University of Tromsø, Tromsø, Norway*

This is a manuscript of an article in preparation for submission and presents initial numerical modelling results and interpretations.

Keywords: Mars; glaciation; glacier; water; climate change; numerical modelling

Abstract: Mars' glacier-like forms (GLFs) are mid-latitude ice rich landforms that are thought to have formed during one or more periods of ice accumulation during the Late Amazonian. However, little is known about the climate that leads to GLF formation or how these ice masses evolved over time. Here we present initial results from a two-dimensional, plane-strain flow model that investigates the climates under which one particular GLF may have formed in Crater Greg, eastern Hellas Planitia. A suite of model experiments were conducted and output was compared directly to geomorphogical evidence of former horizontal and vertical ice limits. The model was driven by a mass balance parameterisation forced by altering the equilibrium line altitude (ELA) through time and is applied under a range of englacial temperature scenarios. For ice temperatures of between 263 and 233 K an ELA range of between 615 and 640 m (above Mars datum) was required to reconstruct the maximum frontal position in the geomorphological record. However, none of these experiments corresponded with the vertical limits on ice thickness provided by moraine heights. Colder englaical temperatures of <243 K, yielding thicker ice, were were required to satisfy the upper vertical constraint and conversely thinner ice with a temperature configuration of at least 20 K warmer (i.e. >263 K) was required to match the lower vertical constraint. This suggests that a spatially varying ice rheology or basal regime may have acted upon the GLF. The response of the GLF to a transient climate experiment, forced by obliquity variations, indicates that the maximum frontal position attained by the GLF was achieved during an initial extended period of climate favourable to ice accumulation. Several terminus standstills were noted during the advance/retreat fluctuations of the GLF terminus throughout the obliquity cycle, thereby providing a plausible transient reconstruction that facilitates the formation of multiple moraines as recorded in the geomorphological record.

5.1. Introduction

High-resolution remotely sensed images of the martian surface have revealed numerous mid-latitude (30 – 60^{o}) landforms that have surface morphologies consistent with viscous deformation and the flow of H_2O ice (e.g. Squres 1978; Lucchitta, 1984; Head et al., 2005; Holt et al., 2008; Head et al., 2010). Collectively, these landforms have become encompassed by the umbrella term viscous flow features (VFFs) and in total

>12,000 VFFs have been identified (Milliken et al., 2003; Dickson et al., 2012; Souness et al., 2012; Levy et al., 2014). Given that water ice is not presently stable across a large proportion of the latitudes where VFFs are located (e.g. Mellon and Jakosky, 1995; Mellon et al., 2004; Byrne et al., 2009), such deposits are thought to have formed under different climatic conditions from today. These climatic perturbations are hypothesised to result from orbital changes of Mars providing preferential conditions for ice accumulation during periods of increased obliquity (Laskar et al., 2002, 2004; Head et al., 2003). The survival of this ice to the present day is related, at least in part, to a now ubiquitous armouring of debris protecting the underlying ice from sublimation (e.g. Fastook et al., 2014).

Glacier-like forms (GLFs) are a distinctive sub-type of VFF similar in planform appearance to terrestrial valley glaciers or debris-covered glaciers (e.g. Arfstrom and Hartmann, 2005; Hubbard et al., 2011; Souness et al., 2012), and have been shown to be <50 Ma, and likely <10 Ma old – making them some of the most recent ice flows on Mars (Arfstrom and Hartmann, 2005; Hartmann et al., 2014). Despite their potential importance as an archive of recent climatic change on Mars, relatively little is known about the processes and climates under which GLF formation occurs, and how they have evolved in the geologically recent past (e.g. Hubbard et al., 2014). On Earth, numerical ice flow modelling provides a useful methodology by which we can link historical or geological observations of glacier fluctuations to the environmental and climatic conditions that were responsible for producing them (e.g. Oerlemans, 1988; Hubbard, 1997a, b). However, applications of a similar nature to Mars mid-latitudes have thus far focused on the large scale VFFs: namely lobate debris aprons (e.g. Colaprete and Jakosky, 1998; Fastook et al., 2014; Parsons and Holt, 2016), lineated valley fill (e.g. Fastook et al., 2011) and concentric crater fill (e.g. Fastook and Head, 2014) and relatively little focus has been given to understanding the formation and evolution of GLFs (Milliken et al., 2003).

Here we present results of a two-dimensional numerical ice flow model forced by equilibrium line altitude (ELA) perturbations to investigate the climates under which one particular GLF may have formed in Crater Greg, eastern Hellas Planitia. Model results are constrained and interpreted with reference to geomorphogical evidence of glaciation in the area concerned. Specifically we investigate: (i) the long-term ELA and

temperature required to best reproduce the maximum frontal position and vertical extent recorded in the geomorphological record; and (ii) the effect and response of the GLF to transient climatic forcing.

5.2. Study site

Crater Greg (centred on ~38.65^{o}S, 113.16^{o}E [Figure 5.1]) is located to the east of Hellas Planitia. It has a diameter of 66 km and is thought to be of Hesperian age (1 – 3 Ga old [Hartmann et al., 2014]). The crater preserves strong evidence of post formation alteration from the action of water, in both liquid and solid state. Numerous landforms within the crater have been attributed as glacial in origin (see Section 5 of Hartmann et al., 2014). A collection of particularly prominent lobate tongues, classified as GLFs, are located on the crater's northern (Figure 5.1c [Hartmann et al., 2003; Marchant and Head, 2003; Kargel, 2004; Arfstrom and Hartmann, 2005; Hubbard et al., 2011; Souness et al., 2012; Hartmann et al., 2014; Brough et al., 2016a]). Age estimates for these GLFs suggest that they are likely <50 Ma old, with a best estimate of ~2-9 Ma (Hartmann et al., 2014). Evidence from global climate models place Crater Greg as one of two locations of high ice accumulation when Mars' orbital obliquity exceeds 45^{o}, and a water source exists at the south polar region (e.g. Forget et al., 2006).

The particular GLF modelled herein (Figure 5.1d) extends downslope at a general angle of ~10^{o} (Hubbard et al., 2011) and appears to converge from a wide upper basin down to a narrow elongate tongue bounded by a sequence of at least three raised arcuate ridges (Figure 5.1e). Based on detailed geomorphological characterisation of the GLF's surface terrain, Hubbard et al. (2011) concluded that the upper basin contained a now degraded and relict GLF and the lower basin zone corresponded to deglaciated terrain. The raised arcuate ridges were interpreted as latero-terminal moraines, thus revealing that the GLF has been subjected to apparently punctuated mass loss and recession since attaining its former maximum extent (Hubbard et al., 2011; Hartmann et al., 2014). Brough et al. (2016a) built on this earlier work and reconstructed a range of former three-dimensional palaeo-ice surfaces of the GLF using Nye's (1951) perfect-plasticity approximation of glacier flow combined with detailed geomorphological mapping. This analysis reveals that the GLF at its maximum extent covered an area of 9.67 km^{2}, had a

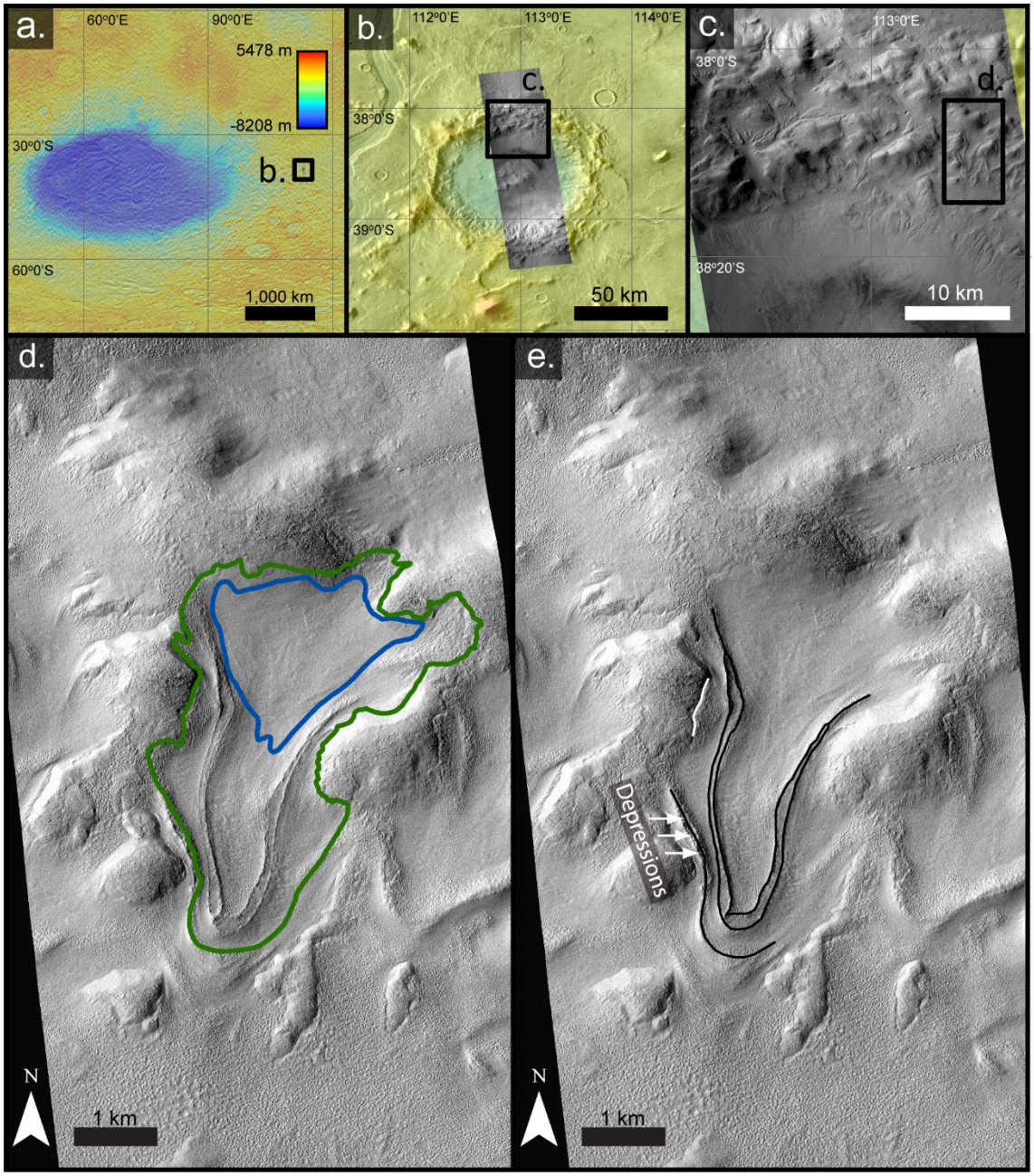

Figure 5.1: *Location of Crater Greg and glacial history of the investigated GLF. (a) – (b) Global and regional context map indicating the location of Crater Greg. Background image is MOLA elevation transparency overlain on a THEMIS-IR day mosaic. (c) Local context of the GLF and landforms of Crater Greg's northern wall, where several GLFs are located (CTX image G05_020121_1412_XN_38S247W). (d) The subject GLF to our modelling reconstruction including the outlines of Brough et al. (2016a) that demarcated the interpreted current (blue line) and former maximum (green line) extent of the GLF (HiRISE image PSP_002320_1415_RED). (e) Schematic illustration of the moraine sequence (black and white lines) recorded in the geomorphological record.*

maximum length and width of 5.2 and 3.5 km, and covered an altitudinal range from 110 to 1040 m above Mars datum. Given the GLF presently has a length and width of 2.3 and 2.5 km, with an area of 2.81 km^2 the GLF has experienced a loss of 6.86 km^2 or ~70 % of its area. Coupling this area loss with differences in elevation between the current surface and reconstructed palaeo-ice surfaces indicates that the GLF had lost between 0.18 and 0.52 km^3 based on the lower (12 kPa) and upper (38 kPa) reconstruction scenarios of Brough et al. (2016a). The preserved geomorphological record hence provides an empirical basis by which applied ice flow modelling can be used to investigate the GLF's former vertical and horizontal limits, ots rheology and the associated climate forcing (Figure 5.1).

5.3. Numerical model

5.3.1. Model description

A time-evolving, plane-strain model of ice flow that is based on a finite-difference, first-order solution of the ice-flow equations (Blatter, 1995; Blatter et al., 1998; Hubbard, 2006) is adapted for the martian environment. The model is based on a first-order approximation of the stokes equations governing ice flow, thereby including longitudinal stress coupling effects, and has been benchmark tested in various synthetic and applied settings under both steady-state and transient conditions (Hubbard, 1997b, 2000, 2006; Hubbard et al., 1998, 2003; Patton et al., 2013). Although such schemes are more elaborate than the often used driving stress approximation, the inclusion of longitudinal stresses demonstrated to be a critical component of valley glacier modelling on Earth (e.g. van der Veen, 1999; Hubbard, 2000), and more recently on Mars (Brough et al., 2016b; Parsons and Holt, 2016), where tensile and compressive forces can be induced as a result of changes in gradients at the glacier bed and surface, or through variability in basal and lateral friction. The numerical scheme has been successfully applied to glaciers on Earth (e.g. Hubbard et al., 1998; Hubbard, 2000; Hubbard et al., 2003) and is fully described in Blatter (1995) and Hubbard (2000).

The boundary conditions required are the glacier (or GLF) bed along a central flowline, down-glacier width distribution, ice rheology, subglacial conditions, and mass balance.

Apart from the bed and the width distribution, these inputs are only poorly constrained for Mars and thus can introduce uncertainty into the modelling process. Nonetheless, choosing reasonable values for these input parameters yield realistic results (e.g. Fastook et al., 2008, 2011). We discuss these requirements in more detail and outline assumptions made in our approach in Section 5.3.2.

5.3.2. Model input

5.3.2.1. Bed profile and width distribution

To constrain the central flowline and corresponding width distribution, the glacial catchment needs to be defined and delineated (Hubbard, 1997b; Parson and Holt, 2016). The catchment was delineated by manual digitisation in ESRI's ArcMap v10.1, using a ~0.25 m per pixel High Resolution Imaging Science Experiment (HiRISE) image (Figure 5.2). The catchment was mapped based on the location of the constraining valley side walls and associated geomorphological evidence (e.g. moraines) and was extended beyond the GLFs headwall and outermost moraine ridge in order to provide a modelling domain greater than the maximum horizontal extent of the former GLF. The central flowline was digitised on screen and converted to nodes at 100 m intervals. Bed elevations were extracted from a 2 m per pixel HiRISE digital elevation model (DEM [stereo pair PSP_002320_1415_RED and PSP_003243_1415_RED]). The DEM was created by Hubbard et al. (2011) and subsequently adapted by Brough et al. (2016a) to remove an inner set of moraine ridges nested behind the outermost moraine limit (e.g. Figure 5.1). The present ice distribution – assumed to not exceed metres to tens of metres thick (Hubbard et al., 2011; Hartmann et al., 2014) – contained within the GLF was not removed. As the exact distribution of this remant ice/debris mass is unknown, we follow Brough et al. (2016a) and assume that the present-day topography with the inner moraine ridges removed represents the former GLF bed. Finally, the width distribution of the modelling domain was calculated orthogonal to each node of the bed profile. The bed topography was fixed for the duration of the experiments.

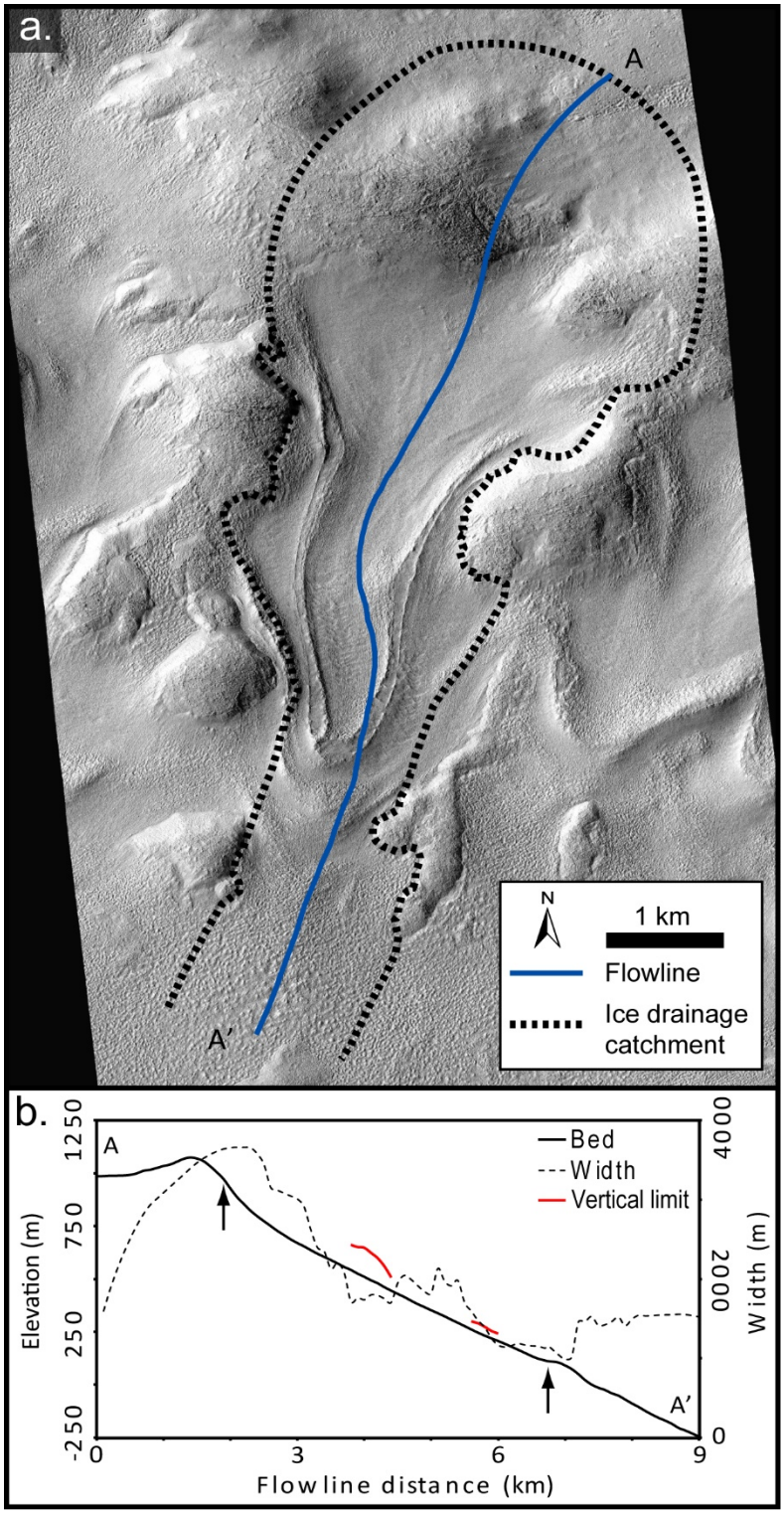

Figure 5.2: *Glacial catchment, bed topography and width distribution of model flowline. (a) Illustration of the delineated ice drainage catchment and flowline used in the model. (b) Topographic profile and width distribution along the flowline. Black arrows indicate the upper and lower marginal extents of the GLF in the geomorphological record. Key indicators of vertical thickness provided by moraine heights are also provided.*

5.3.2.2. Ice rheology

The relationship between stress and strain is determined by Glen's non-linear flow law for ice (Glen, 1955; van der Veen, 1999) that requires definition of a flow-law exponent (n) and a rate factor that equates to bulk viscosity ($A\ [a^{-1}\ bar^{-3}]$), primarily influenced by temperature but also water and debris content. We set the flow-law exponent to the generally used value $n = 3$ (Glen, 1955) and the rate factor is held constant (i.e. isothermal conditions in the interior of the ice). An explanation of the rate factors applied in our experiments is provided in Section 5.4. Although more complex rheologies could be implemented that account for variations in dust and ice grain size (e.g. Goldsby and Kohlstedt, 2001), present understanding of their distribution and influence on martian ice masses is unknown (Parson and Holt, 2016).

5.3.2.3. Basal sliding

The basal boundary condition is assumed frozen and motion is prescribed as zero (i.e. ice is below the pressure melting point); an assumption used in virtually all modelling studies (e.g. Fastook et al., 2008, 2011; Parsons et al., 2011; Parsons and Holt, 2016). This assumption has a physical basis given the lack of liquid water, coupled with low temperatures predicted during climatic periods that favour ice accumulation (e.g. Madeleine et al., 2009; Hartmann et al., 2014) and from results of modelling experiments conducted on VFFs (e.g. Fastook et al., 2011).

5.3.2.4. Mass balance

We used a mass balance function based on the altitudinal-derived mass balance parameterisation of Fastook et al. (2008). The component of their mass balance curve (their Figure 5b) that corresponded to the altitudinal range (-244 to 1075 m) was applied to our modelling domain through a linear regression ($R^2 = 0.99$) to yield a mass balance gradient (i.e. the rate of change in precipitation per metre of elevation) of 0.005 mm water equivalent per m of elevation. We fix the upper limit of accumulation to the upper marginal extent of the GLF and preclude accumulation above this limit.

For the applied model simulations, the maximum distance along the flowline where accumulation occurs is 4.0 km which corresponds to a maximum accumulation rate of ~2.5 mm a^{-1}. Although this accumulation rate is within the range reported from analogous debris-covered glaciers in the Antarctic Dry Valleys (e.g. Kowalewski et al., 2001) and used in modelling studies elsewhere on Mars (e.g. Fastook et al., 2011; Parsons and Holt, 2016), it is substantially lower than those predicted by matrian climate models, which estimate net accumulation rates between ~30 and 70 mm a^{-1} for the regions surrounding Crater Greg during periods of high (>45^{o}) obliquity (Forget et al., 2006).

5.4. Modelling approach and results

Our modelling aims to investigate: (i) the long-term ELA and temperature required to reproduce the GLF's maximum frontal position and vertical extent recorded in the geomorphological record; and (ii) the effect and response of the GLF to transient climatic forcing. All model simulations are initiated from ice-free conditions with a forward integration time-step of one year. Results are output on a 2500-year interval.

To address Aim (i) we simulate climatic change through a stepped ELA lowering from the present-day altitude (nominally set at 1100 m – i.e. above present-day topography). Each of these equilibrium experiments uses a rate factor (A) corresponding to 263 K and were run for 1 Ma until a steady-state was achieved. A collection of equilibrium glacier surface profiles was assembled relating to ELA depressions ranging from 1100 m to 600 m in 50 m intervals (Figure 5.3a). These experiments indicate that an ELA depression to 900 m was required before ice accumulates and persists, and that the maximum frontal position recorded in the geomorphological record lies between an ELA of 650 and 600 m. An ELA of 615 m yields a glacier profile that optiammly corresponds to the available geomorphological evidence (Figure 5.3b).

In the next experiment, the effects of long-term ice temperature on the sensitivity and response of the GLF are assessed. We ran a new suite of model experiments varying the rate factor (A) according to a range of temperatures. The equilibrium sensitivity

experiments commence from an initial temperature of 263 K and were applied under five different ELAs (650, 640, 630, 620, and 615 m). Englacial ice temperature was subsequently reduced in 10 K steps to 233 K and each experiment was run for 1 Ma, until a stead-state glacier profile was obtained.

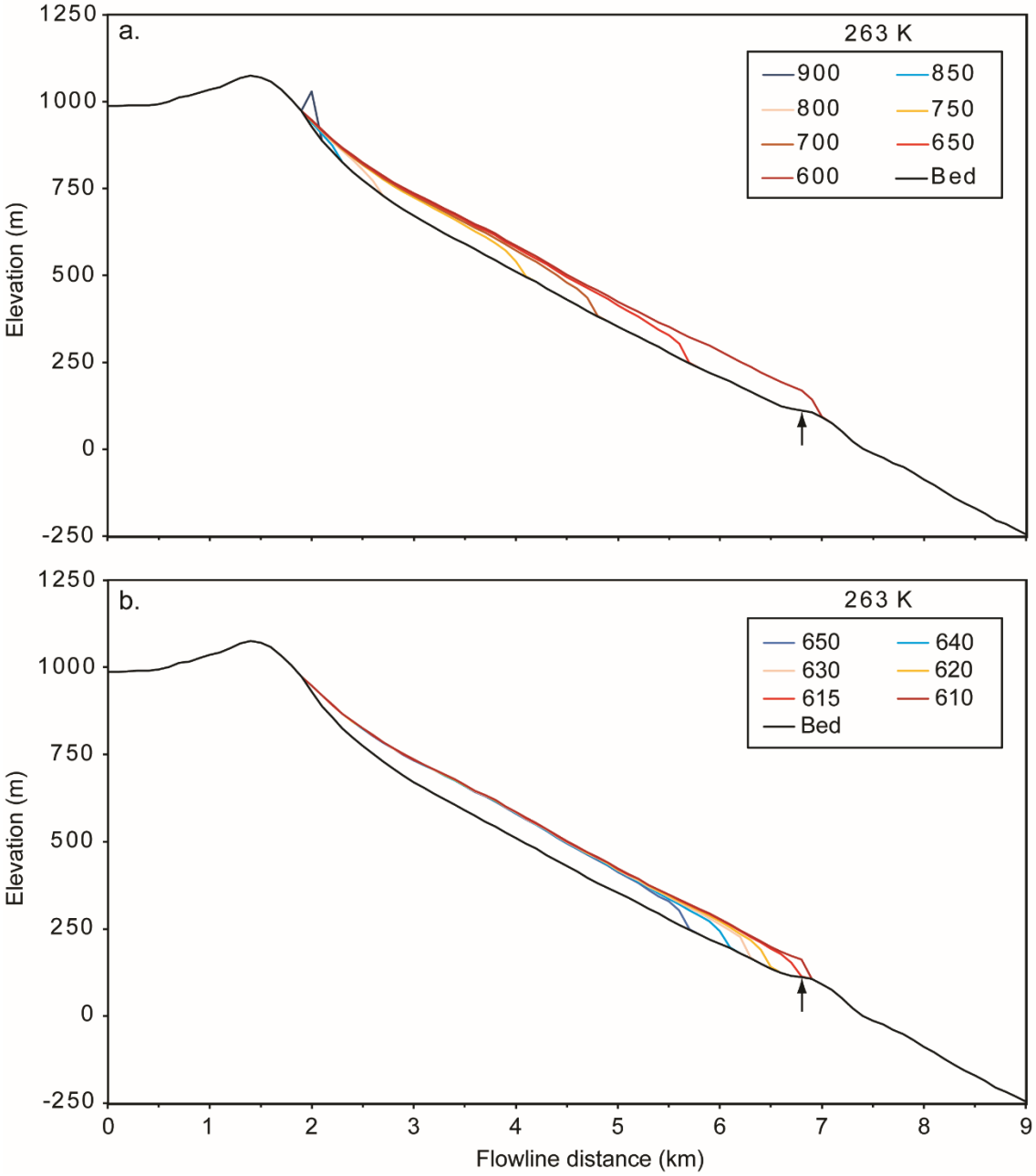

Figure 5.3: *Equilibrium surface profiles of the modelled GLF as a function of stepped ELA lowering. (a) Incremental ELA lowering (coloured lines in metres) from 900 to 600 m. (b) Refined ELA lowering, showing ELA required to match the maximum frontal position from the geomorphological record.*

A collection of steady-state surface profiles showing the effect of temperature is given in Figure 5.4 and summarised in Table 5.1. All modelled GLFs show broadly the same response to decreasing temperature in that they increase: (i) the length of the maximum frontal position; (ii) ice thickness; and (iii) time required to reach steady-state.

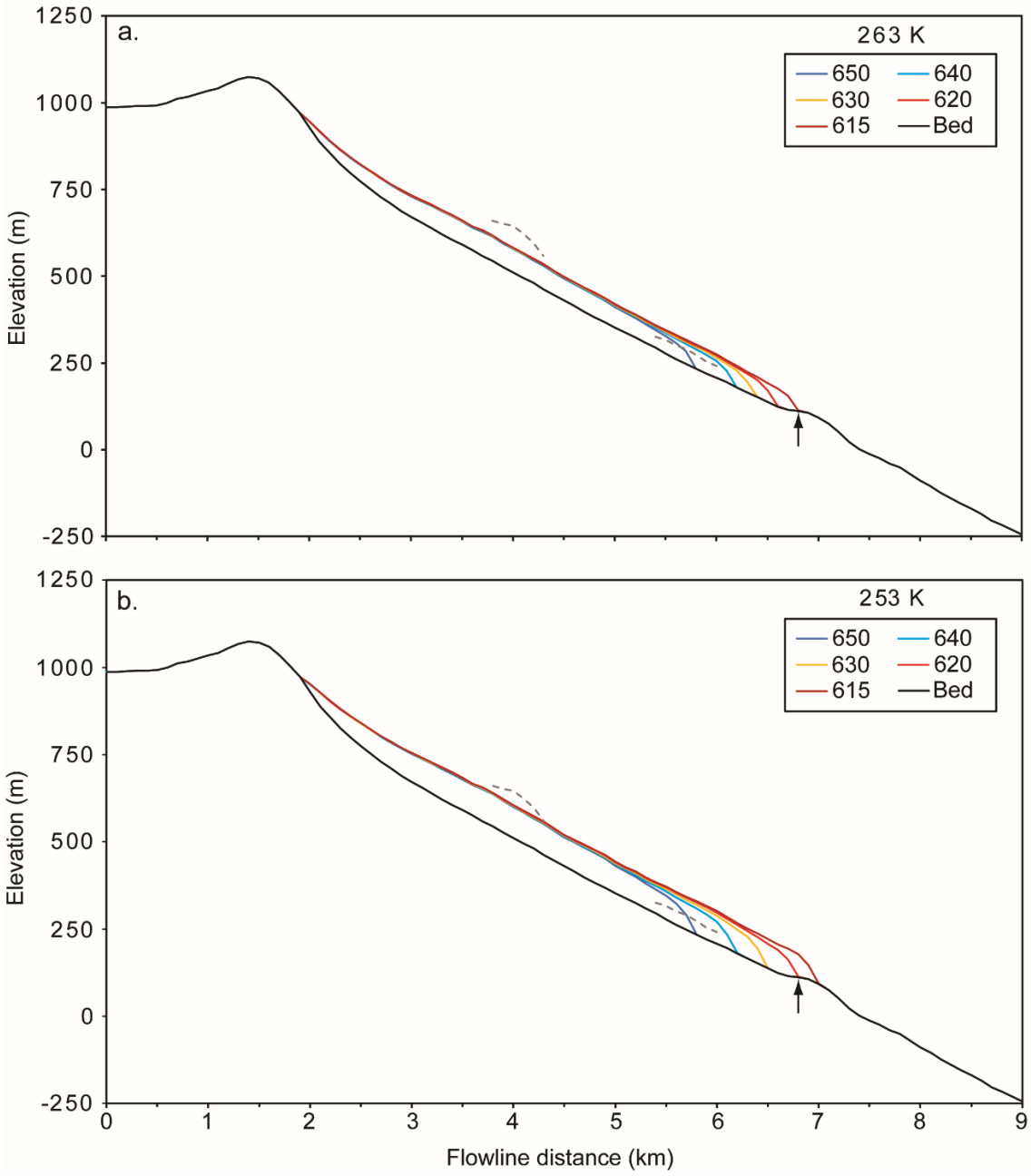

Figure 5.4: *Equilibrium surface profiles of the modelled GLF as a function of stepped temperature and ELA lowering (coloured lines in metres). (a) 263 K. (b) 253 K. (c) 243 K. (d) 233 K. The vertical constraints given by moraine heights are shown by the dashed grey lines.*

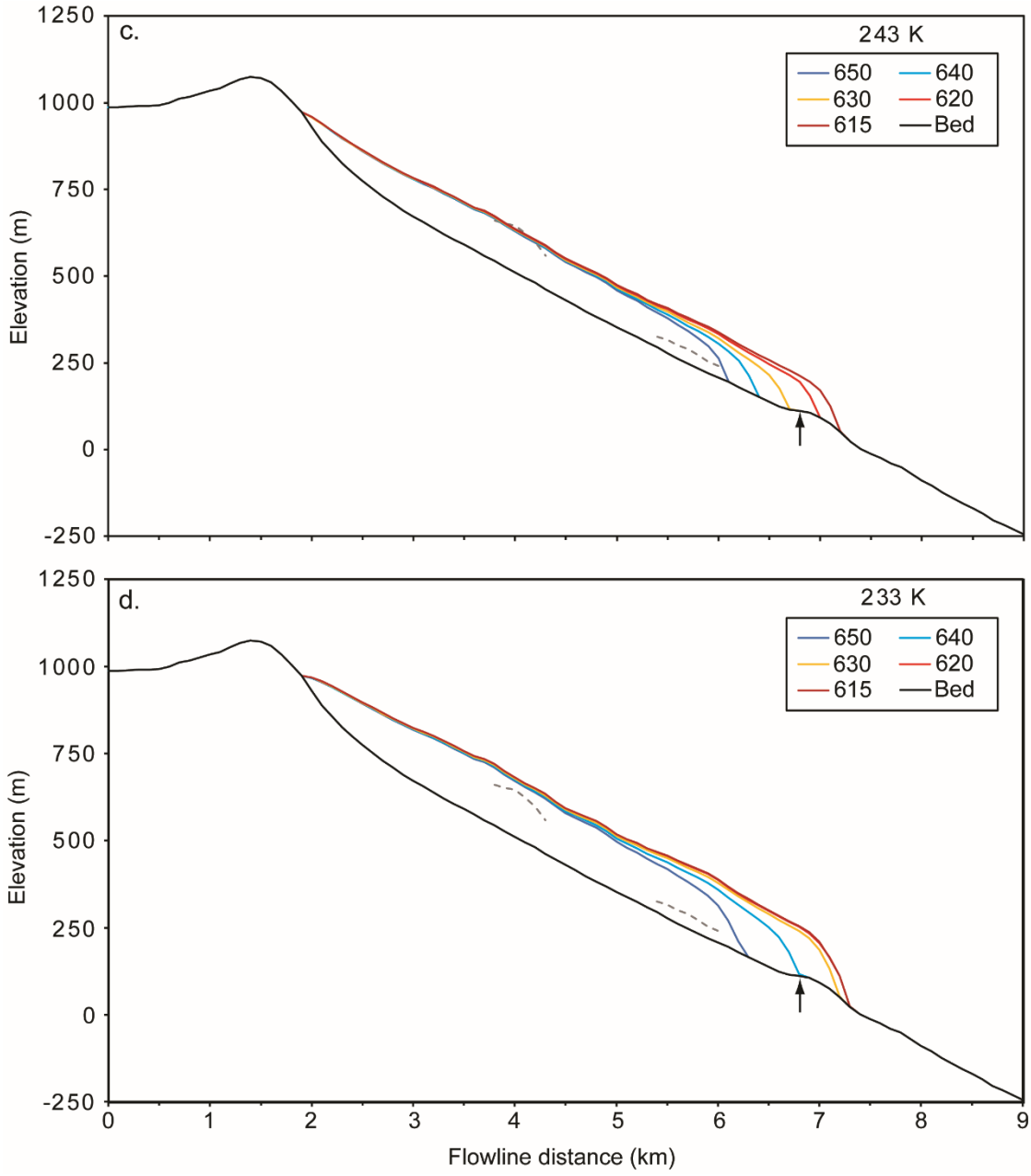

Figure 5.4 continued

Table 5.1: *Steady-state terminus position and formation time of the modelled GLF as a function of stepped temperature lowering. Highlighted in bold are the simulations that 'best fit' the observed terminus position.*

Temperature (K)	ELA (m)	Terminus position relative to moraine (km)	Formation time (ka)
263	650	-1.0	295
	640	-0.6	335
	630	-0.4	285
	620	-0.2	263
	615	**0.0**	**285**
253	650	-1.0	410
	640	-0.6	415
	630	-0.3	415
	620	**0.0**	**405**
	615	+0.2	385
243	650	-0.7	750
	640	-0.4	638
	630	**-0.1**	**590**
	620	+0.2	530
	615	+0.4	515
233	650	-0.5	995
	640	**0.0**	**905**
	630	+0.4	895
	620	+0.5	733
	615	+0.5	685

Comparing modelled results with empirical evidence reveals that the maximum frontal position was attained by one GLF for all temperatures apart from at 243 K where the closest simulation, with an ELA of 630, was 0.1 km short (Figure 5.4). Broadly, a 10 K decrease in temperature equated to a 10 m increase in the ELA required to match the maximum frontal position of the GLF. Comparing the steady-state surface profiles for each temperature to the vertical limits provided by the moraine heights shows that no simulation could satisfy both vertical constraints. At temperatures of 263 and 253 K, the surface profiles fall below the elevation of the upper moraine height and above the lower moraine height (Figure 5.4a – b). For a temperature of 243 K, the steady-state surface profile appears to correspond to the upper moraine height, but is too thick and is raised above the lower moraine (Figure 5.4c). For a temperature of 233 K (Figure 5.4d), the steady-state surface is raised above both vertical constraints – hence, no experiments were applied beyond this temperature.

The formation time required for the simulations that 'best fit' the observed terminus position to reach steady state places an upper and lower formation time of 285 to 905 ka, for our maximum and minimum temperatures of 263 and 233 K, respectively (Table 5.1).

To address Aim (ii) a set of dynamic experiments was conducted to assess the sensitivity and response of the GLF to transient climatic forcing. This was implemented through a series of stepped ELA changes, similar to the approach of Fastook and Head (2014), reflecting known changes in obliquity. Three ELA parameters were imposed: one for obliquity <30°; one for obliquity between 30 and 40°; and one for obliquity >40°. These boundaries were based on the observations that: (i) present day climate is unfavourable for ice accumulation; (ii) ice deposition in mid latitude regions is likely during periods of obliquity >30° (e.g. Head et al., 2003); and (iii) general circulation models place Crater Greg as a foci for ice accumulation during periods of obliquity >45° (Forget et al, 2006), relaxed to >40° here. The duration of each of these obliquity periods is taken from simulation La2004 of Laskar et al. (2004). Based on the upper limit of the best estimate age of 9 Ma (see Section 5.1 [Hartmann et al., 2014]), we commence the experiment prior to this at which obliquity last transitioned from a period below to above 30° (i.e. the transition from an unfavourable to a favourable climate for ice accumulation) and run it through one full obliquity cycle of 2.5 Ma. This corresponds to the period between 10 and 7.5 Ma BP (Figure 5.5). An example of the parameters required to generate a simulation with a maximum extent that corresponds to the geomorphological record is provided in Figure 5.6. The parameters used were an *A* value equal to 263 K and ELAs of 1100, 750, 515 for the <30°, 30 – 40°, and >40° obliquity periods, respectively.

Inspection of Figure 5.6 reveals that from initial ice-free conditions, the GLF grows and advances via a series of stepped cycles, before attaining its maximum extent after 697.5 ka, where there is a 7.5 ka of terminus standstill. This modelled limit collocates nicely with the maximum extent recorded in the geomorphological record. At 802.5 ka, there is a second, 27.5 ka, standstill, which also terminates near to the maximum recorded extent. Significant glacier recession of ~3 km coincides with a change to a climate unfavourable for ice accumulation at 925 ka. From this time onwards, the GLF undergoes further fluctuations in its frontal position, but does not again attain ite

maximum extent – even during a second extended period of >30° obliquity between 1282 and 1624 ka (Figure 5.6).

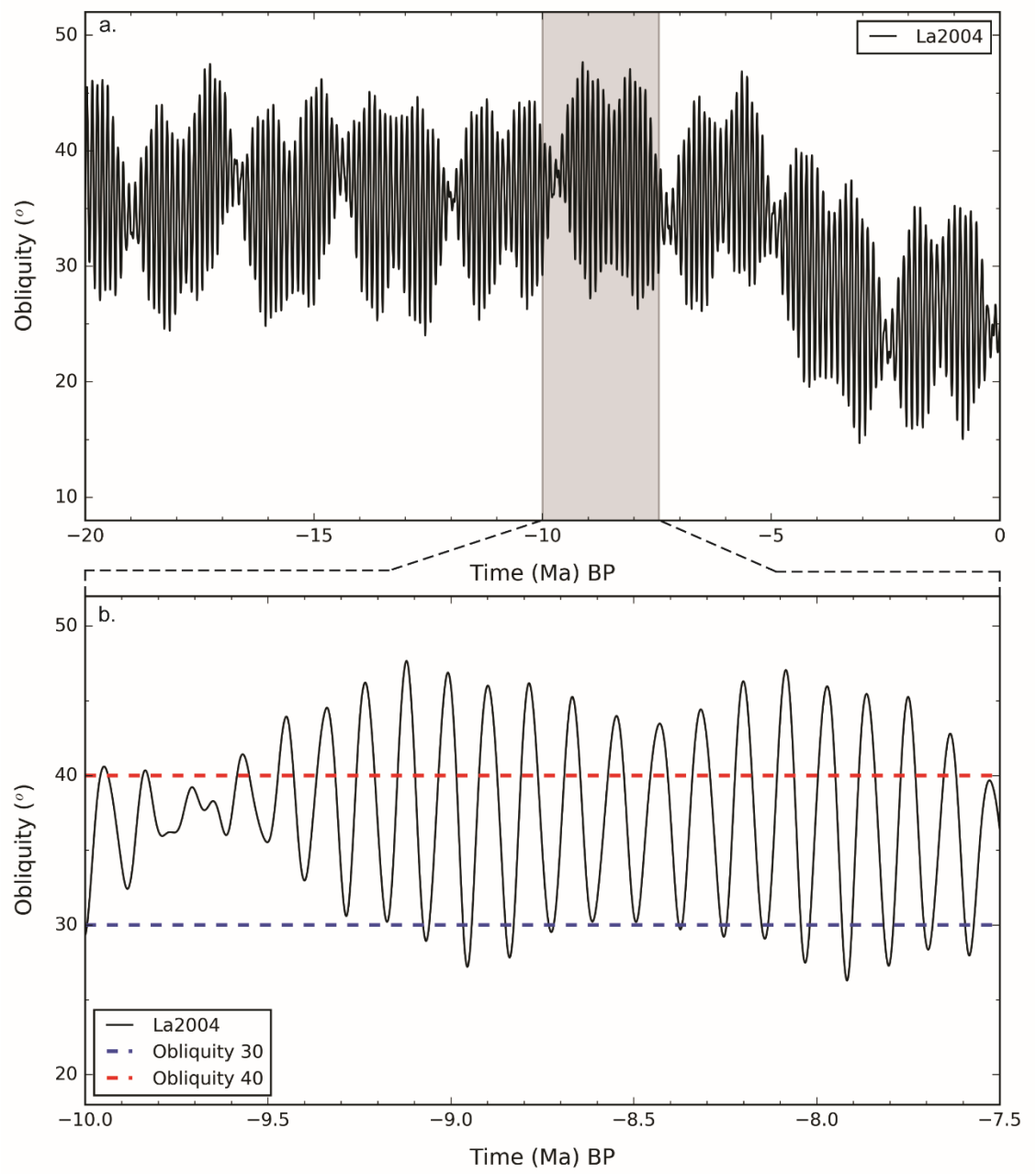

Figure 5.5: *Obliquity scenario La2004 of Laskar et al. (2004). (a) Variations in obliquity over the last 20 Ma. The time period utilised in our transient experiment is highlighted in grey. (b) Obliquity for the period -10.0 to -7.5 Ma BP. The blue and red horizontal lines correspond to the 30 and 40° obliquity thresholds that correspond with an ELA transition.*

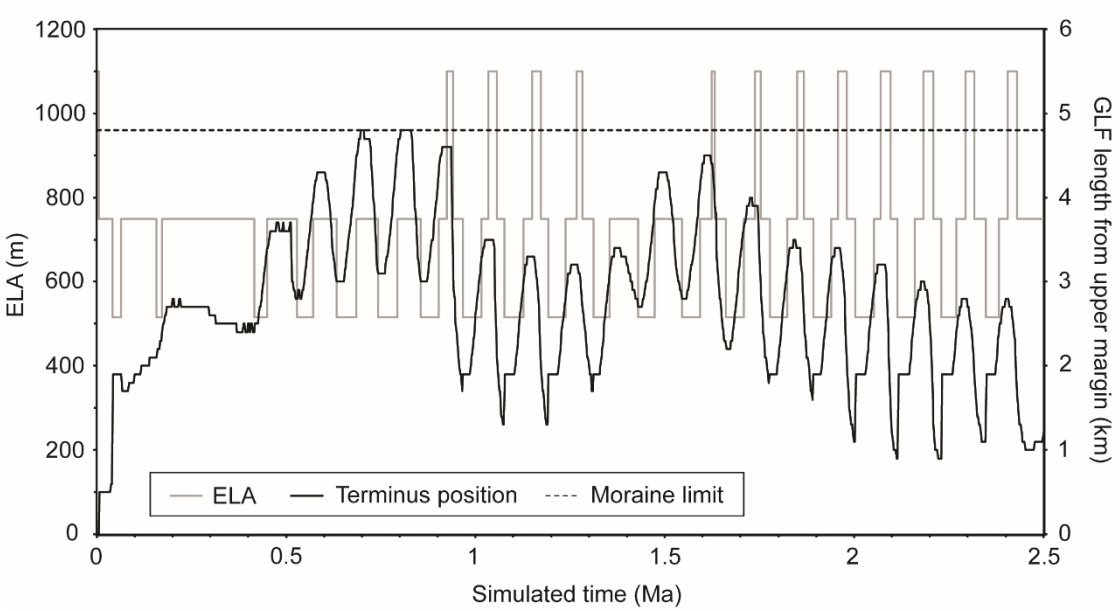

Figure 5.6: *Modelled GLF frontal position as a function of obliquity driven ELA changes. The dashed line gives the limit of the moraine, indicating the maximum-recorded extent of the GLF.*

5.5. Discussion

5.5.1. Crater Greg GLF formation

Our application of a plane-strain ice flow model yields a range of glacier profiles (e.g. Figure 5.4) that match the GLF's maximum frontal position recorded in the geomorphological record (e.g. Hubbard et al., 2011; Brough et al., 2016a). For a temperature of 263 K an ELA of 615 m was required to attain the maximum frontal position and an increased ELA of 640 m was required for a temperature of 233 K. However, no single experiment was able to simultaneously satisfy both of the upper and lower vertical constraints imposed by the mapped moraine heights. At warmer temperatures (263 and 253 K) equilibrium surface profiles appear more consistent with moraine height constraints in the lower sector, but are too thin in the upper sector (Figure 5.4a – b). Conversely, increased ice thickening – due to a more viscous ice mass – associated with colder temperatures (243 K), increases the thickness of the modelled glacier to match the moraine heights in the upper sector, but then raises the glacier surface well above constraining moraine heights in the lower sector (Figure 5.4c). For

the lowest temperature in our simulations (233 K) both the upper or lower moraine height elevations were both exceeded. These experiments tentatively bracket the long-term temperature requirement for GLF formation to be between 263 and 243 k, with a corresponding ELA of between 615 and 630 m. Under these conditions, our modelling indicates a minimum genesis time for GLF formation of between 285 and 590 ka (Table 5.1).

Two principle assumptions of the model are that the ice mass rheology is homogeneous and it has a frozen subglaical condition with no basal motion. However, considering the experiments conducted, then it is quite plausible that these assumptions do not hold. Indeed, it may be quite likely that the englacial/basal thermal regime, debris content and associated impact on ice rheology and basal motion vary both spatially and temporally. One possibility is that thinner ice is achieved through basal motion in the lower sector of the GLF. In such a scenario part of the GLF may have experienced enhanced flow as a result of viscous heat dissipation or geothermal heat flux yielding liquid water at the ice-bed interface. Basal sliding could be related to increased ice thickness in the interior of the ice mass warming the ice above the pressure melting point (e.g. Palli et al., 2003), or through ice strain and friction heating of deformation causing temperate ice to exist near the bed in the ablation area (e.g. Blatter and Hutter, 1991) – both of these conditions occur at high-latitude polythermal glaciers on Earth (see Irvine-Fynn et al., 2011). Enhanced motion as a result of water at the ice-bed interface has also been reported from purely cold-based glaciers (e.g. Echelmeyer and Zhongxiang, 1987; Cuffey et al., 1999). Cuffey et al. (1999) reported glacier sliding over basal boulders at temperatures as low as 256 K from beneath Meserve Glacier in the Dry Valleys of Antarctica – a much used analogue in martian research (e.g. Marchant and Head, 2007; Fastook et al., 2011; Mackay and Marchant 2017). This sliding was reportedly enhanced by high solute concentrations in the interfacial water (Cuffey et al., 1999). Such an interpretation of enhanced flow in the lower portion of the GLF as the result of lubrication at the ice-bed interface is supported by the interpretation of Hubbard et al. (2011) who noted two surface terrains types in the GLFs lower basin that were consistent with, but not definitively from, formation/modification under partial wet-based glacial conditions. Although the spatial and temporal distribution of any such basal motion remains poorly constrained, it is an interesting and important future research avenue to explore and could explain the discrepancy between the upper and

lower vertical constraints noted here. It is also worth noting that the lower moraine ridge appears to have had a proportion of material (~5 m) removed from its crest (Figure 5.1e) which could also account for some of the surface lowering, but not sufficient to explain the elevation difference between the moraine crest and modelled surface profiles (Figure 5.4).

5.5.2. GLF response to climatic forcing

To assess the response and sensitivity of the GLF to long-term transient climate change on Mars we initiated a simple experiment – under conditions favourable to those in the geomorphological record – where such forcing was simulated by obliquity driven ELA changes (Figures 5.5 and 5.6). These experiments revealed several noteworthy points. Firstly, the GLF reaches the maximum extent only during a period of early (0.0 – 0.9 Ma) extended conditions favourable for ice accumulation (i.e. >30^{o} obliquity). Once the obliquity cycle enters into larger amplitude fluctuations that include short-term periods that are unfavourable for ice accumulation (i.e. <30^{o} obliquity), the GLF does not extend as far as its maximum limit throughout the rest of the simulation – even during a second 342 ka period of conditions favourable for ice accumulation. This suggests that the length of this initial extended period of ice accumulation is critical in defining the maximum length of the GLF during the 2.5 Ma obliquity cycle (assuming there is no inherited ice and that the moraine relates to the same depositional sequence). A second point of interest is that given the input forcing, the model demonstrates various terminus standstills particularly when obliquity changes from >40^{o} to <40^{o}. This behaviour can explain the multiple occurrences of moraines noted in the geomorphological record (Figure 5.1 [Hubbard et al., 2011; Brough et al., 2016a]). The configurations that lead to actual moraine formation are likely to be more complex given the range of processes and environments in which they can form (see Barr and Lovell, 2014). However, the transient experiment conducted does yield some encouraging results that resonate nicely with the geomorphological record and give some tentative basis for future investigation.

In addition the long-term behaviour of the GLF will also be influenced by the inclusion of debris, particularly surface debris. Although a thin (<2 cm) layer of debris can increase ablation (Ostrem, 1959), ablation on glaciers is significantly decreased, by

orders of magnitude, under a thicker (10s cm) debris layer (e.g. Kowalewski et al., 2006). Under sufficient debris cover glaciers can become virtually stagnant (Rignot et al., 2002), and the core of glacier ice may persist for millions of years under this protective armouring, as seen in the Dry Valleys of Antarctica (e.g. Sugden et al., 1995; Marchant et al., 2002). The effects of such processes on Mars are of obvious importance, giving a possible scenario for the long-term preservation of ice, but our understanding of these mechanisms and how they affect ice dynamics are still being developed on both Earth (e.g. Rowan et al., 2015) and Mars (e.g. Fastook et al., 2014). Given that the current GLF surface in the upper basin appears to conform to this scenario, with now relict ice persisting under a layer of debris (Section 5.2 [Hubbard et al., 2011]), the incorporation of debris into the long-term cycle needs to be considered (e.g. Fastook et al., 2014; Parsons and Holt, 2016).

5.5.3. Modelling considerations

Although the above discussion offers plausible explanations for the observations and discrepancies in this study, our understanding of many of the processes that affect glaciers in similar settings even on Earth remains poorly constrained. Furthermore, it is prudent to point out the possibility that equifinality could prevail and that several combinations of parameters and values – including some not included in this study – may yield similar results. This issue is difficult to avoid given the limited empirical data available. However, these findings can provide useful insights that can be refined in future studies particularly when new data or evidence becomes available, for example, through constraining geophysical evidence (i.e. radar [Karlsson et al., 2015; Parsons and Holt, 2016]).

5.6. Conclusions

We applied a two-dimensional numerical ice flow model to investigate the conditions under which a GLF formed in Crater Greg, eastern Hellas Planitia. Model results were compared to geomorphogical evidence of current and former GLF geometries. Initial experiments reveal that the model successfully replicated the maximum horizontal

extent of the GLF under an ELA forcing of between 615 and 640 m for our upper (263 K) and lower (233 K) temperature scenarios. However, no single experiment was able to fully reproduce surface profiles that corresponded to both vertical limits provided by moraine heights across the upper and lower glacier simultaneously. Colder temperatures (243 K) were required to match with the upper vertical constraint and conversely warmer temperatures (263 K) were required to match with the lower vertical constraint. This suggests that a spatially and/or temporally varying ice rheology or basal regime may have acted upon the GLF. Based on the interpretation of Hubbard et al. (2011), who described terrain in the lower basin of the GLF that was potentially formed under wet-based conditions, we consider it a possibility that the GLF experienced a period of enhanced flow through basal motion. This represents a potentially important avenue for future research.

The modelled GLF's response to a transient climate, forced by obliquity variations, indicates that its maximum frontal position was related to an initial extended period of climate favourable to ice accumulation. Several prolonged GLF terminus standstills occurred during the advance and retreat of the GLF terminus throughout the obliquity cycle, allowing the formation of multiple moraines. Although the experiment is simple in its approach, the model nicely matches and explains the moraine sequence observed in the geomorphological record.

Acknowledgements

SB is funded by an Aberystwyth University Doctoral Career Development Scholarship. AH gratefully acknowledges support from the Research Council of Norway through its Centres of Excellence funding scheme, project number 223259.

References

Arfstrom, J., & Hartmann, W. K. (2005). Martian flow features, moraine-like ridges, and gullies: Terrestrial analogs and interrelationships. *Icarus, 174*(2), 321-335. doi: 10.1016/j.icarus.2004.05.026.

Barr, I. D., & Lovell, H. (2014). A review of topographic controls on moraine distribution. *Geomorphology, 226*, 44-64. doi: 10.1016/j.geomorph.2014.07.030.

Blatter, H. (1995). Velocity and Stress-Fields in Grounded Glaciers - a Simple Algorithm for Including Deviatoric Stress Gradients. *Journal of Glaciology, 41*(138), 333-344. doi: 10.1017/S002214300001621X.

Blatter, H., & Hutter, K. (1991). Polythermal conditions in arctic glaciers. *Journal of Glaciology, 37*(126), 261-269. doi:10.1017/S0022143000007279.

Blatter, H., Clarke, G. K. C., & Colinge, J. (1998). Stress and velocity fields in glaciers: Part II. Sliding and basal stress distribution. *Journal of Glaciology, 44*(148), 457-466. doi: 10.1017/S0022143000001970.

Brough, S., Hubbard, B., & Hubbard, A. (2016a). Former extent of glacier-like forms on Mars. *Icarus, 274*, 37-49. doi:10.1016/j.icarus.2016.03.006.

Brough, S., Hubbard, B., & Hubbard, A. (2016b). Two-dimensional numerical ice flow modeling of an empirically reconstructed martian glacier-like form. Abstract #1994. *47th Lunar and Planetary Science Conference*, *March 21-25, The Woodlands, Texas.*

Byrne, S., Dundas, C. M., Kennedy, M. R., Mellon, M. T., McEwen, A. S., Cull, S. C., Dauber, I. J., Shean, D. E., Seelos, K. D., Murchie, S. L., Cantor, B. A., Arvidson, R. E., Edgett, K. S., Reufer, A., Thomas, N., Harrison, T. N., Posiolova, L. V., & Seelos, F. P. (2009). Distribution of mid-latitude ground ice on Mars from new impact craters. *Science, 325*(5948), 1674-1676. doi: 10.1126/science.1175307.

Colaprete, A., & Jakosky, B. M. (1998). Ice flow and rock glaciers on Mars. *Journal of Geophysical Research-Planets, 103*(E3), 5897-5909. doi: 10.1029/97je03371.

Cuffey, K. M., Conway, H., Hallet, B., Gades, A. M., & Raymond, C. F. (1999). Interfacial water in polar glaciers and glacier sliding at −17°C. *Geophysical Research Letters, 26*(6), 751-754. doi: 10.1029/1999GL900096.

Dickson, J. L., Head, J. W., & Fassett, C. I. (2012). Patterns of accumulation and flow of ice in the mid-latitudes of Mars during the Amazonian. *Icarus, 219*(2), 723-732. doi: 10.1016/j.icarus.2012.03.010.

Echelmeyer, K., & Zhongxiang, W. (1987). Direct Observation of Basal Sliding and Deformation of Basal Drift at Sub-Freezing Temperatures. *Journal of Glaciology, 33*(113), 83-98. doi: 10.3189/S0022143000005396.

Fastook, J. L., & Head, J. W. (2014). Amazonian mid- to high-latitude glaciation on

Mars: Supply-limited ice sources, ice accumulation patterns, and concentric crater fill glacial flow and ice sequestration. *Planetary and Space Science, 91*, 60-76. doi: 10.1016/j.pss.2013.12.002.

Fastook, J. L., Head, J. W., & Marchant, D. R. (2014). Formation of lobate debris aprons on Mars: Assessment of regional ice sheet collapse and debris-cover armoring. *Icarus, 228*, 54-63. doi: 10.1016/j.icarus.2013.09.025.

Fastook, J. L., Head, J. W., Marchant, D. R., & Forget, F. (2008). Tropical mountain glaciers on Mars: Altitude-dependence of ice accumulation, accumulation conditions, formation times, glacier dynamics, and implications for planetary spin-axis/orbital history. *Icarus, 198*(2), 305-317. doi: 10.1016/j.icarus.2008.08.008.

Fastook, J. L., Head, J. W., Forget, F., Madeleine, J.-B., & Marchant, D. R. (2011). Evidence for Amazonian northern mid-latitude regional glacial landsystems on Mars: Glacial flow models using GCM-driven climate results and comparisons to geological observations. *Icarus, 216*(1), 23-39. doi: 10.1016/j.icarus.2011.07.018.

Forget, F., Haberle, R. M., Montmessin, F., Levrard, B., & Heads, J. W. (2006). Formation of glaciers on Mars by atmospheric precipitation at high obliquity. *Science, 311*(5759), 368-371. doi: 10.1126/science.1120335.

Glen, J. W. (1955). The creep of polycrystalline ice. *Proceedings of the Royal Society of London. Series A. Mathematical and Physical Sciences, 228*(1175), 519. doi: 10.1098/rspa.1955.0066.

Goldsby, D. L., & Kohlstedt, D. L. (2001). Superplastic deformation of ice: Experimental observations. *Journal of Geophysical Research: Solid Earth, 106*(B6), 11017-11030. doi: 10.1029/2000JB900336.

Hartmann, W. K., Thorsteinsson, T., & Sigurdsson, F. (2003). Martian hillside gullies and Icelandic analogs. *Icarus, 162*(2), 259-277. doi: 10.1016/S0019-1035(02)00065-9.

Hartmann, W. K., Ansan, V., Berman, D. C., Mangold, N., & Forget, F. (2014). Comprehensive analysis of glaciated martian crater Greg. *Icarus, 228*, 96-120. doi: 10.1016/j.icarus.2013.09.016.

Head, J. W., Marchant, D. R., Dickson, J. L., Kress, A. M., & Baker, D. M. (2010). Northern mid-latitude glaciation in the Late Amazonian period of Mars: Criteria for the recognition of debris-covered glacier and valley glacier landsystem

deposits. *Earth and Planetary Science Letters, 294*(3-4), 306-320. doi: 10.1016/j.epsl.2009.06.041.

Head, J. W., Mustard, J. F., Kreslavsky, M. A., Milliken, R. E., & Marchant, D. R. (2003). Recent ice ages on Mars. *Nature, 426*(6968), 797-802. doi: 10.1038/Nature02114.

Head, J. W., Neukum, G., Jaumann, R., Hiesinger, H., Hauber, E., Carr, M., Massson, P., Foing, B., Hoffmann, H., Kreslavsky, M., Werner, S., Milkovich, S., van Gasselt, S., & HRSC Co-Investigator Team. (2005). Tropical to mid-latitude snow and ice accumulation, flow and glaciation on Mars. *Nature, 434*(7031), 346-351. doi: 10.1038/Nature03359.

Holt, J. W., Safaeinili, A., Plaut, J. J., Head, J. W., Phillips, R. J., Seu, R., Kempft, S. D., Choudhary, P., Young, D. A., Putzig, N. E., Biccari, D., & Gim, Y. (2008). Radar Sounding Evidence for Buried Glaciers in the Southern Mid-Latitudes of Mars. *Science, 322*(5905), 1235-1238. doi: 10.1126/science.1164246.

Hubbard, A. (1997a). *High resolution modelling of glaciers*. Unpublished Ph. D. Thesis, University of Edinburgh.

Hubbard, A. (1997b). Modelling climate, topography and palaeoglacier fluctuations in the Chilean Andes. *Earth Surface Processes and Landforms, 22*(1), 79-92. doi: 10.1002/(SICI)1096-9837(199701)22:1<79::AID-ESP654>3.0.CO;2-J.

Hubbard, A. (2000). The verification and significance of three approaches to longitudinal stresses in high-resolution models of glacier flow. *Geografiska Annaler, 82A*(4), 471-487. doi: 10.1111/j.0435-3676.2000.00135.x.

Hubbard, A. (2006). The validation and sensitivity of a model of the Icelandic ice sheet. *Quaternary Science Reviews, 25*(17), 2297-2313. doi: 10.1016/j.quascirev.2006.04.005.

Hubbard, A., Blatter, H., Nienow, P., Mair, D., & Hubbard, B. (1998). Comparison of a three-dimensional model for glacier flow with field data from Haut Glacier d'Arolla, Switzerland. *Journal of Glaciology, 44*(147), 368-378. doi: 10.1017/S0022143000002690.

Hubbard, B., Souness, C., & Brough, S. (2014). Glacier-like forms on Mars. *The Cryosphere, 8*(6), 2047-2061. doi: 10.5194/tc-8-2047-2014.

Hubbard, B., Milliken, R. E., Kargel, J. S., Limaye, A., & Souness, C. (2011). Geomorphological characterisation and interpretation of a mid-latitude glacier-like form: Hellas Planitia, Mars. *Icarus, 211*(1), 330-346. doi:

10.1016/j.icarus.2010.10.021.

Hubbard, B., Hubbard, A., Mader, H. M., Tison, J.-L., Grust, K., & Nienow, P. W. (2003). Spatial variability in the water content and rheology of temperate glaciers: Glacier de Tsanfleuron, Switzerland. *Annals of Glaciology, 37*(1), 1-6. doi: 10.3189/172756403781815474.

Irvine-Fynn, T. D. L., Hodson, A. J., Moorman, B. J., Vatne, G., & Hubbard, A. L. (2011). Polythermal glacier hydrology: a review. *Reviews of Geophysics, 49*(4), RG4002. doi: 10.1029/2010RG000350.

Kargel, J. S. (2004). *Mars - A Warmer, Wetter Planet*. London: Springer-Praxis.

Karlsson, N. B., Schmidt, L. S., & Hvidberg, C. S. (2015). Volume of Martian midlatitude glaciers from radar observations and ice flow modeling. *Geophysical Research Letters, 42*(8), 2015GL063219. doi: 10.1002/2015gl063219.

Kowalewski, D. E., Marchant, D. R., Levy, J. S., & Head, J. W. (2006). Quantifying low rates of summertime sublimation for buried glacier ice in Beacon Valley, Antarctica. *Antarctic Science, 18*(03). doi: 10.1017/s0954102006000460.

Laskar, J., Levrard, B., & Mustard, J. F. (2002). Orbital forcing of the martian polar layered deposits. *Nature, 419*(6905), 375-377. doi: 10.1038/Nature01066.

Laskar, J., Correia, A. C. M., Gastineau, M., Joutel, F., Levrard, B., & Robutel, P. (2004). Long term evolution and chaotic diffusion of the insolation quantities of Mars. *Icarus, 170*(2), 343-364. doi: 10.1016/j.icarus.2004.04.005.

Levy, J. S., Fassett, C. I., Head, J. W., Schwartz, C., & Watters, J. L. (2014). Sequestered glacial ice contribution to the global Martian water budget: Geometric constraints on the volume of remnant, midlatitude debris-covered glaciers. *Journal of Geophysical Research: Planets, 119*(10), 2014JE004685. doi: 10.1002/2014je004685.

Lucchitta, B. K. (1984). Ice and debris in the Fretted Terrain, Mars. *Journal of Geophysical Research: Solid Earth, 89*(S02), B409-B418. doi: 10.1029/JB089iS02p0B409.

Mackay, S. L., & Marchant, D. R. (2017). Obliquity-paced climate change recorded in Antarctic debris-covered glaciers. *Nature Communications, 8*, 14194. doi: 10.1038/ncomms14194.

Madeleine, J. B., Forget, F., Head, J. W., Levrard, B., Montmessin, F., & Millour, E. (2009). Amazonian northern mid-latitude glaciation on Mars: A proposed climate scenario. *Icarus, 203*(2), 390-405. doi: 10.1016/j.icarus.2009.04.037.

Marchant, D., & Head, J. W. (2003). Tongue-shaped lobes on Mars: Morphology, Nomenclature, and Relation to Rock Glacier Deposits. Abstract #3091, *Sixth International Conference on Mars, July 20-25, Pasadena, California.*

Marchant, D. R., & Head, J. W. (2007). Antarctic dry valleys: Microclimate zonation, variable geomorphic processes, and implications for assessing climate change on Mars. *Icarus, 192*(1), 187-222. doi: 10.1016/j.icarus.2007.06.018.

Marchant, D. R., Lewis, A. R., Phillips, W. M., Moore, E. J., Souchez, R. A., Denton, G. H., Sugden, D. E., Potter Jr, N., & Landis, G. P. (2002). Formation of patterned ground and sublimation till over Miocene glacier ice in Beacon Valley, southern Victoria Land, Antarctica. *Geological Society of America Bulletin, 114*(6), 718-730. doi: 10.1130/0016-7606(2002)114<0718:fopgas>2.0.co;2.

Mellon, M. T., & Jakosky, B. M. (1995). The distribution and behavior of Martian ground ice during past and present epochs. *Journal of Geophysical Research: Planets, 100*(E6), 11781-11799. doi: 10.1029/95je01027.

Mellon, M. T., Feldman, W. C., & Prettyman, T. H. (2004). The presence and stability of ground ice in the southern hemisphere of Mars. *Icarus, 169*(2), 324-340. doi: 10.1016/j.icarus.2003.10.022.

Milliken, R. E., Mustard, J. F., & Goldsby, D. L. (2003). Viscous flow features on the surface of Mars: Observations from high-resolution Mars Orbiter Camera (MOC) images. *Journal of Geophysical Research-Planets, 108*(E6). doi: 10.1029/2002je002005.

Nye, J. F. (1951). The Flow of Glaciers and Ice-Sheets as a Problem in Plasticity. *Proceedings of the Royal Society of London Series a-Mathematical and Physical Sciences, 207*(1091), 554-572. doi: 10.1098/rspa.1951.0140.

Oerlemans, J. (1988). Simulation of Historic Glacier Variations with a Simple Climate-Glacier Model. *Journal of Glaciology, 34*(118), 333-341. doi: 10.1017/S0022143000007103.

Ostrem, G. (1959). Ice Melting under a Thin Layer of Moraine, and the Existence of Ice Cores in Moraine Ridges. *Geografiska Annaler, 41*(4), 228-230.

Pälli, A., Moore, J. C., Jania, J., Kolondra, L., & Glowacki, P. (2003). The drainage pattern of Hansbreen and Werenskioldbreen, two polythermal glaciers in Svalbard. *Polar Research, 22*(2), 355-371. doi: 10.3402/polar.v22i2.6465.

Parsons, R., & Holt, J. (2016). Constraints on the formation and properties of a Martian lobate debris apron: Insights from high-resolution topography, SHARAD radar

data, and a numerical ice flow model. *Journal of Geophysical Research: Planets*, 2015JE004927. doi: 10.1002/2015je004927.

Parsons, R. A., Nimmo, F., & Miyamoto, H. (2011). Constraints on martian lobate debris apron evolution and rheology from numerical modeling of ice flow. *Icarus, 214*(1), 246-257. doi: 10.1016/j.icarus.2011.04.014.

Patton, H., Hubbard, A., Glasser, N. F., Bradwell, T. and Golledge, N. R. (2013) The last Welsh Ice Cap: Part 1 – Modelling its evolution, sensitivity and associated climate. *Boreas, 42*(3), 471-490. doi: 10.1111/j.1502-3885.2012.00300.x.

Rignot, E., Hallet, B., & Fountain, A. (2002). Rock glacier surface motion in Beacon Valley, Antarctica, from synthetic-aperture radar interferometry. *Geophysical Research Letters, 29*(12). doi: 10.1029/2001gl013494.

Rowan, A. V., Egholm, D. L., Quincey, D. J. and Glasser, N. F. (2015). Modelling the feedbacks between mass balance, ice flow and debris transport to predict the response to climate change of debris-covered glaciers in the Himalaya. *Earth and Planetary Science Letters, 430*, 427-438. doi: 10.1016/j.epsl.2015.09.004.

Souness, C., Hubbard, B., Milliken, R. E., & Quincey, D. (2012). An inventory and population-scale analysis of martian glacier-like forms. *Icarus, 217*(1), 243-255. doi: 10.1016/j.icarus.2011.10.020.

Squyres, S. W. (1978). Martian Fretted Terrain - Flow of Erosional Debris. *Icarus, 34*(3), 600-613. doi: 10.1016/0019-1035(78)90048-9.

Sugden, D. E., Marchant, D. R., Potter, N., Souchez, R. A., Denton, G. H., Swisher Iii, C. C., & Tison, J.-L. (1995). Preservation of Miocene glacier ice in East Antarctica. *Nature, 376*(6539), 412-414. doi: 10.1038/376412a0.

Van der Veen, C. J. (1999). Fundamentals of Glacier Dynamics. Rotterdam: A. A. Balkema.

Summary to manuscript 'Palaeo-glaciers on Mars: modelling their formation and evolution'

Chapter 5 has presented a numerical modelling investigation in to the climates under which a GLF in Crater Greg, eastern Hellas Planitia may have formed. The key outcomes to carry forward are as such:

1. A suite of model experiments were run to investigate the long-term ELA and temperature required to reproduce the GLF's maximum frontal position and vertical extent recorded in the geomorphological record. Results from these experiments can summarised as follows:

    - The maximum horizontal extent of the GLF was replicated under an ELA forcing of between 615 and 640 m for our upper (263 K) and lower (233 K) temperature scenarios.

    - The formation time required for the simulations that 'best fit' the observed terminus position to reach steady state places an upper and lower formation time of 285 to 905 ka, for our maximum and minimum temperatures of 263 and 233 K, respectively.

    - No single experiment was able to fully reproduce surface profiles that corresponded to both vertical limits provided by moraine heights across the upper and lower glacier simultaneously. Colder temperatures (243 K) were required to match with the upper vertical constraint and conversely warmer temperatures (263 K) were required to match with the lower vertical constraint.

2. Given point (1) above, it is suggested that a spatially and/or temporally varying ice rheology or basal regime may have acted upon the GLF, and it is considered a possibility that the GLF experienced a period of enhanced flow through basal motion.

3. A further set of dynamic experiments was conducted to assess the sensitivity and response of the GLF to transient climatic forcing. This was implemented through a series of stepped ELA changes reflecting known changes in obliquity through one full obliquity cycle of 2.5 Ma. Results from this experiment can summarised as follows:

    - The GLF reaches the maximum frontal extent as recorded in the geomorphological record only during a period of early (0.0 – 0.9 Ma) extended conditions favourable for ice accumulation (i.e. $>30^{o}$ obliquity).

    - Once the obliquity cycle enters into larger amplitude fluctuations that include short-term periods that are unfavourable for ice accumulation (i.e. $<30^{o}$ obliquity), the GLF does not extend as far as its maximum frontal limit throughout the rest of the simulation. This suggests that the length of this initial extended period of ice accumulation is critical in defining the maximum length of the GLF during the 2.5 Ma obliquity cycle.

    - Several terminus standstills were noted during the advance/retreat fluctuations of the GLF terminus throughout the obliquity cycle, thereby providing a plausible transient reconstruction that facilitates the formation of multiple moraines as recorded in the geomorphological record.

CHAPTER 6

Conclusions and outlook

One never notices what has been done;
one can only see what remains to be done
Marie Curie

6.1. Conclusions

6.1.1. Summary and contribution of works

6.1.1.1. Chapter 2. Landscapes of polyphase glaciation: eastern Hellas Planitia, Mars

This manuscript presented a geomorphic and structural assessment of a landscape in eastern Hellas Planitia, which is interpreted to be of glacial origin. Mapping, conducted using a combination of Context Camera (CTX) and High Resolution Imaging Science Experiment (HiRISE) imagery, revealed that the landscape was composed of four distinct geomorphic units, and 16 structures. Two units showed significant evidence of glacial flow: (i) at the broad scale the lobate debris apron (LDA) preserved a convex-up profile and numerous arcuate and longitudinal structures indicative of the downslope flow of ice; and (ii) at the more localised scale the glacier-like form (GLF) also preserved several structures indicative of flow and transport of ice downslope, including surface crevassing. A third terrain, degraded glacial material, also showed evidence for the downslope flow of mass, but structures lacked clear indication of a significant ice core and are more akin to slope processes of periglacial environments. Surrounding both the LDA and GLF were numerous moraine-like ridges indicating that mass loss had occurred. Taken together, these observations led to the hypothesis that not only was the landscape glacial in origin but that it had experienced at least two phases of glaciation, with a wider more extensive glacial period being recorded in the LDA, and a secondary, more localised glaciation recorded in the GLF. Analysis of several surface structures, for example the identification of fractures and arcuate transverse ridges, also provided insights into the dynamics of these ice masses suggesting that, much like terrestrial glaciers (e.g. Vaughan, 1993; Goodsell et al., 2005), Mars' viscous flow features (VFFs) have experienced variable flow regimes. Given the above, work presented in Chapter 2 addressed Objectives (1) and (2) of this thesis.

These observations provided further evidence for the hypothesis that Mars' mid-latitudes preserve evidence of multiple phases of glaciation, but extends the spatial scale at which these observations have been reported – until now much of this evidence has been derived in the northern hemisphere (Levy et al., 2007; Dickson et al., 2008; Morgan et al., 2009; Baker al., 2010; Dickson et al., 2010; Sinha and Murty, 2013).

Furthermore, the published manuscript (Brough et al., 2016) provided other researchers with a framework to interpret similar landscapes and features in contemporaneous ice masses, as evidenced in the recent publications of Sinha and Vijayan (2017) and Sinha et al. (2017).

6.1.1.2. Chapter 3. Area and volume of mid-latitude glacier-like forms on Mars

This manuscript presented a population-scale assessment of the area and volume of water stored in present day GLFs. CTX images were used to directly map the outlines of all GLFs in order to derive their current area. From this area, volumetric analysis was conducted using a volume-area scaling approach. These results were subsequently coupled with topographic data from the Mars Orbiter Laser Altimeter (MOLA) to assess potential controlling environmental variables over variations in GLF area and volume. In total 1243 unique GLFs were identified and the main findings were that: (i) GLFs cover an area of 11344 ± 393 km^2, or ~0.01% of the total surface area of Mars; (ii) GLFs have an ice volume between 523 ± 132 km^3 (480 ± 121 Gt) and 1570 ± 397 km^3 (1439 ± 364 Gt). This is equivalent to a global water layer of between 3 ± 1 and 10 ± 3 mm thick; (iii) at the global scale, GLFs are larger at higher latitudes and on shallower slopes; (iv) in the northern hemisphere, GLFs with elevations between 500 and 2500 m, and in the southern hemisphere, GLFs with a northern aspect are also larger on average; and (v) smaller GLFs were located on a wider range of slopes than larger GLFs.

These observations led to a number of broad conclusions being drawn, namely that: (i) GLFs contributed to the present day surface/near-surface water budget, but contained a water equivalent of between one and two orders of magnitude less than other mid-latitude ice deposits; (ii) GLF size is sensitive to insolation and to local meteorological and topographical conditions; (iii) GLF size appeared particularly sensitive to slope, therefore suggesting that like glaciers on Earth, slope process play(ed) an important role in driving GLF motion; and (iv) smaller GLFs are less sensitive to their topographic setting, and as such small GLFs of comparable size are likely to show a heterogeneous response to the same climatic perturbation. Given the above, work presented in Chapter 3 addressed Objectives (1), (2), (3) and (5) of this thesis.

Chapter 3 provided several advances into our understanding of Mars' GLFs. First, present day estimates of the mid-latitude contribution to the surface/near-surface water inventory of Mars (e.g. Levy et al., 2014; Carr and Head, 2015; Karlsson et al., 2015) do not include GLFs. Therefore, these estimate can now be revised upwards to account for the volume of water contained within GLFs. Such information is important to improving our understanding of how the water budget of Mars has evolved over time (e.g. Baker, 2001) and can help to constrain the magnitude and extent of the climatic excursions that are responsible for their formation. Second, although GLFs appeared to show a sensitivity to insolation, for example through preferential poleward facing orientation (Souness et al., 2012), their size is also strongly influenced by variations in their physical environment which act in providing microclimates favourable for the accumulation and/or preservation of ice – some of which (e.g. slope) share a direct relationship with their terrestrial analogues. Finally, the GLF inventory that is provided as part of the supporting material (and will be included with any future publication), presented the most comprehensive and detailed GLF inventory to date in a ready-to-use format with a geographic information system. The production of digital vector outlines are a critical component of analogous studies of glacierised terrains on Earth, where such products are essential for change detection and for the modelling of climatic change (e.g. Huss et al., 2009; Paul et al., 2011).

6.1.1.3. Chapter 4. Former extent of glacier-like forms on Mars

This manuscript built upon the observations of ice mass loss made in Chapter 2 (and Appendix A). It presented a population-scale inventory detailing the locations of GLFs that showed evidence of ice mass loss and recession. Coupled with this inventory, a glacial reconstruction of a typical GLF (located in Crater Greg, eastern Hellas Planitia) was completed, using the perfect plastic approximation for ice flow, in order to quantify its area and volumetric change since its former maximum extent. The main findings were that: (i) 436 GLFs were identified that showed evidence of recession; (ii) relative to the parent population, recessional GLFs were over-represented at latitudes $<40^{o}$ and in areas of high relief in both hemispheres; (iii) the reconstructed GLF had lost an area of 6.86 km^2 and a volume of 0.31 km^3; and (iv) scaling this ice loss to all recessional GLFs yielded a potential planetary volume loss of 135 km^3 from Mars' GLFs. Given the

above, work presented in Chapter 4 addressed Objectives (1), (2), (4) and (5) of this thesis.

The observations reported in Chapter 4 addressed a number of knowledge gaps in relation to the distribution and evolution of GLFs and more broadly mid-latitude ice. Firstly, although several instances of ice mass loss from GLFs had been reported (e.g. Appendix A; Hartmann et al., 2003; Dickson et al., 2008; Hubbard et al., 2011), no such study had identified the extent to which recession had occurred at the global scale. The identification of approximately one third of all GLFs showing evidence of recession indicated that mass loss within the GLF population was not isolated or localised and thus was indicative of changes in global climate. Secondly, analysis of the environmental settings of recessional GLFs showed that latitude and relief exerted some control over GLF sensitivity and response to climatic forcing. These results provided the first quantification of the controls over GLF recession and ice mass loss and showed that GLFs are particularly sensitive to the planetary limit of shallow ground ice stability (e.g. Mellon et al. 2004; Bryne et al., 2009; Schorghofer and Forget, 2012) and that GLFs in areas of higher relief (rougher topography) likely have a shorter response time to climatic perturbations than GLFs in areas of lower relief (smoother topography). Finally, since initial deposition, some GLFs have experienced significant mass loss. Our glacial reconstruction provided the first quantification of both volume and area change and showed that the ice mass had lost ~70 % of its area and a volume of 0.31 km^3 through a combination of vertical thinning and terminus recession.

6.1.1.4. Chapter 5. Palaeo-glaciers on Mars: modelling their formation and evolution

This manuscript extended the investigations into the glacial history of the GLF reconstructed in Chapter 4 and as discussed by previous authors (e.g. Hubbard et al., 2011; Hartmann et al., 2014). It presented initial results from numerical modelling experiments that aimed at investigating the long-term climate that could have led to the formation of the former maximum GLF extent recorded in the geomorphological record. The model is driven by a mass balance term that is forced by altering the equilibrium line altitude (ELA) over time and was applied to steady-state ice temperatures between 263 and 233 K. The ice rheology used in the model followed

Glen's flow law (n = 3), the basal sliding distribution was set to zero (i.e. ice below the pressure melting point), and the mass balance input was derived from the altitudinal parameterisation of Fastook et al. (2008).

Results showed that the numerical model was able to successfully simulate the maximum horizontal extent of the GLF as indicated in the geomorphological record for all ice temperatures, but no simulation was successful in producing a surface profile that was in agreement with both vertical limits, as defined by the moraine heights. A possible explanation for this discrepancy was presented, in that the GLF may have experienced spatially and/or temporally varying ice rheology and/or basal motion. The latter explanation is consistent with the interpretation of Hubbard et al. (2011) who suggested that this GLF might have experienced wet-based conditions at the ice-bed interface. More broadly, this raised an interesting point as to the thermal-regime of GLFs and Mars' wider ice masses and clearly warrants further investigation and research (see Section 6.2). Further experiments invested the response of the GLF to a transient climate that was forced by variations in obliquity. Although simplistic in its approach it highlighted two key points: (i) the length of the initial extended period of ice accumulation is critical in defining the maximum length of the GLF during the 2.5 Ma obliquity cycle; and (ii) several terminus standstills were noticed during the advance and retreat of the GLF throughout the obliquity cycle. These two observations provided a scenario that could facilitate the formation of multiple moraines as recorded in the geomorphological record (e.g. Hartmann et al., 2003; Hubbard et al., 2011). Given the above, work presented in Chapter 5 addressed Objectives (2) and (6) of this thesis.

6.1.2. Overall synthesis

The overall aim of this thesis was to assess the current and former volume and dynamics of mid-latitude GLFs, in order to advance our understanding of the planet's recent glacial history.

At the broadest level Mars' mid-latitudes appear to preserve a complex and spatially heterogeneous record of glaciation (Chapters 2, 3 and 4). GLFs appear to be the manifestation of a more localised, and likely less intense, period of glaciation than that

recorded in the more extensive VFFs (Chapters 2 and 3). Nonetheless, GLFs represent an active component of the near-surface water budget of Mars, locking away an estimated global equivalent water layer of between 3 ± 1 and 10 ± 3 mm (Chapter 3). Furthermore, it has been shown that Mars' GLF population has undergone widespread recession and mass loss since a former maximum extent (Chapters 4), suggesting that these landforms: (i) once contributed a larger volume of water to the near-surface water budget of Mars; and (ii) are sensitive indicators of recent climatic change.

Although our understanding of the origins and subsequent evolution of GLFs is far from complete (see Section 6.2 below), heterogeneity in their distribution and size reveals that they are not purely controlled by insolation forcing that is related to latitudinal position. It is, therefore, likely that regional to local meteorological and topographical conditions also play an important role in GLF ice accumulation and/or preservation, with variation in physical environments providing microclimates favourable for the accumulation and/or preservation of ice (Chapters 3 and 4).

The mechanisms by which GLFs and the wider VFFs flow, suggests that they operate, or have operated, under similar stress and strain regimes as glaciers on Earth and at least some GLFs have experienced variable flow regimes (Chapters 2, 4 and 5). Indeed, the emerging picture shows that Mars GLFs appear to have been dynamically active, and that they have played an important role in altering the surface landscape of Mars through erosion, transport and deposition of material (Chapters 2 and 4).

6.2. Avenues for future work

Despite efforts made in this thesis and more broadly by the research community a number of fundamental glaciological aspects of GLFs remain unknown (see Chapter 1 and Appendix A.4). This is hindered by the overall lack of empirical evidence that has thus far been acquired from Mars's GLFs and associated landscapes that can directly address these knowledge gaps. Nonetheless, with an increasing array of remotely sensed data being acquired, via a variety of techniques (i.e. high-resolution imagery, radar, spectroscopy), it provides us with the opportunity to generate more accurate and

spatially extensive empirical datasets, and should be a priority for future research. For example:

- High-resolution CTX and HiRISE imagery could be used to extend the work performed in Chapter 4 and target/search for local to regional evidence for former ice extents/limits (e.g. moraines, trimlines or kame terraces) or indicators of wet-based glacial conditions/subglacial drainage (e.g. mega-scale glacial lineations or eskers [e.g. Gallagher and Balme, 2015]). Mapping of such landforms when combined with a digital elevation model of sufficient resolution (e.g. CTX or High Resolution Stereo Camera) could allow regional ice loss to be quantified. Studies of this kind have been undertaken on many glaciated and glacierised environments on Earth (e.g. Glasser et al., 2011).

- The continued acquisition of repeat HiRISE imagery raises the possibility that contemporary GLF motion could be measured through feature/speckle tracking. Such endeavours have already proved successful for monitoring sand and dune migration on Mars (Bridges et al., 2012). In this vein, several request have been made by the author of this thesis – and collaborators – to the HiWISH program (https://www.uahirise.org/hiwish/) in a bid to obtain repeat imagery from GLFs where crevassing has been identified (e.g. Appendix A).

- Although hindered by the spatial scale and often steep topographic settings, Shallow Radar (SHARAD) could be used to provide constraints on the ice thickness and bed geometry of GLFs. Several studies have successfully identified the basal interface in VFFs (e.g. Holt et al., 2008; Plaut et al., 2009; Karlsson et al., 2015). Such data would also provide a means to refine the ice volume estimates presented in Chapter 3 and to provide much needed boundary conditions for numerical modelling studies (e.g. Chapter 5).

All of these data sets would provide much needed insights/constraints on the processes and properties of GLF including: ice mass loss; thermal regime; motion; ice thickness; and bed geometry. In this regard the GLF inventory and recessional GLF inventory

presented in Chapters 3 and 4, respectively, could be used to target candidate regions of interest and for cross-checking data availability.

To build upon the work of Chapter 5 efforts should be made to constrain the parameter space that is capable of matching the geomorphological evidence of GLF former extent and change. An initial modelling step would be to include the effects of a spatially and/or temporally varying ice rheology and/or basal regime and the numerical model utilised in this study can include such effects. Moreover, this model incorporated a number of assumptions for parameters that were used to drive the model simulations. Future work should seek to better constrain these parameters for the specific study site; for example, temperature and ice accumulation rates could be incorporated from climate simulations from general circulation models (e.g. Forget et al., 2006), although these endeavours may be hindered by the resolution differences in modelling domains. Such efforts have proven insightful for better understanding the climatic conditions required for VFFs to form (e.g. Fastook et al. 2011) and in reconstructing palaeo-ice sheets in Mars' low-latitudes (e.g. Fastook et al., 2008; Soueck et al., 2015).

More broadly, numerical modelling could help us to improve our understanding of GLF ice rheology. By combining a spatially-distributed, higher-order, ice-flow model with SHARAD-derived geometry or crevasse location/morphology, that act as calibration data, it would be possible to use an iterative approach to test a range of values for properties that influence ice rheology (e.g. temperature, flow-law exponent, ice grain size) in an effort to constrain the range of values that best-fits with the observations (e.g. Hubbard and Hubbard, 2000; Parson and Holt, 2016). Overall it is clear that the biggest limiting factor in the use of numerical modelling studies of Mars' GLFs, and by extraction VFFs, is the acquisition of sufficient boundary conditions for the modelling domain – again pointing us towards the need for empirical data.

References

Baker, D. M. H., Head, J. W., & Marchant, D. R. (2010). Flow patterns of lobate debris aprons and lineated valley fill north of Ismeniae Fossae, Mars: Evidence for extensive mid-latitude glaciation in the Late Amazonian. *Icarus, 207*(1), 186-

209. doi: 10.1016/j.icarus.2009.11.017.

Baker, V. R. (2001). Water and the martian landscape. *Nature, 412*(6843), 228-236. doi: 10.1038/35084172.

Bridges, N. T., Ayoub, F., Avouac, J. P., Leprince, S., Lucas, A., & Mattson, S. (2012). Earth-like sand fluxes on Mars. *Nature, 485*(7398), 339-342. doi: 10.1038/nature11022.

Brough, S., Hubbard, B., Souness, C., Grindrod, P. M., & Davis, J. (2016). Landscapes of polyphase glaciation: eastern Hellas Planitia, Mars. *Journal of Maps, 12*(3), 530-542. doi: 10.1080/17445647.2015.1047907.

Byrne, S., Dundas, C. M., Kennedy, M. R., Mellon, M. T., McEwen, A. S., Cull, S. C., Dauber, I. J., Shean, D. E., Seelos, K. D., Murchie, S. L., Cantor, B. A., Arvidson, R. E., Edgett, K. S., Reufer, A., Thomas, N., Harrison, T. N., Posiolova, L. V., & Seelos, F. P. (2009). Distribution of mid-latitude ground ice on Mars from new impact craters. *Science, 325*(5948), 1674-1676. doi: 10.1126/science.1175307.

Carr, M. H., & Head, J. W. (2015). Martian surface/near-surface water inventory: Sources, sinks, and changes with time. *Geophysical Research Letters*, 2014GL062464. doi: 10.1002/2014gl062464.

Dickson, J. L., Head, J. W., & Marchant, D. R. (2008). Late Amazonian glaciation at the dichotomy boundary on Mars: Evidence for glacial thickness maxima and multiple glacial phases. *Geology, 36*(5), 411-414. doi: 10.1130/g24382a.1.

Dickson, J. L., Head, J. W., & Marchant, D. R. (2010). Kilometer-thick ice accumulation and glaciation in the northern mid-latitudes of Mars: Evidence for crater-filling events in the Late Amazonian at the Phlegra Montes. *Earth and Planetary Science Letters, 294*(3-4), 332-342. doi: 10.1016/j.epsl.2009.08.031.

Fastook, J. L., Head, J. W., Marchant, D. R., & Forget, F. (2008). Tropical mountain glaciers on Mars: Altitude-dependence of ice accumulation, accumulation conditions, formation times, glacier dynamics, and implications for planetary spin-axis/orbital history. *Icarus, 198*(2), 305-317. doi: 10.1016/j.icarus.2008.08.008.

Fastook, J. L., Head, J. W., Forget, F., Madeleine, J.-B., & Marchant, D. R. (2011). Evidence for Amazonian northern mid-latitude regional glacial landsystems on Mars: Glacial flow models using GCM-driven climate results and comparisons to geological observations. *Icarus, 216*(1), 23-39. doi:

10.1016/j.icarus.2011.07.018.

Forget, F., Haberle, R. M., Montmessin, F., Levrard, B., & Head, J. W. (2006). Formation of glaciers on Mars by atmospheric precipitation at high obliquity. *Science, 311*(5759), 368-371. doi: 10.1126/science.1120335.

Gallagher, C., & Balme, M. (2015). Eskers in a complete, wet-based glacial system in the Phlegra Montes region, Mars. *Earth and Planetary Science Letters, 431*, 96-109. doi: 10.1016/j.epsl.2015.09.023.

Glasser, N. F., Harrison, S., Jansson, K. N., Anderson, K., & Cowley, A. (2011). Global sea-level contribution from the Patagonian Icefields since the Little Ice Age maximum. *Nature Geosci, 4*(5), 303-307. doi: 1 0.1038/ngeo1122.

Goodsell, B., Hambrey, M. J., Glasser, N. F., Nienow, P., & Mair, D. (2005). The structural glaciology of a temperate valley glacier: Haut Glacier d'Arolla, Valais, Switzerland. *Arctic Antarctic and Alpine Research, 37*(2), 218-232. doi: 10.1657/1523-0430(2005)037[0218:Tsgoat]2.0.Co;2.

Harbor, J. M. (1995). Development of glacial-valley cross sections under conditions of spatially variable resistance to erosion. *Geomorphology*, *14*(2), 99-107. doi: 10.1016/0169-555x(95)00051-1.

Hartmann, W. K., Thorsteinsson, T., & Sigurdsson, F. (2003). Martian hillside gullies and Icelandic analogs. *Icarus, 162*(2), 259-277. doi: 10.1016/S0019-1035(02)00065-9.

Hartmann, W. K., Ansan, V., Berman, D. C., Mangold, N., & Forget, F. (2014). Comprehensive analysis of glaciated martian crater Greg. *Icarus, 228*, 96-120. doi: 10.1016/j.icarus.2013.09.016.

Holt, J. W., Safaeinili, A., Plaut, J. J., Head, J. W., Phillips, R. J., Seu, R., Kempf, S. D., Choudhary, P., Young, D. A., Putzig, N. E., Biccari, D., & Gim, Y. (2008). Radar Sounding Evidence for Buried Glaciers in the Southern Mid-Latitudes of Mars. *Science, 322*(5905), 1235-1238. doi: 10.1126/science.1164246.

Hubbard, A., & Hubbard, B. (2000). The potential contribution of high-resolution glacier flow modelling to structural glaciology. *Geological Society, London, Special Publications, 176*(1), 135-146. doi: 10.1144/GSL.SP.2000.176.01.10.

Hubbard, B., Milliken, R. E., Kargel, J. S., Limaye, A., & Souness, C. (2011). Geomorphological characterisation and interpretation of a mid-latitude glacier-like form: Hellas Planitia, Mars. *Icarus, 211*(1), 330-346. doi: 10.1016/j.icarus.2010.10.021.

Huss, M., Farinotti, D., Bauder, A., & Funk, M. (2008). Modelling runoff from highly glacierized alpine drainage basins in a changing climate. *Hydrological Processes, 22*(19), 3888-3902. doi: 10.1002/hyp.7055.

Karlsson, N. B., Schmidt, L. S., & Hvidberg, C. S. (2015). Volume of Martian midlatitude glaciers from radar observations and ice flow modeling. *Geophysical Research Letters, 42*(8), 2015GL063219. doi: 10.1002/2015gl063219.

Levy, J. S., Head, J. W., & Marchant, D. R. (2007). Lineated valley fill and lobate debris apron stratigraphy in Nilosyrtis Mensae, Mars: Evidence for phases of glacial modification of the dichotomy boundary. *Journal of Geophysical Research, 112*(E8). doi: 10.1029/2006je002852.

Levy, J. S., Fassett, C. I., Head, J. W., Schwartz, C., & Watters, J. L. (2014). Sequestered glacial ice contribution to the global Martian water budget: Geometric constraints on the volume of remnant, midlatitude debris-covered glaciers. *Journal of Geophysical Research: Planets, 119*(10), 2014JE004685. doi: 10.1002/2014je004685.

Mellon, M. T., Feldman, W. C., & Prettyman, T. H. (2004). The presence and stability of ground ice in the southern hemisphere of Mars. *Icarus, 169*(2), 324-340. doi: 10.1016/j.icarus.2003.10.022.

Morgan, G. A., Head, J. W., & Marchant, D. R. (2009). Lineated valley fill (LVF) and lobate debris aprons (LDA) in the Deuteronilus Mensae northern dichotomy boundary region, Mars: Constraints on the extent, age and episodicity of Amazonian glacial events. *Icarus, 202*(1), 22-38. doi: 10.1016/j.icarus.2009.02.017.

Parsons, R., & Holt, J. (2016). Constraints on the formation and properties of a Martian lobate debris apron: Insights from high-resolution topography, SHARAD radar data, and a numerical ice flow model. *Journal of Geophysical Research: Planets*, 2015JE004927. doi: 10.1002/2015je004927.

Paul, F., Frey, H., & Le Bris, R. (2011). A new glacier inventory for the European Alps from Landsat TM scenes of 2003: challenges and results. *Annals of Glaciology, 52*(59), 144-152. Doi: 10.3189/172756411799096295.

Plaut, J. J., Safaeinili, A., Holt, J. W., Phillips, R. J., Head, J. W., Seu, R., Putzig, N. E., & Frigeri, A. (2009). Radar evidence for ice in lobate debris aprons in the mid-northern latitudes of Mars. *Geophysical Research Letters, 36*(2), L02203. doi: 10.1029/2008gl036379.

Schorghofer, N., & Forget, F. (2012). History and anatomy of subsurface ice on Mars. *Icarus, 220*(2), 1112-1120. doi: 10.1016/j.icarus.2012.07.003.

Sinha, R. K., & Murty, S. V. S. (2013). Evidence of extensive glaciation in Deuteronilus Mensae, Mars: Inferences towards multiple glacial events in the past epochs. *Planetary and Space Science, 86*, 10-32. doi: 10.1016/j.pss.2013.09.002.

Sinha, R. K., & Vijayan, S. (2017). Geomorphic investigation of craters in Alba Mons, Mars: Implications for Late Amazonian glacial activity in the region. *Planetary and Space Science, 144*, 32-48. doi: 10.1016/j.pss.2017.05.014.

Sinha, R. K., Vijayan, S., & Bharti, R. R. (2017). Study of ice-related flow features around Tanaica Montes, Mars: Implications for late amazonian debris-covered glaciation. *Icarus, 297*, 217-239. doi: 10.1016/j.icarus.2017.07.002.

Souček, O., Bourgeois, O., Pochat, S., & Guidat, T. (2015). A 3 Ga old polythermal ice sheet in Isidis Planitia, Mars: Dynamics and thermal regime inferred from numerical modeling. *Earth and Planetary Science Letters, 426*, 176-190. doi: 10.1016/j.epsl.2015.06.038.

Souness, C. J., & Hubbard, B. (2013). An alternative interpretation of late Amazonian ice flow: Protonilus Mensae, Mars. *Icarus, 225*(1), 495-505. doi: 10.1016/j.icarus.2013.03.030.

Souness, C., Hubbard, B., Milliken, R. E., & Quincey, D. (2012). An inventory and population-scale analysis of martian glacier-like forms. *Icarus, 217*(1), 243-255. doi: 10.1016/j.icarus.2011.10.020.

Vaughan, D.G. (1993). Relating the occurrence of crevasses to surface strain rates. *Journal of Glaciology*, *39*(132), 255-266. doi: 10.1017/S0022143000015926.

Appendix A

Glacier-like forms on Mars

A ship in port is safe,
but that's not what ships are built for
Grace Hopper

Glacier-like forms on Mars

Bryn HUBBARD[a], Colin SOUNESS[a] and Stephen BROUGH[a]

[a]*Department of Geography and Earth Sciences, Aberystwyth University, Aberystwyth, UK*

Link to published article

This is a manuscript of an article published by Copernicus Publications in *The Cryosphere* on 05/11/2014, available online: http://dx.doi.org/10.5194/tc-8-2047-2014.

Citation for published paper

Hubbard, B., Souness, C., & Brough, S. (2014). Glacier-like forms on Mars. *The Cryosphere*, *8*(6), 2047-2061. doi: 10.5194/tc-8-2047-2014.

Keywords: Mars; Ices; Mars, climate; Mars, surface; Geological processes

Abstract: Over 1300 glacier-like forms (GLFs) are located in Mars' mid-latitudes. These GLFs are predominantly composed of ice-dust mixtures and are visually similar to terrestrial valley glaciers, showing signs of downhill viscous deformation and an expanded former extent. However, several fundamental aspects of their behaviour are virtually unknown, including temporal and spatial variations in mass balance, ice motion, landscape erosion and deposition, and hydrology. Here, we investigate the physical glaciology of martian GLFs. We use satellite-based images of specific examples and case studies to build on existing knowledge relating to: (i) GLF current and former extent, exemplified via a GLF located in Phlegra Montes; (ii) indicators of GLF motion, focusing on the presence of surface crevasses on several GLFs; (iii) processes of GLF debris transfer, focusing on mapping and interpreting boulder trains on one GLF located in Protonilus Mensae, the analysis of which suggests a best estimate GLF flow speed of 7.5 mm a^{-1} over the past 2 Ma; and (iv) GLF hydrology, focusing on possible supraglacial gulley networks on GLFs. On the basis of this information we summarise the current state of knowledge of the glaciology of martian GLFs and identify future research avenues.

A.1. Introduction

Numerous similarities exist between ice-rich landforms on Mars and Earth (e.g. Colaprete and Jakosky, 1998; Marchant and Head, 2003, Forget et al., 2006). Glacier-like forms (GLFs), which comprise one particular sub-group of these features, are strikingly similar in planform appearance to terrestrial valley glaciers (Figure A.1). However, despite this similarity, the fundamental glaciology of martian GLFs remains largely unknown. Improving this knowledge would enhance our understanding both of the specific landforms concerned and of broader planetary issues such as: (i) how Mars' present-day landscape was formed; (ii) the presence and phase state of H_2O on Mars' surface; and (iii) how Mars' climate has changed in geologically recent times. The aim of this paper is to summarize and develop our understanding of the fundamental physical glaciology of Mars' GLFs. As well as summarising existing knowledge, we provide new observations and interpretations of glacial landforms on Mars and outline potential avenues for future research. Although, in common with other interpretations of

Mars' surface features, we adopt a model based on terrestrial analogues, several fundamental controls over martian glaciation contrast sharply with those on Earth. For example, Mars' gravity, at ~3.7 m s^{-2}, is less than 40% of Earth's. Mars' surface temperature varies between ~-130 and +27 °C, with a mean of ~-60 °C (Read and Lewis, 2004), ~75 °C lower than on Earth. Finally, the partial pressure of H_2O in Mars' near-surface atmosphere is ~1 μbar, making the planet's surface ~1000 times drier than Earth's.

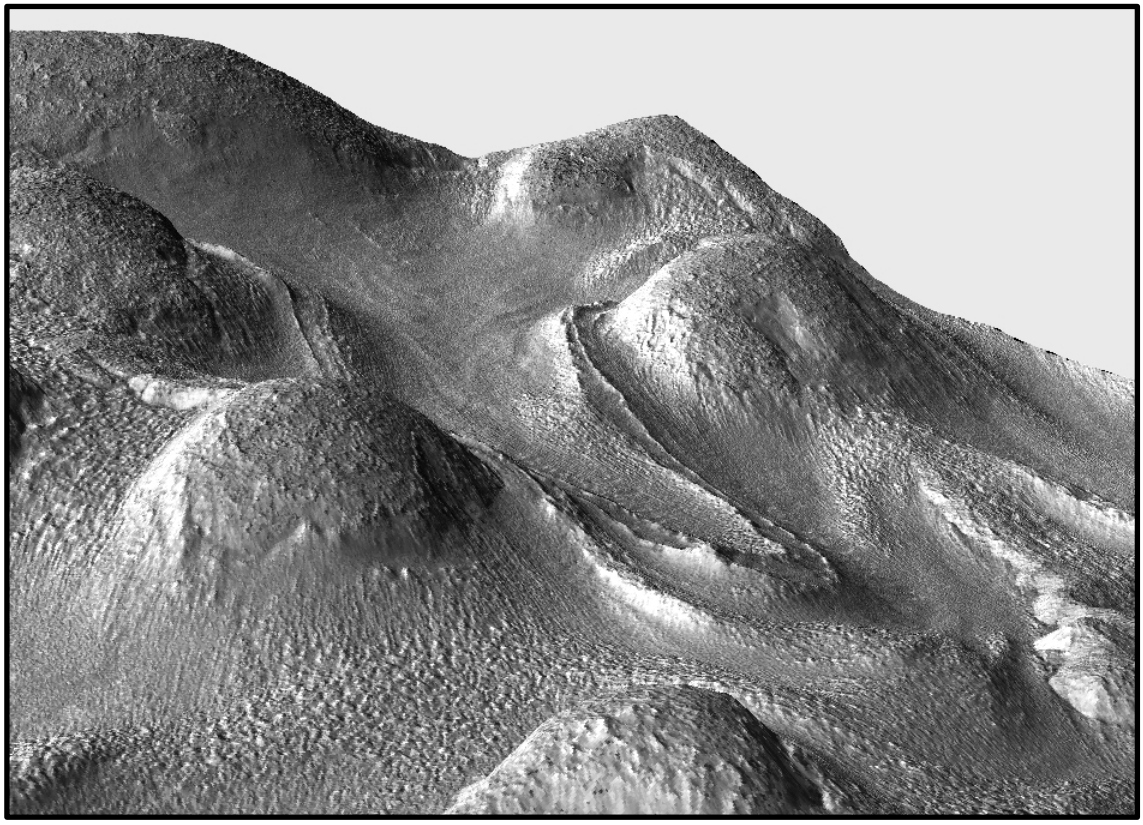

Figure A.1: *A three-dimensional image of a typical martian GLF (#948 in the inventory of Souness et al., 2012), which is ~4 km long and ~600 m in altitudinal range. The GLF shows evidence, through deformed chevron-like surface ridges, of down-slope flow, is longer than it is wide and is bounded on all sides. This particular, well-studied GLF is also bounded by a series of well-defined moraine-like ridges. Image reproduced after Hubbard et al. (2011).*

Since this paper is primarily intended for readers who are primarily interested in the terrestrial cryosphere, and who may not therefore be familiar with the literature relating to the martian cryosphere, a list of the acronyms used herein is given in Table A.1.

Table A.1: *List of commonly used terms and corresponding acronyms*

Term	Acronym
Glacier-like form	GLF
Viscous flow feature	VFF
Lobate debris apron	LDA
Lineated valley fill	LVF
Moraine-like ridge	MLR
Mars Reconnaissance Orbiter	MRO
Context (Camera)	CTX
High Resolution Imaging Science Experiment	HiRISE
Shallow Radar	SHARAD

A.1.1. Background

A.1.1.1. GLF classification, location and form

Mars' mid-latitude regions, between ~20 and ~60° N and S, host numerous landforms and surface deposits that bear a striking resemblance to small-scale terrestrial ice masses (e.g. Souness et al., 2012). These landforms, being composed predominantly of H_2O ice (Holt et al., 2008; Plaut et al., 2009) and exhibiting surface morphologies consistent with viscous flow (Marchant and Head, 2003; Head et al., 2010), have come to be known collectively as viscous flow features or VFFs (Milliken et al., 2003; Souness and Hubbard, 2012). Glacier-like forms, or GLFs, are a distinctive sub-type of VFF that are elongate and similar in appearance and overall morphology to terrestrial valley glaciers. GLFs thereby generally form in small cirque-like alcoves or valleys, appear to flow downslope between bounding sidewalls, and terminate in a distinctive tongue which may or may not feed into a higher order ice-rich terrain type. GLFs thereby represent the lowest-order component of what Head et al. (2010) referred to as Mars' integrated

glacial landsystem. According to this model, GLFs flow and may merge downslope to form broad, rampart-like lobate debris aprons (LDAs [Squyres, 1978; Squyres, 1979]). LDAs may, in turn, coalesce, typically from opposing valley walls, to form lineated valley fills (LVFs), which take the form of complex and contorted surfaces that often exhibit no obvious flow direction.

In their inventory of Mars' GLFs, Souness et al. (2012) inspected >8,000 CTX images, covering ~25% of the martian surface, and identified 1309 individual forms, reporting the location (Figure A.2) and basic morphometry of each. Hereafter, we refer to specific GLFs through their classification number in this inventory, available as a supplement accompanying Souness et al. (2012). Of the total population, 727 GLFs (56%) were found in the northern hemisphere and 582 (44%) in the southern hemisphere, with GLFs showing a preference for the mid-latitudes (centred on a mean latitude of 39.3^{o} in the north and -40.7^{o} in the south). Although Souness et al. (2012) did not normalise their GLF count to (spatially variable) image coverage, inspection of Figure A.2 strongly suggests that GLFs are locally clustered in both hemispheres, for example along the so-called "fretted terrains" (Sharp, 1973) of Deuteronilus Mensae, Protonilus Mensae and Nili Fossae in the north and around the Hellas Planitia impact crater in the south (Figure A.2). GLF morphometry was found to be remarkably similar between the two hemispheres, with a mean GLF length of 4.91 km in the north and 4.35 km in the south, and a mean GLF width of 1.26 km in the north and 1.34 km in the south. Similar to on Earth, a pronounced preference for a poleward orientation was also found, with GLFs having a mean bearing of 26.6° (NNE) in the northern hemisphere and 173.1° (SSE) in the southern hemisphere – indicating a strong sensitivity to insolation. These inter-hemispheric similarities in distribution and morphometry indicate that all martian GLFs share a high degree of commonality in terms of composition and formation. These are considered below.

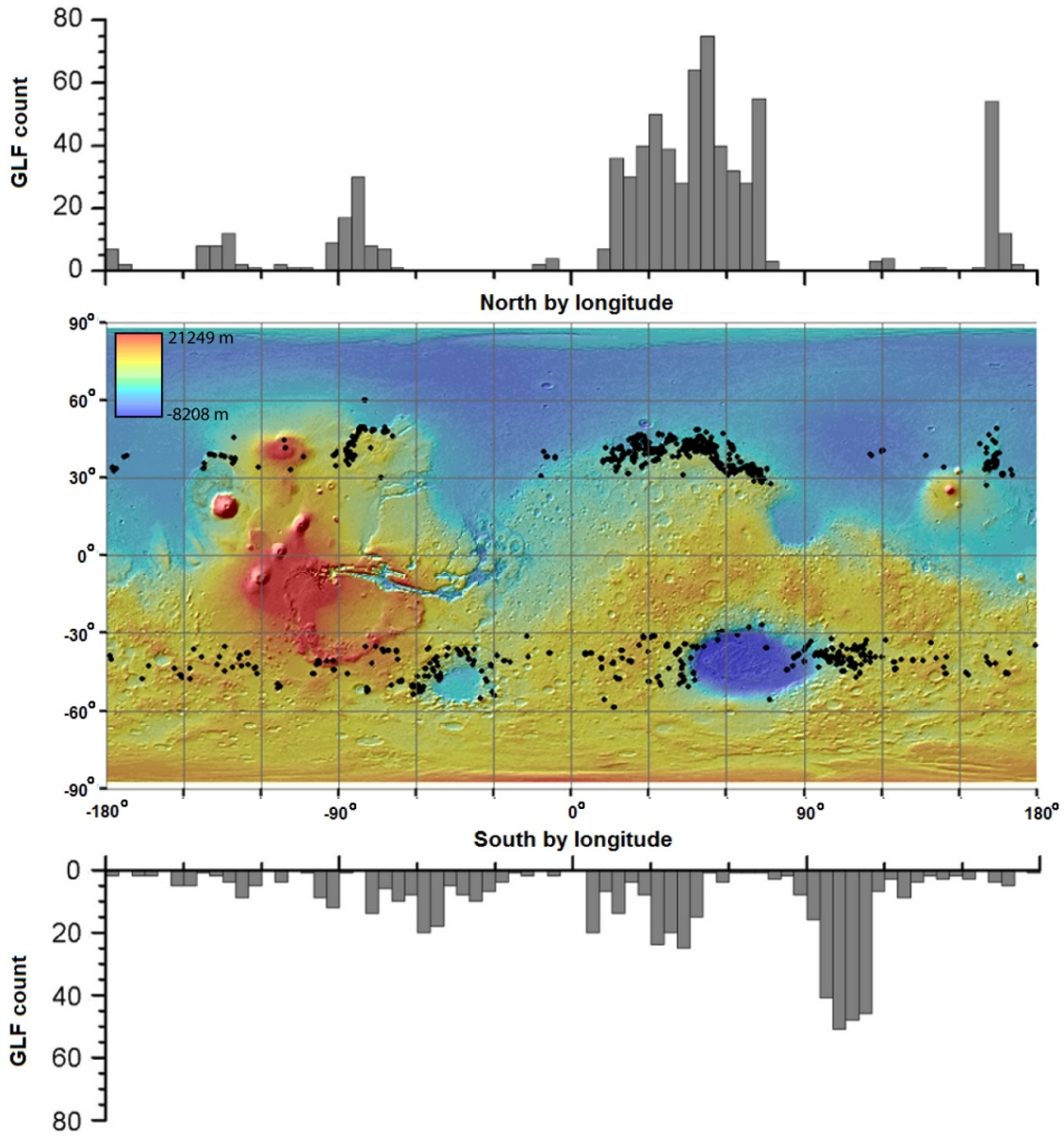

Figure A.2: *The spatial distribution of Mars' 1,309 GLFs as identified by Souness et al. (2012).*

A.1.1.2. GLF composition

The precise composition of GLFs is still unknown due to the fact that they are almost ubiquitously covered in a layer of fine-grained regolith. Debate surrounding the amount of water ice involved in VFF composition (including GLFs) has led to varying feature-scale interpretations being proposed, including as ice assisted talus flows (~20 – 30% ice [Squyres 1978; 1979]), rock-glaciers (~30 – 80% ice [Colaprete and Jakosky, 1998;

Mangold, 2003]), and debris-covered glaciers (>80% ice [Head et al., 2005; Li et al., 2005]). Since the distinctions between these forms, and between them and 'standard' glaciers, is not sharply defined even on Earth, we are not yet in a position to definitively attribute martian equivalents. We therefore follow the convention of much of the published literature and refer to these forms as 'glacier-like', accepting that they may eventually, when more information becomes available, be more accurately sub- or re-classified as related forms such as rock glaciers or mass flows. That said, the latter is unlikely to hold universally on Mars since many GLFs do not show distinctive source areas for their mass, many have lost substantial mass since their formation, and many appear from radar data to be composed largely of water ice. Hubbard et al. (2011) noted that boulder incisions into the unconsolidated surface of GLF #948 located in the north wall of Crater Greg, Eastern Hellas, were some decimetres deep, representing a minimum surface dust thickness at this location. There have been very few direct observations of the interior of GLFs, but Dundas and Byrne (2010) reported the capture of very recent meteorite strikes that indicated the presence of relatively clean (i.e., debris poor) massive ice at a depth of some centimetres to metres below the surface. Furthermore, data from the shallow radar (SHARAD) sensor, mounted on the Mars Reconnaissance Orbiter (MRO), suggest that many VFFs (including GLFs) may well be composed of massive H_2O ice with minimal lithic content (Holt et al., 2008; Plaut et al., 2009). These findings led to the widespread acceptance that H_2O ice accounts for the dominant portion of GLF mass. However, the presence of a lithic component has been demonstrated by ice fade through sublimation following recent impact exposures (Dundas and Byrne, 2010), and the precise proportions of ice-rock mixture, particularly at depth, are still unknown.

A.1.1.3. GLF formation

A continuing point of discussion relates to precisely how and when GLFs formed. It is generally agreed that GLFs are now largely relict forms dating to a past, but relatively recent, martian ice age (see Kargel, 2004). While it is thought that Mars' last major ice age ceased when the planet's obliquity changed from ~35 to ~25^{o} between four and six million years ago (Laskar et al., 2004), evidence of a subsequent, late-Amazonian ice age has been proposed (e.g. Head et al., 2003). It is thought that during periods of short-

term obliquity cycles (~100 ka) between ~2 and ~0.5 Ma BP, obliquity still intermittently exceeded 30°. During these periods, increased high-latitude solar radiation led to the melting of Mars' polar caps, the release of moisture into the atmosphere and its precipitation as snow or condensation above or within the ground at lower latitudes (e.g. Forget et al., 2006; Hudson et al., 2009; Schon et al., 2009). This ice deposition extends well into Mars' mid-latitudes, where it appears to have survived, preserved beneath surface regolith, until the present day. Still, the mechanisms by which GLFs first accumulated sufficient ice-rich mass to flow downslope and acquire their distinctive surface morphologies remain uncertain.

A.2. The glaciological characteristics of martian GLFs

A.2.1. Approach and methods

Each of the following sections both summarizes published information and supplements that information with new data from the analysis of images acquired by MRO's Context Camera (CTX), at a resolution of ~6 m per pixel, or High Resolution Imaging Science Experiment (HiRISE) camera, at a resolution of ~0.3 m per pixel. Maps were constructed from these images using ArcMap Geographic Information System software and interpretations additionally drew on elevation data produced by the Mars Orbiter Laser Altimeter (MOLA), at a typical resolution of 128 pixels per degree, mounted on the Mars Global Surveyor spacecraft.

A.2.2. GLF extent

Recent observations suggest that current GLFs are the remnants of a once far larger ice mass (e.g. Dickson et al., 2010; Sinha and Murty, 2013) that was most extensive during a hypothesised last martian glacial maximum, or LMGM (Souness and Hubbard, 2013). Such an expanded former extent has been inferred from detailed regional geomorphological reconstructions, for example identifying former ice limits from variations in surface texture and the existence of distal moraine-like ridges, or MLR.

Allied to local topography, such reconstructions have allowed the recreation of both former ice extent and local ice-flow directions (e.g. Dickson et al., 2010). However, debate persists concerning both the precise timing of the LMGM and the extent and volume of ice coverage at the time. The complexity of this issue is compounded by the timescales involved, with best estimates currently placing the LMGM at ~5 – 6 Ma BP, but possibly continuing closer to the present day (Section A.1.1.3 above [Touma and Wisdom, 1993; Head et al., 2003]).

The outlines of many GLFs are clearly demarcated by the presence along their margins and front of bounding MLRs (Arfstrom and Hartmann, 2005). These landforms are commonly raised above the present GLF surface and are texturally distinct from their surroundings. One particular Amazonian-aged (~10 Ma BP) GLF located in Crater Greg, Eastern Hellas (246.84°E, -38.15°N [#948]) has been the focus of much study (e.g. Hartmann et al., 2003; Kargel, 2004; Hubbard et al., 2011; Hartmann et al., 2014). In an analysis of this particular GLF, Hubbard et al. (2011) described a sequence of up to four distinct raised bounding ridges located along the GLF's margins. The authors also described two surface terrain types in the GLF's lower tongue, 'linear terrain' and 'mound and tail terrain', as being possible exposed subglacial bedforms. Overall, this led these authors to suggest the GLF's moraine-bounded outline presently represents a glacial basin in which the lower zone now comprises an exposed former glacier bed, while the basin's upper zone still hosts a degraded ice mass. In this case, therefore, the present day GLF outline incorporates both an ice mass and its immediate proglacial area. This particular GLF's multiple bounding moraines were also interpreted in terms of a general recession punctuated by several (at least three) episodes of minor re-advance or still-stand.

At a larger scale, GLFs form the first-order of the martian glacial landsystem (Section A.1.1 above [Head et al., 2010]), which is present throughout substantial parts of the planet's northern and southern mid-latitudes (Milliken et al., 2003; Souness and Hubbard, 2012). Many of the ice masses forming this landsystem are thought to have been substantially more advanced and thicker in the past, having important implications for reconstructions of climatic variability on Mars. For example, Dickson et al. (2008) reconstructed former glacial limits in the Protonilus Mensae region (54.55^{o}E, 40.80^{o}N) based on the identification and mapping of former glacial high-stands. The analysis

indicated a maximum ice thickness of >2 km at LMGM and a downwasting of at least 920 m since then. Although reconstructed flow directions were questioned in detail by Souness and Hubbard (2013), this analysis indicates substantially thicker ice in the geologically-recent martian past.

Several studies have also pointed out that GLFs appear to be distinctive from the underlying ice-rich (LDA or LVF) material onto which they appear to have flowed (e.g. Levy et al., 2007; Baker et al., 2010; Sinha and Murty, 2013). This material contrast has been interpreted as signifying the possibility of a marked age difference between the two surfaces, suggesting two or more glacial events with at least one small-scale or 'local' glacial phase advancing over an earlier 'regional' glaciation (e.g. Head et al., 2003; Levy et al., 2007; Dickson et al., 2008; Sinha and Murty, 2013).

Glacial activity has also been identified outside of the mid-latitude regions. As well as the well-studied polar ice caps (e.g. Seu et al., 2007; Phillips et al., 2008), degraded glacier-like features have been described surrounding the shield volcano of Arsia Mons (239.00^{o}E, -0.31^{o}N [Head and Marchant, 2003]) and in high latitude craters (266.45^{o}E, 70.32^{o}N [Garvin et al., 2006]). The identification of features and landforms of glacial origin across vast areas of Mars' present surface has also led to suggestions that continental glaciation may once have occurred on Mars (Kargel and Strom, 1992; Kargel et al., 1995; Fastook et al., 2014; Hobley et al., 2014).

A.2.2.1. Case study: reconstructing former GLF extent

GLF #146 (164.48^{o}E, 34.13^{o}N) is ~12 km long, ~5 km wide and located in the Phlegra Montes region of Mars' northern hemisphere (Figure A.3). This region is largely formed from several massifs that stretch from the north-eastern section of the Elysium Volcanic Province to the dichotomy lowlands. GLF #146 is located on the southern tip of a massif range and converges from a wide upper basin between two rock outcrops in to an elongate lower tongue. The main tongue of this GLF shows distinctive surface lineations and textures that indicate the presence of three separate major flow units. Several arcuate linear raised features or MLRs are located in the foreground of the

current GLF. This particular case is of interest because these MLRs are located some distance from the GLF's current margin, indicating formation at some time in the past when the GLF was at a more advanced position than at present.

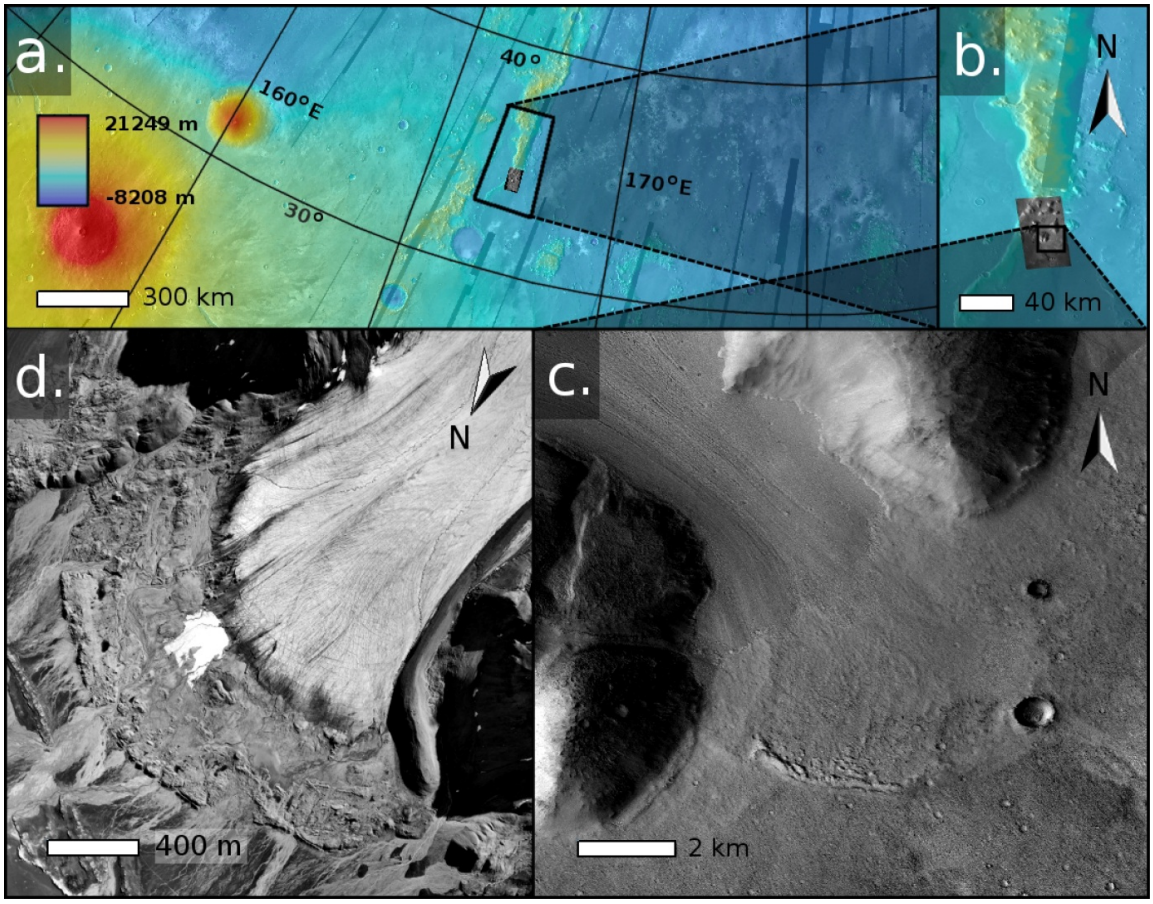

Figure A.3: *Case study illustrations of the former extent of martian GLF #146 showing background MOLA elevation images (a and b), and a CTX image expansion (c). The forefield of terrestrial Midre Lovénbreen, Svalbard, is shown for comparison (d).*

The geomorphological interpretation of GLF #146 (Figure A.4), reconstructed from CTX images alone, reveals that the region in front of the current GLF is characterised by two distinctive terrain types. At the broadest scale, both terrains are clearly part of the ice-rich, fretted terrain found throughout Mars' mid-latitudes but particularly characteristic of Deuteronilus Mensae, Protonilus Mensae and Nili Fossae (Sharp, 1973). However, both terrains also differ in several important details, indicating distinctive mechanisms of formation and/or subsequent history. The first terrain type,

'arcuate terrain', forms a ~3.3 km-wide band around the GLF's current margin. This terrain is characterised by arcuate ridges whose shadows indicate that they are raised above the adjacent ground, forming distinct local topographic highs ~0.1 – 1.7 km long and 5 – 10 m wide. These ridges show distinct similarities in morphology and spatial relationships to MLRs identified elsewhere on Mars (Arfstrom and Hartmann, 2005), which are the martian equivalent of terminal moraines on Earth (e.g. Figure A.3d). The arcuate ridges forming this terrain increase in size and coherence away from the GLF's margin (Figure A.4) such that they are almost unbroken along the terrain's full distal edge. The ridges are smaller and more fragmented nearer to the GLF's margin. The second terrain type, 'smooth terrain', extends beyond the arcuate terrain for 100s of km into the forefield's lower plains. This terrain appears at the broadest scale to be visually smooth with few undulations relative to the arcuate terrain. Close inspection also indicates irregular mottling and a greater concentration of impact craters on the smooth terrain than on either the arcuate terrain or the GLF proper (Figure A.4).

The location and characteristics of the two proglacial terrain types outlined above provide some basis for their interpretation. We infer that the arcuate area directly in front of the GLF represents the geologically-recent former extent of the GLF. Like on Earth, the MLRs represent the former locations of the GLF's terminus, with the outermost MLR representing the maximum former extent of the GLF and each subsequent ridge representing a former terminal position (of minor advance or slowdown) during a period of general GLF recession. The sequence of multiple terminal MLRs thereby implies that the GLF has undergone a cyclic or punctuated recession. The lower density of craters on the GLF and its encompassing arcuate terrain relative to the outer smooth terrain is consistent with the younger age for the deposition or exposure of the former. Indeed, the general lack of resolvable craters on the arcuate terrain and on the GLF itself, although insufficient in number to analyse formally, suggests that the feature is of a geologically very young age. On a regional scale, other degraded ice-related features have been reported in the north western region of Phlegra Montes (Dickson et al., 2010), suggesting that this region may also have been subject to large-scale glaciation in the recent past and that it now hosts only diminished remains.

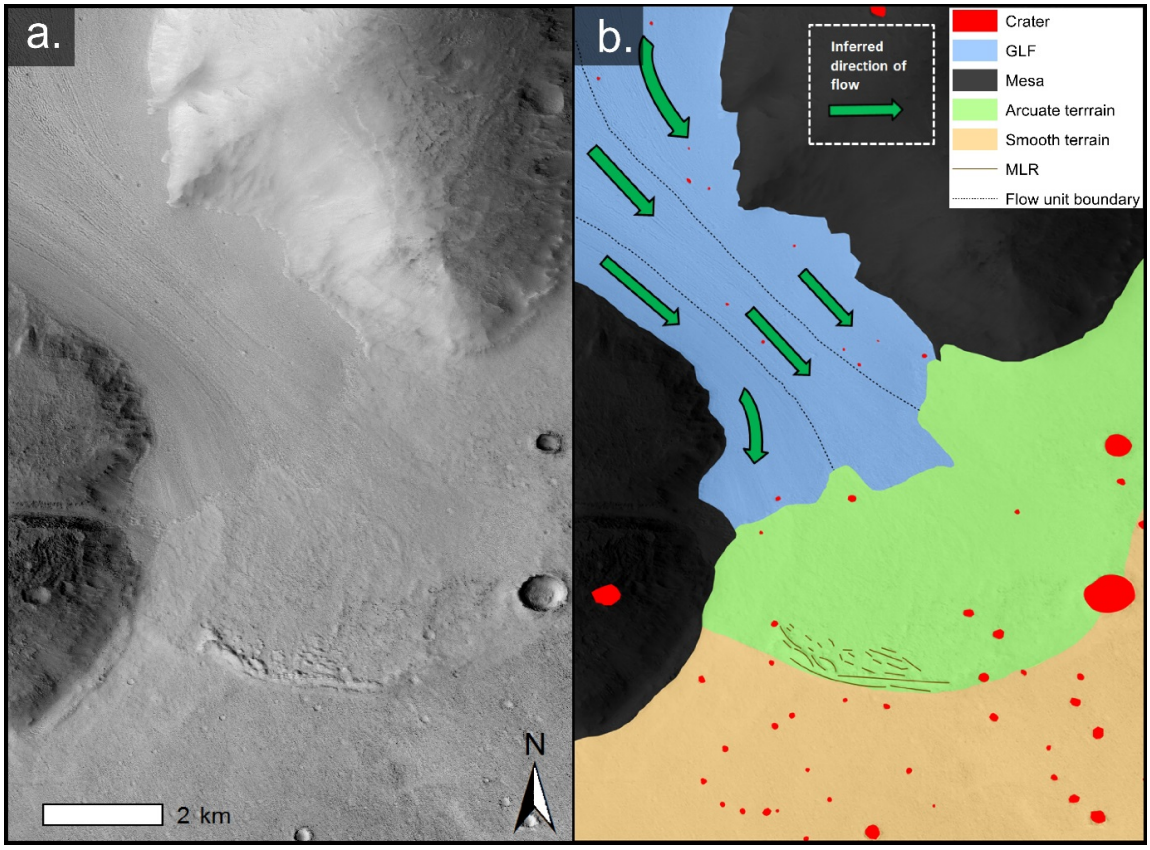

Figure A.4: *GLF #146 CTX image expansion (a) and geomorphological interpretation (b).*

Overall, we interpret the GLF located in Phlegra Montes as an ice-rich mass that was once much larger than its current extent, with the outer MLR marking its former maximum extent. The continuity of the smooth plains to the east, combined with a lack of further evidence of ice-related processes suggests that the GLF reported here marks the outer limit of glacial activity of the Phlegra Montes region. It appears that the GLF coalesced from a wide upper basin into a narrow tongue before spreading out onto the flatter plains, much like a piedmont glacier on Earth. Subsequently the GLF's terminus has retreated ~3.3 km to its current position, apparently through periods of cyclic or punctuated standstill, particularly early on during the period of general recession. Similar evidence for GLFs representing degraded landforms has been presented elsewhere in Mars' mid-latitudes (e.g. Hubbard et al., 2011; Souness and Hubbard, 2013) indicating it is possible that GLFs were once a much larger feature on Mars' surface. Further, the appearance of deposits indicating the GLFs former extent would also imply that GLFs have been active and dynamic in the past.

A.2.3. GLF motion

While no data have yet been obtained that reveal either rates of GLF movement or the mechanisms responsible for that movement, GLF motion has been both modelled and inferred from their overall lobate shape and the presence of flow structures on their surface. These flow structures are typically shaped like chevrons (e.g. Figure A.1) consistent with a transverse surface velocity profile similar to that measured at terrestrial glaciers, i.e. increasing inwards from the glacier's lateral margins towards the centreline, where velocity is highest above the thickest ice. There is therefore little doubt that GLFs have moved, at least through viscous deformation. However, there is no evidence that mass is continuing to accumulate on present day GLFs, nor that they are still moving. In an effort to shed some light on the likelihood of GLF motion, Milliken et al. (2003) applied the multi-component constitutive relation of Goldsby and Kohlstedt (2001) to typical ranges of VFF temperature, slope and (assumed) ice grain size. For a 10 m thick VFF deposit, Milliken et al. (2003) estimated shear stresses of $10^{-1.5} - 10^{-2.5}$ MPa and consequent strain rates on the order of $10^{-11} - 10^{-16}$ s^{-1}. Based on these rates, the authors estimated it would take between 3 ka and 300 Ma, respectively, to produce a shear strain of 100%, which was in broad agreement with age estimates of the VFF ($10^5 - 10^7$ a). Although the application of this stress-strain relationship to martian VFF conditions represented a major advance, the model was not distributed spatially and was not therefore applied to, nor considered, any particular VFF geometry. Moreover, the possible presence of liquid water within or below VFFs was (and still is) also unknown. All VFF motion was therefore assumed to occur through deformation of a spatially homogeneous ice-dust mixture.

A.2.3.1. Crevassing as an indicator of GLF motion

Fracturing is a universal diagnostic indicator of high tensile strain rates within terrestrial ice masses. Further, the orientation of individual crevasses and the size and shape of crevasse fields reflect the strain rate, and strain history, of specific parcels of ice (e.g. Herzfeld and Clarke, 2001). Crevasses have been reported on a variety of ice-rich surfaces on Mars. For example, fractures observed on the floor of certain craters in

Xanthe Terra formed part of what Sato et al. (2010) described as 'chaotic' terrain. Pierce and Crown (2003) also reported transverse cracks in debris apron deposits in eastern Hellas, and interpreted them specifically as brittle extensional crevasses. Fractures have also been observed at the edge of high (>800 m) icy scarps on Mars' north and south polar ice caps (Byrne et al., 2013). These fractures appear to act as planes of weakness for occasional collapse events that have been observed in repeat satellite images (Russell et al., 2008). Kargel (2004) made specific reference to the presence of crevassing on martian GLFs, where the varying size, morphology and overall state of preservation of crevasses were interpreted in terms of formation over a considerable period of time, possibly continuing to the present day. This indicates that Mars' GLFs do appear to be, at least in some cases, still actively flowing.

Below, we present an analysis, based on new data, of the extent and nature of crevasses visible on the surface of martian GLFs.

A.2.3.2. Concentration and location of crevassed GLFs

From an overall population of ~1300 GLFs (Souness et al., 2012), surface crevasses are present on 64 individual forms (~5% of the total population). Of these crevassed GLFs, 37 (57.8%) are located in the northern hemisphere and 27 (42.2%) in the southern hemisphere (Figure A.5a). While this inter-hemispheric division mirrors that of the overall GLF population of 55.5% on the northern hemisphere and 44.5% in the southern hemisphere (Figure A.2), crevassed GLFs are preferentially clustered in certain regions relative to their parent GLFs populations. These clusters are particularly notable in northwest Argyre in the southern hemisphere and in Deuteronilus Mensae and Protonilus Mensae in the northern hemisphere (Figure A.5). Crevassing therefore occurs, or is at least more readily visible (i.e. exposed by the absence or excavation of supraglacial regolith), in these specific areas.

Crevassing occurs where tensile strain rate of ice exceeds a critical threshold (Vaughan, 1993). Such high strain rates can result from several factors including local changes in mass balance, ice surface and/or bed slope, ice thickness, and basal traction. Similar to crevassed ice masses on Earth, many of the crevasse fields identified on Martian GLFs

fall into one of a small number of repeated patterns, illustrated below through examples of four sets of crevasses from two martian GLFs.

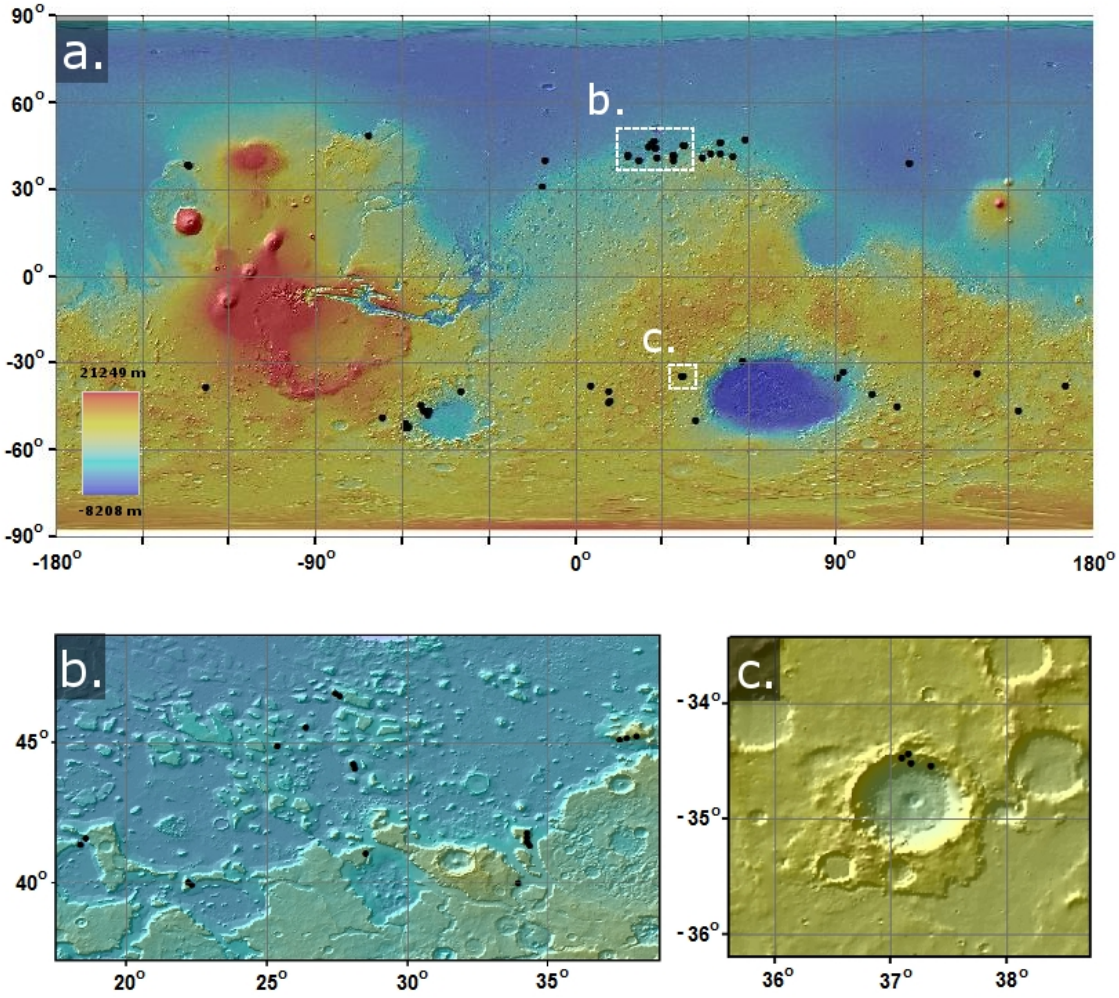

Figure A.5: *The distribution of crevassed GLFs on Mars (a), with expansions of case study GLF locations in Deuteronilus Mensae (b) and western Hellas Planitia (c).*

4.2.3.3. Examples of GLF crevasse morphologies and their interpretation

Example crevasse set #1 (ECS1 [Figure A.6]) is on GLF #1054, located to the east of the large Hellas Planitia impact crater in Mars' southern hemisphere (102.65°E, -40.85°N). This particular GLF exhibits two crevasse sets. ECS1 (Figure A.6c), comprises a dense cluster of transverse linear crevasses, typically 100 – 250 m long and up to 50 m wide, that coincide with an abrupt increase in slope, just down-flow of the

point at which the GLF flows out of a cirque-like alcove. The location and transverse orientation of ECS1 conforms to longitudinal extension associated with the acceleration of GLF #1054 as it flows over its cirque lip and moves down a steeper slope. The physical setting, strain regime and pattern of these crevasses are similar to icefalls, which are commonplace on terrestrial valley glaciers.

ECS2 (Figure A.6d) is also located on GLF #1054, but in its upper reaches. This set of linear crevasses forms a discontinuous band aligned adjacent and parallel to the GLF's headwall contact, similar to glacier bergschrunds in Earth. On Earth, bergschrunds indicate gravity-driven ice flow away from the headwall of a glacier where the ice surface slope is locally sufficiently steep to induce brittle fracture (Mair and Kuhn, 1994).

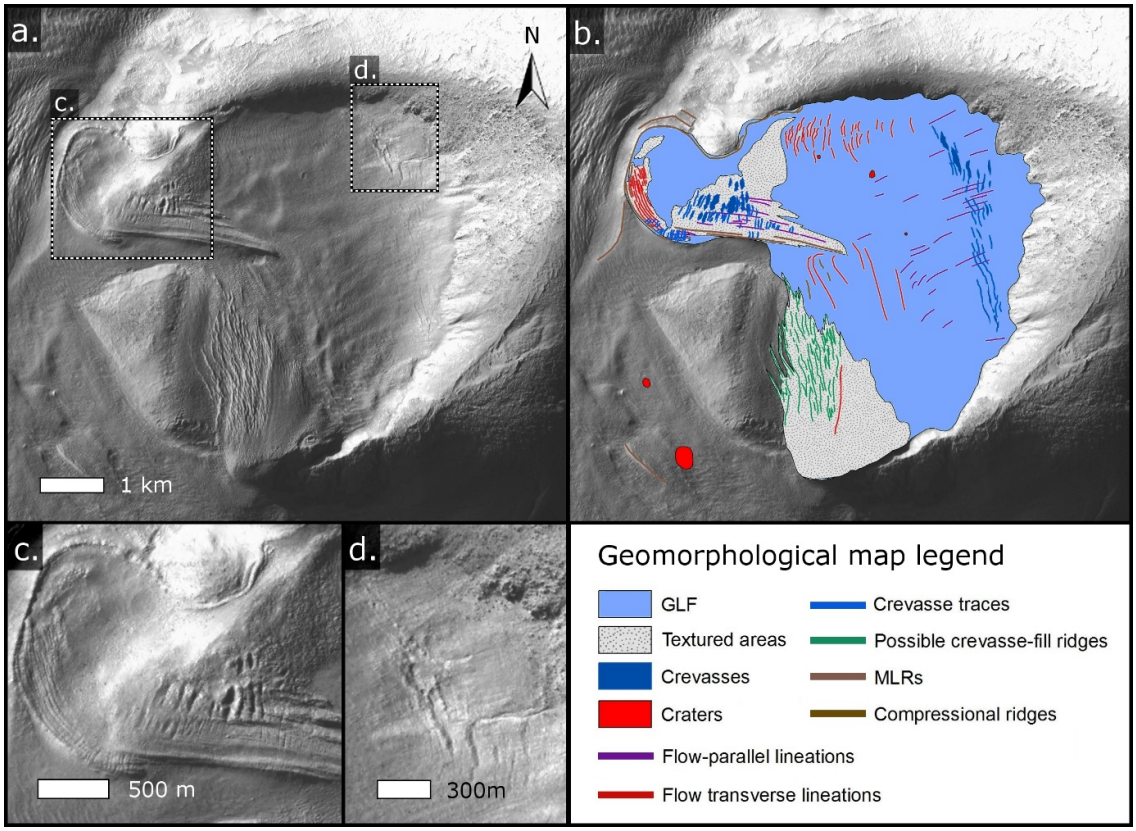

Figure A.6: *CTX image of crevassed GLF #1054, located in eastern Hellas (Figure A.5a) (a), along with its geomorphological interpretation (b) and expansions of two crevasse sets (c and d).*

ECS3 (Figure A.7) is on GLF #541, located in Deuteronilus Mensae in Mars' northern hemisphere (38.18°E, 45.14°N). This crevasse field is located along the GLF's western flank (Figure A.7b) and consists of multiple, highly-degraded fractures that extend towards the GLF's centreline from its lateral margin. These crevasses are aligned slightly up-valley, and progressively rotate towards a more transverse alignment towards the GLF's terminus. On Earth, such a crevasse pattern indicates the presence of extensional lateral shear within a glacier, caused by friction between the ice and the valley walls. Once formed, the crevasses rotate in accordance with a general increase in longitudinal ice velocity away from the valley-sides and towards a glacier's centreline. The similar morphology of the crevasses observed on GLF #541 (Figure A.7b) and the lateral crevasses on terrestrial glaciers indicate that martian GLFs are, or have been, characterized by a similar geometry and velocity field to terrestrial valley glaciers. This particular case provides evidence that GLFs both thicken towards their centreline (where on Earth such valleys are typically parabolic in cross section; Harbor 1995), and that the associated increase in ice thickness causes a corresponding increase in ice velocity.

ECS4 (Figure A.7c) is located near the terminus of GLF #541. This crevasse field comprises longitudinally-orientated crevasses that are located along the approximate centreline of the GLF and diverge laterally as the terminus of the glacier spreads to form a piedmont lobe (Figure A.7c). A series of major ridges is also present in this zone, located just up-flow of an apparent bedrock protuberance. These ridges are aligned orthogonal to the GLF's flow direction and to ECS4. The crevasses forming ECS4 are virtually identical in context and shape to longitudinal crevasses on Earth's glaciers, formed by transverse extension. In this case, we interpret ECS4 as forming through a combination of transverse extension, associated with the spreading of the piedmont lobe, and longitudinal compression as the terminus of the GLF abuts the bedrock protuberance. This interpretation is consistent with the transverse ridges in front of GLF #541, which are similar to compressional ridges, or push moraines, commonly found in the proglacial areas of valley glaciers on Earth. It is also apparent from Figure A.7 that the edges of the crevasses forming ECS4 are particularly sharply-defined, suggesting that they are young and have been subjected to minimal degradation relative to other examples (e.g. ECS2 [Figure A.6d]).

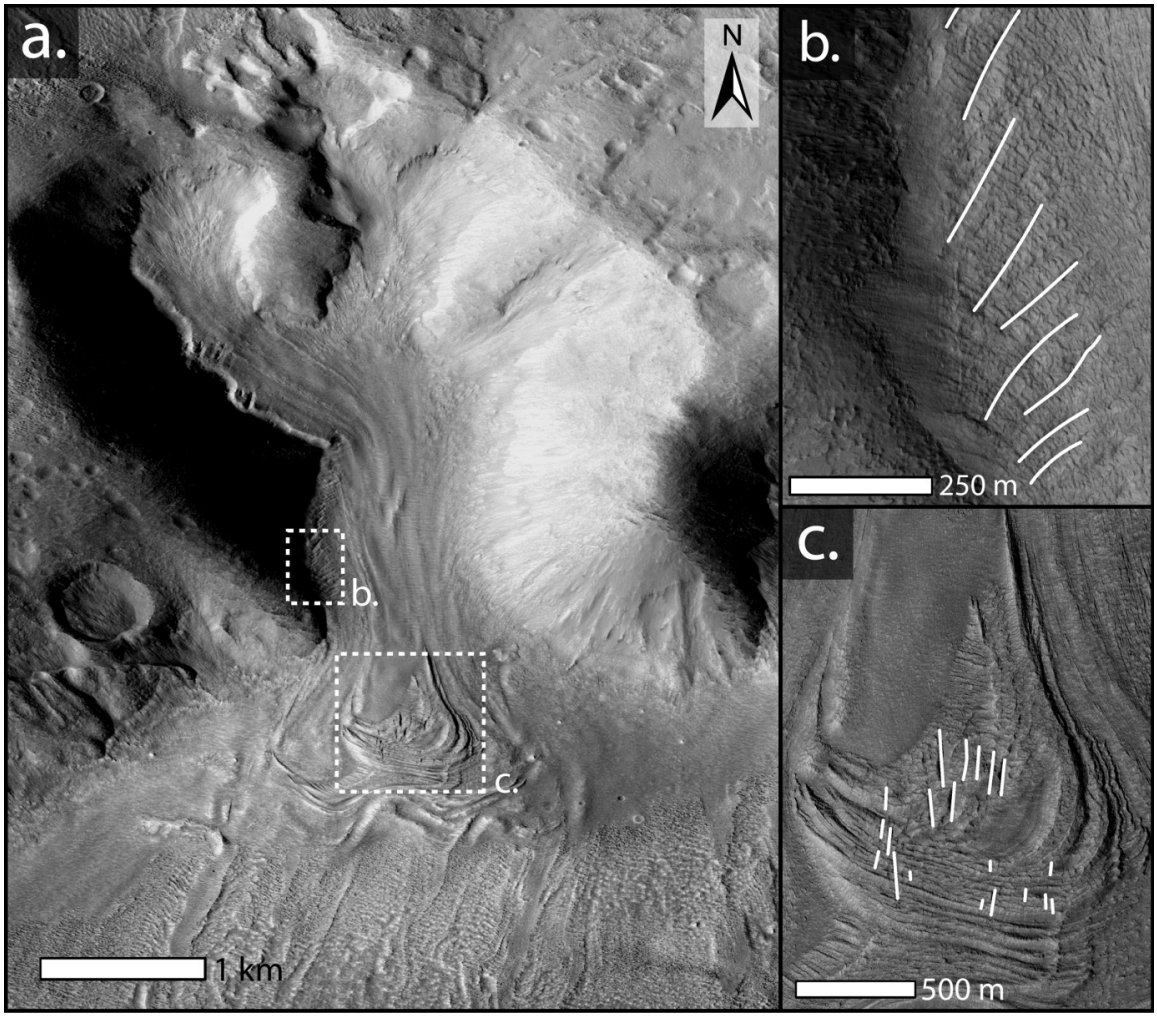

Figure A.7: *CTX image of crevassed GLF #541, located in Deuteronilus Mensae (Figure A.5b) (a), along with expansions of two crevasse sets (b and c).*

The presence of crevasses on martian GLFs indicates that their deformation can be achieved through brittle fracture as well as ductile flow. The interpretations of such crevasse fields presented above indicates that high GLF strain rates can be caused by several factors that are similar to terrestrial ice masses, including: (i) variable bed slope; (ii) lateral drag at shear margins (e.g. along valley sides), and (iii) spatial variations in traction at the ice-bed interface. These case studies also suggest that GLFs share certain geometrical and dynamic characteristics with Earth's glaciers, such as a parabolic cross-section and its associated transverse velocity profile, characterized by faster motion along the centreline than along the margins. These observations also show that crevasses on Mars' GLFs range from highly degraded to sharp-edged, suggesting that

crevasses have been formed over a considerable length of time, possibly continuing to the present day.

A.2.4. GLF debris transfer and deposition

The presence of MLRs on Mars' GLFs (Section A.2.2 above), implies the entrainment, transport and deposition of substantial volumes of debris. While very little research has been directed specifically at evaluating how and to what extent GLFs (or VFFs more broadly) have shaped Mars' landscape, some relevant information is available. For example, lithic debris can be supplied to the uppermost reaches of GLFs from steep bounding headwalls that appear to be composed of weathered bedrock and unstable boulder-rich deposits (Hubbard et al., 2011). These authors likened this 'incised headwall terrain' to ice-marginal lateral moraines on valley glaciers on Earth. The base of this headwall was composed of a strip of boulder-rich deposits, some tens of metres wide, into which closely-spaced parallel incisions had been cut, similar in appearance to water-related erosional gullies on Earth. Below this incised headwall terrain, several boulders appeared to have rolled downslope and come to rest on the surface of the GLF (their Figure 4.7b). Such headwalls thereby supply both coarse-scale rock-fall and, if the headwall gullies are eroded fluvially, fine-scale washed debris to the GLF surface.

Many GLFs also appear to host medial moraines, present as raised linear deposits, typically metres to tens of metres wide and up to some kilometres long, which are aligned parallel to the direction of flow. Moreover, these lineations occasionally correspond to the common edge of two adjoining adjacent source flow units such as a tributary flow unit joining a glacier's trunk or flow re-converging after splitting around a bedrock protrusion or nunatak. Both situations closely correspond to the most common mechanism of medial moraine formation on Earth – as coalesced lateral moraines.

A.2.4.1. Case study: supra-GLF boulder trains

Substantial coarse debris appears to be present on the surface of GLF #498 (Figure A.8), located on the inner edge of the southern rim of Moreaux Crater in Protonilus Mensae (44.06ºE, 40.82ºN). GLF #498 is ~2 km wide and ~12 km long from terminus to confluence where two major source areas converge into a single north-flowing trunk. Surface landforms and textures indicate the presence of numerous smaller source areas along the GLF's flanks. This GLF is unusual and interesting because it exhibits extensive surface boulder deposits that are not confined to the GLF's margins but are located throughout the GLF, extending right to its centre. This supra-GLF debris is largely formed of boulder-sized material that protrudes conspicuously above the host terrain, making them clearly visible on the high-resolution HiRISE images used to map the feature. Indeed, hundreds of individual boulders, which are commonly 1 – 5 m across, can readily be identified in the images (Figure A.8d – e). A geomorphological map of this GLF (Figure A.9) reveals that much of this debris appears to belong to one of nine clusters or populations, labelled A – I on Figure A.9. Here, Populations A, B and C represent 1 – 2 km long, elongate boulder trains located in a medial supra-GLF position as one major tributary enters the principal tongue from the west. All three populations are conformable with surface lineations and raised textured areas as they together bend northwards as they join the GLF's main channel. Approximately 3 km down-flow of Population C, Population G is notably elongate, extending for more than 2 km along the GLF but attaining a width of no more than ~20 m. This boulder train rests on the west-facing flank of a raised supra-GLF MLR and appears as a continuation of Population C. In contrast, Populations D and H to the east and E, F and I to the west all appear to extend over ~50 – 100 m away from steep and rocky valley-side walls.

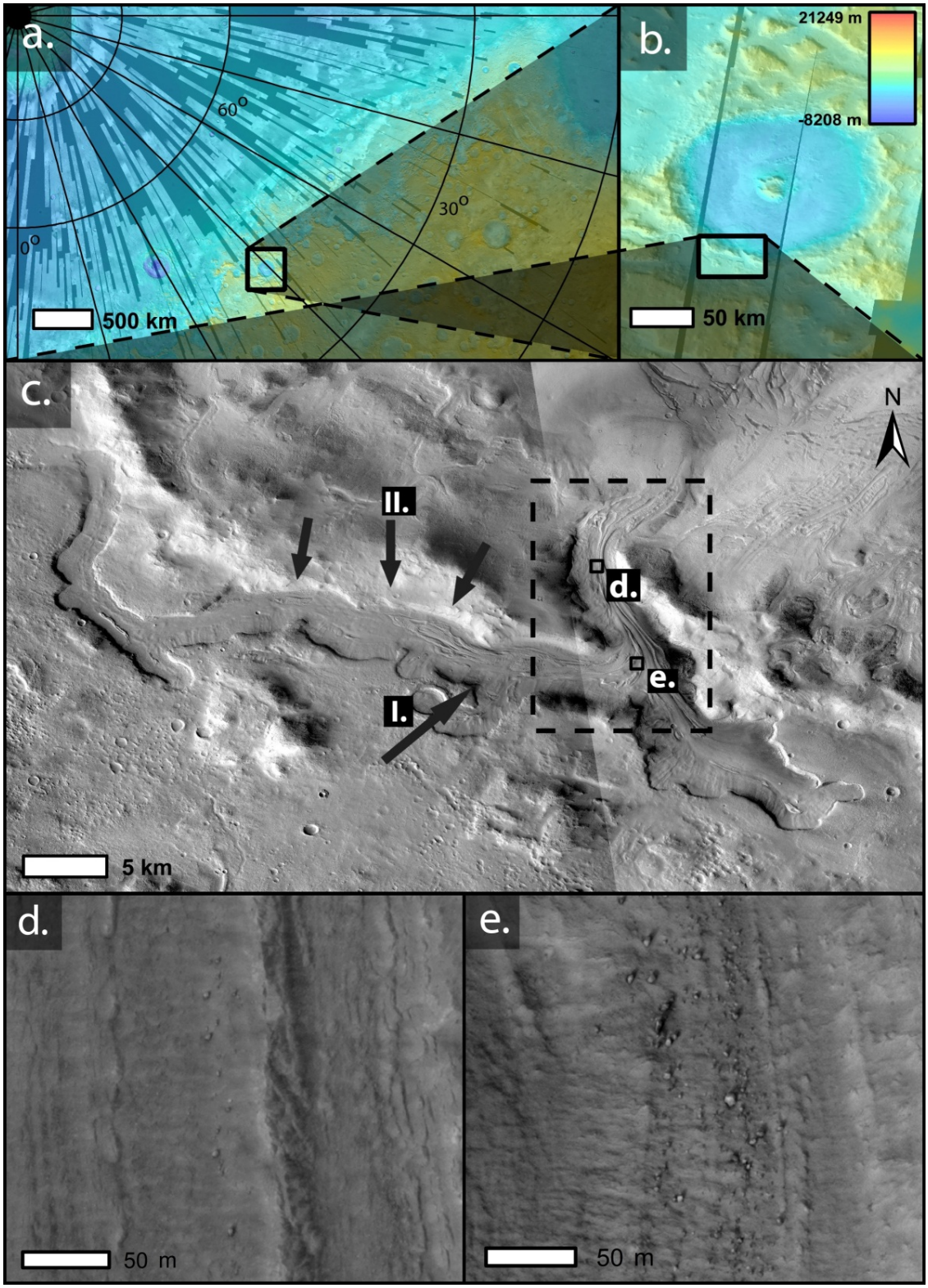

Figure A.8: *GLF #498, located in Protonilus Mensae showing background MOLA elevation images (a and b), a HiRISE image expansion (c), along with two examples of surface boulder exposures (d and e). Arrows marked I. and II. on (c) indicate likely source areas for supra-GLF boulders illustrated on Figure A.9 and discussed in the text. The dashed box is expanded in Figure A.9.*

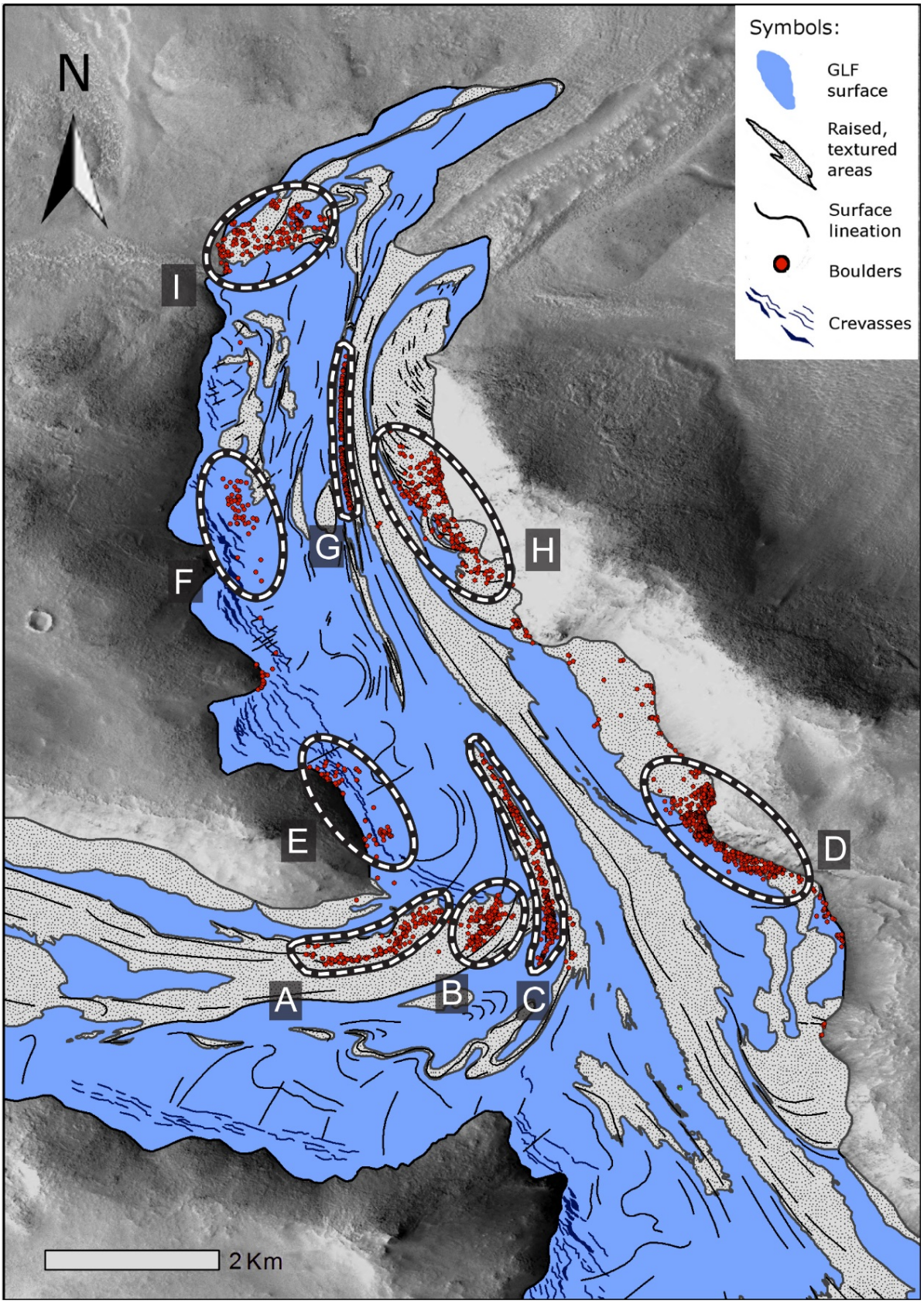

Figure A.9: *Geomorphological map and interpretation of boulder clusters A – I located on the surface of GLF #498, illustrated in Figure A.8.*

It is apparent from Figure A.9 that boulders have been supplied to several locations on the surface of GLF #498 and that they have subsequently moved across the GLF. Some of this movement may have been by active rolling, particularly away from immediate valley-side supply areas and towards the GLF's centreline, such as in the cases of Populations D, E, F, H and I. However, some or all of these populations may also have experienced passive redistribution, with boulders being advected with GLF motion. Without knowledge of the precise source area and maximum reach of individual boulders it is not possible to determine the component of passive advection in these cases, but it could have been anything up to the maximum dimension of these populations, ~2 km. In contrast, there appears to be no local source area for the boulders forming trains A, B, C and G; the boulders comprising these elongate trains are almost certainly sourced from further up-GLF. Inspection of Figure A.8c indicates that the closest likely source areas for these trains are from along the steep northern margin of the GLF's trunk for Populations A and B (marked 'II.' on Figure A.8c) and as a medial moraine extending from a promontory separating the GLF trunk from a tributary flowing into it from the south for Population C (marked 'I.' on Figure A.8c). Both of these likely source areas are at least 8 km up-flow of their corresponding supra-GLF boulder populations. In this case, and assuming that Populations C and G are part of the same feature, then the boulders at the far end of Population G appear to have been transported at least 15 km (8 km from the head of the tributary flow unit to Population C and a further 7 km to the distal end of Population G). In the absence of any firm age constraint on this particular GLF, we adopt a 'best estimate' age for its formation of 2 Ma, at the onset of the proposed 'late Amazonian' ice age, and a likely age range from 5 Ma, the middle of the last major ice age on Mars, to 0.5 Ma, the end of the proposed 'late Amazonian' ice age (Section A.1.1.3 above). Thus, if boulder transport was initiated at the time of GLF formation from point "I." on Figure A.8c it follows that, for those boulders to have been transported passively to the distal end of Population G, GLF #498's minimum centreline velocity was within the range of 3 – 30 mm a^{-1}, with a best estimate value of 7.5 mm a^{-1}.

Finally, the nature of boulder train elongation on the surface of GLF #498 is consistent with more rapid motion along the approximate centreline of the GLF (Populations A, B, C and G, which are highly elongate) than at its margins (Populations D, E, F, H and I,

which are less elongate), providing independent support for the normal, plan-form flow pattern reconstructed from crevasse patterns on other GLFs (Section A.2.3 above).

A.3. GLF hydrology

A.3.1. Present day GLF hydrology

Although still debated in detail (e.g. Ehlmann, 2014; Haberle, 2014), early Mars appears to have been both warmer and wetter than at present (Kargel, 2004). Current surface conditions are relatively cold and dry (see Section A.1 above), and are consequently no longer conductive to the survival of surface water. Nonetheless, seasonal variations in temperature are sufficient to induce occasional melting as evidenced, for example, by the intermittent discolouration of surface slope deposits in the southern mid-latitudes, inferred by McEwen et al. (2011) to indicate the effects of occasional near-surface moisture. Further, the presence of gullies incised into unconsolidated sediments has been interpreted as the result of intermittent fluvial erosion (Balme et al., 2006, 2013; Dickson and Head, 2009; Soare et al., 2014), as were similar gullies incised into pro-GLF headwall materials on the well-studied GLF #948 located in Crater Greg, Eastern Hellas (Hubbard et al., 2011).

A.3.1.1. Case study: supra-GLF channel networks

Despite evidence, summarized above, pointing to the intermittent melting of near-surface ice in Mars' mid and low-latitudes, such melting has, to our knowledge, in only one case been associated with GLFs. Hubbard et al. (2011) reported the presence of numerous incisions, typically ~1 m wide and tens of metres long, linking the edges of frost or contraction polygons (their 'polygonized terrain') on the surface of GLF #948 (their Figure 9). These were preferentially aligned sub-parallel to the ~10° local slope and they were interpreted as gullies formed by fluvial erosion resulting from the occasional melting of ice located immediately below the GLF's unconsolidated dust mantle. This interpretation, however, was proposed only tentatively because the incised segments were short and did not link up to form a coherent network; also, because

liquid water is not stable on Mars' cold, dry and low-pressure surface. Here, we extend this analysis to other GLFs to evaluate the nature and degree of recurrence of this landform in other, similar settings.

Because of the small scale of the polygons and incisions involved, target GLFs for the present study were restricted to those with high-resolution, HiRISE coverage, revealing at least six with extensive areas of surface incision. While four of these are located within or near to Hellas Planitia's Crater Greg (GLF #930, 947, 948 and 951) the other two are located on the dichotomy boundary in Protonilus Mensae (GLF #1310[1] and 390). Examination of these incised supra-GLF zones, one of which is presented for illustration in Figure A.10, reveals similar dimensions and slope-parallel orientation to those observed on GLF #948. Individual incised segments are also, in all cases, limited in length to a maximum of some tens of metres, while none of the cases identified develops a coherent tributary-based drainage network (e.g. Figure A.10). These similarities strongly indicate that all such incised terrains have been formed and subsequently influenced by a similar process set, operating widely in Mars' mid-latitudes. These characteristics are consistent with the formation of incisions by occasional surface melting, perhaps beneath a thin layer of surface dust, enhancing albedo and local energy transfer (e.g. Nicholson and Benn, 2006), on the relatively steep edges of surface periglacial patterned ground (Gallagher et al., 2011). The short reach length and absence of a coherent channel network is also consistent with the short-lived nature of any such liquid water, evaporating away before sufficient discharge can develop to form a supra-GLF drainage network.

A.3.2. Former GLF hydrology

With the notable exception of the proposed intermittent small-scale surface melting proposed above (Section A.3.1 above), present-day GLFs show little or no sign of the presence or influence of liquid water. For example, no evidence of pro-GLF fluvial

[1] This particular GLF is visible in HiRISE image ESP_019213_2210, which was acquired after the inventory of Souness et al. (2012). We therefore give it the next-available designation of #1310.

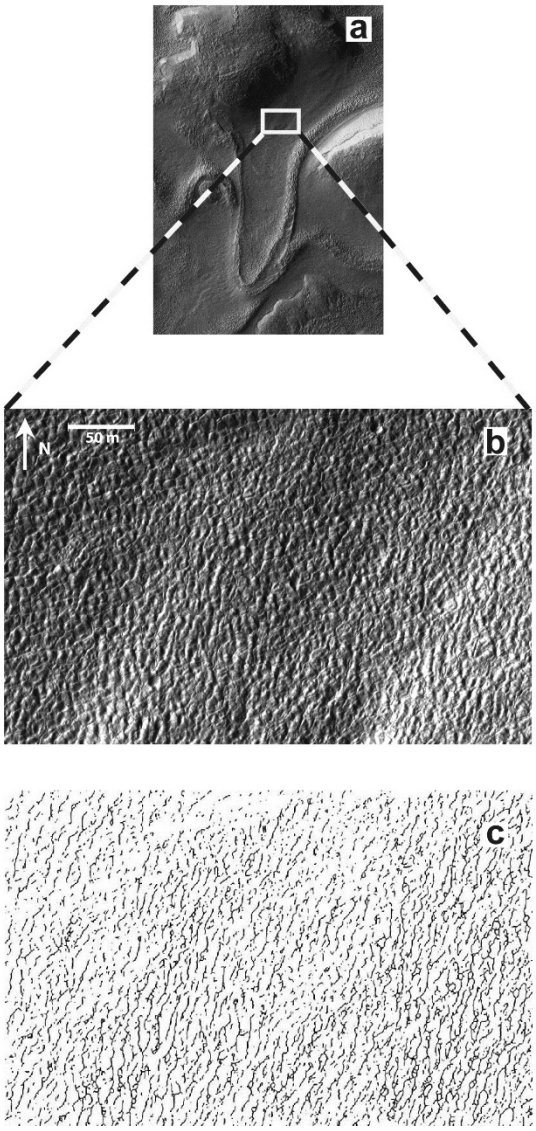

Figure A.10: *Surface incisions on GLF #947 (a) imaged by HiRISE to supplement those reported on GLF #948 by Hubbard et al. (2011), with an expansion of the incised terrain (b) and trace of incised segments (c).*

activity has been reported, and flow is almost certainly achieved solely through ice deformation, whether ductile or brittle (Section A.2.3 above). Current martian GLFs therefore appear to be cold throughout. However, this may not have always been the case, even up to the recent geological past. Indeed, the recently-expanded extent and thickness of GLFs during the LMGM (Section A.2.2 above) makes insulation of the bed beneath thick ice more likely than at present. Although former ice thicknesses are not known, precluding thermal modelling, large-scale regional glaciation has been proposed (Kargel and Strom, 1992; Kargel et al., 1995; Fastook et al., 2014) and several

landforms have been interpreted as indicative of, or consistent with, former wet-based glaciation. These include, for example, MLRs, the formation of which was proposed by Arfstrom and Hartmann (2005) possibly to involve subglacial squeezing. At the larger scale (and longer time span), sinuous and anastomosing ridge networks, elongate bedforms and large-scale grooves located in southern Argyre Planitia (~30 – 55 °S) were interpreted by Banks and Pelletier (2008) and Banks et al. (2009) as subglacial eskers, mega-scale glacial lineations (MSGL) and glacial erosional grooving respectively. The formation of these features would have required the area to have been covered by a large, wet-based ice mass (e.g. Bernhardt et al., 2013). To form MSGL, this ice mass would also have to have been, for some period of time, sliding rapidly over its substrate, almost certainly lubricated by subglacial water (e.g. Clark, 1994). Although these features are undated, Banks and co-workers (2008; 2009) considered them to have been formed in pre-Amazonian times.

More recently, Hubbard et al. (2011) interpreted the basin of GLF #948 in terms of an upper zone occupied by a remnant dust-mantled ice mass, and a lower zone now exhibiting relict bedforms. These bedforms were classified as ‘mound and tail’ terrain and ‘linear’ terrain and were likened to terrestrial drumlins and MSGL respectively. Since both of these landforms are predominantly associated with wet-based glacial conditions on Earth, these authors proposed that such conditions may have prevailed beneath GLF #948 at a time in the past when it had expanded and thickened to fill its moraine-bounded basin. This interpretation, however, was considered side-by-side with an alternative - not involving wet-based glaciation - based on the mound and tail and linear terrains representing degraded supra-GLF forms, in this case wind-blown dune deposits and exposed longitudinal foliation respectively. Finally, Hubbard et al. (2011) also reported the presence of ‘rectilinear ridge’ terrain located outside the current GLF basin, as enclosed by the well-defined MLRs. This terrain was likened to moraine-mound complexes on Earth, the formation of which again suggests either the direct presence of water, if formed as outwash deposits (Lukas, 2005) or crevasse fills (Sharp, 1985), or of polythermal glaciation if formed by glacial thrusting (Hambrey et al., 2005). However, the possibility of cold-based formation, in this case as proglacial thrust-blocks, was not entirely discounted.

A.4. Summary

With the aid of high-resolution imagery, particularly from the CTX and HiRISE cameras, several major advances have been made in a short period of time concerning Mars' mid-latitude GLFs. Thus, it is now known with some certainty that:

- Many GLFs were previously more extensive and thicker than at present, possibly now representing the remnants of former large ice sheets. In Section A.2.2.1 above we identify a distinctive proglacial zone ~3 km wide surrounding a GLF located in Phlegra Montes. This zone, bounded along its distal edge by MLRs is interpreted as having been recently deglaciated and is likened to a similar proglacial region bounding Midre Lovénbreen, Svalbard, on Earth.

- GLFs flow slowly downslope through a combination of ductile and (less common) brittle deformation. In Section A.2.3.3 above we identify and interpret four contrasting sets of crevasses located on two martian GLFs in terms of variable strain regimes. These crevasses are also shown to range from being relatively fresh in appearance, implying a correspondingly young age, to appearing blunt and degraded, implying earlier formation and possibly a relict current condition.

- GLFs have the ability to transport debris, forming large bounding moraines and depositing boulder trains extending for several kilometres along-GLF. In Section A.2.4.1 above we identify an extensive supra-GLF debris train which we interpret in terms of passive transport from specific ice-marginal supply points. Reconstructing boulder transport distances since GLF formation (over the range 5.0 to 0.5 Ma ago, with a best estimate age of 2.0 Ma BP) yields a corresponding provisional GLF surface velocity range of 3 - 30 mm a^{-1}, with a best estimate of ~7.5 mm a^{-1}.

- GLFs currently show little influence of liquid water, confined to postulated intermittent surface melting which is insufficient to form coherent supra-GLF drainage. In Section A.3.1.1 above we illustrate that such supra-GLF incised

channels occur on several GLFs and are not confined to the single instance at which they have hitherto been reported. However, more extensive former GLFs, and/or their predecessor ice masses, may have been partially wet-based.

Despite this information, many of the most fundamental glaciological aspects of GLFs remain unknown. These include the following:

- It is not known whether GLFs are currently active or whether they are decaying relics of previously active forms. Diagnostic indicators of such activity would include any evidence of motion (addressed below) and for a GLF to have a surface profile that is in balance – as indicated by a spatially-distributed numerical model of GLF flow - with current climatic conditions.

- The previous extent of GLFs, and their putative parent ice sheets, is still only poorly understood. This requirement could be addressed through additional field mapping at a variety of spatial scales, based on CTX or High Resolution Stereo Camera images at the regional scale to HiRISE images at a local scale. Such mapping could be targeted at identifying markers of former ice extent such as specific surface terrains, subglacial deposits and ice-marginal moraines.

- The thermal regime of former GLFs is unknown, and the possibility of partial wet-based conditions remains unproven and their extent unevaluated. These issues could be evaluated empirically or theoretically, ideally through a combination of both. Empirical evidence might include the identification of indicators diagnostic of wet-based conditions (e.g. bedforms such as MSGL) or of subglacial drainage (e.g. meltwater channels or eskers). Theoretically, former thermal regime could be estimated from the application of a thermomechanically-coupled ice-flow model to reconstructed former ice mass geometries under realistic climatic conditions for the time.

- The basic mass-balance regime of GLFs is unknown. Whatever the spatial expression of this regime, there is no compelling climatological reason for it to comply with the common terrestrial valley-glacier model of net accumulation at

high elevations gradually giving way to net ablation at low elevations. This is possibly the most challenging unknown GLF property to elucidate, and would likely require several lines of evidence to be combined. Central to these might be a regional evaluation of GLF extent in the light of corresponding regional variations in meteorological conditions. A modelling approach may also shed some light of the mass-balance regime of GLFs, for example, through comparing modelled GLF geometries and flow with empirical data under a variety of modelled mass-balance patterns.

- The 3-D geometry and internal structure of GLFs is unknown. Although SHARAD radar data are available and capable of mapping ice thickness, the data are of fairly coarse resolution and have limited spatial coverage. Very little information is therefore available to allow the basal interface of GLFs to be identified and mapped. This property is also critically important because spatially-distributed models of ice mass flow depend sensitively on accurate bed geometry. In this case, new and existing SHARAD data could usefully be mined to locate intersections with known GLFs, providing a first approximation of bed profiles. Further to that, modelling-based sensitivity analyses (to GLF depth) could also be used to constrain likely bed geometries.

- Mechanisms of GLF motion are poorly known and, apart from the estimate of 3 – 30 mm a^{-1} presented herein (Section A.2.4.1 above), it has not yet been possible to measure surface velocities on any martian GLF. Further research based on indicators of surface displacement – such as the boulder analysis presented herein – could usefully be used to refine the range we propose. As the period of time between repeat HiRISE images of certain GLFs increases it may also become possible to identify contemporary GLF motion on the basis of feature or speckle tracking. Indeed, a single such measurement would provide a major advance in our understanding of the dynamic glaciology of martian GLFs, particularly if the GLF concerned could also be modelled.

- GLF-related landforms such as lineations, drumlin-like forms, surface cracks/gullies and possible eskers remain largely unexplored and their basic

morphometric characteristics are unreported. Targeted mapping from HiRISE images remains the best way to identify and evaluate such landforms. The online inventory accompanying Souness et al. (2012) would provide a suitable starting point for identifying candidate regions of interest.

- Although considered to be rich in water-ice, the internal composition of GLFs remains unknown, despite these material properties having important implications for GLF dynamics and our ability to model GLF behaviour accurately. Apart from direct sampling in the future, which is unlikely in the medium-term, SHARAD data analysis may be combined with numerical modelling to further constrain the internal composition of GLFs. Opportunistic images, for example shortly following a meteorite impact, may also continue to yield information relevant to GLF sub-surface conditions.

These issues deserve research attention to improve our understanding of the surface features of Mars and, glaciers being effective recorders of climate change, the planet's past environmental conditions. It is also worth noting that the well-insulated base of thick ice masses represents one of the most likely geologically-recent environments on Mars for the existence of the wet and relatively warm conditions that are conducive to life.

Acknowledgements

We acknowledge the HiRISE team, University of Arizona, and NASA/JPL for making the HiRISE images we investigate herein available to the public. We thank Ajay Limaye for preparing the 3-D image presented in Figure A.1. We also thank Matthew Balme, Wilfried Haeberli, Michael Kuhn and Sara Springman for reviewing or commenting on an earlier version of the manuscript, and Martin Schneebeli for Editing.

References

Arfstrom, J., & Hartmann, W. K. (2005). Martian flow features, moraine-like ridges, and gullies: Terrestrial analogs and interrelationships. *Icarus, 174*(2), 321-335. doi: 10.1016/j.icarus.2004.05.026.

Baker, D. M. H., Head, J. W., & Marchant, D. R. (2010). Flow patterns of lobate debris aprons and lineated valley fill north of Ismeniae Fossae, Mars: Evidence for extensive mid-latitude glaciation in the Late Amazonian. *Icarus, 207*(1), 186-209. doi: 10.1016/j.icarus.2009.11.017.

Balme, M. R., Gallagher, C. J., & Hauber, E. (2013). Morphological evidence for geologically young thaw of ice on Mars: A review of recent studies using high-resolution imaging data. *Progress In Physical Geography*, *37*(3), 289-324. doi: 10.1177/0309133313477123.

Balme, M., Mangold, N., Baratoux, D., Costard, F., Gosselin, M., Masson, P., Pinet, P., & Neukum, G. (2006). Orientation and distribution of recent gullies in the southern hemisphere of mars: Observations from High Resolution Stereo Camera/Mars Express (HRSC/MEX) and Mars Orbiter Camera/Mars Global Surveyor (MOC/MGS) data. *Journal of Geophysical Research: Planets*, *111*(E5). doi:10.1029/2005JE002607.

Banks, M. E., & Pelletier, J. D. (2008). Forward modeling of ice topography on Mars to infer basal shear stress conditions. *Journal of Geophysical Research: Planets*, *113*(E1). doi: 10.1029/2007JE002895.

Banks, M. E., Lang, N. P., Kargel, J. S., McEwen, A. S., Baker, V. R., Grant, J. A., Pelletier, J. D., & Strom, R. G. (2009). An analysis of sinuous ridges in the southern Argyre Planitia, Mars using HiRISE and CTX images and MOLA data. *Journal of Geophysical Research: Planets*, *114*(E9). doi:10.1029/2008JE003244.

Bernhardt, H., Hiesinger, H., Reiss, D., Ivanov, M., & Erkeling, G. (2013). Putative eskers and new insights into glacio-fluvial depositional settings in southern Argyre Planitia, Mars. *Planetary and Space Science*, *85*, 261-278. doi: 10.1016/j.pss.2013.06.022.

Byrne, S., Russel, P., Pathare, A., Becerra, P., Molaro, J., Mattson, S., & Mellon, M. T. (2013). Fracturing the icy polar cliffs of Mars. Abstract #1659, *44th Lunar and Planetary Science Conference*, *March 18-22, The Woodlands, Texas*.

Clark, C. D. (1994). Large-scale ice-moulding: a discussion of genesis and glaciological significance. *Sedimentary Geology*, *91*(1-4), 253-268. doi: 10.1016/0037-0738(94)90133-3.

Colaprete, A., & Jakosky, B. M. (1998). Ice flow and rock glaciers on Mars. *Journal of Geophysical Research: Planets*, *103*(E3), 5897-5909. doi: 10.1029/97JE03371.

Dickson, J. L., & Head, J. W., (2009). The formation and evolution of youthful gullies on Mars: Gullies as the late-stage phase of Mars' most recent ice age. *Icarus*, *204*(1), 63-86. doi: 10.1016/j.icarus.2009.06.018.

Dickson, J. L., Head, J. W., & Marchant, D. R. (2008). Late Amazonian glaciation at the dichotomy boundary on Mars: Evidence for glacial thickness maxima and multiple glacial phases. *Geology, 36*(5), 411-414. doi: 10.1130/g24382a.1.

Dickson, J. L., Head, J. W., & Marchant, D. R. (2010). Kilometer-thick ice accumulation and glaciation in the northern mid-latitudes of Mars: Evidence for crater-filling events in the Late Amazonian at the Phlegra Montes. *Earth and Planetary Science Letters, 294*(3-4), 332-342. doi: 10.1016/j.epsl.2009.08.031.

Dundas, C. M., & Byrne, S. (2010). Modeling sublimation of ice exposed by new impacts in the martian mid-latitudes. *Icarus*, *206*(2), 716-728. doi: 10.1016/j.icarus.2009.09.007.

Ehlmann, B. L. (2014). The First Billion Years - Warm and Wet vs. Cold and Icy? Abstract #1245, *Eighth International Conference on Mars, Pasadena, March 14-18, California.*

Fastook, J. L., Head, J. W., & Marchant, D. R. (2014). Formation of lobate debris aprons on Mars: Assessment of regional ice sheet collapse and debris-cover armoring. *Icarus, 228*, 54-63. doi: 10.1016/j.icarus.2013.09.025.

Forget, F., Haberle, R. M., Montmessin, F., Levrard, B., & Head, J. W. (2006). Formation of glaciers on Mars by atmospheric precipitation at high obliquity. *Science, 311*(5759), 368-371. doi: 10.1126/science.1120335.

Gallagher, C., Balme, M. R., Conway, S. J., & Grindrod, P. M. (2011). Sorted clastic stripes, lobes and associated gullies in high-latitude craters on Mars: Landforms indicative of very recent, polycyclic ground-ice thaw and liquid flows. *Icarus*, *211*(1), 458-471. doi: 10.1016/j.icarus.2010.09.010.

Garvin, J. B., Head, J. W., Marchant, D. R., & Kreslavsky, M. A. (2006). High-latitude cold-based glacial deposits on Mars: Multiple superposed drop moraines in a

crater interior at 70 degrees N latitude. *Meteoritics & Planetary Science*, *41*(10), 1659-1674. doi: 10.1111/j.1945-5100.2006.tb00443.x.

Goldsby, D. L., & Kohlstedt, D. L. (2001). Superplastic deformation of ice: Experimental observations. *Journal of Geophysical Research: Solid Earth*, *106*(B6), 11017-11030. doi: 10.1029/2000JB900336.

Haberle, R. M. (2014). Mars: The First Billion Years - Warm and Wet vs. Cold and Icy? Abstract *#1270, Eighth International Conference on Mars, March 14-18, Pasadena, California.*

Hambrey, M. J., Murray, T., Glasser, N. F., Hubbard, A., Hubbard, B., Stuart, G., Hansen, S., & Kohler, J. (2005). Structure and changing dynamics of a polythermal valley glacier on a centennial timescale: Midre Lovenbreen, Svalbard. *Journal of Geophysical Research-Earth Surface*, *110*(F1). doi: 10.1029/2004JF000128.

Harbor, J. M. (1995). Development of glacial-valley cross sections under conditions of spatially variable resistance to erosion. *Geomorphology*, *14*(2), 99-107. doi: 10.1016/0169-555x(95)00051-1.

Hartmann, W. K., Thorsteinsson, T., & Sigurdsson, F. (2003). Martian hillside gullies and Icelandic analogs. *Icarus, 162*(2), 259-277. doi: 10.1016/S0019-1035(02)00065-9.

Hartmann, W. K., Ansan, V., Berman, D. C., Mangold, N., & Forget, F. (2014). Comprehensive analysis of glaciated martian crater Greg. *Icarus, 228*, 96-120. doi: 10.1016/j.icarus.2013.09.016.

Head, J. W., & Marchant, D. R. (2003). Cold-based mountain glaciers on Mars: Western Arsia Mons. *Geology, 31*(7), 641-644. doi: 10.1130/0091-7613(2003)031<0641:cmgomw>2.0.co;2.

Head, J. W., Mustard, J. F., Kreslavsky, M. A., Milliken, R. E., & Marchant, D. R. (2003). Recent ice ages on Mars. *Nature, 426*(6968), 797-802. doi: 10.1038/Nature02114.

Head, J. W., Marchant, D. R., Dickson, J. L., Kress, A. M., & Baker, D. M. (2010). Northern mid-latitude glaciation in the Late Amazonian period of Mars: Criteria for the recognition of debris-covered glacier and valley glacier landsystem deposits. *Earth and Planetary Science Letters, 294*(3-4), 306-320. doi: 10.1016/j.epsl.2009.06.041.

Head, J. W., Neukum, G., Jaumann, R., Hiesinger, H., Hauber, E., Carr, M., Massson, P., Foing, B., Hoffmann, H., Kreslavsky, M., Werner, S., Milkovich, S., van Gasselt, S., & HRSC Co-Investigator Team. (2005). Tropical to mid-latitude snow and ice accumulation, flow and glaciation on Mars. *Nature, 434*(7031), 346-351. doi: 10.1038/Nature03359.

Herzfeld, U. C., & Clarke, G. K. C. (2001). Analysis of crevasse patterns as indicators of ice dynamics using structural glaciology and geostatistical classification. IP21A-0674, *American Geophysical union, Fall Meeting, December 10-14, San Francisco, California*.

Hobley, D. E. J., Howard, A. D., & Moore, J. M. (2014). Fresh shallow valleys in the Martian midlatitudes as features formed by meltwater flow beneath ice. *Journal of Geophysical Research-Planets, 119*(1), 128-153. doi: 10.1002/2013je004396.

Holt, J. W., Safaeinili, A., Plaut, J. J., Head, J. W., Phillips, R. J., Seu, R., Kempft, S. D., Choudhary, P., Young, D. A., Putzig, N. E., Biccari, D., & Gim, Y. (2008). Radar Sounding Evidence for Buried Glaciers in the Southern Mid-Latitudes of Mars. *Science, 322*(5905), 1235-1238. doi: 10.1126/science.1164246.

Hubbard, B., Milliken, R. E., Kargel, J. S., Limaye, A., & Souness, C. J. (2011). Geomorphological characterisation and interpretation of a mid-latitude glacier-like form: Hellas Planitia, Mars. *Icarus, 211*(1), 330-346. doi: 10.1016/j.icarus.2010.10.021.

Hudson, T. L., Aharonson, O., & Schorghofer, N. (2009). Laboratory experiments and models of diffusive emplacement of ground ice on Mars. *Journal of Geophysical Research: Planets*, *114*(E1). doi:10.1029/2008JE003149.

Kargel, J. S. (2004). *Mars: A warmer, wetter planet.* London, Springer-Praxis.

Kargel, J. S., & Strom, R. G. (1992). Ancient glaciation on Mars. *Geology*, *20*(1), 3-7. doi: 10.1130/0091-7613(1992)020<0003:AGOM>2.3.CO;2.

Kargel, J. S., Baker, V. R., Beget, J. E., Lockwood, J. F., Pewe, T. L., Shaw, J. S., & Strom, R. G. (1995). Evidence of Ancient Continental-Glaciation in the Martian Northern Plains. *Journal of Geophysical Research-Planets, 100*(E3), 5351-5368. doi: 10.1029/94je02447.

Laskar, J., Correia, A. C. M., Gastineau, M., Joutel, F., Levrard, B., & Robutel, P. (2004). Long term evolution and chaotic diffusion of the insolation quantities of Mars. *Icarus, 170*(2), 343-364. doi: 10.1016/j.icarus.2004.04.005.

Levy, J. S., Head, J. W., & Marchant, D. R. (2007). Lineated valley fill and lobate debris apron stratigraphy in Nilosyrtis Mensae, Mars: Evidence for phases of glacial modification of the dichotomy boundary. *Journal of Geophysical Research, 112*(E8), E08004. doi: 10.1029/2006je002852.

Li, H., Robinson, M. S., & Jurdy, D. M. (2005). Origin of martian northern hemisphere mid-latitude lobate debris aprons. *Icarus*, *176*(2), 382-394. doi: 10.106/j.icarus.2005.02.011.

Lukas, S. (2005). A test of the englacial thrusting hypothesis of 'hummocky' moraine formation: case studies from the northwest Highlands, Scotland. *Boreas*, *34*(3), 287-307. doi: 10.1111/j.1502-3885.2005.tb01102.x.

Mair, R., & Kuhn, M. (1994). Temperature and movement measurements at a bergschrund *Journal of Glaciology*, *40*(136), 561-565. doi: 10.1017/S0022143000012442.

Mangold, N. (2003). Geomorphic analysis of lobate debris aprons on Mars at Mars Orbiter Camera scale: Evidence for ice sublimation initiated by fractures. *Journal of Geophysical Research, 108*(E4), 8021. doi: 10.1029/2002je001885.

Marchant, D., & Head, J. W. (2003). Tongue-shaped lobes on Mars: Morphology, Nomenclature, and Relation to Rock Glacier Deposits. Abstract #3091, *Sixth International Conference on Mars, July 20-25, Pasadena, California.*

McEwen, A. S., Dundas, C. M., Mattson, S. S., Toigo, A. D., Ojha, L., Wray, J. J., Chojnacki, M., Byrne, S., Murchie, S. L., & Thomas, N. (2011). Recurring slope lineae in equatorial regions of Mars. *Nature Geoscience*, *7*, 53-58. doi: 10.1038/ngeo2014.

Milliken, R. E., Mustard, J. F., & Goldsby, D. L. (2003). Viscous flow features on the surface of Mars: Observations from high-resolution Mars Orbiter Camera (MOC) images. *Journal of Geophysical Research-Planets, 108*(E6), 5057. doi: 10.1029/2002je002005.

Nicholson, L., & Benn, D. I. (2006). Calculating ice melt beneath a debris layer using meteorological data. *Journal of Glaciology*, *52*(178), 463-470. doi: 10.3189/172756506781828584.

Phillips, R. J., Zuber, M. T., Smrekar, S. E., Mellon, M. T., Head, J. W., Tanaka, K. L., Putzig, N. E., Milkovich, S. M., Campbell, B. A., Plaut, J. J., Safaeinili, A., Seu, R., Biccari, D., Carter, L. M., Picardi, G., Orosei, R., Mohit, P. S., Heggy, E., Zurek, R. W., Egan, A. F., Giacomoni, E., Russo, F., Cutigni, M., Pettinelli, E.,

Holt, J. W., Leuschen, C. J., & Marinangeli, L. (2008). Mars north polar deposits: Stratigraphy, age, and geodynamical response. *Science*, *320*(5880), 1182-1185. doi: 10.1126/science.1157546.

Pierce, T. L., & Crown, D. A. (2003). Morphologic and topographic analyses of debris aprons in the eastern Hellas region, Mars. *Icarus*, *163*(1), 46-65. doi: 10.1016/S0019-1035(03)00046-0.

Plaut, J. J., Safaeinili, A., Holt, J. W., Phillips, R. J., Head, J. W., Seu, R., Putzig, N. E., & Frigeri, A. (2009). Radar evidence for ice in lobate debris aprons in the mid-northern latitudes of Mars. *Geophysical Research Letters, 36*(2), L02203. doi: 10.1029/2008gl036379.

Read, P. L., & Lewis, S. R. (2004). *The Martian Climate Revisited: Atmosphere and Environment of a Desert Planet.* Chichester: Springer-Praxis.

Russell, P., Thomas, N., Byrne, S., Herkenhoff, K., Fishbaugh, K., Bridges, N., Okubo, C., Milazzo, M., Daubar, I., Hansen, C., & McEwen, A. (2008). Seasonally active frost-dust avalanches on a north polar scarp of Mars captured by HiRISE. *Geophysical Research Letters*, *35*(23). doi:10.1029/2008GL035790.

Sato, H., Kurita, K., & Baratoux, D. (2010). The formation of floor-fractured craters in Xanthe Terra. *Icarus*, *207*(1), 248-264. doi: 10.1016/j.icarus.2009.10.023.

Schon, S. C., Head, J. W., & Milliken, R. E. (2009). A recent ice age on Mars: Evidence for climate oscillations from regional layering in mid-latitude mantling deposits. *Geophysical Research Letters*, *36*(15). doi:10.1029/2009GL038554.

Seu, R., Phillips, R. J., Alberti, G., Biccari, D., Bonaventura, F., Bortone, M., Calabrese, D., Campbell, B. A., Cartacci, M., Carter, L. M., Catallo, C., Croce, A., Croci, R., Cutigni, M., Di Placido, A., Dinardo, S., Federico, C., Flamini, E., Fois, F., Frigeri, A., Fuga, O., Giacomoni, E., Gim, Y., Guelfi, M., Holt, J. W., Kofman, W., Leuschen, C. J., Marinangeli, L., Marras, P., Masdea, A., Mattei, S., Mecozzi, R., Milkovich, S. M., Morlupi, A., Mouginot, J., Orosei, R., Papa, C., Paterno, T., Persi del Marmo, P., Pettinelli, E., Pica, G., Picardi, G., Plaut, J. J., Provenziani, M., Putzig, N. E., Russo, F., Safaeinili, A., Salzillo, G., Santovito, M. R., Smrekar, S. E., Tattarletti, B., & Vicari, D. (2007). Accumulation and erosion of Mars' south polar layered deposits. *Science*, *317*(5845), 1715-1718. doi: 10.1126/science.1144120.

Sharp, M. (1985). "Crevasse-fill" ridges - a landform type characteristic of surging glaciers? *Geografiska Annaler*, *67A*(3-4), 213-220. doi: 10.2307/521099.

Sharp, R. P. (1973). Mars: Fretted and Chaotic Terrains. *Journal of Geophysical Research, 78*(20), 4073-4083. doi: 10.1029/Jb078i020p04073.

Sinha, R. K., & Murty, S. V. S. (2013). Evidence of extensive glaciation in Deuteronilus Mensae, Mars: Inferences towards multiple glacial events in the past epochs. *Planetary and Space Science, 86*, 10-32. doi: 10.1016/j.pss.2013.09.002.

Soare, R. J., Conway, S. J., & Dohm, J. M. (2014). Possible ice-wedge polygons and recent landscape modification by “wet” periglacial processes in and around the Argyre impact basin, Mars. *Icarus*, *233*, 214-228. doi: 10.1016.j.icarus.2014.01.034.

Souness, C. J., & Hubbard, B. (2012). Mid-latitude glaciation on Mars. *Progress In Physical Geography*, *36*(2), 238-261. doi: 10.1177/0309133312436570.

Souness, C. J., & Hubbard, B. (2013). An alternative interpretation of late Amazonian ice flow: Protonilus Mensae, Mars. *Icarus, 225*(1), 495-505. doi: 10.1016/j.icarus.2013.03.030.

Souness, C. J., Hubbard, B., Milliken, R. E., & Quincey, D. (2012). An inventory and population-scale analysis of martian glacier-like forms. *Icarus, 217*(1), 243-255. doi: 10.1016/j.icarus.2011.10.020.

Squyres, S. W. (1978). Martian Fretted Terrain: Flow of Erosional Debris. *Icarus, 34*(3), 600-613. doi: 10.1016/0019-1035(78)90048-9.

Squyres, S. W. (1979). The Distribution of Lobate Debris Aprons and Similar Flows on Mars. *Journal of Geophysical Research, 84*, 8087-8096. doi: 10.1029/Jb084ib14p08087.

Touma, J., & Wisdom, J. (1993). The Chaotic Obliquity of Mars. *Science*, *259*(5099), 1294-1297. doi: 10.1126/science.259.5099.1294.

Vaughan, D.G. (1993). Relating the occurrence of crevasses to surface strain rates. *Journal of Glaciology*, *39*(132), 255-266. doi: 10.1017/S0022143000015926.